Ulm University

Institute of Medical Systems Biology

Prof. Dr. Hans A. Kestler

LOGICAL MODELLING OF MOLECULAR CROSSTALKS FOR THE PREDICTION OF COMPLEX PHENOTYPES

Dissertation submitted in partial fulfilment of the requirements for the degree of „Doctor rerum naturalium“ (Dr. rer. nat.) of the International Graduate School in Molecular Medicine Ulm

Nensi Ikonomi
born in Durrës

Ulm, 2022

1. Current dean of the medical faculty: Prof. Dr. Thomas Wirth

2. Chairman of the Graduate School: Prof. Dr. Bernd Knöll

3. Thesis Advisory Committee:

    - First supervisor: Prof. Dr. Hans A. Kestler

    - Second supervisor: Prof. Dr. Michael Kühl

    - Third supervisor: Prof. (apl.) Dr. Malte Buchholz

4. External reviewers:

    - Prof. Stefano Toppo, PhD

    - Prof. Dr. Helen Morrison

5. Day doctorate awarded: 13.06.2023

Some results gained in this thesis have previously been published in the following publications:

- **Ikonomi N.***, Kühlwein S.D.*, Schwab J.D.*, Kestler H.A. (2020). Awakening the HSC: dynamic modeling of HSC maintenance unravels regulation of the TP53 pathway and quiescence. *Frontiers in Physiology*, 848.

- **Ikonomi N.***, Kühlwein S.D.*, Schwab J.D.*, Kestler H.A. (2022). Discrete Logic Modeling of Cell Signaling Pathways. In: Zi Z., Liu X. (eds) *TGF-Beta Signaling*. Methods in Molecular Biology. Humana, New York, NY. 2488: 159-181.

- Schwab J.D.*, **Ikonomi N.***, Werle S.D.*, Weidner F.M.*, Geiger H., Kestler H.A. (2021). Reconstructing Boolean network ensembles from single-cell data for unraveling dynamics in the aging of human hematopoietic stem cells. *Computational and Structural Biotechnology Journal*, 19:5321-5332.

- Weidner F.M.*, Schwab J.D.*, Werle S.D.*, **Ikonomi N.***, Lausser L., Kestler H.A. (2021). Capturing dynamic relevance in Boolean networks using graph theoretical measures. *Bioinformatics*, 37(20): 3530-3537.

- Schwab J. D., Kühlwein S.D., **Ikonomi N.**, Kühl M., Kestler H. A. (2020). Concepts in Boolean network modeling: What do they all mean? *Computational and Structural Biotechnology Journal*, 18: 571-582.

Currently in revision/preparation:

- Werle S.D.*, **Ikonomi N.***, Weidner F.M., Lausser L., Schwab J.D., Maier J., Buchholz M., Gress T. M., Kestler A.M.R., Kestler H.A. (2022). Pancreatic neuroendocrine tumors - A systems biology approach to define mechanisms, phenotypes, and drivers in patient cohorts. *Cancers*.

$*$ **equal contribution**

Acknowledgements for this dissertation have been removed due to privacy issues.

TABLE OF CONTENTS

List of abbreviations VII

1 Introduction 1

1.1 Overview on Systems biology 1

1.2 Dynamic modelling 4

1.2.1 Boolean network models 6

1.3 Investigation and prediction possibilities of network dynamics 10

1.4 Background on the biological use cases 15

1.4.1 Ageing 15

1.4.2 Cancer 17

1.5 Aims of the thesis 19

1.6 Synopsis of the thesis 20

2 Methods 21

2.1 Boolean network models 21

2.1.1 Simulation of Boolean network models 22

2.1.2 Robustness analysis within Boolean network models 23

2.1.3 Target identification in Boolean network models 24

2.2 Model setup strategies 26

2.2.1 Manual establishment of literature-based Boolean network models 26

2.2.2 Automatic reconstruction of Boolean network models 28

2.3 Model analysis and validation 33

2.3.1 Model analysis strategies 34

2.3.2 Model validation 36

2.4 Predicting dynamic relevance via graph theoretical measures 39

2.4.1 Collection of Boolean network models 40

2.4.2 Evaluation of dynamic impact after perturbation 40

2.4.3 Static measures 41

2.4.4 Ranking gene impacts 42
2.4.5 Evaluation of node connectivity 43
2.5 Statistics and visualisation 43
3 Results 44
3.1 Modelling the physiological maintenance and ageing of HSCs 44
3.1.1 The homeostatic maintenance of HSCs 45
3.1.2 Discussion – Modelling the HSC maintenance 72
3.1.3 The NF-κB signalling during HSCs ageing 77
3.1.4 Discussion – Modelling HSC ageing via personalised ensembles 88
3.2 Modelling pNETs' progression and targeted interventions 91
3.2.1 A Boolean network model of pNETs initiation and progression 93
3.2.2 Simulation of frequently mutated pNETs drivers 110
3.2.3 Integration of foreign feature classification in dynamic predictions 113
3.2.4 Attractor-specific activities validation 116
3.2.5 Identification of new tumour drivers 119
3.2.6 Prediction of efficacy and resistance of mTORC1 inhibitors 123
3.2.7 Automatic screening to predict potential targets in pNETs 126
3.2.8 Discussion – Modelling pNETs 129
3.3 Predicting dynamic relevance via graph theoretical measures 135
3.3.1 Identification of static measures predicting dynamic impact 135
3.3.2 Characterisation of a new class of dynamic drivers 138
3.3.3 Gatekeeper nodes exchange mutual information with hubs 139
3.3.4 Perturbation of gatekeepers impacts biological phenotypes 140
3.3.5 Evaluation of gatekeepers in the pNET model 141
3.3.6 Discussion – Predicting dynamic relevance via static measures 144
4 General Discussion 147
4.1 Biological complexity: is less more in defining phenotypical landscapes? 147
4.2 Modelling strategies and challenges in Boolean networks 148
4.3 Capturing heterogeneity: towards personalised modelling 150
5 Summary 152
6 References 154
7 Appendix 220

LIST OF ABBREVIATIONS

&; $\wedge$ and

|; $\vee$ or

!; $\neg$ not

$\subseteq$ is a subset of

$\in$ is member of

$\cup$ set union

$\propto$ is proportional to

$\mathbb{N}$ set of natural numbers

$\mathbb{R}$ set of real numbers

$\mathbb{B}$ set of Boolean values

ADP adenosine diphosphate

AKT protein kinase B

AP1 activator protein 1

Apaf-1 apoptotic protease-activating factor 1

APC adenomatous polyposis coli protein

ARF1 ADP-ribosylation factor 1

ATRX ATRX chromatin remodeller

ATM ataxia-telangiectasia mutated

AUC area under the curve

b betweeness

BASC binarization across multiple scales

BCL2 B-cell lymphoma 2

BIRC3 baculoviral IAP Repeat Containing 3

BMI polycomb ring finger protein

CARD14 caspase recruitment domain family member 14

c Clustering coefficient

CDH1 E-cadherin

CCND1 cyclin D1

CCNE1 cyclin E1

CDC42 cell division control protein 42 homolog

CDK4/6 cyclin dependent kinase 4/6

CEBPα CCAAT enhancer binding protein alpha

C. elegans Caenorhabditis elegans

CFL1 cofilin-1

cFOS Fos proto-oncogene

CIP2A cancerous inhibitor of PP2A

CYLD CYLD Lysine 63 Deubiquitinase

c-Jun Jun proto-oncogene

CITED2 Cbp/p300-interacting transactivator 2

CSNK2A1 casein kinase 2 alpha 1

CTNNB1 β-catenin

CYCS cytochrome C

D diameter

d distance

DAXX death-domain assiciated protein

DNA desoxyribonucleic acid

DP Determinative Power

E2F transcription factor E2F

4E-BP1 eukaryotic translation initiation factor 4E-binding protein 1

EGFR epidermal growth factor receptor

eIFs eukaryotic initiation factors

EMT epithelial to mesenchymal transition

ERC1 ELKS/RAB6-interacting/CAST family member 1

ERK extracellulat signal-regulated protein kinase

ET1 endotelin 1

ETS1 ETS Proto-Oncogene 1

ESE2 E74 like ETS transcription factor 5

ERV endogenous retroviral elements

f function

FACS fluorecence-activated cell sorting

FAK1 focal adhesion kinase

FGF fibroblast growth factor

FLI1 friend leukemia integration 1

FOXO forkhead Box-O

FOXO1 forkhead Box-O1

FOXO3A forkhead Box-O3

G0 gap zero phase

G1 gap one phase

GATA2 GATA binding protein 2

GEO Gene Expression Omnibus

GFI1 growth factor independent 1

GLI1 glioma-associated oncogene homolog 1

GRN gene regulatory network

GSK3β glycogen synthase kinase 3 beta

GTP guanosine triphosphate

H Hamming distance

HD normalised Hamming distance

HIF1 hypoxia inducible factor 1

HSC Hematopoietic stem cell

hub higly connected component

IGF insulin-like growth factor

IGFR insulin-like growth factor receptor

IKBKB inhibitor of nuclear factor-kappa B kinase subunit beta

IL17 interleukin 17

IQGAP1 IQ motif-containing GTPase-activating protein 1

IRAK4 interleukin-1 receptor-associated Kinase 4

IRS insulin receptor substrate

JNK c-Jun-N-terminal kinase

k degree

KEGG Kyoto Encyclopedia of Genes and Genomes

LAT linker for activation of T-Cells

LKB1 liver kinase B1

LYN LYN Proto-Oncogene

LT-HSC Long-term hematopoietic stem cell

MALT1 mucosa-associated lymphoid tissue lymphoma translocation protein 1

MAPK mitogen-activated protein kinase

MCL1 induced myeloid leukemia cell differentiation protein

MDM2 mouse double minute 2

MEF myeloid elf-1-like factor

MEK mitogen-activated kinase kinase

MEKK1 mitogen-activated kinase kinase kinase 1

MEN1 Menin 1

MI mutual information

mRNA messenger RNA

mTOR mammalian target of rapamycin

mTORC1 mammalian target of rapamycin complex 1

mTORC2 mammalian target of rapamycin complex 2

MYC Myc proto-oncogene

n number of nodes in a network

NEK2 NIMA related kinase 2

NF-κB nuclear factor kappa-light-chain-enhancer of activated B-cells

NFKBIA NFKB Inhibitor Alpha

NM negative mismatch

NP complexity class nondeterministic polynomial time

NS non-selected

NSC neural stem cell

$\mathcal{O}$ big O notation for time complexity

ODE ordinary differential equation

P complexity class polynomial time

p16 cyclin-dependent kinase inhibitor 2A

p18 cyclin-dependent kinase inhibitor 2C

p19 p19Arf, cyclin-dependent kinase inhibitor 2A

p21 cyclin-dependent kinase inhibitor 1A

p27 cyclin-dependent kinase inhibitor 1B

p57 cyclin-dependent kinase inhibitor 1C

PAK4 p21-activated kinase 4

PNEC pancreatic neuroendocrine carcinoma

PNET pancreatic neuroendocrine tumour

PDAC pancreatic ductal adenocarcinoma

PDK1 pyruvate dehydrogenase kinase 1

PIDD1 P53-Induced Death Domain Protein 1

PI3K phosphoinositide 3-kinase

PIP2 phosphatidylinositol 4,5-bisphosphate

PIP3 phosphatidylinositol-3,4,5-triphosphate

PM positive mismatch

PP2A protein phosphatase 2A

PPI protein protein interaction graph

PUMA p53 upregulated modulator of apoptosis

PTEN phosphatase and tensin homolog

RAC1 Ras-related C3 botulinum toxin substrate 1

RAF1 rapidly accelerated fibrosarcoma

RAS rat sarcoma

RASSF1A Ras association domain family 1 isoform A

RB retinoblastom

RHEB GTP-binding protein Ras homolog enriched in brain

ROC receiver operating characteristic

ROS Reactive oxygen species

rk ranking

RNA ribonucleic acid

RSK 90-kDa ribosomal S6 kinase

S6K ribosomal protein S6 kinase

SAT satisfiability problem for classical propositional logic

SCF stem cell factor

SDE stochastic differential equation

SETD7 SET domain-containing 7 histone lysine methyltransferase

SKP2 S-phase kinase associated protein 2

SP1 SP1 transcription factor

SLUG1 snail family transcriptional repressor 2

ST-HSC Short-term hematopoietic stem cell

STAT3 signal transducer and activator of transcription 3

SVM support vector machine

t point in time

TGFβ Transforming growth factor beta

TJ Tight Junction

TNFRSF13C TNF receptor superfamily member 13C

TNFSF13B TNF superfamily member 13B

TNFSF14 TNF superfamily member 14

TNoM Threshold Number of Misclassification

TP53 tumour protein 53

TPO thrombopoietin

TRAF5 TNF receptor associated factor 5

TSC1/2 tuberous sclerosis complex 1/2

TWIST1 twist-related protein 1

PU.1 Spi1 proto-oncogene

scRNA-seq single-cell RNA sequencing

UCHL1 ubiquitin carboxyl-terminal hydrolase isozyme L1

VB Vertex betweeness

VEGF vascular endothelial growth factor

VEGF vascular endothelial growth factor receptor

VHL Von Hippel-Lindau

WHO World Health Organisation

x Boolean variable of gene

$x(t)$ state at time t

$x'(t)$ perturbed state at point in time t

1

INTRODUCTION

This work focuses on unravelling new mechanisms in cellular pathways to understand complex phenotypical landscapes.The principles behind gene regulation and mathematical modelling approaches are briefly described. In this context, Boolean network models will be introduced. Afterwards, the described approaches will be applied to model the maintenance and ageing process of hematopoietic stem cells (HSCs) and the development and therapeutic targeting of pancreatic neuroendocrine tumours (pNETs). An overview on the content is summarised in Figure 1.

1.1 Systems biology: holistic view to summarise complex phenotypical landscapes

Understanding and controlling the complex mechanisms governing biological phenotypes has always been the final goal of past and modern biology. No matter how complex the outcome of a biological process is, it mostly comes down to the interactions between deoxyribonucleic acid (DNA), ribonucleic acid (RNA), and proteins [106]. Information on any functional activity is encoded by the DNA in form of genes (exception is made for RNA viruses). When the information encoded by a certain gene is required, the latter is transcribed into messenger RNA (mRNA), which is then translated into proteins [106, 253]. Following this ground principle, each regulatory module in a cell accomplishes different functions and can interact with others to form a complex gene regulatory network (GRN) [253]. To unravel the mechanisms governing these complex regulatory networks, molecular biology approaches have been focused on investigating single interactions by collecting different experimental results at each of the described regulatory levels (e.g. DNA sequences, protein-protein interaction data, or gene expression profiles) [314, 253].

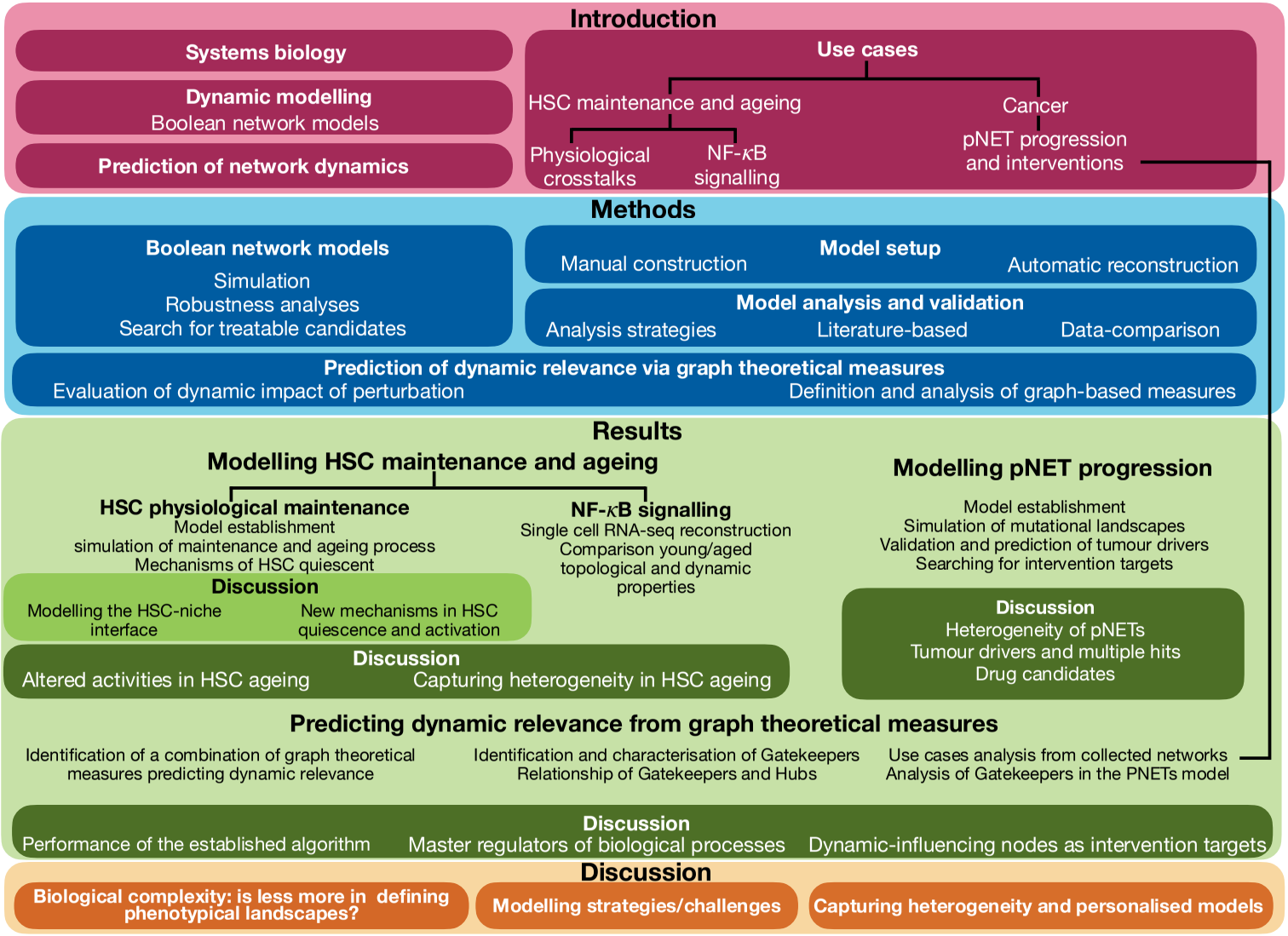


Figure 1: **Overview of this dissertation.**

These results allow a detailed glance at a given regulatory dependency included in the investigated process. Nevertheless, the knowledge on single interactions is often not enough to understand the overall resulting phenotypical landscape generated by the dynamic behaviour of the underlying regulatory network [314, 694, 701]. Consequently, complex biological behaviours such as disease development are often the result of an overall dysregulation of the pathways involved in the GRN [111, 694]. Systems biology proposes a holistic view of the understanding of biological behaviours by considering the system in its entirety. A substantial section of systems biology investigations shifts the attention from the single interactions to the collection and summarisation of all involved regulations to create a global mathematical model [701]. Such models aim to capture the complexity of phenotypical landscapes and formulate hypotheses on their regulations [314]. The knowledge gained from systems biology approaches can be synergised to experimental efforts to guide and suggest testable hypotheses [253, 365](Figure 2).

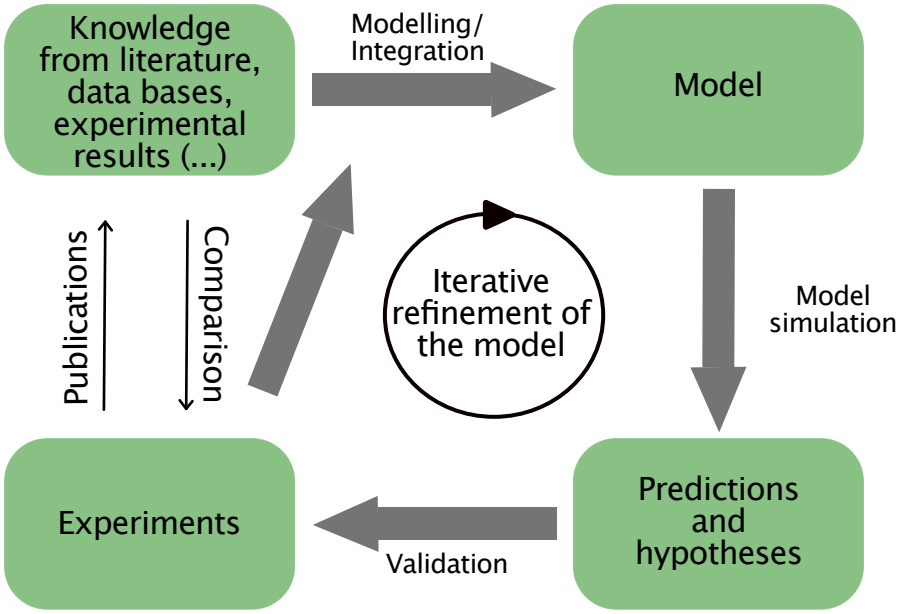


Figure 2: **Systems biology as an holistic, iterative approach.** Systems biology is an interdisciplinary field that investigates biological, clinical, chemical, physical, and computational research. It proposes a holistic perspective to regulatory processes by proposing an integration of existing knowledge to generate mathematical models [165, 64]. These can be simulated to predict phenotypical behaviours which can in turn be validated by targeted laboratory experiments. Results from the experimental efforts can then be integrated iteratively to refine the model.

1.2 Dynamic modelling

Mathematical models applied in systems biology can be either static or dynamic. Static models, such as clustering techniques, search for similarities among genes expression profiles. This results in the ability of grouping sets of genes based on similar expression profiles which can be also cohesive in biological functionality [315, 538]. However, these modelling approaches often can not capture temporal changes in the system which are instead a fundamental characteristics of dynamic models [538]. Understanding the changes of the systems over time comes with the advantage of understanding their dynamics. Biological networks describe dependencies among their components via regulatory interactions that can influence the final level of gene expression or protein activity of a certain compound [550]. As a result, the network describing a certain process consists of a set of regulatory interactions (edges) connecting different proteins or genes (nodes). Graphically, this set of interactions is depicted in an interaction graph [550]. Nevertheless, these types of representations are not *per se* informative regarding the dynamic behaviour of the system, which is only possible by considering time as a variable [56]. Hence, a variety of dynamic modelling approaches have been proposed to describe the dynamic behaviour of GRNs. Mainly, these approaches differ in terms of complexity and abstraction leading to the division in qualitative (e.g. discrete) and quantitative (e.g. continous) models (Figure 3). Modelling approaches that allow a precise quantification in terms of compound concentrations, ordinary differential equation (ODE) or stochastic differential equation (SDE) models, are usually restricted to smaller processes due to the limited amount of available kinetic parameters [542, 550]. Vice versa, qualitative modelling approaches that do not require the initial knowledge of these parameters are more suitable for the dynamic description of larger systems. Examples of these types of modelling approaches are Boolean network models [297], or Fuzzy logic models [196, 197]. The choice of the most suitable modelling approach depends mostly on the underlying biological question and the availability of information. Additionally the type of modelling approach will also affect the simulation complexity and potentially further limit the size of simulated models [442]. On these grounds, discrete modelling approaches are particularly applicable when studying large interaction networks involving multiple cascades and their crosstalks (Figure 3).

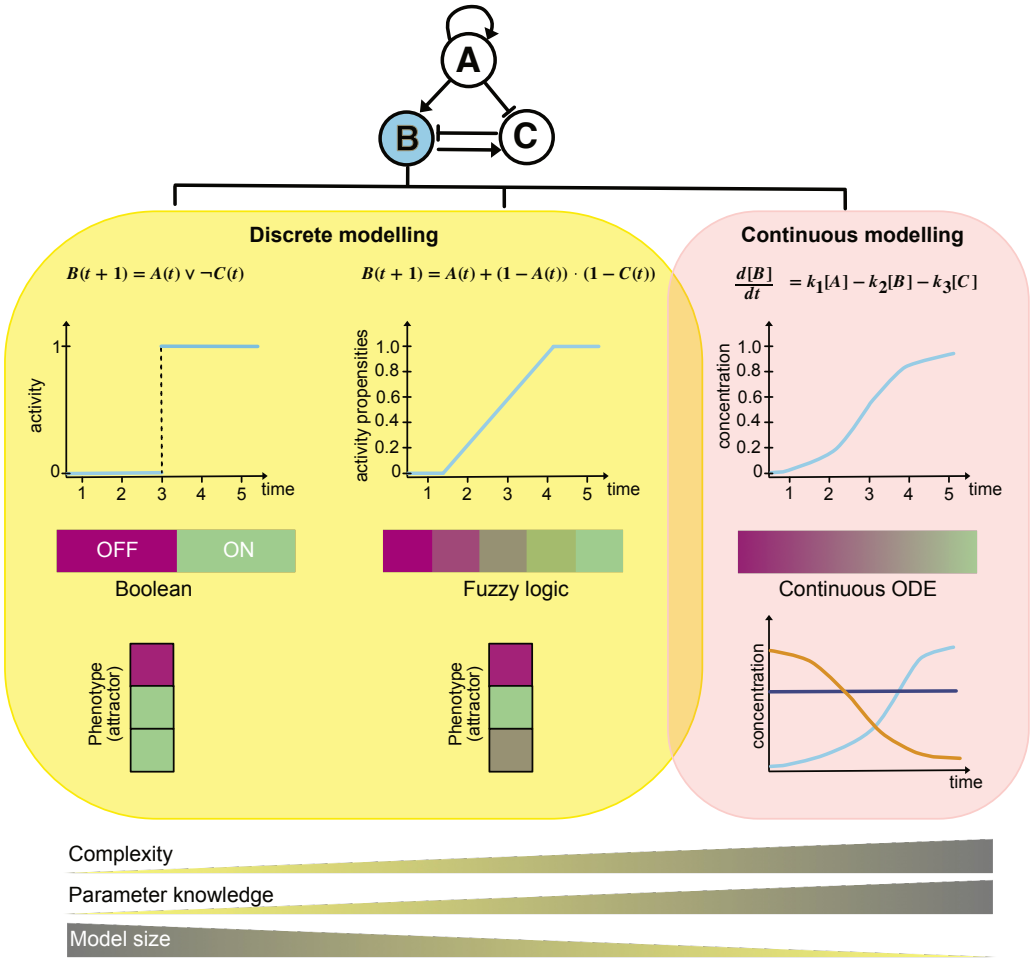


Figure 3: **The complexity of dynamic models.** Depending on the biological question, network size, and available kinetic details (lower level bars), different modelling approaches are available. Discrete models such as Boolean networks can either describe activation by the "ON/OFF" switch or by applying other notions, such as fuzzy logic. Both rely on attractors for the phenotype description (left yellow box). Continuous modelling can be feasible in the case of rather small networks, where enough parameter knowledge is present. Here, interactions can be described as differential equations, depending on concentrations and time as continuous variables. Phenotype description is depicted by the concentration of components through time (right pink box). Adapted by permission from Springer Nature Customer Service Centre GmbH: Springer Nature, Methods in Molecular Biology [255], Copyright © 2022, Springer Science Business+Media, LCC (2022).

1.2.1 *Boolean network models*

Boolean network models are one of the simplest dynamic models [11]. Despite their simplicity, they can describe complex biological behaviours ranging from physiology [236, 254], to ageing [598], to cancer [113, 428, 692].
Boolean networks contain a set of n variables $X = \{x_1, x_2, ..., x_n\}, x_i \in \mathbb{B}\{0, 1\}$. Regulatory dependencies among variables are described by means of logical operators AND (&; $\wedge$), OR (|; $\vee$) and NOT (!; $\neg$), and are summarised in a set of Boolean functions $F = \{f_1, f_2, ..., f_n\}, f_i : \mathbb{B}^n \rightarrow \mathbb{B}$ [297] (Figure 4A).

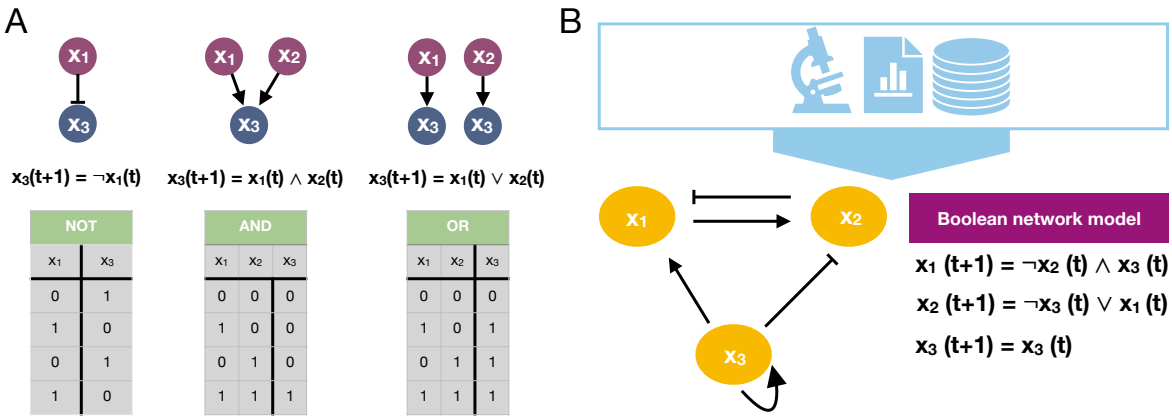


Figure 4: **Boolean logical operators and network construction.** Logical operators AND ($\wedge$), OR ($\vee$), and NOT ($\neg$) are used to construct Boolean functions (A). All possible results of a Boolean function based on logical connectivities can be summarised and depicted in truth tables. Boolean network models can be generated by both literature statements or driven from expression data (B). The interaction graph (left) depicts regulatory interactions between compounds present in the network but is not sufficient to describe dynamic behaviour over time. Here, arrows indicate activatory interactions, and bar headed lines indicate inhibitory interactions. To do so, Boolean models are composed of a set of Boolean functions (here on the right) describing the relationships among their nodes. A toy model is depicted to show an interaction graph and the representation of the Boolean network model.

These functions integrate information on regulatory interactions from a variety of possible sources. Particularly, there are two major approaches in constructing Boolean network models: either by manual reconstruction via extensive literature search, or by automatic network reconstruction strategies starting from gene expression data [244] (Figure 4B). Each compound x_i in the network is regulated by its own Boolean function f_i which defines whether x_i is present/active/1 or absent/inactive/0 [297]. Thus, the state of a given Boolean network at a specific discrete point in time t is defined by a vector $\vec{x}(t) = (x_1(t), ..., x_n(t))$ including

the activities of all compounds x_i within the network at this particular point in time (Figure 4B). Given that each compound x_i has two possible activity states, the total state space corresponds to 2^n states [297]. The dynamic behaviour over time can be simulated by updating Boolean functions to generate transitions from one state to the successor one $\vec{x}(t) \mapsto \vec{x}(t+1)$ [297]. Depending on the updating strategy, Boolean network models can be divided into synchronous [297, 298], asynchronous [225] and probabilistic Boolean networks [592] (Figure 5).

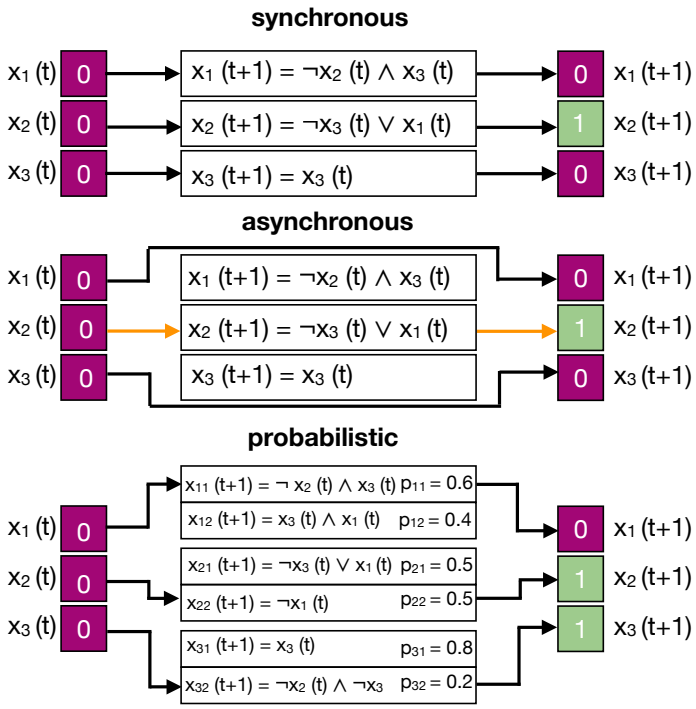


Figure 5: **Update schemes of Boolean network models.** In synchronous Boolean network models, all Boolean functions are updated at each time step. In asynchronous Boolean network models, one randomly chosen function (marked in orange) is updated at each time step. Probabilistic updates schemes allow for multiple Boolean functions per node, each having a certain probability p of being applied at each state transition. At each transition, one of the possible functions is selected per variable x_i and is updated. The activity of the nodes x_i at the point in time t is listed on the left in coloured squares. The arrows represent the updating of the model from time t to its successor state at time t+1. Boolean functions are depicted inside the rectangles. In the figure, dark purple refers to inactive nodes, while green refers to active nodes. This figure has been modified from Schwab, Kühlwein, Ikonomi et al. [572], licensed under CC BY 4.0, https://creativecommons.org/licenses/by/4.0/.

In synchronous Boolean network models, all Boolean functions are updated simultaneously at each step in time t [297, 298]. In asynchronous Boolean network models, one function is randomly chosen and updated at each point in time [225]. In contrast to synchronous and asynchronous Boolean network models, in probabilistic Boolean network models, each node can be associated with multiple Boolean functions, each one with a different probability of occurring p [592]. Here, the state transition is achieved by choosing one of the possible functions accordingly to their likelihood of occurrence and then synchronously updating the state of the model for all nodes (Figure 5) [8, 573].
The dynamics of a network can be displayed in a state transition graph (Figure 6). Here, in contrast to interaction graphs, nodes represent the state of the network at a certain point in time, while edges show the transition from one state to its successor [8, 709]. Notably, in the state transition graph of synchronous Boolean network models each state of the network has only one unique possible successor state. In contrast, in asynchronous and probabilistic Boolean network models a state may have multiple successor states (Figure 6) [543].
Under a synchronous update scheme, due to their finite number of states (in total 2^n), Boolean network models eventually converge on recurring sequences of states called attractors. Depending on the sequence of recurrent states, there are single state (fixed points) and multiple state (cyclic) attractors [244, 297] (Figure 6). Of note, probabilistic models might also not end in any attractor [572, 244, 543]. All states leading to a certain attractor define its so-called basin of attraction [543]. The larger this basin of attraction is, the higher is the probability for an attractor to be relevant [709]. Again, attractors of synchronous models have disjoint basins of attraction while in asynchronous models or probabilistic models these basins of attraction may overlap [543] (Figure 6).

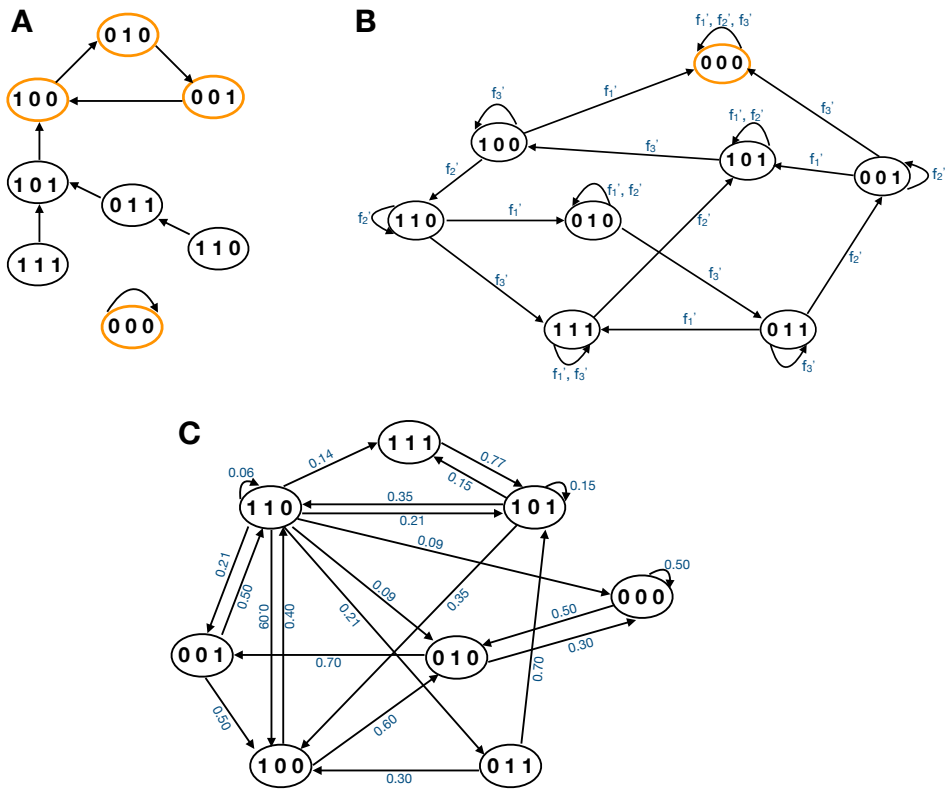


Figure 6: **State transition graphs.** Dynamics of Boolean network models can be displayed as a state transition graph. A state in a synchronous Boolean network (A) has only one unique successor state while a state in an asynchronous Boolean network model (B) or probabilistic Boolean network model (C) can have multiple successor states. The updated Boolean function (either f_1' or f_2' or f_3') for each state transition of the asynchronous model are depicted above the corresponding edges. For the probabilistic state graph (C) the p-values showing the probability for the corresponding transition are depicted. Attractors (in orange) represent the long-term behaviour of the network. All states leading into the same attractor represent its basin of attraction. This figure has been modified from Schwab, Kühlwein, Ikonomi et al. [572], licensed under CC BY 4.0, https://creativecommons.org/licenses/by/4.0/.

From an interpretative perspective, attractors describe the long-term behaviour of the model and are associated with biological phenotypes [249, 248]. This is crucial for the iterative modelling process, allowing attractors to be validated and compared to experimental results, finally allowing the refinement of the network [255, 314, 315].

1.3 Investigation and prediction possibilities of network dynamics

The simulation of dynamics of Boolean models can predict dynamic behaviours. Generally, dynamic simulations can be performed on either the entire state space of the investigated model (exhaustive simulations) [113, 236], or on a subset of initial states corresponding to known conformations of the modelled biological system [254]. As a result, in the first case, the investigator will have access to the entire set of attractors retrievable from the system, while, in the second, the limited amount of starting states might lead to only a subset of them. When analysing the dynamics of a model for the first time, or in case of missing information on relevant starting states, it is common and advisable to attempt to explore the entire state space of the model [254, 255]. This will provide an overview on all attractors, and corresponding phenotypes, retrievable from the model, and, through their basin of attraction, on their representativeness within the state space [254, 692]. However, given the exponential growth of the state space, it eventually becomes unfeasible to exhaustively simulate Boolean network models with a high number of nodes ($n \geqslant 30$) in a reasonable amount of time [244]. To circumvent this issue, efficient approximation algorithms have been developed, such as the so-called satisfiability problem (SAT)-solver which have been applied to the exhaustive simulation of Boolean models [8, 103]. However, while the SAT-solver will exhaustively retrieve the complete set of attractors of a system, this will not retrieve also their basins. Hence, to evaluate basins of attractions of large networks, it will be required to sample subparts of the state graph as starting states of the system [572].
This computational limitation becomes even more accentuated when studying perturbations of the systems. Besides assessing the biological representativeness of an established network model, perturbation studies can also be used to search for promising intervention targets or to investigate disease drivers [254, 428] (Figure 7). This can be achieved by fixing the state of a node to either "1" or "0" during the simulation. This *in silico* perturbation relates to over expression or knockout experiments performed in laboratory setups [255, 541].

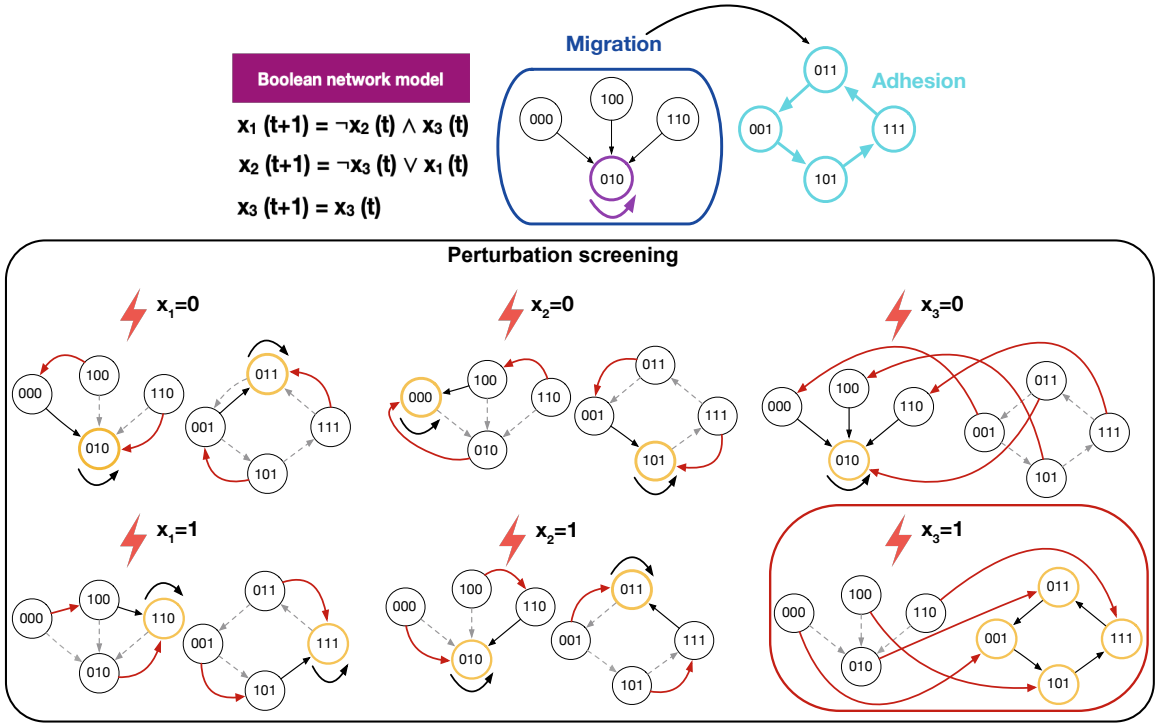


Figure 7: **Screening for intervention targets.** Systematic intervention screening can support the identification of intervention targets. In the figure, an intervention screening of a toy model of three nodes is presented. In the example, the two attractors of the model depict an invasive phenotype (migration) and an adherent one (adhesion). By performing the screening it appears that fixing the node x_3 to one leads to the disappearance of the invasive attractor leaving only the adherent one. Of interest, some perturbations might lock the system into the invasive phenotype, while others might lead to new attractors.

Hence, perturbations of Boolean models are a crucial part of the network dynamics investigation. Furthermore, a screening to test all possible single or multiple intervention targets is of interest in the perspective of identifying new interventions (Figure 7). Due to exponential growth of dynamic complexity with network size [572, 688], combined with the concomitant increase of combinations to test in multiple targeting, the possibility of complete dynamic investigations becomes even more limited [572] (Figure 8). However, to limit the amount of simulations to be performed, some approaches have been developed to perform targeted screening based on desired final behaviours of certain components of the model [571].

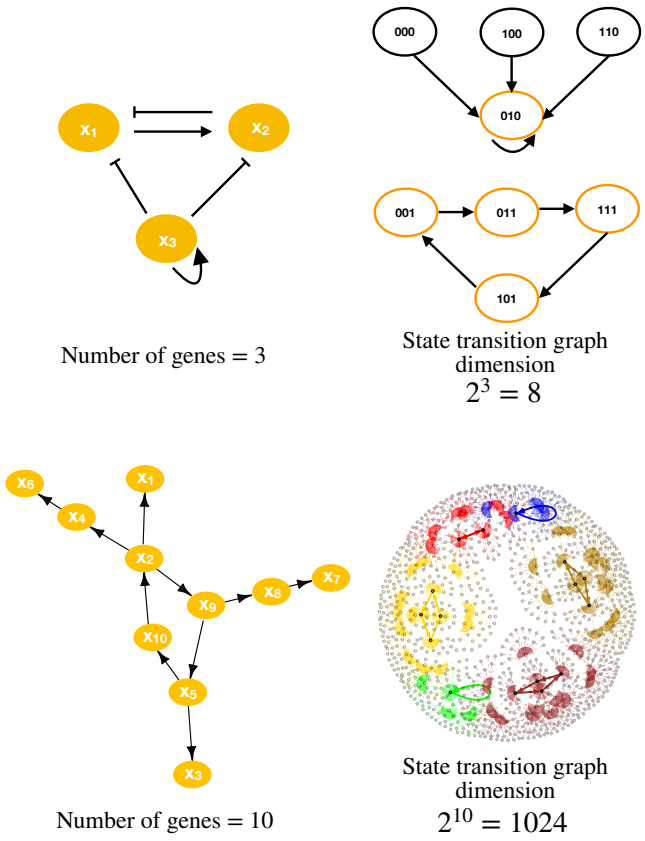


Figure 8: **Complexity growth in interaction and state transition graphs.** Complexity of of state transition and interaction graphs scales differently in relation to network size (n). Two toy models with respectively three (A) and and ten (B) nodes are depicted. As shown, while interaction graphs grow linearly with network size (left side A and B), state transition graphs grow exponentially, in the order of 2^n (right side, A and B). This exponential increase of state spaces limits the feasibility of exhaustive network simulations.

Nevertheless, the issue of predicting dynamic effects without certain knowledge of the investigated system (e.g. expected activities, or known targets) is still open. From this perspective, the study of network theory and topologies might enlighten the problem. In biologically motivated networks, different studies have pointed out that only a limited amount of nodes are responsible for the dynamic behaviour of the system [271]. Nevertheless, identifying these dynamic drivers is not an obvious task. Unlike the state graph, the interaction graph does not scale exponentially with network size (Figure 8). This brings attention to the possibility of using interaction graph-based measures as predictors of dynamic influencing nodes [572, 407, 763] (Figure 9). This idea is sustained by already existing results

linking interaction graph-based measures to dynamic activities [43, 271, 763].

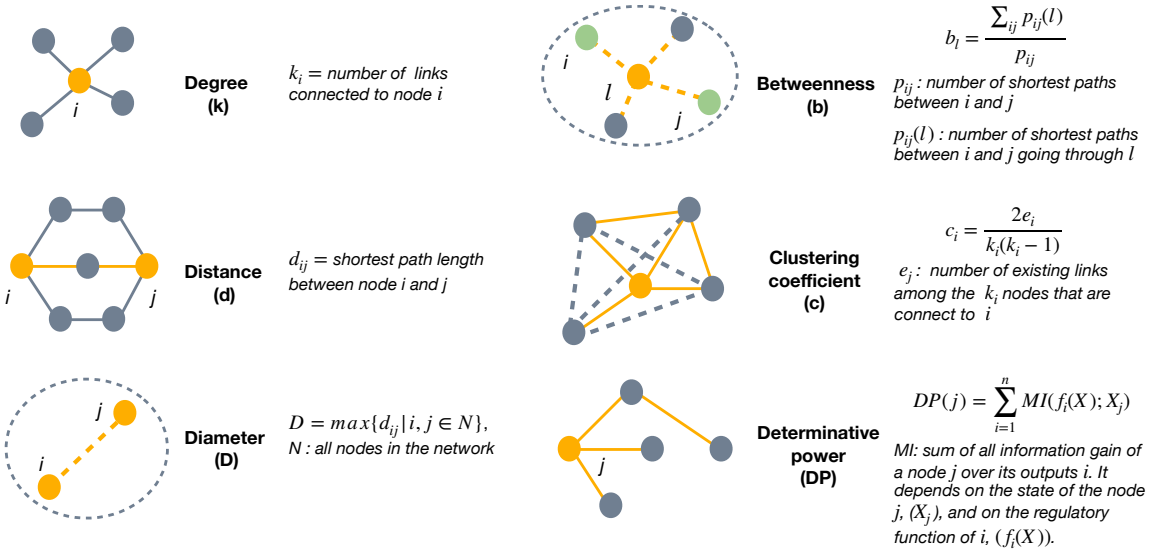


Figure 9: **Overview of common interaction graph-based measures.** The figure depicts a set of commonly applied interaction graph-based measures in network theory [164, 231, 407, 763]. Definitions are illustrated both in graphs and formulae. For each topological measure, the corresponding formal mathematical definition is depicted on the right of each graph. From top to bottom and from left to right, degree (k) measures the number of connections one node has. Distance (d) is the length of the shortest path existing between two nodes. Diameter (D) is the maximum distance between any two nodes in a given network. Betweenness (b) is the fraction of those shortest paths between all pairs of vertices that pass through one vertex of the network. The clustering coefficient measures the percentage of existing links among the neighbourhood of a given node. Determinative power (DP) represents a sum of all "information gains" obtained over the outputs of a node given knowledge of this node state. Relevant nodes and links for each measure are depicted in orange.

Biological networks are considered to be scale-free based on topological studies of protein-protein interaction networks (PPI) [30, 304]. In directed networks, each component has several in- and out-going edges which can be summarised as an in-degree and an out-degree [13, 30]. The majority of components in scale-free networks have few connections and only a small number of components is highly connected, called hubs [30] . Hub nodes have been firstly identified as master dynamic influencing nodes since their removal was related to lethal phenotypes [43, 271]. In addition to hubs, other interaction graph-based measures have been suggested in network theory (Figure 9), but their potential implication in predicting dynamic behaviours is still to be unravelled [164, 231, 407, 763]. Network motifs are considered

regulatory building blocks of networks, determining recurrent structural patterns in the interaction graph [17, 431] (Figure 10).

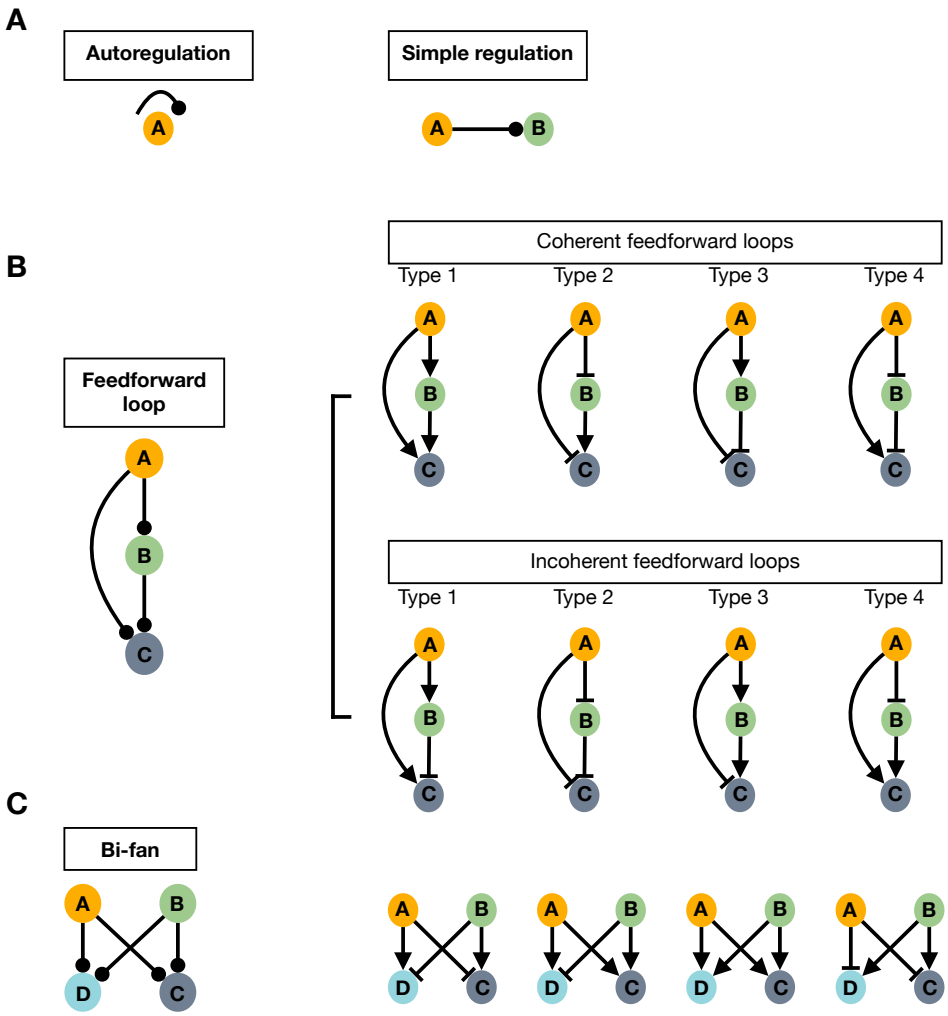


Figure 10: **Overview of common network motifs.** (A) Simple regulation and autoregulation can serve as a reference for understanding the dynamic functions of network motifs. (B) Feedforward loops are commonly three-node motifs found in biological networks (left). In this motif, the product of gene A regulates both genes B and C, while B also regulates gene C. They are divided into coherent (right upper part) and incoherent ones (right lower part). (B) the bi-fan motifs are four node motif commonly found in biological regulatory networks, in which the products of nodes A and B regulate both genes C and D. Commonly found types of bi-fan are depicted (right). Arrows indicated activation dependencies, bar-headed lines represent inhibition, while round-ended lines represent both types of regulation (inhibition or activation).

In fact, feedback (such as positive and negative autoregulations) or simple positive or negative regulations are interaction structures that can be found frequently in biological networks [17, 550]. These simple structures involve only one or two nodes, and have been associated with certain dynamic response patterns. For instance, while negative autoregulation can speed up responses and reduce fluctuations, positive autoregulation slow-down responses and increases variations [17, 550]. Moving to more complex motifs, short feed-forward loops have also been shown to impact the stability of PPI [10]. Together with the latter, also bi-fan motives have been recurrently found in PPIs [256] (Figure 10). Nevertheless, more complex network motifs (involving more than two nodes) might not be the most suitable predictors of dynamic behaviours, since it was shown that from the same motif multiple dynamic behaviours can be retrieved [256].

1.4 Background on the biological use cases

In the presented work, Boolean network modelling approaches were applied to two major biological contexts, namely physiological ageing and cancer. For what concerns ageing, two approaches the studying of the physiological maintenance of HSCs and their ageing process via the kappa-light-chain-enhancer of activated B-cell (NF-κB) signalling were applied. Instead, molecular pathways involved in tumourigenesis and progression were studied in the context of pNETs. In the following subsections, both topics will be introduced.

1.4.1 *Ageing*

Ageing is a physiological process, which starts directly after the end of the development program of an organism and proceeds until the end of its lifespan [222, 228]. This process results in the accumulation of diverse deleterious changes in the cells and tissues that increase the risk of disease and death [222, 223, 228]. Ageing increases the vulnerability to certain diseases, such as cancer, chronic lung disease, heart pathologies, and diabetes, together with the decrease in physiological functions and fertility [228, 560, 644, 650]. However, there are certain organisms reported to be less affected by ageing. Hydra, a small freshwater cnidarian polyp, shows regenerative abilities after loss or damage of any part of its body independently of the age [644]. Likewise, the fertility of naked mole-rats seems to be unchanged until old age [57]. Based on the sum of the above-mentioned deleterious events, the physiologic age of an individual can be calculated. The latter can be in contrast to the "true age" or "chronological age", which simply refers to the age of the organism [223]. The average lifespan expectancy of humans has dramatically increased over time, with an exponential increase in the last century, pushing the average

up to 80 years in 1980 [650, 459]. This increase is mainly imputable to extrinsic causes (or stochastics), such as the reduction of accidents, increased socioeconomic and nutritional status, improved sanitation, and reduction of death by infectious diseases [650]. Of notice, the longest-lived human died at the age of 122 years old [137, 522]. Besides extrinsic causes, intrinsic ones that are related to genetic and post-developmental mechanisms of the organism are still a major limitation in the understanding of the ageing process [650]. Among these, common characteristics of ageing have been identified in mammals. In general, ageing is related to a progressive decrease in physiological capacity: exemplarily, a decrease in glomerular filtration rate and maximal heart rate decrease linearly after the age of 30 in humans [593]. In addition, a decrease in the ability to respond adaptively to environmental stimuli is also registered [3, 650]. This correlates to a general inability to maintain homeostasis [3, 650]. At the tissue level, this translates into tissue-specific changes in the biochemical composition, such as age-related alteration in oxigen radical levels, and increased DNA damage at the cellular level [40, 378, 488, 576, 650]. Given this altered homeostatic behaviour, intense attention has been put in long-lived cells responsible for supplying tissue renewal after development, namely somatic stem cells [505, 506, 657]. Hence, the mechanistic understanding of the homeostatic processes regulating somatic stem cell activation is pivotal in the study of ageing [505, 506, 657].

1.4.1.1 *Physiological maintenance of HSCs*

Adult stem cells are a rare population of cells entitled to the regenerative potential of cells belonging to a certain tissue in the adult organism. In contrast to germline stem cells of invertebrates which are constantly cycling [610], mammalian adult stem cells are predominantly in a quiescent, non-dividing Gap zero (Go) state [40, 512]. HSCs are among the best-studied adult stem cells population, and their quiescence has been linked to their long-term regeneration capacity of the blood system [358, 89]. HSCs are normally found in a quiescent condition, which can be exited by entering the cell cycle for two crucial tasks, namely self-renewal or differentiation [147, 512]. The first is required to maintain a stable pool of HSCs, while the second is responsible for generating differentiated blood cells [90, 358]. To accomplish the maintenance of HSCs a set of intrinsic and extrinsic factors are required [700]. Different studies have pointed out the relevance of intrinsic regulators such as tumour protein p53 (TP53), forkhead box (FOXO), Ataxia-telangiectasia mutated (ATM), and the mechanistic target of rapamycin (mTOR) pathway [89, 358, 355]. In addition, this intrinsic network is maintained and stimulated by the surrounding specialised environment of the HSCs in the bone marrow, named the "stem cell niche" [614, 700]. The interplay between intrinsic and extrinsic regulation of HSCs holds the key to their homeostatic maintenance and is far from being mechanisti-

cally understood [700]. Even more importantly, alterations in the balance between activation and quiescence of HSCs can determine the insurgence of diseases such as leukaemia, or result in age-related phenotypes [27, 338, 682].

1.4.1.2 *Ageing of the HSCs and the NF-κB pathway*

The altered activity of HSCs in ageing has been linked to an impaired immune response [27, 338, 682]. Here, increased production of myeloid cells over lymphoid ones is associated with a diminished immune competence in the elderlies and, likely, with an increased chance of developing acute myeloid leukaemia (AML) [338, 533]. This shift towards the myeloid cell type differentiation also impairs long-term self-renewal ability [338, 533]. Besides, ageing of HSCs is considered a heterogenous process differently affecting single HSCs from the same population [122, 362]. Likely, this might reflect the variegated activity levels observed within populations of quiescent HSC [63, 696]. The molecular mechanisms of HSCs ageing are primarily described in phenotypic terminology, with several identified molecular hallmarks [122, 362]. These are metabolic activation, reactive oxygen species (ROS) production, impaired autophagy, loss of polarity, cellular senescence, telomere extension, and increased DNA damage [122, 362]. Altogether, these impaired activities relate to the increased presence of inflammatory signals, and therefore on the role of their downstream pathways, such as the nuclear factor kappa light chain enhancer (NF-κB) signalling pathway [122]. The activation of the NF-κB has been implicated in the differentiation process of HSCs during ageing [229, 495]. Here, extended inflammatory signalling causes the massive activation of NF-κB pathway, priming differentiating cells to the myeloid lineage via the transcription factor encoded by the Spi1 proto-oncogene (PU.1)[229, 495]. Nevertheless, the main players and mechanisms regulating the ageing of HSCs and the related NFκB pathway are still not well characterised [122, 229].

1.4.2 *Cancer*

Cancer is classified as the leading cause of death of the 21st century [50]. More than 100 different cancers and subtypes of cancers are known [218, 219], with each subtype associated to specific organs [218, 219]. Worldwide, an estimated number of 19.3 million new cancer cases and almost 10 million cancer deaths occurred only in 2020, with a predicted cancer burden increase of 47% by 2040 [597, 626]. The development of cancers follows a multistep process, where different steps reflect genetic alterations that drive a progressive transformation of human cells into a highly malignant derivate [218, 219]. Cancer driving mutations can both be inherited or sporadically appear during the lifespan of an individual [218, 219]. Besides

the vast heterogeneity of tumour entities, a set of common hallmarks of cancer have been postulated already at the beginning of the century: self-sufficiency in growth signals, evasion of programmed cell death (apoptosis), limitless replicative potential, sustained angiogenesis, and tissue invasion and metastasis [217, 218, 219]. With the advance of cancer research, new hallmarks have been postulated: avoiding immune destruction, deregulation of cellular energetics, genome instability and mutation ability, and tumour-promoting inflammation [217, 218, 219].

1.4.2.1 *Pancreatic neuroendocrine neoplasms*

pNETs are the second most common epithelial neoplasms in the pancreas [445, 719, 726]. pNETs account for around 2% of all pancreatic neoplasms, however their incidence has doubled over the past 30 years [445, 719, 726]. In 2017, the World Health Organization (WHO) classified human pNETs into two groups: well-differentiated and poorly differentiated ones, also called pancreatic neuroendocrine carcinomas (pNECs) [719]. pNETs are further sub-classified into grades (G), ranging from 1 to 3 based on their proliferative activity assessed by the proliferation marker protein Ki-67 (Ki-67) labelling index and mitotic rate [31, 719]. In addition, further classification can be made based on hormonal secretion into functional and non-functional tumours [31, 719]. Previous research efforts have revealed extensive alterations in a set of genes involved in the tumoural process: menin 1 (MEN1), death-domain associated protein (DAXX)/ATRX chromatin remodeler (ATRX) , and genes in the mTOR pathway (e.g. tuberous sclerosis protein (TSC)) [277, 559, 666]. While hyperactivation of the mTOR pathway is a common hallmark of pNETs, MEN1 mutations are the most common drivers of tumour formation and are associated with a generally worse prognosis [169, 719]. Nevertheless, the underlying molecular mechanisms of pNET formation and grade progression are widely unexplored [31, 719].

1.5 Aims of the thesis

This thesis aims to investigate new relationships between molecular regulatory pathways that play a role in the context of ageing and cancer from a systems biology perspective. Different strategies to establish and analyse Boolean network models will be designed, used, and compared. Based on these, three major areas will be investigated. Two will regard the application of Boolean models to unravel mechanisms and new markers of HSC ageing and pNETs progression. The third, instead, will focus on the investigation of network theory aspects to design a strategy to efficiently individuate dynamic influencing nodes in Boolean models.

For the HSC ageing section the following points will be investigated:

- Is it possible to understand and reconcile the regulatory crosstalk and mechanisms behind the maintenance of HSCs?
- How does this maintenance get altered during ageing? And, how does the niche influence the ageing of HSCs?
- Is it possible to capture the heterogeneity of HSCs activities by directly reconstructing personalised models of human HSC populations?
- Are there potential markers that distinguish the heterogeneity of the HSC ageing in different individuals?

For the oncology section focusing on pNETs the following points will be investigated:

- Given the sparse knowledge on pNETs molecular mechanisms, is it possible to better characterise pathways leading to the phenotypes generated by different mutations?
- Is it possible to individuate new tumour drivers for pNETs?
- Is it possible to individuate new drug targets for pNETs?

In addition, topological properties of biologically motivated regulatory networks will be explored to determine genes responsible of shifting the phenotypic landscape of dynamic models. In particular, the following points will be addressed:

- Is it possible to individuate interaction graph based properties able to capture dymanic relevance of biologically motivated models?

- Do nodes selected by these topological properties have particular or new properties?
- Do these nodes also have biological relevance, and therefore be considered as candidates for drug targets and disease drivers?

1.6 Synopsis of the thesis

This work approaches the study of complex phenotypes in ageing and cancer via Boolean network models. On the one hand, both literature curated and automatic reconstruction strategies were developed and employed, focusing on single-cell expression-based reconstructions of personalised ensembles of models. On the other hand, both dynamic and interaction-graph-based approaches were designed to analyse Boolean network models. Additionally, a study using foreign features for classification based on patients' cohorts' expression profiles was integrated into the analysis of attractor patterns. Overall, these strategies were applied to identify disease drivers, intervention targets, and disease and ageing progression regulatory mechanisms.

2

METHODS

This thesis deals with the modelling of regulatory networks applying Boolean networks models. For this reason, the materials and methods section includes a brief mathematical description of Boolean network models and explains simulation strategies applied in the present work. Subsequently, the establishment process of the Boolean models developed in this thesis is discussed. First, the development of manually constructed models is described. This includes the model on HSC maintenance in the bone marrow niche environment and the one dealing with pNET tumour progression and interventions. In addition to manually constructed models, automatic reconstruction of model ensembles of age-dependent alterations within the NF-κB pathway based on single-cell RNA-sequencing (scRNA-seq) data have been obtained. For the reconstruction of these models from time series of single-cell gene expression data, a binarisation of the data is required first, which will be discussed together with a newly tailored model reconstruction strategy. Subsequently, data-based analyses used in this work will be discussed to support the model-generated hypotheses on therapeutic targets and mechanistic regulations. The methods section ends with the implementation of a method for the inference of interaction graph-based measures able to select for nodes responsible of influencing the network dynamics.

2.1 Boolean network models

Boolean network models are characterised by a set $X = \{x_1, ..., x_n\}$ of variables $x_i, i \in \{1, ..., n\}$ that represent n genes or proteins [8, 297]. Each variable x_i can have an either positive (active) or negative (inactive) value, $x_i \in \{0, 1\}$ [297] possible states. Regulatory interactions within the model are summarised in a set $F = \{f_1, ..., f_n\}$ of Boolean functions. Each function $f_i, i \in \{1, ..., n\}$ is constructed via logical connectives (AND (&, $\wedge$), OR (|, $\vee$), and NOT (!, $\neg$)). Each value of each variable in the Boolean network is determined by its Boolean function.
The state of a Boolean network at a certain point in time t, is defined by a vector $\vec{x}(t) = (x_1(t), \ldots, x_n(t))$. Considering all combinations of value assignments to the

n variables, the total number of states in the network sums to 2^n possible states [297].
Based on the transit from one state to the successor one, there are three main paradigms of updating schemes. Namely, these are synchronous [297, 298], asynchronous [225] and probabilistic [592] Boolean network models. Within the scope of this work, only synchronous updating schemes were considered. In synchronous Boolean network models, all Boolean functions are updated at the same time at each step in time t [8].
Simulations were performed using the R-package BoolNet [454].

2.1.1 *Simulation of Boolean network models*

Dynamic simulations of Boolean network models can be performed on the entire state space (exhaustive simulation approach) [113, 236]. Alternatively, it is possible to simulate starting from initial starting states that correspond to known biological conditions of interest [428, 598]. In this case, the mechanistic regulation leading to this long-term behaviour can be investigated by following the state transitions towards an attractor [428, 598].
Note that an exhaustive attractor search analyses the whole state space, being therefore demanding in terms of memory and runtime (both are $\mathcal{O}(2^n)$) [244]. This might imply a limitation in network sizes (up to 29 nodes [454]) for which the exhaustive approach is applicable [244]. To circumvent this limitation it is possible to either start simulations from a reduced set of randomly drawn initial states or to apply Boolean satisfiability problem (SAT) algorithms. Dubrova and Teslenko [138] proposed such a mapping to SAT for synchronous Boolean network models.
While the SAT algorithm exhaustively retrieves attractors for a certain Boolean model, it can not give information about the basin size of each attractor [244]. The "sat.exhaustive" algorithm, that is included in BoolNet [454], searches for trajectories and checks if the last state of the latter is present at least twice. If a path does not contain a loop (where the last state is present twice in the considered path), the path length is doubled and the search continues [138].
Nevertheless, basin sizes can be estimated by sampling random starting states [692]. Combining the SAT search with the estimation of basins by randomly drawn starting states can give an overview of the attractor landscape and their basin in large network models. In the present work, SAT search was applied for attractor computation. In addition, for the pNET model, attractors were also analysed based on the extension of their basin of attraction. Basin estimation were computed by 10,000 randomly drawn starting states. Of note, simulation results for the pNET model were not significantly altered by the sampling size of the initial starting states in the basin (Appendix Figures A1-A2). In accordance, also Cho and

colleagues [92] showed similar basin behaviours by sampling the same number of states in a large model on colorectal cancer.

2.1.2 *Robustness analysis within Boolean network models*

Scale-free networks, including biological networks, display a high error tolerance [12, 314]. Hence, this resistance to noise can be exploited to identify biologically meaningful networks [298]. In addition, it is assumed that, while noise will not influence the long-term behaviour of a biologically motivated network, randomly generated ones will suffer more from perturbations [760]. This peculiarity is also used to assess the stability of biologically motivated models [760]. The introduction of noise into a Boolean network is commonly induced by randomly flipping nodes in the network states [15, 299, 502].
In the present work, two main approaches will be employed to evaluate network stability both based on resistance to perturbation. The first one relates to the different effect of noise between biologically motivated models and randomly drawn ones. In this approach, single bit-flips are applied to the original network state $\vec{x}(t)$, leading to the generation of a perturbed state, $\vec{x'}(t)$. Both successor states $\vec{x}(t+1)$ and $\vec{x'}(t+1)$ of the original $\vec{x}(t)$ and perturbed $\vec{x'}(t)$ starting states are then computed. Then, the distance between the two successor states is measured using the normalised Hamming distance (HD) (equation 2)[184]. The Hamming distance (H) measures the number of different bits between two state vectors and can be formally described as (equation 1):

$$H(\vec{x}, \vec{x}') = \sum_{i=1}^{n} | \vec{x_i} - \vec{x_i}' | \tag{1}$$

The normalisation is performed by dividing the measured H by the number n of bits in the vectors [184] (equation 2):

$$HD(\vec{x}, \vec{x'}) = \frac{H(\vec{x}, \vec{x'})}{n} \tag{2}$$

The distance is an indicator of the ability of the Boolean network to maintain its functionality under noisy conditions. A normalised Hamming distance of zero indicates that the applied bit-flip (mutation) does not affect evaluated network behaviour. The normalised Hamming distance is then computed for a defined number of randomly drawn states. In addition, the same procedures are also applied to a set of randomly generated Boolean networks, to compare the effect of noise between the biologically motivated networks and the randomly generated ones. This is a computer-intensive test, resulting in the calculation of a p-value to evaluate if the null hypothesis *"the Hamming distance for the biologically-motivated network*

is larger or equal than the distance for randomly drawn networks" can be rejected, as follows (equation 3):

$$\frac{\sum_{i}^{r}(HD_{rnd_i} > HD_c)}{r} \tag{3}$$

Here HD_{rnd_i} represents the mean Hamming distance over all states of one random network rnd_i and r is the total number of random networks tested. HD_c represents the mean normalised Hamming distance overall the measured states of the constructed network. P-values $p < 0.001$ are considered to be significant. This test procedure is included in the BoolNet package [454]. The method was applied in the manually constructed literature-based HSC maintenance model, where 1000 randomly drawn states were considered and 1000 randomly generated networks were computed for comparison.
The second approach to measure stability is based on the ability of the network to compensate for the introduction of noise. In this case, noise is applied again in form of bit-flips to the basin of attraction. Robustness is evaluated by the ability to reach the same attractor before and after perturbation. Again, a set of randomly drawn states is computed and attractors resulting from each state are calculated. Next, each state is perturbed and attractors are calculated again. To evaluate the robustness of the network, the resulting attractor of each random state and its perturbed copy is compared. In the case of the present work, this assessment was made starting from one million randomly generated states. The noise was applied in form of bit-flips, and one, two, and three flips per state were applied to an independent simulation setting. Each setting was repeated in triplicate. This procedure was applied to investigate the stability of the manually constructed literature-based HSC maintenance model.

2.1.3 *Target identification in Boolean network models*

Biological networks are considered to be stable against random bit-flip perturbations, which resemble the effect of noise [12, 314]. Nevertheless, stable interventions where one or more compounds in the network are set constantly to a certain value (0 or 1), can widely affect the dynamic behaviour of the system. These conditions simulate wet-laboratory knockout and overexpression experiments. Hence, by stably perturbing targets of interest, the effect of potential therapeutic interventions or disease drivers can be assessed [572]. Laboratory screening of promising interventions is cost-intensive and can be time-consuming [571, 760]. Therefore, automatic *in silico* screenings based on the dynamic perturbation of Boolean network models can help to identify new intervention targets [571]. The Java application ViSiBooL [569, 571] was applied in the present work to screen for meaningful intervention targets in the established Boolean network models. This automatic screening ap-

proach allows the selection of which attractors may or may not be present in the perturbed network and the expected final behaviour of nodes of interest in the network. In addition, it is possible to set the number of intervention combinations m [571]. Based on these specifications, a SAT-solver performs all possible intervention combinations in parallel (in total $\sum_{i=1}^{m} \binom{c}{i} \cdot 2^i$), and returns a list of interventions that show the pre-indicated long-term behaviour [571]. This approach was applied to the pNETs model, taking into account up to two combinations of interventions and assuming that all nodes in the network could be altered except for the output nodes Cyclin E (CCNE1) and tight junctions (TJ). The simulation was performed with the aim of eliminating the aggressive attractor patterns (showing proliferation, detachment, and angiogenesis) starting from the MEN1 loss condition.
The identification of disease drivers based on network dynamics is also of interest. Within this work, the identification of disease drivers was performed by the set up of a newly established strategy based on the study of basin of attractions. In particular, a node is selected a potential disease driver based on the percentage (%) of times it is found to be active (1) or inactive(0) in the basin of attraction of an attractor, or a set of attractors, of interest (in this case a disease-matched attractors). Given that the start states are randomly sampled, the mean activity of 0.5 is expected for nodes within the basin of attraction having potentially any impact on the resulting attractor pattern. As a consequence, nodes activity percentages higher or lower than one standard deviation from this mean are selected as disease drivers. To confirm the role of a selected node as a disease driver, the corresponding perturbation suggested by the basin activity is simulated and the attractor landscape finally evaluated. An example of the analysis is presented in Figure 11 with a toy model of 3 nodes. Within the presented work, the disease driver screening was applied to the pNETs model, starting from a set of 100 million randomly sampled start states. In addition, from the set of identified drivers, nodes presenting a high or low probability of activation in the basin that matched their activity in both quiescent and aggressive matched phenotypes were excluded (AMP-activated protein kinase (AMPK) and Tumor protein 53 (TP53) for the wildtype (WT) condition). In other words, a node selected as a lowly active driver, but always inactive in quiescent and aggressive attractor patterns is not considered to be influencing the overall behaviour. Please note, that an exception was made for TP53 knockout in the WT condition, where the attractor landscape simulation was performed as a comparison to the TP53 knockout in the MEN1 loss condition.

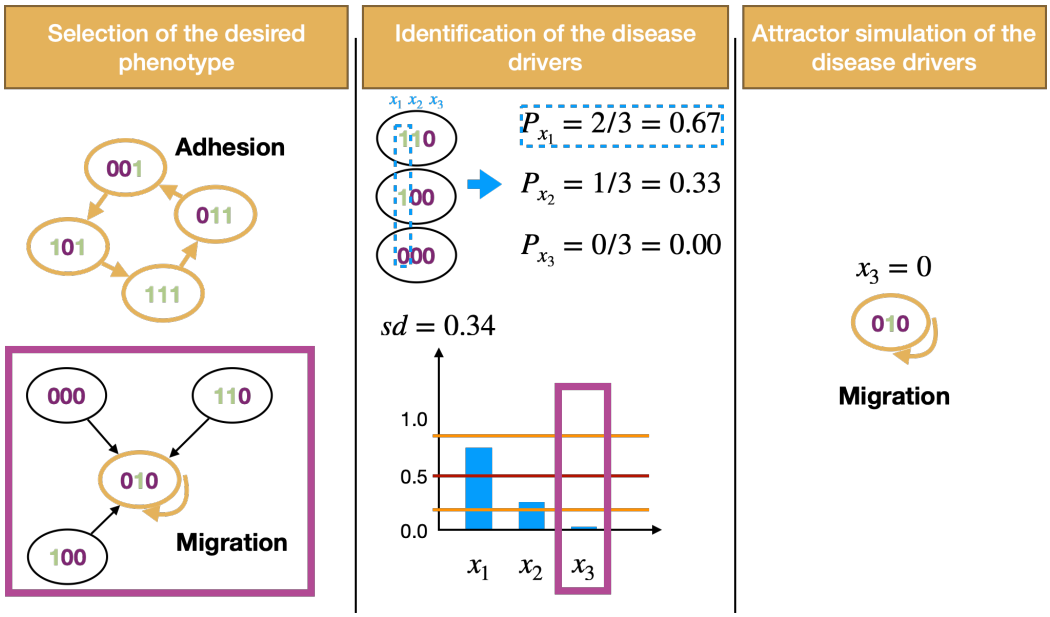


Figure 11: **Toy model for the disease driver screening**. A toy model of the disease driver screening strategy is depicted. First an attractor of interest is selected, in this case the migration inducing one (left pannel). The basin of attraction of the attractor of interest is then screened and frequency of activities of each node is calculated (middle pannel). Then, nodes whose frequency of activities is higher or lower of one standard deviation are selected. Finally, the corresponding perturbation is simulated and the attractor related phenotype is evaluated (right pannel).

2.2 Model setup strategies

Within the scope of this work, Boolean network models were created using a literature search or time series of gene expression data. The following sections describe the individual models setups.

2.2.1 *Manual establishment of literature-based Boolean network models*

All manually curated models require first the collection literature statements about regulatory dependencies, and successively their translation into Boolean regulatory functions. This process is rather complex and normally requires different iterations of model construction, simulation, and validation. Exemplarily, literature results are often presenting contradicting results, which can be evaluated independently during the modelling process by simulation and evaluation of the attractor landascapes. The general manual modelling framework described below is also presented by Ikonomi et al. [255].

In the first place, literature on a certain biological problem should be gathered. In this perspective, a first round of literature search starting from general review papers and further detailing the single interactions was performed. In this phase, the aim is to detect the initial set of nodes relevant to the analysed process. Once this is done, further refinement of the model is performed by deepening the literature screening and by support of interaction databases (e.g. BioGRID [617]). This approach allows the modeller to acquire a first general expertise of the examined regulatory process. Additionally, when approaching the manual establishment of a model, the cellular context should be taken into account. This avoids the inclusion of regulatory dependencies not specific for the investigated cell regulatory contexts. Exemplarily, it is not said a priori that results gathered in lung cancer can also be valid in pNETs. The inclusion of external regulatory dependencies is normally considered in the refinement of the model. Here, alternative cellular contexts are considered when realtable to the one in exam. Exemplarily, general regulations from pancreatic endocrine cells could be integrated when modelling pNETs. Alternatively, regulatory dependencies can be transferred when knowledge is available on similar behaviours for the investigated nodes or interactions of two cell types. As an example, both HSC and neural stem cells (NSC) rely on low ROS levels and potentially similar environmental conditions for maintaining quiescence [600]. Hence, common regulation in the context of ROS regulations could be hypothesised for these two stem cell types. Nevertheless, the amount of regulatory dependencies extracted by similar cellular contexts might also depend on the amount of data available on the system under examination. In any case, in all presented models, results obtained from human and mouse models data were prioritised, together with the ones selectively observed in the interested systems.
In the second place, the collected literature statements are translated into Boolean regulatory functions. To combine regulatory dependencies, some general rules were followed. In first modelling phases, alternative activators of a node are combined with an OR operator, while all inhibitors are added with an AND NOT operator. This general rule construction assumption holds true until further information is available. Exemplarily, if information on cooperative activity for two components of the model is present, they can be connected with an AND operator. Linear connections all taking place in one regulatory framework were summarised in one node (PI3K phosphorylation steps in the activation of AKT are summarised as a unique dependency). Whenever possible, different regulatory levels (e.g. transcription, protein modifications, degradation) were connected via and AND operator. This implies that a node will be activated only if all its regulatory levels, from transcript to protein stability, are not inhibited and stimulated.
In the presented work, two Boolean network models investigating the HSC physiological maintenance and activation network, and the pNET network were con-

structed. The following sections briefly describe the specific literature search for their establishment.

2.2.1.1 *HSC physiological maintenance and activation*

The first regulatory process investigated in this work concerns the physiological maintenance in the bone marrow niche of HSCs. This crucial task is accomplished by general maintenance of HSC quiescence and a niche-mediated activation in presence of certain external signals [614, 700]. Following the modelling framework described above, from the first screening of general reviews, a set of regulators involved in cell cycle regulation, metabolism, senescence, and apoptosis was selected. Extrinsic regulations were collected and summarised in quiescence inducing signals, mainly responsible for inducing cell cycle inhibitors, and cycling signal, found to stimulate cell cycle entering. Afterwards, further interactions were retrieved by searching the specific terms including processes and specific genes of interest (such as e.g. "cell cycle regulation HSC", "quiescence regulation HSC", "mTORC HSC") in NCBI and Google Scholar. Wherever possible, findings obtained in the HSC regulatory context were favoured. Studies from both mouse models and from human HSCs (when available) were considered. For all components of the model, different levels of regulation were included (from transcription to post-translational modifications).

2.2.1.2 *pNET model*

The second manually constructed literature-based model that was created in this thesis deals with the understanding of the development and progression of pNETs. While little information is known on the molecular mechanisms of these tumours [31, 719], previous research efforts have revealed the frequent presence of alterations in a set of genes involved in the tumoural process: MEN-1, DAXX, ATRX, and genes in the mTOR pathway [277, 559, 666]. Hence, these genes were screened in the context of pNETs both by specific findings and more general reviews. Hence search terms such as "mTOR pNETs", "MEN-1 pNETs" were searched in Google Scholar and NCBI. Whenever possible, regulations retrieved from evidence in pNETs have been favoured. Additionally, the curated databases BioGRID [617] and Metacore^{TM} (Thomson Reuters Inc., Carlsbad, CA) were used to identify further possible interactions of components that were further integrated.

2.2.2 *Automatic reconstruction of Boolean network models from expression data*

Boolean models can be constructed both via manual construction combining literature statements or automatically reconstructed based on expression data. Since

gene expression data consists of values $\in \mathbb{R}$ while Boolean network models work with binary values, the gene expression values first have to be binarised. In the following sections, the unsupervised binarisation of gene expression data and the automatic reconstruction of Boolean networks from expression data will be described. Besides, given that the reconstruction will be based on single-cell RNA sequencing data, a newly established combined pipeline for reconstruction will be applied. The GSE138544 dataset [507] was used to reconstruct Boolean network ensembles describing the age-dependent changes of NF-κB signalling pathway in the progression of ageing.

2.2.2.1 *Dataset for network reconstruction*

The GSE138544 [507] dataset containing samples of human isolated peripheral blood LT-HSCs ($lin^-CD34^+CD38^-CD45RA^-CD49f^+$) was used for reconstruction. Single-cell RNA sequencing was performed on a NovaSeq6000. The dataset contains single-cell expression samples from four young (ages 19, 21, 37, 40) and four aged (ages 61, 66, 68, 70) human individuals (two males and two females per group) as grouped by Ratliff and colleagues [507]. 83 to 94 single-cell measurements are available per individual. Given the focus of the reconstruction approach on the NF-κB pathway, only the genes included in the NF-κB signalling (101 in total) as described in the hsa04064 Kyoto Encyclopedia of Genes and Genomes (KEGG) database [288] were considered.

2.2.2.2 *Expression data binarisation*

Binarisation across multiple scales (BASC) algorithms suggested by Hopfensitz et al. [245] are two approaches for the binarisation of gene expression data. In the case of this work, the BASC A algorithm implemented in the R-package BiTrinA [455] was used. This approach uses a series of step functions to get a robust binarisation threshold [245]. The algorithm is conceptually based on three computational stages. First, the input values of the expression data are ordered in an ascending manner to generate an initial step function. Next, step functions with fewer discontinuities are calculated employing a dynamic programming approach. The aim of this procedure is to minimise the Euclidean distance to the initial step function. Finally, the data is binarised by applying a unique threshold computed based on the strongest discontinuities in the step function. Note that, not all expression data can be equally well binarised based on the identified threshold. For this reason, a p-value is computed providing a measure of the reliability of the binarisation for the found threshold.
For the GSE138544 [507], 96 genes of the NF-κB pathway were significantly binarised (p-value< 0.05), and were used for reconstruction.

2.2.2.3 *Generation of pseudo-time-series from single-cell expression data*

All automatic network reconstruction algorithms depend largely on the amount of available data, especially on the time points available for reconstruction which is frequently limited [245]. Nevertheless, this limitation can be overcome by taking advantage of the emerging single-cell high-throughput data, where each sample presents a potentially large set of single-cell measurements. Experimental results indicate that populations of LT-HSCs can depict interchangeable activity states, implying that a population of LT-HSCs dynamically transits from one expression activity level to the other [63, 696]. Based on this knowledge, in the present work, the generation of time series was made by assuming that within the same group of cells coming from an individual, each one can be a potential predecessor or successor the state of each other single-cell measurement. As a result, each single cell sample x is treated as a pseudo-time point, scaling up considerably the number of tuples of predecessor time steps $x(t)$ and $x(t+1)$. Given a total number of single-cell measurements b the number of possible couples of predecessor-successor states is (equation 4):

$$\binom{b}{2} \tag{4}$$

Additionally, since each state in a give tuple can act bidirectionally as predecessor or successor, the total amount of possible tuples sums up to (equation 5):

$$\binom{b}{2} \cdot 2 \tag{5}$$

For the NF-κB signalling network reconstruction during human HSC ageing, 1000 tuples of data points were randomly drawn and used as time points to generate pseudo-time series of length two. This procedure was repeated for each of the eight groups of LT-HSCs.

2.2.2.4 *Reconstruction of Boolean networks from binarised pseudo-time-series*

In the scope of this thesis, a hybrid pipeline named *"filtered best-fit"* approach is applied to infer large Boolean network ensembles of the NF-κB signalling pathway during human HSC ageing. The approach aims to boost the speed of reconstruction, which allows the reconstruction of large models. To do so, the strategy combines the detection of a selection of input candidates suggested by Maucher et al. [412], which serves now as a preprocessing step for the exact reconstruction algorithm by Lähdismäki et al. [341]. The latter is included in the R-package BoolNet [454]. The combined approach was initially set up in the dissertation of Julian Schwab [568] and subsequently applied as part of the single-cell expression automatic reconstruction pipeline. Altogether, the *"filtered best-fit"* provides an initial structure

of the candidate interactions to be included in the model, that are subsequently fed to the best-fit algorithm.

The algorithm of Maucher et al. [412] infers regulatory dependencies from binary time-series of data relying on the relevance of monotonicity for biological functions [412, 611]. The algorithm determines which variables $x_i \in \{0,1\}$ are relevant for a Boolean function $f_i : \{0,1\}^n \to \{0,1\}$ based on Pearson correlation. Under the monotonicity assumption, it is possible to show that a function $f_i : \{0,1\}^n \to \{0,1\}$ depends on the i-th element of the random variable $X \in \{0,1\}^n$ distributed according to a product distribution D, if and only if the Pearson correlation of x_i and $f(X)$ is non-zero for non-zero variances [412]. Based on this principle, the algorithm identifies input variables with a selected minimum influence for each regulatory compound individually. To do so, the Pearson correlation between each input value and the value of the regulatory compound is computed. If the correlation is above a specific threshold the interaction between a putative input and the regulatory compound is considered relevant. This process is iterated for each regulatory compound in the network.

While the algorithm of Maucher et al. [412] infers regulatory dependencies, the *best-fit extension* from Lähdismäki et al. [341] allows for reconstruction of Boolean functions from time series of expression data. The *best-fit* approach tests all possible combinations of inputs for each Boolean function to fit the dynamics of the given time series as correctly as possible. In more detail, the algorithm screens for the subset $X^{'}$ of all genes X, with up to k inputs. Finding Boolean functions which match the measured observations in the time series data corresponds to solving the consistency problem [9].

To solve this problem, the algorithm detects Boolean functions f which distinguish between true T and false F examples in the given data. This is done based on a partially defined Boolean function $(\mathrm{pdBf}(T,F))$, with $T,F \in \{0,1\}^k$, and k being the pre-defined maximum number of possible inputs.

$(\mathrm{pdBf}(T,F))$ includes true examples $T = \{X^{'}(t) \in \{0,1\}^k : x_i(t+1) = 1\}$ and false examples $F = \{X^{'}(t) \in \{0,1\}^k : x_i(t+1) = 0\}$. Each tuple of predecessor x(t) and successor x(t+1) time points is added in the $(\mathrm{pdBf}(T,F))$ as T or F.

Next, the error associated with input combinations $X^{'}$ is computed. The number of inconsistencies in the $(\mathrm{pdBf}(T,F))$ is calculated by intersecting $T \cap F$. This means the same function is not expected to have both a true and false output. The algorithm aims to minimise inconsistencies. Thus this intersection coincides with the error associated with the input combinations. In more detail, let us assume that positive weights $\omega(x) > 0$ are given to all variables $x_i \in T \cup F$ and the weights of all subsets $S \subseteq T \cup F$ are calculated (Equation 6) [341]:

$$\omega(S) = \sum_{x \in S} \omega(x) \tag{6}$$

Now, the error ϵ of function f is defined as (Equation 7):

$$\varepsilon(f) = \omega(T \cap F(f)) + \omega(F \cap T(f)) \tag{7}$$

Afterwards, the input combinations with the least error ε are chosen. Finally, a Boolean function based on these inputs is defined (Equation 8). The Boolean function is constructed using a truth table, which is filled by iterating through all examples $x \in T \cup F$ over all time steps $t = 1, \ldots, j$ (where j denotes the current measurement). The final output-vector is described as follows:

$$f_i^t = \begin{cases} 0, & \text{if} \quad x \in F \wedge f_i^{t-1} = ? \\ 1, & \text{if} \quad x \in T \wedge f_i^{t-1} = ? \\ *, & \text{otherwise} \end{cases} \tag{8}$$

Here, the i-th variable of f can either be inactive $\{0\}$, active $\{1\}$, undefined $\{?\}$ or a conflict $\{*\}$. f^0 is intialised as $f^0 = (?, \ldots, ?)$.
The output of the approach finally yields sets of regulatory functions for each compound included in the data. In the age-related NF-κB reconstruction approach, 100 networks were sampled based on the output of *"filtered best-fit"* for each individual. In addition, the procedure from sampling of tuples to generation of the network ensemble was repeated 20 times for each of the 8 individuals, leading to a total amount of 2000 reconstructed networks per individual, as depicted in Figure 12.

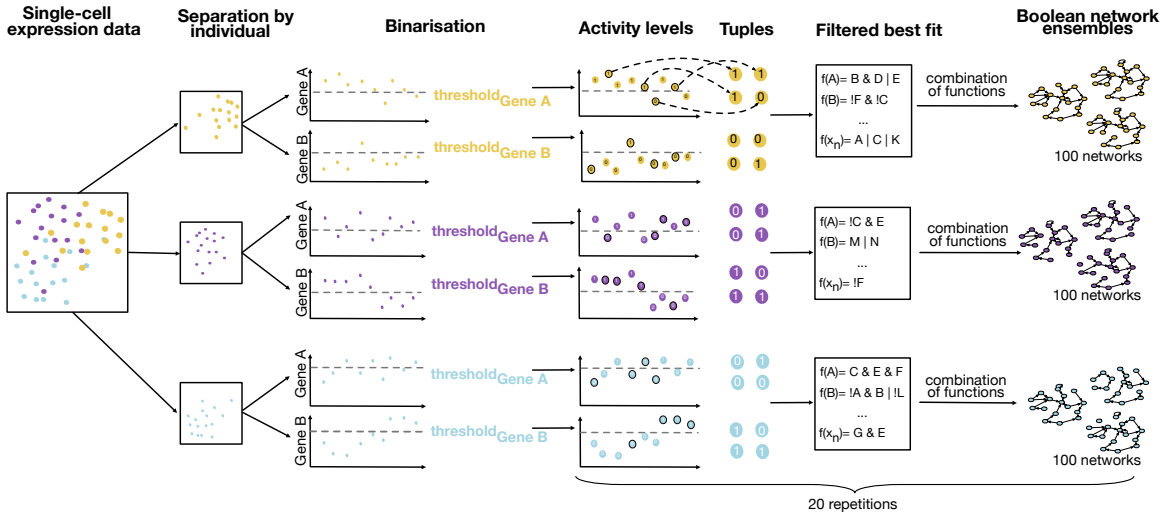


Figure 12: **Schematic overview of the pipeline for network ensemble reconstruction**. The pipeline starts with selecting single-cell RNA sequencing samples from each group (yellow, purple, and turquoise - here samples of single cells are coming from the same individual). Data points are randomly sampled and sequentially ordered to create pseudo-time points. Then, data are binarised and tuples are formed. The generated tuples are used for the *"filtered best-fit"* reconstruction algorithm. From the reconstructed Boolean functions, an ensemble of Boolean models is obtained by randomly sampling reconstructed regulatory dependencies. This figure has been modified from Schwab, Ikonomi et al. [570], licensed under CC BY 4.0, https://creativecommons.org/licenses/by/4.0/.

2.3 Model analysis and validation

Once generated, independently from the construction strategies, models are simulated to formulate hypotheses regarding mechanistic regulations and general behaviours. In the case of reconstruction strategies, together with dynamics, also some interaction-graph based features of the ensembles can give insights on further regulatory hypotheses. Nevertheless, before formulating mechanistic hypotheses, models need to be validated to show that their characteristics resemble the ones observed in the described biological process. To do so the long-term behaviour of the model needs to be analysed and interpreted. Model validation can be performed by both literature validation, laboratory experiments, or by comparison of the long term behaviour to available gene expression data. In addition, ensembles of Boolean models can also be structurally validated.
Different strategies in analysing the attractor landscapes and interaction graph-based properties (only in the case of network ensembles) have been applied in the present work. The validation of the three presented Boolean network models has

been supported by matching model results to experimental results. In addition, ensembles of Boolean models for the age-related alteration of the NF-κB pathway in HSCs have been also validated structurally. The pNET attractor activities have also been validated via comparison to binarised gene expression data from healthy pancreas and pNET samples [546].

2.3.1 *Model analysis strategies*

2.3.1.1 *Representation and interpretation of attractors*

Attractors represent the long-term behaviour of Boolean network models and have been connected to biological phenotypes [249, 248]. While the number of attractors and their length gives insights on the system stability and heterogeneity, their interpretation is crucial in formulating new regulatory hypotheses in the modelled biological process.
Different strategies can be applied when interpreting attractor patterns. First, they can be analysed via read-out nodes activities, such as "Go-phase", "Apoptosis", "Senescence", or "Tight junctions". These particular nodes can be included in the modelling process, and can support the interpretation of attractor patterns, especially in larger networks. Such types of nodes are included in both the manually constructed models investigated in this work. In addition, phenotypical interpretation can be inferred also by the activity of certain nodes, representing the output of a certain process. This characterisation of the attractor landscape has been applied to the pNET model, where multiple tumour phenotypes have been characterised within the same attractor landscape. In particular, cellular phenotypes such as proliferation, quiescence, Go-alert, detachment and angiogenesis were characterised. CCNE1 and E2 factor (E2F) activities were applied to select for proliferating phenotypes. In their absence, the phenotype is considered quiescence if mTORC1 is inactive too. A quiescent state with mTORC1 activity is instead considered as a Go-alert phenotype, priming cells to enter cell cycle. The detachment was evaluated based on the inactivity of the node tight junctions. Instead, angiogenesis was considered present when both vascular endothelial growth factor (VEGF) and Vascular endothelial growth factor receptor (VEGFR) were active in the attractor landscape. These phenotypes were evaluated both in combination, and independently in the pNETs model simulations. For the evaluation of pNETs mutational landscape and mTORC1 resistance, the combination of the defined phenotypes was considered. Hence, in each attractor, the presence of the different read-outs for each phenotype was evaluated and quantified based on the estimation of the specific basin representation. This results in a determination of the attractor landscape via combination of phenotypical readouts (as shown in Figure 31 and Figure 36). Instead, for the evaluation of the dynamic drivers and intervention targets, the abundance of each

read-out phenotype across all attractors is evaluated independently from the others. An example of the different interpretation and representation of attractors in terms is presented in Figure 13, with an example extracted from the pNET model.

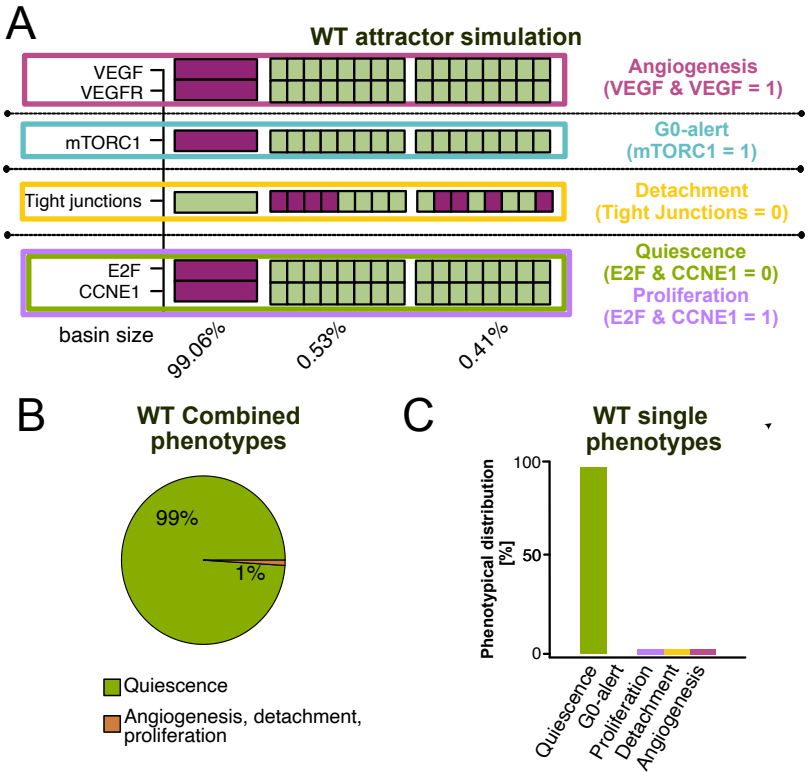


Figure 13: **Example of attractor interpretation and representation**. The interpretation of read-out phenotypes and their representation is presented based on the WT simulation of the pNET model. Nodes used to interpret the pNET model phenotypes are extracted from the attractor pattern (A). On the side of each node, the criteria for assigning the specific phenotypes are reported. The estimated basin sizes are reported under each attractor. In the attractor pattern, green boxes indicate activation, while dark purple ones indicate inactivation. Phenotypes present in each attractor then are combined and weighted based on their basin of attraction (B). In the pie chart, 99% of the phenotype is covered by quiescence, represented by the single state attractor. Instead, the two cyclic attractors cover 1% of the basin connected to angiogenesis, detachment, and proliferation. The two combined phenotypes can be broken down independently into single phenotypes (C). Again percentages for each phenotype overall the attractor landscape corresponds to the estimated basins of attraction. In this case, overall the attractor landscape, 99% is represented by quiescence, while angiogenesis, detachment, and proliferation cover the 1%. This visualisation is considered more intuitive when comparing the effect of many perturbations on the attractor landscape.

When dealing with ensembles of Boolean models, attractors have been analysed in terms of the probability of attractor patterns within the same ensemble. In particular, node activities are expressed as active states normalised by the number of total states of the attractor. This procedure yields the probabilities of each gene to be active within the entire attractor landscape of one network. Next, these probabilities are summed up for all network simulations within one ensemble and the repeated runs and normalised again by ensemble size and the number of repeated runs. This results in an average probability of genes being active in the long-term behaviour of the entire ensemble over the repeated reconstruction runs.

2.3.1.2 *Interaction-graph based analyses of network ensembles*

To investigate age-related structural changes in the ensemble reconstructed from single-cell RNA sequencing data of human LT-HSCs, a variety of structural alterations has been investigated. In particular, the following interaction-graph and network reconstruction based were analysed:

- The number (#) of nodes that are unregulated. These nodes are set to a constant value (0/1) in the Boolean networks (**fixed genes**)
- The number (#) of nodes that have connectivity of 0. These nodes are disconnected from the rest of the graph (**isolated genes**)
- The mean number (#) of incoming edges across the ensemble of networks (**mean input**)
- The mean number (#) of potential regulatory functions retrieved for each gene in the reconstruction strategy (**mean function**)
- The number (#) of network motifs. Based on their proven biological impact, this analysis has been focused on feed-forward loops and bifans [17, 550].

Note that, the motif search has been performed using the igraph R-package (Version 1.2.6, [108]).

2.3.2 *Model validation*

2.3.2.1 *Attractor comparison to gene expression data*

In addition to literature-based validation, the resulting attractor activities of the pNETs model were checked using microarray data from healthy and pNET cancer tissues of the RIP1-Tag2 mouse model. Here, the dataset referenced as GSE73514

(3 healthy tissues, 3 hyperplastic islets, 3 angiogenic islets, 5 tumours, 5 metastasis-like tumors, 3 metastatic tumors) was considered [546]. RNA was extracted and hybridised on Affymetrix GeneChip Mouse Gene 1.0 ST arrays.
As for reconstruction, the gene expression data needs to be binarised before comparison to the attractor pattern. In this case, the selected dataset includes labels that can be exploited for binarisation. For this reason, a supervised binarisation method is suitable for this scenario. Here, the best binarisation threshold for each investigated gene of the pNET model was determined by computing all possible thresholds and evaluating the performing one in therms of sensitivity and specificity. The calculation of binarisation thresholds was performed with the R-implementation pROC [521]. The performance of the binarisation method can be visualised via receiver operating characteristic (ROC) curves. ROC curves are plots depicting sensitivity against 1− specificity, as the threshold is moved over the range of all possible values [39, 212] . Sensitivity (or recall) is defined as the proportion of true positive results that are detected correctly as positive [521, 39] (Equation 9). Instead, specificity denotes the proportion correctly classified negative results [39, 212] (Equation 10).

$$\mathit{sensitivity} = \frac{\mathit{true}\quad \mathit{positives}}{\mathit{true}\quad \mathit{positives} + \mathit{false}\quad \mathit{negatives}} \tag{9}$$

$$\mathit{specificity} = \frac{\mathit{true}\quad \mathit{negatives}}{\mathit{true}\quad \mathit{negatives} + \mathit{false}\quad \mathit{positives}} \tag{10}$$

Here, true negative/true positive define cases in which the results are correctly classified as positive/negative ones. False-positive/false-negative, instead, define the condition in which a result is miss-classified as positive/negative ones [39, 212].
In optimal conditions, both sensitivity and specificity are equal to one [39]. As a consequence, a binarisation threshold close to this optimum would be desirable. To evaluate the performance of the classifier, the area under the curve (AUC) is computed by the sum of trapeziums (Equation 11) [39, 149]. For the calculation of each trapezium the starting coordinates (x_k, y_k) and terminal coordinates (x_{k+1}, y_{k+1}) in the plot of the ROC curve are considered. Here, the maximal range of the coordinates $m \in \mathbb{N}$, whereas the coordinates x_k, as well as $y_k \in [0, 1]$.

$$\mathrm{AUC} = \sum_{k=1}^{m-1} (x_{k+1} - x_k) \cdot \frac{y_k + y_{k+1}}{2} \tag{11}$$

2.3.2.2 *Comparison to classification results*

In the presented work, a strategy based on foreign feature classification experiments was designed to compare similarities between attractor landscapes for different perturbation experiments and expression profiles of patients cohorts with

the corresponding alterations. When dealing with classification experiments, on the contrary of the dynamic modelling approach, the labels assigned to each class represent the assigned phenotype. Therefore, all expression profiles of patients having tumours previously classified e.g. histo-pathologically as carcinomas, or bearing a certain mutations such as MEN1, will belong to the same class. In this case, the classification experiments will determine the best manner to separate two classes and identify an expression signature. When dealing with the presented foreign classification approach, an external, or foreign class, to the one on which a binary classification experiment is performed is reclassified using the decision boundaries of that binary classification. In particular, assignment of foreign classes to binary classification tasks for differently mutated patients cohorts was considered as a measure of similarity or purity among the different cohorts. Hence, a foreign class assigned with higher frequency to one of the original ones is assumed to have certain similarities in the molecular expression profile to one of the two classes. By performing this combination of binary classsification experiments and reclassification of the foreign class for all potential combinations of classes in the dataset, it is possible to infer a general interpretation of similarities of the expression profiles present in the examined dataset. The distribution of assignments is then compared to the similarity of attractor landscapes, not only for validating model predictions, but also to integrate information from patients cohorts expression profiles in a new fashion to formulate further hypotheses on the effect of e.g. different alterations.
In the present work, this strategy was applied to investigate different driving mutations in pNETs, creating a parallelism between phenotypical landscapes hypothesed by model simulations and common features shared by differentially mutated patients cohorts. In the specific scenario, the GSE117851 [79] dataset, containing 47 pNETs tumour specimens (8 MEN1 mutated, 9 DAXX mutated, 7 double mutated, and 17 WT for the two mutations) was used. The dataset contains human pNETs specimens, from which RNA was extracted and hybridized to HGU133A2 (Affymetrix) to profile gene expression. For the binary classification tasks the analysis was performed via linear support vector machines, focusing on the 200 top features based on threshold number of misclassification (TNoM) scoring [38]. The experiments were conducted as 5x5 cross-validation (CV) analyses.
A multi class classifier experiment was also performed to investigate the potential of different pNETs and lung tumours with neuroendocrine properties datasets to be classified. The applied multi class classifier was a one against one support vector machine. To construct the decision on all groups or classes to be separated, one base classifier for each pair of classes is computed. Each classifier predicts one of two classes and then a majority vote is performed for the ensemble decision. The output of the multi class classifier was depicted in form of a confusion matrix where each entry represents the probability of that class to be assigned in the cor-

responding one. Also in this case, classification experiments were performed via linear SVMs, focusing on the 200 top features based on Threshold Number of Misclassification (TNoM) scoring [38]. The experiments were conducted as 5x5 cross-validation (CV) analyses. With this approach three datasets were analysed. First the above-described GSE117851 [79]. Secondly another human pNETs dataset grouped via histo-pathological features was analysed. This was the GSE73338 [432, 546], containing 95 human pNETs speciments (63 non functional, 17 insulinomas, 7 metastases, 9 normal pancreas), where RNA was extracted and hybridised on a custom 18.5K human oligo microarrays. Finally the GSE19945 dataset including lung tumours with neuroendocrine profiles was used. All 59 samples (35 small-cell lung cancer, 11 large cell neuroendocrine cancer, 5 squamous cell carcinoma, 8 normal lung) were obtained by tumour surgical resections. RNA was extracted and hybridised on a Agilent Human 0.6K miRNA Microarray G4471A.

2.3.2.3 *Structural validation of ensembles of Boolean network models*

The validation of the automatic reconstruction approach was performed via comparison of the reconstructed regulatory dependencies with the ones reported in the STRING-DB database [603]. To do so, two matrices were combined: the first considering consistency of regulatory interaction within the network ensembles, the second considering the existence of a given interaction in the STRING-DB database[603]. The matrix of the ensemble of networks reports an entry of 1 at the position (i, j) if the compound i is present in the regulatory function of the compound j. Otherwise, 0 is included. When multiple regulatory dependencies are reconstructed for the same node, the union across all present regulatory dependencies was considered. For the STRING-DB interactions, a similar matrix was constructed. In this case, a match (1) was assigned if the regulatory dependency was present by either a direct interaction or an indirect one via one maximal additional node. The interaction considered were selected among those either present in curated databases or experimentally validated. Finally, these two matrices were combined to obtain a matching matrix. Here, 1 indicated that there is a match between interactions present in the ensemble as well as in STRING-DB. If no interaction is reported in the ensemble a 0 is assigned. Finally, an entry of -1 is assigned to a mismatch, where the interaction is found in the ensemble but not in the STRING-DB, or only exist via more than one intermediate node

2.4 Predicting dynamic relevance via graph theoretical measures

Other than exploring and getting insights on new regulatory mechanisms within phenotypical landscapes, another aim of this work is to investigate the possibility

that interaction graph-based measures, referred in the present work also as "static measures", can predict dynamic altering nodes. The approach takes its fundaments on two ground ideas. First, exhaustive attractor computation is limited to a rather small network. This is because the state transition graph scale up exponentially with the network size [572]. Due to the smaller search space, measures of interaction graph-based properties can be calculated on a faster time scale than their dynamic counterparts. Second, there is already evidence that some particular set of nodes in a network can be responsible for its dynamic behaviour [271]. Hence, the question addressed in this thesis is whether there are interaction graph-based measures able to select nodes whose perturbation can shift the dynamic behaviour of the system. Especially in large networks where exhaustive perturbation analyses can be impaired, such strategy could support fast and efficient detection of disease drivers and intervention targets.
In the following, the main methods applied to individuate and validate combinations of interaction graph-based measures able to predict dynamic influencing nodes are presented. The established method was applied to a collection of biologically motivated Boolean models that is also described.

2.4.1 *Collection of Boolean network models*

To address the aim of the project, several biologically motivated Boolean network models were extracted from the interactive modelling of the biological networks database (Cell Collective) [232]. This search yielded a selection of 35 Boolean networks, ranging in size from 5 to 51 genes, with an average of 20 nodes. The median number of nodes in networks is 18, with an interquartile range of 10.5 (from 12.5 to 23). The number of regulations ranged from 12 in a network of 7 nodes to 158 in a network of 32 nodes, with an average of 48 connections for an overall number of 684 nodes.

2.4.2 *Evaluation of dynamic impact after perturbation*

To evaluate the dynamic prediction power of static measures, the first requirement was to quantify and rank the dynamic impact of applied node perturbations. Hence, three dynamic measures were considered to quantify the changes in the attractor landscape after perturbation of a node. In all these measures, attractors were collapsed to single state ones. This was done by considering that each attractor a belonging to the set of attractors of a network, defined as $\mathcal{A}(N)$, can be considered as a vector $\vec{a} = (a_1, \ldots, a_m)$ of trinary variables $a_m \in \{0, 1, 0.5\}$ indicating presence, absence or oscillating behaviour.
The first dynamic measure considered was the gain of attractors (G_n) after per-

turbation. This measure returns the number of attractors present in the perturbed condition that were not present in the unperturbed set of attractors. The second measure defines the loss of attractors (L_n) and returns the number of attractors in the unperturbed model for which there is no match in the perturbed set of attractors. Finally, the third measure considers the minimal Hamming distance HD_n, which quantifies the minimal shift in attractors caused by the perturbation. In more detail, all attractors in the perturbed system are compared to the set of attractors in the unperturbed one. HD_n measures the Hamming distance to the one which most closely resembles its pattern of activities. The Hamming distance was calculated as previously described in the methods (section 2.1.1). Finally, these three measures were aggregated to compute a vector specifying the dynamic impact I of each node n as follows:

$$I = \frac{1}{3}\left(rk\left(G\right) + rk\left(L\right) + rk\left(HD\right)\right) \tag{12}$$

$rk(.)$ denotes the ranking function. Here, nodes in a network N can be ranked according to their dynamic impact after perturbation. The dynamic impact I_n of an individual compound n can be extracted from $I = (I_n)_{n=1}^{m}$, being m the number of nodes.

2.4.3 *Static measures*

A range of static measures that assign individual values to each node according to the specific properties of the networks' topology was initially investigated in the master thesis of Felix Weidner [687]. All these measures are computed based on the interaction graph, defined as:

$$\mathcal{I} = \mathcal{G}(\mathcal{V}, \mathcal{E}) \tag{13}$$

containing a set $\mathcal{V}$ of nodes connected via directed edges $\mathcal{E}$.
To evaluate the best candidates able to predict dynamic behaviours feature selection experiments were performed. The classification was performed applying all possible combinations of the static features over all nodes of all investigated networks N. Each node n was labelled with its dynamic impact measured by I_g. For classification, k-Nearest-Neighbour, random forest, and support vector machine algorithms were applied. Classification performance was measured using 10x10 and leave-one-subset-out (LOSS, leaving out one network) cross-validation (CV). The two static measures vertex betweenness (VB) and determinative power (DP) were overrepresented over the best-performing feature combinations, and thus further considered as best predicting static measures. Below, both measures are briefly defined.

2.4.3.1 *Vertex betweenness*

The definition of vertex betweenness VB_n is based on the set of shortest paths s_{ij} between nodes n_i and n_j, $n_i \neq n_j$, and its subset $s_{ij}(n)$ of paths which pass node n:

$$VB_n = \sum_{n_i, n_j \in \mathcal{V} \setminus \{n\}} \frac{|s_{ij}(n)|}{|s_{ij}|}. \tag{14}$$

Hence, this measure computes the shortest paths between nodes of a system.

2.4.3.2 *Determinative power*

Determinative power relates to the network entropy and assigns high scores to a node n if knowledge about the state of this node confers a high gain of information about the state of its output nodes, defined in terms of mutual information [231, 407]. The determinative power DP_n of a node n is defined by utilising the binary Shannon entropy: $h(p_n) = -p_n \log_2(p_n) - (1 - p_n) \log_2(1 - p_n)$, where $p_g = P(X_g = 1)$ describes the probability of a random, binary variable X_n taking the value $x_n = 1$ [407]. The support of a given Boolean regulation function f_n is defined as the set of states which are mapped to an output of 1 by the function, formally defined as $\mathcal{S}(f_n) = \{x : f_n(x) = 1\}$. The decrease of uncertainty regarding the values of genes in the support of f_n inferred from the knowledge of the state of node n' is described using mutual information (MI) [99]:

$$MI(X_n; f_{n'}(X)) = h\left(\sum_{x \in \mathcal{S}(f_{n'})} p_x\right) - \sum_{b \in \{0,1\}} P(X_n = b) h\left(\sum_{x \in \mathcal{S}(f_{n'})} P(X = x | X_n = b)\right) \tag{15}$$

Here p_x denote the probability of state x and $X = (X_g)_{n=1}^{m}$.
Finally, this yields the determinative power of node n as DP_n by summing over all m outputs n' of node n:

$$DP_n = \sum_{n'=1}^{m} MI(X_n; f_{n'}(X)) \tag{16}$$

As the maximal value of $MI(X_n, f_{n'}(X))$ is one, whereas the values of the determinative power of a node range between zero and the number of outputs of the node [492].

2.4.4 *Ranking gene impacts*

Besides evaluating single measures of VB and DP, also their union $VB \cup DP$ and intersection $VB \cap DP$ were analysed. The aim was to verify whether combination

of these two measures could be even more predictive of the dynamic impact. To do so, $U \in [1\%; 100\%]$ denotes the percentage of all m genes. VB_U denotes the top scoring gene set:

$$VB_U = \left\{ g : r_n \leqslant \left\lceil Un \right\rceil, r = rk(VB) \right\}, \tag{17}$$

where $r = (r_n)_{n=1}^{m}$. DP_U is defined analogously. To determinate whether a stricter or broader criterion should be chosen for labelling a gene as having high impact the comparison between statics and dynamics is conducted for all possible sizes $U \in [1\%; 100\%]$ of the selected set. Based on this threshold, genes are defined as either high or low impact.

2.4.5 *Evaluation of node connectivity*

Connectivity of compounds in the interaction graph is considered to be relevant to determine high-impact nodes [43, 202, 230]. In fact, so called hub nodes, which are highly connected components, are known to be master regulators of biological processes [43, 202, 230]. Connectivity is quantified using z-scores C_n (Equation 18) for a given gene n, where δ_n is the total degree of node n, while $\bar{\delta}$ is the average total degree of all nodes in the network. σ is the corresponding standard deviation of these total degrees in the same network.

$$C_n = \frac{\delta_n - \bar{\delta}}{\sigma} \tag{18}$$

A hub is then defined as a node having a z-score in connectivity of $C_n \geqslant 2.5$ [202].

2.5 Statistics and visualisation

R version 4.0.0 [503] (www.r-project.org) was used for statistical analyses and visualisation.
Experimental data were analysed by the Wilcoxon test, with significant values considered for $p - value < 0.05$. When appropriate, Bonferroni correction was applied for multiple comparisons.

3

RESULTS

The results are divided into three sections specifically addressing one of the introduced topic presented in this work. Each section is followed by a tailored short discussion that only comprises the results concerning the specific part of the work. For the results concerning the physiological maintenance and the ageing process of HSCs, a literature-based and a data-driven approach were applied. Here, the main regulators governing HSC quiescence and activation, as well as the age-related NF-κB pathway, were studied and discussed in terms of regulatory mechanisms and modelling strategies. The investigations regarding the HSCs physiology and ageing are followed by the presentation of a Boolean model that aims to unravel mechanisms and suggest targeted interventions in pNETs. The results end with an investigation concerning the prediction power of interaction graph-based measures in term of dynamic behaviours. Here, besides defining a method to identify these dynamic predictors, a validation based on the results of the PNETs model is performed and discussed.

3.1 Modelling the physiological maintenance and ageing of HSCs

Ageing is a biological process that heterogeneously limits organisms in their regeneration potential and maintenance of homeostatic activities [560, 644]. Given that most of post-developmental regeneration activities are carried out by somatic stem cells, these are of central interest in the study of ageing [505, 506, 657]. In particular, the understanding of mechanisms governing the physiological maintenance and activation of these cells is pivotal in the further investigation of their deregulation in ageing [505, 506, 657]. While the main intrinsic and extrinsic regulators of HSCs maintenance have been individuated, the understanding of their crosstalk and regulatory mechanisms is still far from being unravelled. [700]. In the present work, the mechanisms governing HSC maintenance together with the age-related NF-kB pathway [89, 358] were investigated.

3.1.1 *The homeostatic maintenance of HSCs*

HSCs are characterised by the ability to self-renew, to expand their own pool, and to generate differentiated blood cells for the entire lifespan of an organism [61, 496, 557, 623]. Under homeostatic conditions, HSCs are maintained as a quiescent population of cells that can be activated in the presence of external upcoming stimuli from the bone marrow niche [48, 88, 159, 489]. This dormant state is believed to contribute to the long-term preservation of HSCs and is a result of a crosstalk between intrinsic regulators and niche signals [27, 682]. Fine-tuning of dormancy the awakening of HSCs is of crucial relevance for correct hematopoiesis. In fact, not responsive dormant HSCs would cause hematopoietic failure, while highly active HSCs would lead to the exhaustion of the population [697]. As a result, alteration of these responses is also involved in ageing and leukemia development [505, 506, 657].
The maintenance of HSCs is obtained by the regulation of their cell cycle, metabolism, and survival activities [27, 682, 697]. Crucial regulators of quiescence such as TP53, Polycomb ring finger protein (BMI1), ATM, mTORC1, and ROS have been identified [89, 358, 355]. In particular TP53, previously widely linked to damage response and survival [419, 643, 671], has been shown to have a homeostatic role in HSCs maintenance by promoting their quiescence [161, 376]. However, mechanisms and crosstalk governing the switch from dormant quiescent HSCs (or LT-HSC) to activated and more prone to enter the cell cycle HSCs (or short term HSCs (ST-HSC)) are largely still unknown [27, 682].
Besides intrinsic factors, HSCs are regulated by the signals from the bone marrow niche. The niche is defined as the specialised bone marrow environment where the HSCs reside [565]. Classically, two types of niches have been individuated: the endosteal and the vascular ones. The endosteal niche is responsible for the maintenance of quiescence and is composed mainly of osteoblastic lineage cells. In this context, hypoxic condition and signals promoting quiescence such as Transforming growth factor beta (TGF-β) set HSCs to a dormant state [182, 199, 278, 329, 621, 672, 750]. On the other hand, the vascular niche (characterised principally by endothelial and stromal cells) creates a milieu that supports proliferation, differentiation, and trans-endothelial migration of HSCs [182, 199, 278, 329, 621, 672, 750]. Here, higher oxygen concentrations and cycling stimulating signals such as Stem cell factor (SCF), Fibroblast growth factor (FGF), and other growth factors are mostly present. Overall, these signals stimulate HSC activation and cycling [366, 104]. Nevertheless, the exact components in terms of cellular compositions of the bone marrow niche are still under investigation [170].
To investigate the mechanisms governing HSCs maintenance and in particular their exit from quiescence, the intrinsic and extrinsic regulators of HSCs were integrated

in a Boolean network model. The established model (Table 1) comprises the three main axis of HSCs physiologic maintenance (cell cycle, metabolism, and survival), together with their crosstalk regulations (Figure 14). Extrinsic stimuli from the niche have been summarised as quiescence signals regulating cell cycle inhibitors, or as cycling signals activating the Rat sarcoma protein (RAS)/ Phosphoinositide 3-kinase (PI3K) axis. In total, the network consists of 37 nodes and 78 regulatory interactions (Figure 14).

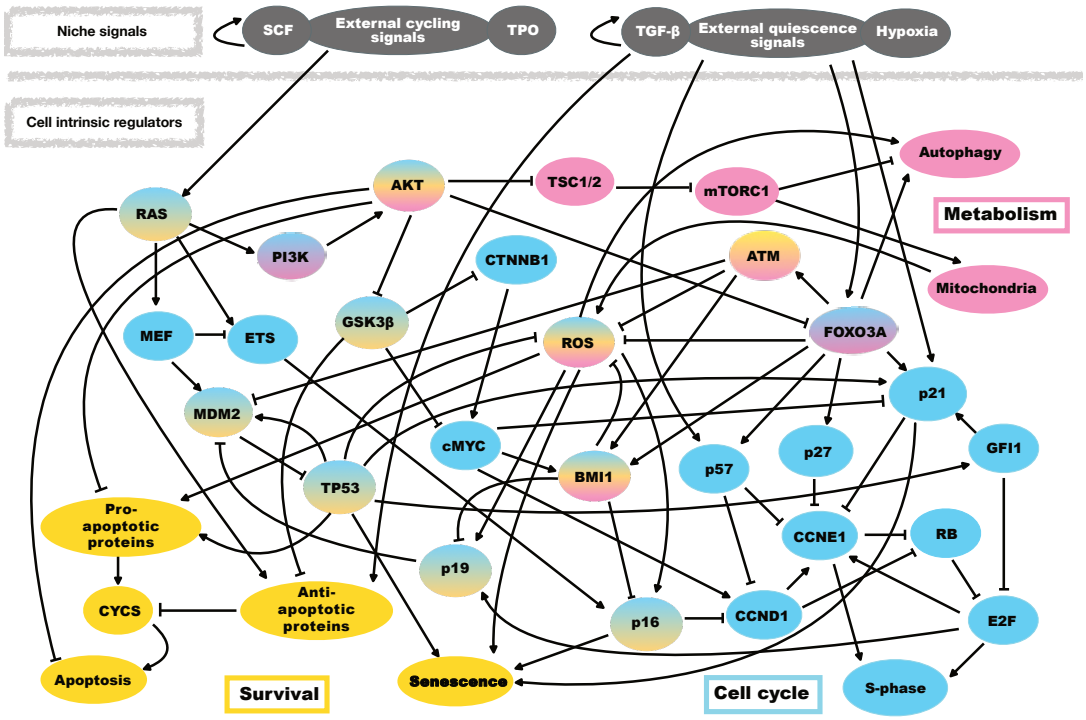


Figure 14: **Interactions within the HSC maintenance network.** External niche factors as well as regulations within the hematopoietic stem cells are summarised within one model. Regulatory activating interactions are depicted by arrows while bar-headed lines represent inhibiting regulations. Affected mechanisms and involved proteins are separated by colours. Niche upcoming signals are reported on top of the figure and are separated from the cell intrinsic regulations. The figure has been modified from Ikonomi et al. [254], licensed under CC BY 4.0, https://creativecommons.org/licenses/by/4.0/.

Table 1: Boolean functions of the HSC model and their descriptions modified from Ikonomi et al. [254], licensed under CC BY 4.0, https://creativecommons.org/licenses/by/4.0/. All proteins are abbreviated in accordance with the current nomenclature. Logical connectives are depicted by & (=AND), | (=OR), and ! (=NOT).

	Node; $t+1$	**Boolean network function;** t	**Description**
Inputs	External quiescence signals	External quiescence signals	TGF-β and hypoxia are the most prominent for promoting quiescence in HSC [41, 142, 494, 496, 558, 620].
	External cycling signals	External cycling signals	SCF and thrombopoietin (TPO) are widely studied for maintenance of HSC self renewal and cell cycle entry [144, 300, 336, 349, 399, 496, 499, 660].
Metabolism	PI3K	RAS	PI3K is a common activated downstream target of RAS [95, 233, 399].
	TSC1/2	¬AKT	Protein kinase B (AKT) inhibits TSC1/2 [399, 496, 682].
	mTORC1	¬TSC1/2	TSC1/2 inhibits activation of mammalian target of rapamycin complex 1 (mTORC1) and thereby cellular metabolism and cellular growth [382, 399, 496, 682].
	FOXO3A	External quiescence signals ∧ ¬AKT	Forkhead box O3 (FOXO3A) expression is directly triggered by hypoxic conditions, here summarised as external quiescence signals [28, 620]. The main described inhibitory regulation of FOXO3A protein is through AKT which leads to its phosphorylation, export from the nucleus by 14-3-3 proteins and loss of downstream transcription of target genes [54, 55, 399, 619, 620].

Table 1: Boolean functions of the HSC model and their descriptions modified from Ikonomi et al. [254], licensed under CC BY 4.0, https://creativecommons.org/licenses/by/4.0/. All proteins are abbreviated in accordance with the current nomenclature. Logical connectives are depicted by & (=AND), | (=OR), and ! (=NOT).

	Node; $t+1$	**Boolean network function;** t	**Description**
Metabolism	ATM	FOXO3A	In HSC, ATM expression and protein activity is dependent on the transcription factor FOXO3A [715].
	Mitochondria	mTORC1	Mitochondria activity and number are increased during cell growth by mTORC1 signalling [84, 173, 283, 382, 727].
	ROS	Mitochondria $\vee \neg$ATM $\vee \neg$ FOXO3A $\vee$ $\neg$BMI1 $\vee \neg$TP53	Increase of ROS levels are caused by cell activated metabolism via mitochondrial biogenesis, where the cellular metabolism naturally shifts to the oxydative one [84, 382]. FOXO3A, ATM, and TP53 independently repress ROS by inducing the expression of anti-oxydant enzymes [262, 263, 382, 433, 567, 620, 646, 647, 715]. Alternatively, loss of BMI1 can impair mitochondrial activity and aberrantly increase the ROS levels. [2, 372, 487, 516, 567].
	Autophagy	FOXO3A $\wedge$ ROS $\wedge \neg$ mTORC1	FOXO3A set up in HSC the correct program for an autophagic response which is triggered by presence of high ROS and absence of growth signals, like active mTORC1 [382, 399, 433, 443, 680, 681].

Table 1: Boolean functions of the HSC model and their descriptions modified from Ikonomi et al. [254], licensed under CC BY 4.0, https://creativecommons.org/licenses/by/4.0/. All proteins are abbreviated in accordance with the current nomenclature. Logical connectives are depicted by & (=AND), | (=OR), and ! (=NOT).

	Node; $t+1$	**Boolean network function;** t	**Description**
Cell cycle	RAS	External cycling signals	Different cycling promoting signals can trigger the activation of the RAS/PI3K [144, 300, 349, 496, 660].
	ETS	$RAS \wedge \neg MEF$	ETS Proto-Oncogene 1 (ETS) is up-regulated by RAS and inhibited by myeloid elf-1-like factor (MEF) [340, 376, 555].
	MEF	RAS	MEF is activated downstream of RAS [340, 376, 555]
	GSK3β	¬AKT	AKT phosphorylates and inhibits glycogen synthase kinase 3 beta (GSK3β) [399, 405, 496, 682].
	CTNNB1	¬GSK3β	GSK3β phosphorylates and inhibits β-catenin (CTNNB1) [135, 241, 247, 417, 520]
	cMYC	$CTNNB1 \wedge \neg GSK3\beta$	MYC protoncogene (cMYC) is regulated by CTNNB1 [417, 452, 698]. Moreover, stability of cMYC is impaired by phosphorylation from GSK3β [413, 520, 710].

Table 1: Boolean functions of the HSC model and their descriptions modified from Ikonomi et al. [254], licensed under CC BY 4.0, https://creativecommons.org/licenses/by/4.0/. All proteins are abbreviated in accordance with the current nomenclature. Logical connectives are depicted by & (=AND), | (=OR), and ! (=NOT).

	Node; $t+1$	**Boolean network function;** t	**Description**
Cell cycle	BMI1	cMYC $\vee$ (FOXO3A $\wedge$ ATM)	BMI1 is highly expressed in all the HSC populations, indipendently from their activation status [489, 496]. MYC positively affects transcription of BMI1 [204, 282, 509, 517]. FOXO3A also up-regulates the transcription of BMI1 through Cbp/p300-interacting transactivator 2 (CITED2) [28, 87, 620]. Additionally ATM can preserve the stability of BMI1 by controlling the level of stressors (ROS), as shown in ATM -/- mouse models [262, 263, 310, 647, 715]. Given that FOXO3A directly regulates the activation of ATM [262, 263, 310, 647, 715], these two compounds are assumed to work on the same axis of regulation. MYC is hypothesised to be responsible of BMI1 activity during active cycling.

Table 1: Boolean functions of the HSC model and their descriptions modified from Ikonomi et al. [254], licensed under CC BY 4.0, https://creativecommons.org/licenses/by/4.0/. All proteins are abbreviated in accordance with the current nomenclature. Logical connectives are depicted by & (=AND), | (=OR), and ! (=NOT).

	Node; $t+1$	**Boolean network function;** t	**Description**
Cell cycle	MDM2	$(TP53 \vee MEF) \wedge \neg p19 \wedge \neg ATM$	Mouse double minute 2 (MDM2) is transcriptionally activated by TP53 [224, 226, 242, 335, 380, 438, 485, 493, 585, 596]. Additionally, the transcription of MDM2 is independently sustained from MEF [340, 376, 555]. p19Arf (p19) competes with MDM2 for the binding TP53, thus preventing its inactivation [620, 585, 587]. ATM can phosphorylate both TP53 and MDM2 destabilising their binding and thus preserving TP53 being inactivated [294, 416, 427, 585, 715]
	TP53	$\neg$MDM2	MDM2 inhibits TP53 activity through binding to its transactivation site or acting as a E3 ubiquitin ligase and inducing proteosomal degradation [1, 2, 226, 242, 335, 376, 438, 485, 493, 585, 596].
	p57	External quiescence signals $\vee$ FOXO3A	Cyclin-dependent kinase inhibitor 1C (p57) is the only member of the KIP family induced by TGFβ, which is a quiescence inducing signal [41, 496, 558, 722, 720]. Moreover, FOXO3A can also induce expression of p57 [433, 496, 722, 720].

Table 1: Boolean functions of the HSC model and their descriptions modified from Ikonomi et al. [254], licensed under CC BY 4.0, https://creativecommons.org/licenses/by/4.0/. All proteins are abbreviated in accordance with the current nomenclature. Logical connectives are depicted by & (=AND), | (=OR), and ! (=NOT).

	Node; $t+1$	**Boolean network function;** t	**Description**
Cell cycle	p21	(TP53 $\vee$ FOXO3A $\vee$ External quiescence signals $\vee$ GFI1) $\wedge \neg$cMYC	Cylcin-dependent kinase inhibitor 1A (p21) is transcriptionally activated by either TP53, FOXO3A, or external quiescence signals [22, 141, 143, 405, 496, 649, 667]. Alternatively, p21 transcript has shown to be down-regulated after loss of growth factor independent 1 (GFI1) [239, 745]. cMYC is a transcriptional repressor of p21 [26, 452, 517]
	p27	FOXO3A	FOXO3A is a transcripional activator of Cyclin-dependent kinase inhibitor 1B (p27) [405, 433, 649, 667].
	GFI1	TP53	TP53 regulates the transcription of GFI1 [2, 376].
	RB	$\neg$CCND1 $\wedge \neg$CCNE1	Retinoblastoma protein (RB) family is inhibited by phosphorylation from cyclin D1 (CCND1) and E1 (CCNE1) in a cooperative way. First, CCND1 leads to partial phosphorylation that is enhanced by CCNE1 [496, 586, 636].

Table 1: Boolean functions of the HSC model and their descriptions modified from Ikonomi et al. [254], licensed under CC BY 4.0, https://creativecommons.org/licenses/by/4.0/. All proteins are abbreviated in accordance with the current nomenclature. Logical connectives are depicted by & (=AND), | (=OR), and ! (=NOT).

	Node; $t+1$	**Boolean network function;** t	**Description**
Cell cycle	E2F	$\neg$RB $\wedge$ $\neg$GFI1	RB proteins are a tumour suppressor protein family that inhibits cell checkpoint between gap1 (G1)- synthesis (S)- phase by directly binding E2F or complexing with it to the promote for target genes [186, 496, 586, 636]. Loss of GFI1 causes increase of E2F levels [239, 745].
	CCND1	$\neg$p16 $\wedge$ $\neg$p57 $\wedge$ cMYC	CCND1 activation marks the exit from Go state. CCND1 is inhibited by cyclin-dependent kinase inhibitor 2A (p16) by direct binding and preventing the interaction with cyclin associated kinases (CDK) [47, 489, 496, 586]. Furthermore, CCND1 presence in the nucleus is restricted by p57 which can cause its sequestration in the cytoplasm [410, 636, 764]. Finally, expression of CCND1 is controlled by cMYC [452, 556].
	CCNE1	$\neg$p57 $\wedge$ (($\neg$p21 $\wedge$ $\neg$p27) $\vee$ CCND1) $\wedge$ E2F	Transcription factor E2F (E2F) is the main transcriptional regulator of CCNE1 [489, 496]. p57 is an inhibitor of CCNE1 [636, 489]. The CIP/KIP (p21, p27) family is also responsible for inhibition of CCNE1 [489, 496]. CCND1 can also bind p21 and p27, imparing their binding to CCNE1 and thus promoting its activation [585, 586, 636, 489].

Table 1: Boolean functions of the HSC model and their descriptions modified from Ikonomi et al. [254], licensed under CC BY 4.0, https://creativecommons.org/licenses/by/4.0/. All proteins are abbreviated in accordance with the current nomenclature. Logical connectives are depicted by & (=AND), | (=OR), and ! (=NOT).

	Node; $t+1$	**Boolean network function;** t	**Description**
	S-phase	$E2F \wedge CCNE1$	Activation of CCNE1 and E2F induce the entry into the S-phase of the cell cycle [221, 496, 585].
Survival	AKT	PI3K	PI3K activates AKT by phosphorylation [399, 496, 682].
	p19	$(E2F \vee ROS) \wedge \neg BMI1$	p16 and p19 are expressed by the same gene locus. BMI1 represses the expression of p19 [265, 354, 487, 567]. E2F induces instead its transcription [380, 585, 762]. Similar effects are shown in ROS presence. [262, 263, 354, 382, 388, 447, 487, 577, 585, 620]
	p16	$(ETS \vee ROS) \wedge \neg BMI1$	BMI1 represses the expression of p16 [265, 354, 487, 516, 567]. ETS can induce the expression of p16 [555]. Alternatively, oxydative stress can upregulate p16 [262, 263, 382, 388, 447, 577, 620].
	Pro-apoptotic proteins	$ROS \wedge TP53 \wedge \neg AKT$	Pro-apoptotic proteins are expressed in the presence of high levels of ROS and cellular stress mainly by TP53. The main pro-apoptotic protein that is regulated by TP53 is Puma [22, 462, 485, 510]. AKT can inhibit pro-apoptotic proteins by phosphorylation [283, 301, 606].

Table 1: Boolean functions of the HSC model and their descriptions modified from Ikonomi et al. [254], licensed under CC BY 4.0, https://creativecommons.org/licenses/by/4.0/. All proteins are abbreviated in accordance with the current nomenclature. Logical connectives are depicted by & (=AND), | (=OR), and ! (=NOT).

	Node; $t+1$	**Boolean network function;** t	**Description**
Survival	Anti-apoptotic proteins	$(RAS \vee \text{External quiescence stimuli}) \wedge \neg GSK3\beta$	The B cell lymphoma 2 (BCL2) and induced myeloid leukemia cell differentiation protein (MCL1) are anti-apoptotic proteins studied in HSCs [62, 183, 220, 325, 474, 501, 662, 675, 733]. They are activated either downstream of RAS activation or by cell contact to the osteoblastic niche [62, 183, 220, 325, 474, 501, 662, 675, 733]. GSK3β destabilises MCL1 by mediating its phosphorylation [413, 417, 436, 677].
	CYCS	Pro-apoptotic proteins $\wedge$ ¬Anti-apoptotic proteins	Release of cytocrome C (CYCS) depends on the balance between pro- and anti-apoptotic proteins [136, 470, 476].
	Apoptosis	$CYCS \wedge \neg AKT$	The release of CYCS causes activation of effector caspases and apoptosis [136, 470, 476]. AKT can phosphorylate and inhibits effector caspases [301, 283, 606].
	Senescence	$(p16 \wedge ROS) \vee (TP53 \wedge ROS \wedge p21)$	Senescence occurs in the presence of aberrant ROS levels which trigger the reactivation of p16 or of the TP53/p21 axis [470, 583, 682]

The exhaustive simulation of the model lead to the identification of four single state attractors (Figure 15). Since the network contains two input nodes (external quiescence and external cycling), each attractor shows a different combination of these nodes. Given that input nodes represent niche stimulations, a condition without the presence of any stimuli from the environment surrounding HSCs is considered not realistic considering the niche context (attractor 1). Therefore, this attractor was excluded for further analyses. Below, the remaining attractors are described. Attractor patterns were compared to experimental evidence on HSCs and each one was assigned to a known phenotype of HSCs. The results of this comparison are described in detail below and shortly summarised in Table 2.

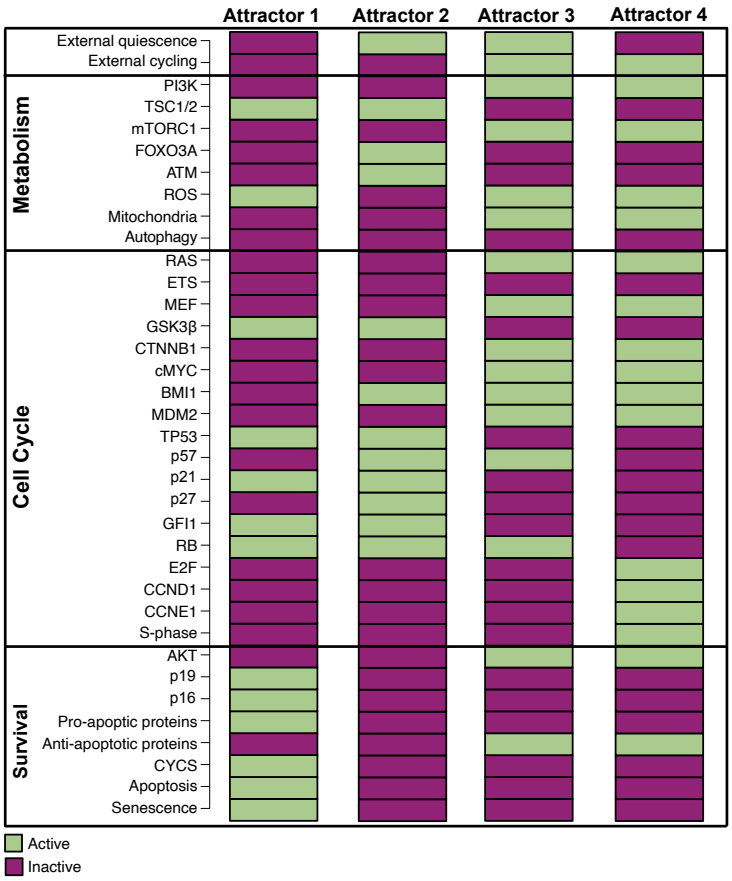


Figure 15: **Attractor landscape of the HSC model** Simulation of the HSC model revealed four attractors that are dependent on the combinations of the two external inputs (external quiescence and external cycling). Components of the model are listed on the left separated into investigated pathways. The state of each component is identified by coloured rectangles. Green indicates active nodes, dark purple denotes inactive ones. The figure has been modified from Ikonomi et al. [254], licensed under CC BY 4.0, https://creativecommons.org/licenses/by/4.0/.

Attractor 2 is affected by quiescent external stimulation, while external cycling factors are absent. This attractor shows neither activation of the cell cycle nor active metabolism or cell growth (Figure 15). Instead, many inhibitors of the cell cycle are active. No apoptosis is observable, although TP53 is active. Pro-apoptotic proteins and ROS that are required for apoptosis induction [136, 470, 476] are inactive. The obtained attractor pattern was matched to the experimental reported activities of quiescent HSCs (or LT-HSCs) (Table 2). The maintenance of low ROS [382, 84, 85], and low metabolic rates via AKT/mTORC1 [33, 63, 84, 85, 267, 382, 523] are pivotal for guaranteeing the HSC quiescence. To this aim, the anti-oxydant activity of FOXO3A, ATM and TP53 is crucial in maintaining such low stress rate [382, 433, 620]. Interestingly, Jang et al. [267] could select for highly dormant HSCs just by sorting HSCs via their ROS levels. The isolated HSCs also showed absence of p16, expression of TP53 and p57 and down-regulated mTORC1 signalling. From the cell cycle enter point of view, quiescent HSCs are reported to have low levels of RAS [181] and low levels of its downstream target MYC, a central stimulator of CCND1 expression, and thus cell cycle entry [63, 161, 698]. Finally, for TP53, a cell-cycle related activity in quiescent HSCs is reported via the induction of GFI1 [161, 376, 485].
Attractor 3 presents the activity of both external stimuli. Similarly to attractor 2, the cell cycle (S-phase) is not active based on these external conditions. Hence, this attractor also depicts quiescent behaviour. However, this time RAS/PI3K signalling as well as mTORC1, ROS, and cMYC are active. Moreover, in the attractor 3, many cell cycle inhibitors (p21, p27, GFI1) and ROS regulators (FOXO3A and ATM) are inactive. Also, apoptosis is still inactive. This might be due to inactive TP53 and the activation of the anti-apoptotic proteins. Activated HSCs are considered still to be quiescent, but they show an increased tendency to enter cell cycle [63]. Attractor 3 was matched with the expression levels of activated HSCs (or ST-HSCs) (Table 2). This is mainly reported to be reached via an activation of metabolic activities via the AKT/mTORC1 axis [33, 63, 84, 85, 267, 382, 523] and loss of cell cycle regulators [161, 496]. Cyclins also start getting expressed, even though cells are still in Go-phase [63]. This is visibile in the attractor patterns via the activation of cMYC, another marker of activated HSCs [63, 161, 698]. Also in the attractor, nevertheless, the S-phase node is not active. This is due to the activity of cell cycle inhibitor p57. Thus, model-based activity is also consistent with experimental observations indicating p57 as the crucial regulator of quiescence in HSC [410, 764, 636, 653], which is maintained by several quiescence-inducing external stimuli [501, 558, 41].
The presence of cycling stimulation regulates attractor 4. Here, proliferative components such as cyclins are active, while cell cycle inhibitors are inactive. Due to S-phase, a cycling HSC phenotype can be assumed [496, 477] (Table 2).

Table 2: **Analysis and comparison of attractor patterns.** The attractor patterns described in the text are listed and divided by analysed processes. For each node activity and experimental evidence was matched. The table has been modified from Ikonomi et al. [254], licensed under CC BY 4.0, https://creativecommons.org/licenses/by/4.0/.

	Process	Attractor activity	Experimentally matched activity	Associated HSC phenotype
Attractor 2	Metabolism	inactive ROS	[63, 84, 85, 267, 382]	Quiescent HSC
	Metabolism	inactive mTORC1	[33, 63, 84, 85, 267, 382, 523]	
	Metabolism	active FOXO3A	[382, 433, 620]	
	Metabolism	active ATM	[382, 433, 715, 620]	
	Cell cycle	inactive MYC	[63, 161, 698]	
	Cell cycle	active TP53	[161, 267, 376, 485]	
	Cell cycle	active p57	[74, 410, 764, 636, 653]	
	Cell cycle	active p21	[161, 496]	
	Cell cycle	active p27	[161, 496]	
	Cell cycle	active GFI1	[376, 485]	
	Cell cycle	inactive S-phase	[477, 496]	
Attractor 3	Metabolism	active ROS	[63, 84, 85, 267, 382]	Activated HSC
	Metabolism	active mTORC1	[33, 63, 84, 85, 267, 382, 523]	
	Metabolism	inactive FOXO3A	[382, 433, 620]	
	Metabolism	inactive ATM	[382, 433, 715, 620]	
	Cell cycle	active MYC	[63, 161, 698]	
	Cell cycle	inactive TP53	[161, 267, 376, 485]	
	Cell cycle	active p57	[74, 410, 636, 653, 764]	
	Cell cycle	inactive p21	[161, 496]	
	Cell cycle	inactive p27	[161, 496]	
	Cell cycle	inactive GLI1	[161, 267, 376, 485]	
	Cell cycle	inactive S-phase	[496, 477]	
Attractor 4	Cell cycle	active CCND1	[496, 477]	Cycling HSC
	Cell cycle	active CCNE1	[496, 477]	
	Cell cycle	active E2F	[496, 477]	
	Cell cycle	active S-phase	[496, 477]	

Model simulations could recapitulate the main behaviours observed in HSCs maintenance from dormancy, to activation, to cycling. In addition, the intrinsic wiring

was shown to respond and adapt to signal stimulations. This supports the consolidated hypothesis that a niche-stem cell crosstalk determines the long-term behaviour of HSCs [27, 682, 697].

3.1.1.1 *From dormancy to cycling - modelling the awakening of HSCs*

After assessing the ability of the model to predict phenotypes of HSCs, the temporal behaviour was studied to unravel regulatory mechanisms governing HSCs awakening. HSCs can be activated upon stimulation to enter the cell cycle transiting from dormancy, to activation, to active cycling [496, 697, 162, 700, 699].

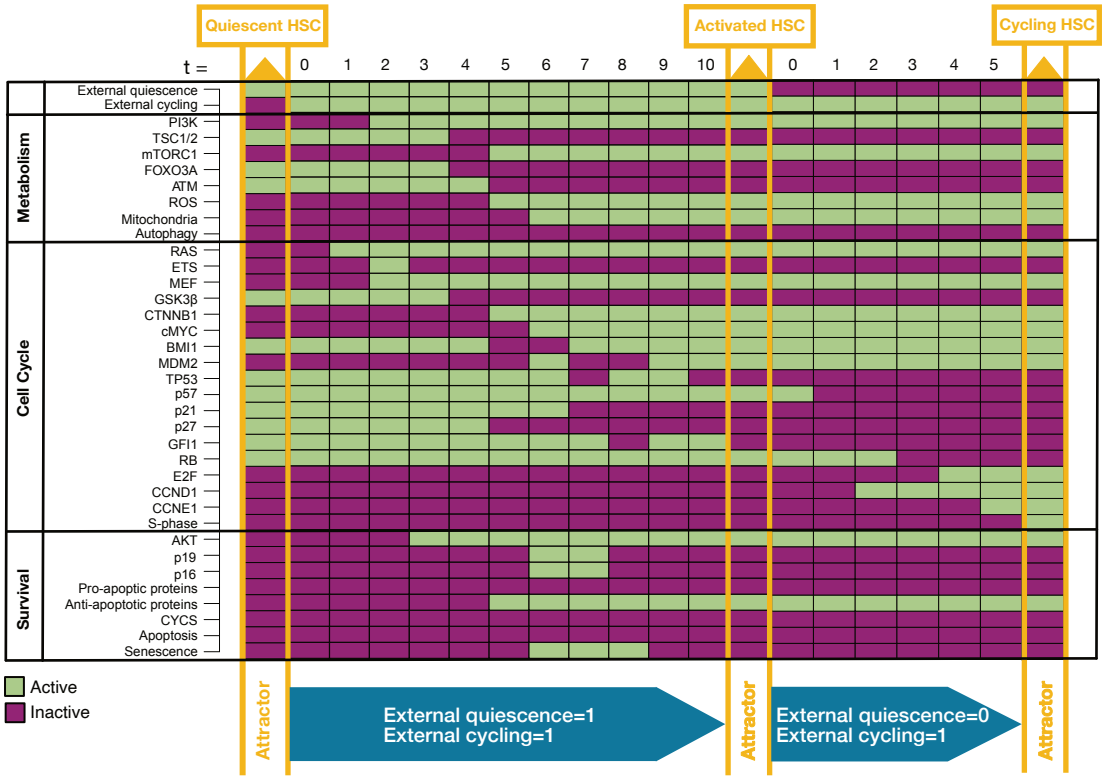


Figure 16: **The HSC progression thorough the different activation stages**. The figure shows the progression from quiescent to activated to cycling HSC depending on the activation of external stimulations. Attractors are highlighted in orange. Activated external stimuli are depicted in blue boxes below. Components of the model are listed on the left separated into pathways. The state of each component is depicted by coloured rectangles. Light green indicates active compounds, dark purple indicates inactive ones. The figure has been modified from Ikonomi et al. [254], licensed under CC BY 4.0, https://creativecommons.org/licenses/by/4.0/.

To correctly depict this process, the retrieved attractors are assumed to depend on each other. Hence, it was investigated whether single HSCs phenotypes could transit into each other by alteration of external niche factors (Figure 16).
To simulate HSC activation, cascades were studied starting from only quiescence stimuli, to combination of quiescence and cycling ones, to only cycling ones.
The cascade simulation of the awakening process was initiated from the dormant HSC matched attractor. The impact of activating both external inputs was studied. The progression towards the attractor took 10-time steps (Figure 16). First, the presence of external quiescent stimuli led to up-regulation of cell cycle inhibitors (p57, p21, p27). The additional presence of the external cycling stimuli induced a stabilisation of RAS and PI3K signalling (time step zero to four). The stabilisation of RAS and AKT induced the activation of cMYC by down-regulation of GSK3β. In turn, cMYC led to loss of cell cycle inhibitor p21 (time step three to seven). On the other hand, AKT activity induced mTORC1 signalling and repressed FOXO3A (time steps three to seven). Hence, the activation of mTORC1 directly activated mitochondria and the production of ROS. ROS activation got further sustained by FOXO3A inhibition and, consequently, ATM (time steps three to seven). Loss of ATM in the absence of p19 stabilised MDM2 that, in turn, down-regulated TP53 and its downstream target GFI1 (time steps six to ten). The stabilisation of active MDM2 gets further maintained by the activation of MEF in response to RAS activation (from time step 2). The described cascades converged onto the attractor depicting an activated HSC. This cascade, including both external niche factors, shows a destabilisation of TP53 based on the activity of RAS/AKT and their downstream regulated compounds.
Starting from this attractor, the system was simulated by removing the external quiescence stimuli starting from the activated HSC attractor. This time the attractor depicting a cycling HSC is reached in 5-time steps. Due to the lack of the external quiescence input, the simulated cascade resulted into the cycling HSC attractor. In particular, the lack of active cell cycle inhibitors induced the regulation of RB, CCND1, CCNE1, and finally to the activation of the S-phase entry (time steps one to four). Once the S-phase node is activated, the phenotype is considered to represent an active cycling activity.
In addition, the possibility that a strict change of environment could induce a direct transition from dormancy to cell cycle entry is hypothesised. Such situation is correlated to stress hematopoiesis, such as a response to injury or infection [29]. Here, an increased onset of inflammatory signal triggers a quick and consistent activation of quiescent HSCs [170]. The simulation was performed by inducing directly the activation of external cycling stimuli starting from the quiescent LT-HSC attractor (Figure 17). Again, the system ends into the cycling HSC attractor following a similar cascade to the one described above. In fact, the simulation transits from a set of

states similar to the ones depicting an activated HSC (time steps eight to nine). This result also hints to a certain preserved continuity in HSCs regulation and activation levels.
The analysis of network-based cascades indicates a dependency of HSCs from niche factors. This influence is transmitted downstream to the intrinsic wiring of the system. Here, model-based simulations could show switching activity between HSC entities governed by a crosstalk among different pathways (Figure 16, Figure 17).

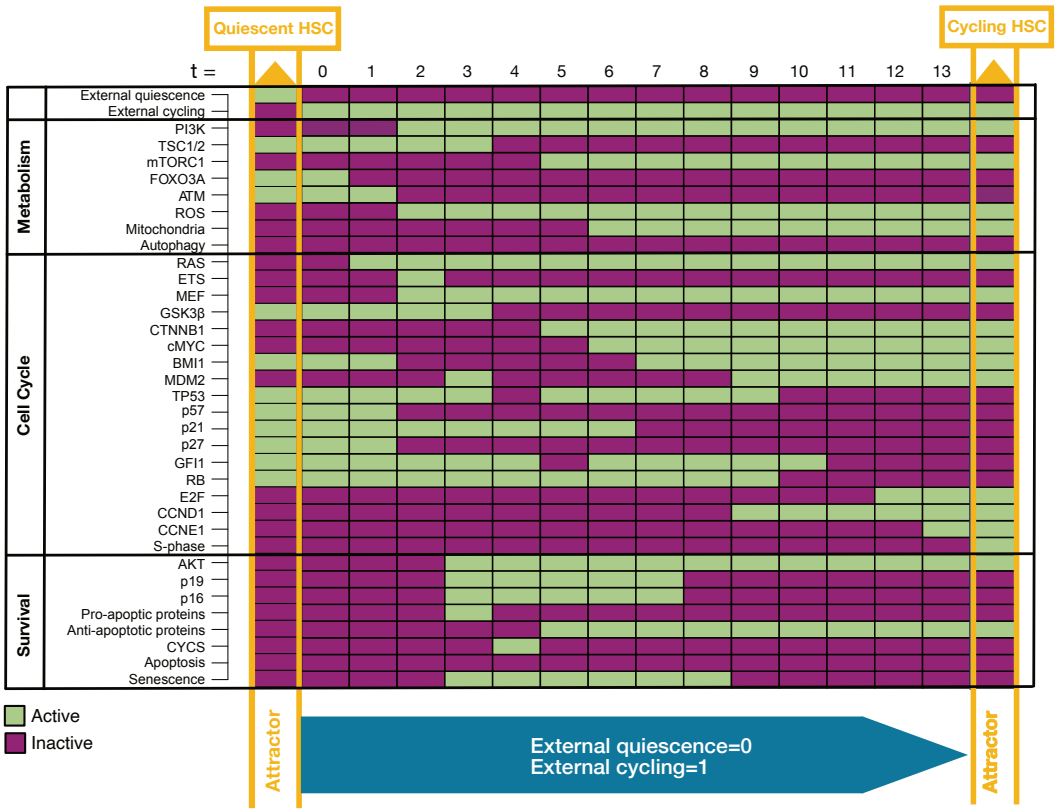


Figure 17: **Direct activation of dormant HSCs**. The figure shows the progression from a quiescent to a cycling HSC depending on the activation of external stimulations. Attractors are highlighted in orange. Activated external stimuli are depicted in blue boxes below. Components of the model are listed on the left separated into pathways. The state of each component is depicted by coloured rectangles. Light green indicates active compounds, dark purple indicates inactive ones. The figure has been modified from Ikonomi et al. [254], licensed under CC BY 4.0, https://creativecommons.org/licenses/by/4.0/.

3.1.1.2 *Balancing quiescence - a novel mechanism in maintaining HSCs*

Different regulators have been reported to be involved in the maintenance of HSC quiescence. While their phenotypical effect on the activity of HSC populations is

described, mechanisms balancing these behaviours are still to be clarified. In particular, certain proteins involved in HSC maintenance intensely crosstalk and play an essential role in both HSC activation and survival. A central example of such regulators is TP53. TP53 activity is known to be down-regulated by MDM2 and is mainly known for its involvement in cellular survival [279, 440, 514]. Furthermore, MDM2 expression is triggered by TP53 itself, setting a negative feedback loop in its own regulation [279, 440, 514]. Nevertheless, this classic view on TP53 is assumed to be somehow uneven in HSCs to allow a certain level of TP53 activity connected to the maintenance of quiescence. In the cascade simulations (Figure 16, Figure 17), alterations in TP53 regulation could be observed while moving from one HSC activation state to the other. In fact, in dormant quiescent HSCs the activity of TP53 is maintained through a FOXO3A-ATM axis that destabilises MDM2 activity. In activated HSCs, instead, external cycling signals cause an up-regulation of the RAS/PI3K axis. This activation has two major effects that ultimately down-regulate TP53. First, AKT activation causes a down-regulation of FOXO3A and ATM (Figure 16). Second, RAS activation up-regulates MEF, a transcriptional activator of MDM2. As a result, MDM2 and TP53 as well as its downstream target the cell cycle inhibitor GFI1, eventually are down-regulated. Model-based results suggest that TP53 activity in steady state conditions is balanced by a crosstalk of intrinsic and extrinsic factors, finely tuning its activity in the regulation of HSC quiescence.
The hypothesised mechanism of TP53 regulation was further investigated by performing *in silico* knockouts on the model. In the following paragraphs, model perturbations will be compared to phenotypes of mouse models. To verify the model prediction power, the general long-term behaviour and the impact on TP53 was assessed.

3.1.1.3 *FOXO3A and ATM knockouts: the guardians of ROS maintenance*

FOXO3A and ATM are two major regulators of ROS in quiescent HSCs [27, 382]. Mouse models for FOXO3A knockout [404, 646, 647, 715] and ATM knockout [262, 263, 404, 465] show increased ROS, p19, and p16 levels in the HSC compartment, affecting the HSC quiescence and survival. This leads to impaired self-renewal and repopulation ability of the quiescent LT-HSCs. However, it a normal differentiation in hematopoiesis is still observable [262, 263, 404, 646, 647, 715].
The observed phenotypes described in the mouse models could be matched to the perturbed attractors for FOXO3A and ATM (Figure 18). The quiescent HSC attractor shows senescence and apoptosis activation and increased ROS levels due to the activation of p16 and p19. In particular, activation of p19 sustains TP53 activation. The latter, in the presence of ROS, can trigger apoptosis and senescence.

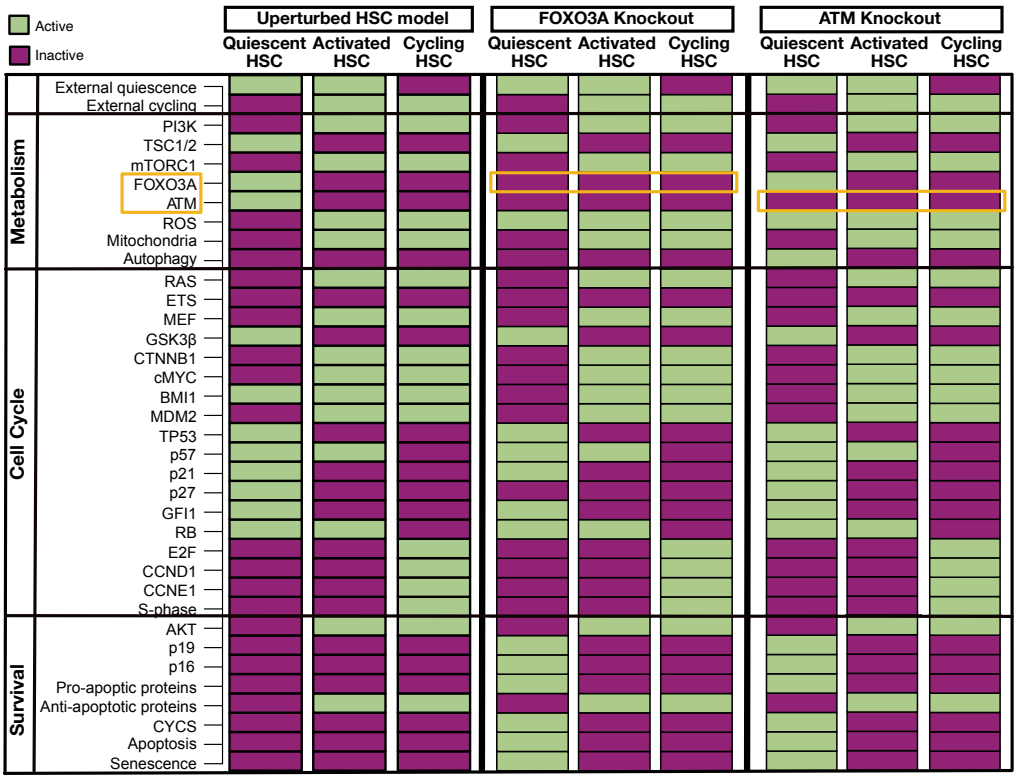


Figure 18: **Knockout phenotypes of ATM and FOXO3A.** An *in silico* knockout of FOXO3A or ATM increases ROS levels but only induces apoptosis and senescence in the quiescent HSC attractor. Proteins are listed on the left with their pathway affiliations. For comparison, the attractors of the unperturbed network are reported on the left. The state of each protein is represented by colored rectangles. Activity is represented in light green and inhibition in dark purple.The figure has been modified from Ikonomi et al. [254], licensed under CC BY 4.0, https://creativecommons.org/licenses/by/4.0/.

The attractor characterising the activated HSCs is less affected by the perturbation. Additionally, the cycling HSC attractor is not altered. This result is also in line with the mechanisms shown in the cascade analysis (Figure 16). In fact, model-based predictions showed that FOXO3A and ATM are already inactivated in activated HSC after activation of PI3K/AKT signalling. This model-based result might explain the normal hematopoiesis seen in the FOXO3A and ATM mouse models [262, 715]. Moreover, in the FOXO3A depleted mice, it was shown that the depletion of the HSCs comes from the dormant LT-HSC population [715], again supporting the model predictions.

3.1.1.4 *BMI1 knockout: the gatekeeper of self-renewal*

BMI1 is a crucial regulator of self-renewal and is stably expressed in the HSC compartment [372, 487, 516]. In accordance, the BMI1 knockout in mice shows a huge effect on the phenotype, leading to defect in self-renewal, depletion of the HSC compartment, and shortened life-span [372, 487, 516]. This effect is accompanied by increased ROS levels and increased p16 and p19 expression, which eventually induces apoptosis and senescence [372, 487, 516].
These phenotypical traits are also observable in the perturbed attractor patterns. Here, BMI1 loss induces a substantial impairment of cell cycle entry for the HSCs in all obtained attractors (Figure 19). All attractors show senescence, and the quiescent HSC attractor shows also apoptosis. The attractor depicting the cycling HSCs does not have an activation of S-phase. Based on the model-hypothesised regulatory mechanism (Figure 16), loss of BMI1 would directly affect p16 and p19 upregulation, causing impaired quiescence and activation among the three HSC phenotypes.
Various possibilities to partially rescue the phenotype of BMI1 loss have been suggested. One of these is the loss of TP53 which is reported to rescue the apoptotic phenotype [6, 682]. This result is confirmed in the model simulations when TP53 is perturbed together with BMI1 (Figure 19). Again, these simulations confirm that an increase of ROS and p19 activate TP53 and direct its activity towards pro-apoptotic behaviour.

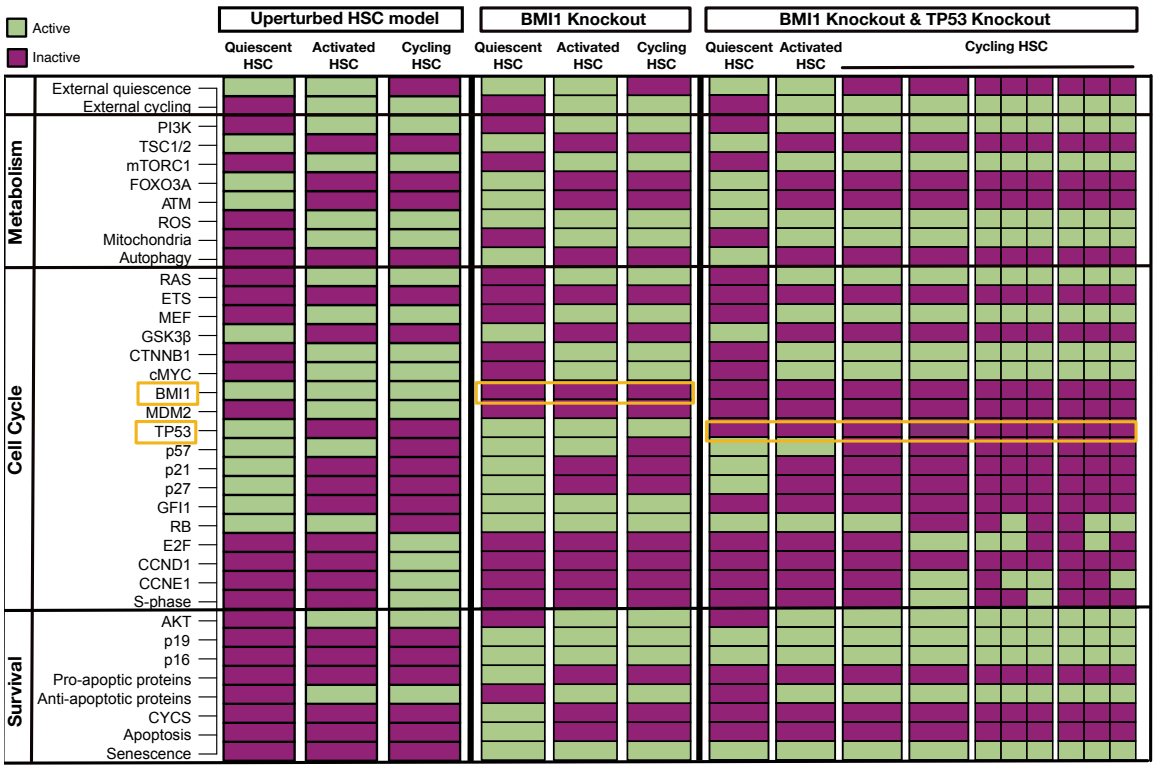


Figure 19: **BMI1 loss impairs self-renewal** (left part). An *in silico* knockout of BMI1 impairs cell cycle entry for all HSC populations. Proteins are listed on the left with their pathway affiliations. TP53 partially rescues a BMI1 knockout (right part). An *in silico* knockout of BMI1 and TP53 rescues the impact of a loss of BMI1 by impairing apoptosis. For comparison, the attractors of the unperturbed network are reported on the left. Proteins are listed on the left with their pathway affiliations. The state of each protein is represented by coloured rectangles. Activity is represented in light green and inhibition in dark purple. The figure has been modified from Ikonomi et al. [254], licensed under CC BY 4.0, https://creativecommons.org/licenses/by/4.0/.

3.1.1.5 *TP53 and MEF knockouts: the perturbation of quiescence*

TP53 knockout has any major implications on hematopoiesis in mice [2, 376, 485, 634]. However, the concomitant loss of GFI1 after TP53 gives an advantage in competitive assays due to a less regulated quiescent state [2, 376, 485, 634]. A matching attractor pattern is observable in the *in silico* simulation with no significant induction of apoptosis (Figure 20). Moreover, also in the quiescent HSC attractor GFI1 gets inactivated. The inactivation of GFI after TP53 was observed also in the cascade investigation (Figure 16). Hence, the perturbed quiescent HSC TP53 knockout attractor matches partially with the unperturbed activated HSC one (Figure 16). In addition, the TP53 perturbed attractor pattern

shows the increase of ROS, in line with literature results [370]. The activation of ROS in HSCs has also been connected to a more active state, prone to enter the cell cycle [27, 382] further sustaining the correctness of the retrieved attractor pattern.

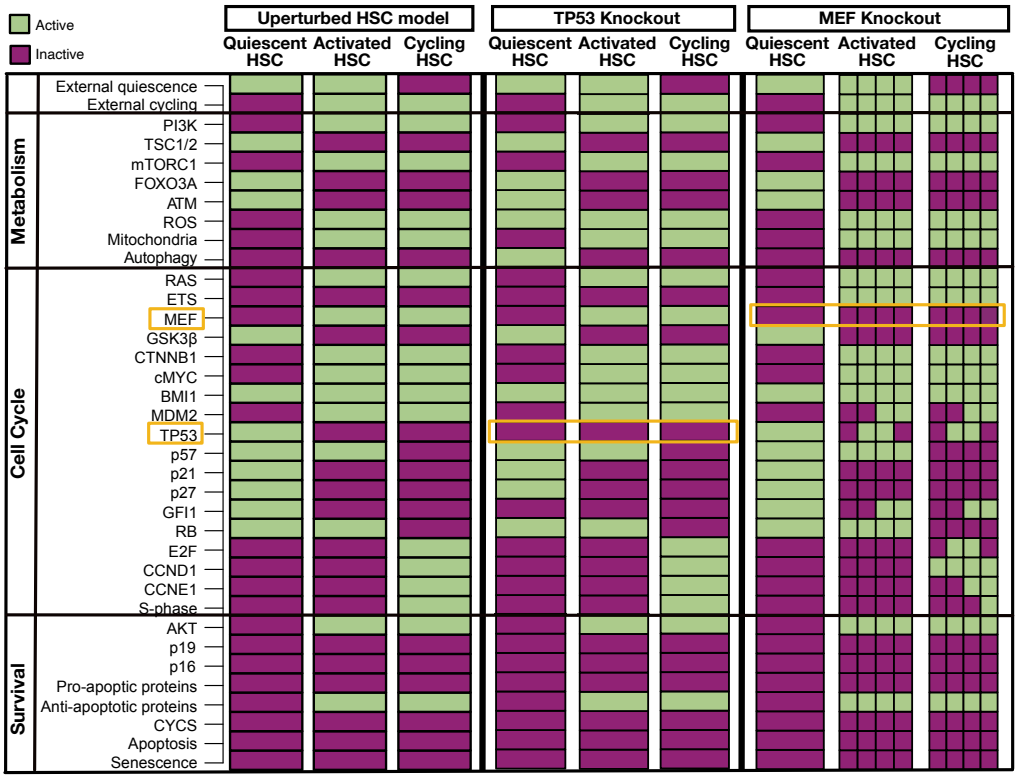


Figure 20: **TP53 and MEF knockouts.** TP53 knockout has minor impact on the HSC populations. An *in silico* knockout of TP53 causes loss of GFI1 in quiescent HSCs and increased ROS levels. ST-HSC and cycling ones are not impacted. MEF knockout stabilises TP53. An *in silico* knockout of MEF stabilised TP53 and enhanced quiescence. Here, the ST-HSC and the cycling HSCs show a sustained activity of GFI1 and cycling HSCs are impaired in entering S-phase. For comparison, the attractors of the unperturbed network are reported on the left. Proteins are listed on the left with their pathway affiliations. Proteins are listed on the left with their pathway affiliations. The state of each protein is represented by coloured rectangles. Activity is represented in light green and inhibition in dark purple. The figure has been modified from Ikonomi et al. [254], licensed under CC BY 4.0, https://creativecommons.org/licenses/by/4.0/.

After accessing the loss of TP53, the effects of its over stabilisation were also analysed (Figure 20). The results were compared to a mouse model causing MDM2 down-regulation via MEF deletion [340, 376]. MEF knockout mice show a stabilisation of TP53 connected to an enhancement of quiescence [340, 376]. Likewise,

the attractor describing a cycling HSC showed enhanced quiescence due to loss of S-phase. In accordance also the activated HSC attractor shows now TP53 and GFI1 activity. Hence, the stabilisation of homeostatic TP53 is hypothesised to affect the transition from one HSC phenotype to another, mainly by the maintenance of GFI1 activity. The unperturbed cascade confirms the depicted behaviour: loss of GFI1 activity happens during the transition between the quiescent and the activated HSC.

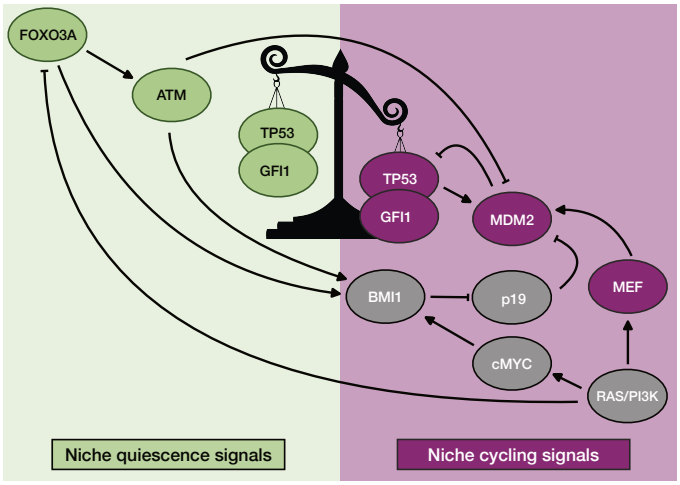


Figure 21: **General description of TP53 and quiescence regulation in HSC.** Homeostatic activity of TP53 is promoted by ROS regulators ATM and FOXO3A. Unbalance of TP53 activity is promoted by MEF that stabilises the transcription of MDM2. Furthermore, the unbalanced activity of TP53 is maintained by niche regulation: quiescence promoting environment favours ROS regulators; Cycling promoting environment promotes MEF expression. The figure has been modified from Ikonomi et al. [254], licensed under CC BY 4.0, https://creativecommons.org/licenses/by/4.0/.

The HSC maintenance model could recapitulate the phenotype observed in a variety mouse models. Moreover, the perturbation results sustain the hypothesis concerning the general mechanism of regulation of TP53 and maintenance in HSCs. When ATM, FOXO3A, or BMI1 are depleted, increased ROS and p19 lead to activation of TP53. This effect switches its activity towards the impairment of cell cycle progression and leads to apoptosis and senescence. In homeostatic conditions, instead, the same regulators guide the TP53 activity towards quiescence by down-regulating ROS and p19. The presented simulations also show and confirm the relevance of the RAS/PI3K axis in down-regulating TP53 in activated HSCs. The loss of MEF down-regulates MDM2 in activated and cycling HSCs. This loss causes an impaired entry in the S-phase despite the presence of external cycling stimula-

tions. The general regulatory mechanism hypothesis based on model simulations is summarised in (Figure 21).

3.1.1.6 *Simulating ageing-towards a systemic view of HSCs ageing*

Ageing is the main risk factor for functional decline of HSCs, defects in immunity, and increased occurence of haematological abnormalities, such as insurgence of blood tumours [170, 420]. The HSC maintenance model was shown to extensively describe and predict the maintenance regulation of HSCs under physiological conditions. For this reason it will also be applied to investigate age-related alterations. To model ageing, three perturbation simulations were performed (Figure 22).
Ageing is widely connected with an increase of inflammation [122, 170, 420], hence the first setup simulated a knockin of the ROS stressors in the system (Figure 22). The resulting perturbed attractor pattern shows increased apoptosis and senescence in the quiescent HSC population. In particular, the attractor pattern shows activation of pro-apoptotic proteins, and p19. Results from HSCs models in age-related dysfunctions such as telomere shortening also report an increase of apoptosis driven by activation of p19 and p53 up-regulated modulator of apoptosis (PUMA) [435, 530, 714, 751]. In addition, apoptosis is partially observed in aged bone marrow populations [468], whereas elderly human HSCs up-regulate genes associated with DNA repair and cell death [484]. This increased expression of apoptotic markers during ageing was also recently observed by Zeng and colleagues [747] when analysing different subpopulations of murine HSCs single-cell transcriptomic profiles. Moreover, a switching role of TP53 in ageing conditions under stress towards apoptosis induction is observed in HSCs [272, 280, 281]. On the other hand, the attractors depicting activated and cycling HSCs are not altered. This suggests that niche signals might counteract the increase of stressors observed in ageing. Especially, based on the regulatory mechanisms governing the HSC model, this might be driven by pro-survival and proliferation signals.
Additionally to the increase of inflammation and stress, the stem cell niche is also chronically altered during ageing [170]. Recent studies have shown that ageing involves an increase in adipogenic cells [551], further attributed to a decline in osteogenic cell fate determination [296, 339, 464, 735]. Hence, mesenchymal precursors are assigned to an adipogenic cell fate rather than an osteogenic one [759]. The decline of the osteogenic specification is further accompanied by a remodelling of the niche vasculature, which results enlarged in diameter [545, 659]. This vascular response is also common in acute inflammatory conditions, where again HSCs are found to be more activated [545, 630, 673].

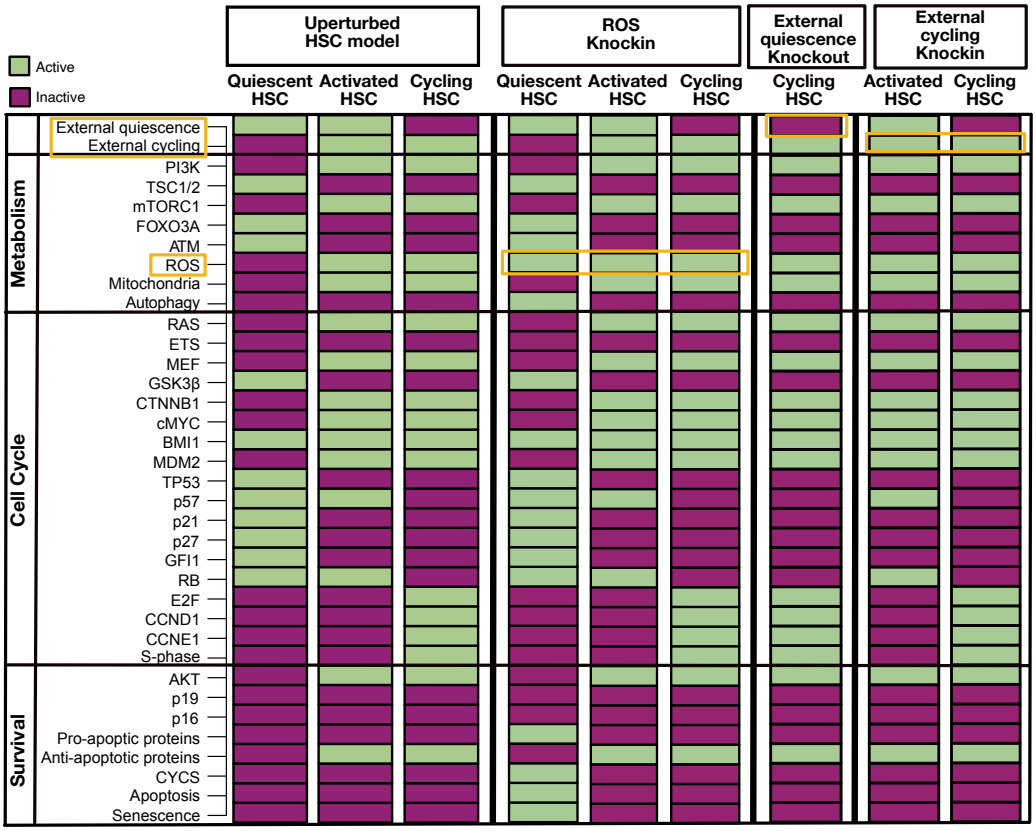


Figure 22: **Ageing simulations on the HSC model.** Different network perturbations aimed at modelling ageing are depicted. The HSCs attractor patterns show in general favoured activities towards activated or cycling HSCs. Finally, in the presence of high uncontrolled levels of stressors (ROS) the quiescent HSC population undergoes senescence and apoptosis. For comparison, the attractors of the unperturbed network are reported on the left. Proteins are listed on the left with their pathway affiliations. Proteins are listed on the left with their pathway affiliations. The state of each protein is represented by coloured rectangles. Activity is represented in light green and inhibition in dark purple.

Altogether, this can be translated within the modelling setting into a general decrease of quiescence signals in favour of cycling inducing ones. This niche remodelling condition is represented in two different experimental setups (Figure 22). On the one hand, quiescence stimuli are knocked out, simulating a complete loss of quiescence promoting niche environment (external quiescence = 0). On the other hand, a milder situation is considered where cycling promoting signals invade the quiescence signalling reserved space, thus causing the presence of a mixed environment (external cycling = 1). The first scenario leads to an attractor pattern that includes only actively cycling HSCs, thus showing a most severe case without any residual quiescent HSC. The second instead, leads to the presence of activated and

cycling HSCs. In both simulation scenarios, the completely quiescent HSC attractor is not present. Interestingly, this time, the rewiring of the niche, while not inducing apoptotic behaviours in the quiescent HSC population, leads to its progression into an activated or cycling HSC. In accordance, one of the most established phenotypical hallmarks of HSC ageing is related to increased number of HSCs together with an increased expression of genes involved cell cycle, myeloid lineage specification, and myeloid malignancies (such as cMYC) [484]. In particular, genes involved in MAPK/ERK are up-regulated [484]. Finally, aged HSCs also show increased metabolic activity [81, 665], which in model-based simulations is concomitant with mitochondrial activity and HSC activation and cycling.
The presented results indicate and match different ageing-related behaviours observed in HSCs. In addition, it is reported that some HSCs are also protected from ageing in particular regions of the niche [545]. This leads to the idea of an heterogeneous spectrum in the ageing activities of HSCs. This heterogeneity is fragmentally captured by the different model simulations that enclose different combinations of possible scenarios. Hence, based on perturbation results, it is hypothesised that all of these possibilities could coexist in a spacial environment of the HSC niche, including unperturbed quiescent HSCs in areas of the niche where physiological stimulations are preserved during ageing too. Such a variety of perturbation possibilities could also explain the long lasting maintenance of HSCs which, even though defective, will not get exhausted before the end of the individual lifespan [122, 170, 420].

3.1.1.7 *Robustness analyses*

Each organism is constantly exposed to environmental stimuli and changes. Nevertheless, biological systems are considered to be robust and are able to adapt to changes [314]. This property was investigated in the HSC model in the form of resistance to noise. As a first measure for robustness, the impact of noise on the state transitions in the model was compared to the response of randomly generated Boolean networks (Figure 23). Noise was simulated using random bit flips. The normalised Hamming distance between the successor states of the original state and the perturbed copy was calculated. Smaller Hamming distance can be interpreted as a better ability to compensate noise. The results show a mean Hamming distance of 0.028 for the constructed HSC model. In contrast, the mean normalised Hamming distance over all random networks is 0.034. The calculated p-value is below 0.0001. Thus, it can be concluded that the established model is significantly more robust to noise than a set of randomly generated networks of the same size (Figure 23). Second, the robustness of the network was computed based on its attractors. Also in this case, their robustness was measured by the addition of noise by random bit flips in their basin of attraction. The simulation

was run in triplicates, flipping 1, 2, and 3 nodes of each random state. The results showed that equal attractors are reached for perturbed and unperturbed states in 95%(±0.0003)/89%(±0.0001)/85%(±0.0005), for the simulation with 1/2/3 random bit flips (reported mean and standard deviation).

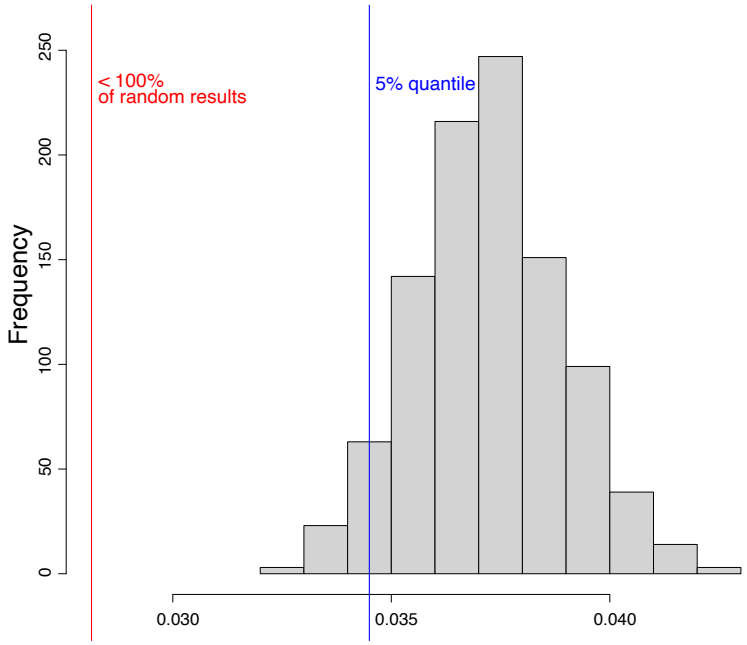


Figure 23: **Robustness analysis.** 1000 randomly drawn states of the HSC model were mutated by bit flip and their successor states were computed. The successor states of the mutated and the original states were then compared using the normalised Hamming distance (red line). The same analysis was performed for 1000 randomly generated networks of the same size (histogram). The blue line shows the 5% quantile. The figure has been taken from Ikonomi et al. [254], licensed under CC BY 4.0, https://creativecommons.org/licenses/by/4.0/

3.1.2 *Discussion – Modelling the HSC maintenance*

3.1.2.1 *The challenges in modelling the HSC behaviour at the niche interface*

The behaviour of HSCs is tightly regulated by an intense crosstalk with the bone marrow niche [170]. The presented model attempts to summarise niche stimulation in the form of inputs, as either quiescent or cycling ones. This choice might be seen an over-simplification of the complex network of signals surrounding the HSC. However, it has been shown that, due to its crucial relevance, HSC maintenance is redundantly regulated by multiple sources. Exemplarily, p57, which is considered the central gatekeeper of quiescence [410, 489, 636, 653, 764], is regulated by a multiplicity of endosteal stimulations including TGF-β, TPO and hypoxia [41, 143, 501, 558]. Following the idea of redundancy, the loss of hypoxic conditions alone will not lead to a complete lack of p57 activity [143]. In the same direction, the loss of single developmental pathways has been shown not to affect HSC maintenance, indicating again that a multiplicity of signals conquer to the same task [391, 392, 240, 177, 285, 473]. An over dissection of the single influence of each external signal might also lead to contradictory results. For example, SCF and TPO have been associated with quiescence *in vivo* [501, 639, 732]. However, these factors are commonly applied to sustain the proliferation and expansion of HSC *in vitro* [145, 172]. This differential behaviour suggests the possibility that cross-regulation among quiescence signals exists. For instance, it has been shown that TGF-β signalling, highly present in the endosteal niche [41, 721], is able to repress the cytokine-induced activation of PI3K by inhibiting the formation of lipid rafts [721]. Hence, while future model developments might pave the way to the possibility of modelling single niche stimulation, the present model is able to successfully represent the HSCs maintenance in light of cumulative stimulations. Other mathematical modelling approaches successfully described HSC differentiation by suggesting cumulative signalling environments [191, 526, 525]. As a result, it is reasonable to consider an environment with predominant quiescence or cycling stimuli.

Model-based simulations showed also phenotypes connected to the co-presence of both quiescence and cycling inducing stimuli, as sort of grey zones with a balance between the two signals (Figure 15, Figure 16). This result is actually in line with different experimentally-derived niche models that suggest activated HSCs to be found in regions of the niche that are boundaries between the two different environments [452, 700]. Murphy et al. [452], describe HSCs able to self-renew and proliferate to be found in the connection between the endosteal and the stromal area of the bone marrow. Also, Trumpp et al. [700, 652] hypothesised a similar regulation, describing the presence of a quiescent compartment reservoir with specialised cells maintaining dormant HSCs. Again, they hypothesise a "self-renewing

endosteal niche" as the one present at the boundaries of this region when HSCs can get activated and more responsive [700, 652].
Another advantage of the dual-input modelling setting is its low number of assumptions. In fact, model-based results implicate that, by simply combining sets of stimuli, new quiescent promoting niche environments in potentially new regions of the bone marrow could be found. This consideration is in accordance with the recent experimental observations that describe the presence of dormant HSCs in lowly oxygenised regions of sinusoids [499, 261].

3.1.2.2 *Balancing quiescence and activation - reconciling the hypotheses of HSC maintenance*

Besides modelling the niche interface, the HSC maintenance network also summarises the intrinsic wiring governing HSCs quiescence and activation. Different phenotypic characterisations of dormant and activated HSC describing differential expression patterns have been published [63, 161, 267, 489, 698]. The model retrieved attractors could match these expression patterns. Moreover, two different mechanisms of quiescence maintenance were suggested based on *in silico* cascades in these two HSC subpopulations.
Model-based regulations indicate that in dormant HSCs quiescence is preserved by a tight regulation of the ROS levels (Figure 16, Figure 21). This is achieved by a combination of intrinsic factors induced by external stimuli. Accordingly, it has been observed that keeping oxidative stress low in quiescent HSC is fundamental for preserving their integrity and survival [267, 382, 620]. In fact, despite the activity of TP53 and the lack of survival stimuli, activation of apoptosis is impaired in model-based results due to the high hampering of cellular stress. Interestingly, it has been shown that HSCs have a high expression of induced MCL1, an anti-apoptotic protein activated in the presence of survival stimuli [474]. This would initially contradict the modelling results, where dormant HSCs are maintained without the activation of survival cycling stimulations. However, this study was performed on the entire subset of HSC (dormant and activated HSCs) and progenitor cells. Similarly, if the the whole attractor landscape is considered, an expression of anti-apoptotic proteins is also observable. Sustaining the model-based hypothesis of maintenance of dormant HSCs, Kobayashi et al. s [323, 324] recently published a study describing the ideal setting for *in vitro* maintenance of quiescent HSCs. In their work, the authors actually show that hypoxic conditions in the presence of minimal residual cytokine stimuli set the best environment for the maintenance of quiescence [323]. For the activated HSC attractor pattern, instead, the increase of ROS caused by metabolic activities is counteracted by activation of survival stimuli via the cycling input. This is in accordance with experimental results indicating that activation of AKT and

mTORC1 signalling triggers cellular metabolism and prompts the HSC to enter the cell cycle [33, 84, 85, 523].
Finally, it could also be shown that dormant and activated HSCs have different responsiveness in terms of time-steps required to enter the cell cycle once stimulated. This is also in line with the observation that actually activated HSCs (or ST-HSCs) are more reactive and can quickly enter the cell cycle [161, 452, 696, 699].

3.1.2.3 *A new regulatory mechanism in HSC maintenance*

Based on the simulation modelling of the progression from a quiescent HSCs towards entry into the cell cycle, a mechanism regulating the homeostatic activity of TP53 was suggested. Here, it was proposed that the awakening of the HSC follows the initial activation of cellular metabolism. This will then induce the rewiring of the intrinsic network of ROS sensors (FOXO3A and ATM) and finally led to a loss of cell cycle regulators connected to quiescence such as TP53, p21, and p27. In the end, with the loss of quiescence signals, the HSC can rapidly enter the cell cycle. Stress sensors have been shown to be fundamental for regulating HSC quiescence [27, 382, 620]. The expression of FOXO3A is directly connected to the hypoxic environment, and this leads in turn to the up-regulation of active ATM [620, 715]. The latter, besides being an independent regulator of cellular stress, is also involved in the activation of TP53 [27, 382, 620, 715]. Thus, the simulations indicate that in the dormant HSC ATM is responsible for the regulation of active TP53. This activation is actually new to the HSC maintenance context, where ATM activity towards TP53 is mainly reported in the survival context [22], as enforced from the fact that ATM seems to be required for TP53 immediate regulation of irradiation in quiescent HSC [330, 435]. Nevertheless, besides its well-defined role in DNA damage response, ATM has already been shown to regulate activation of TP53 under physiological conditions in the context of homeostatic cellular metabolism outside of the HSC context [21]. Here, it has been suggested that activation of TP53 by ATM is involved in the reduction of ROS [21].
Model-based results suggest that in presence of an active metabolic activity and increased ROS levels HSCs get activated (Figure 16, Figure 17). In detail, when RAS and PI3K are activated by external stimuli, FOXO3A is down-regulated by the AKT/mTORC1 signalling potentially also down-regulating ATM. This regulation is in accordance with the fact that in activated ST-HSC, FOXO3A is already excluded from the nucleus of HSCs [715]. Consequently, in this condition, TP53 is mainly regulated by the MEF/MDM2 and the BMI1/p19 axis, as confirmed also by experimental results [1, 376, 682]. These regulators set the down-regulation of TP53 and GFI1 in the progression towards the ST-HSC phenotype. In accordance, TP53 is down-regulated in ST-HSCs [161, 267, 485].

Finally, the modelling results also support the hypothesis that TP53 activity is actually context- and environment-dependent [22], as shown and further enforced by the knockout simulations (Figures 16-Figure 20). The mechanistic hypothesis of the regulatory wiring is further encouraged by the predictive power towards a variety of *in silico* knockouts that can faithfully recapitulate the phenotype of analog mouse models

3.1.2.4 *Modelling ageing - a context and space dependent hypothesis on the heterogeneity of HSCs ageing*

The model results based on ageing reported perturbations showed a potentially multi-faced representation of HSC ageing. In fact, based on different combinations of perturbations to the system the attractor landscape was able to capture different activities reported in the description of the ageing phenotype of HSCs. Interestingly, these results follow again the idea of a "context-dependent" regulation of HSCs.
The over-expression of ROS signals in the model lead to the depletion of the quiescent LT-HSC compartment via apoptosis and senescence activation (Figure 22). Instead, when also niche signals are perturbed in ageing-like condition, while again stressors are up-regulated due to the internal wiring, the quiescent cells results again depleted but this time in favour of their progression towards activated or cycling HSCs (Figure 22). While on the one hand the shown pattern might explain the insurgence of leukaemia in aged individuals due to hyper-activation of HSCs [170], on the other hand the age-dependent alteration in the niche might confer a trade-off mechanism to rescue HSC activity. In support of this model-based hypothesis, Gutierrez-Martinez et al. [208] show that aged HSCs show a diminished apoptotic priming in response to DNA damage due to the down-regulation of ATM signalling. This is actually in line with the simulation setup where niche stimulations are perturbed. Here, TP53 and ATM are down-regulated by survival signals coming from the perturbed niche stimuli. Interestingly, the same authors could show that the apoptotic response rates could be reverted to the young phenotype when aged HSCs are transplanted in young recipient [208]. This condition matches the model simulation in which only ROS stressors are over expressed without altering the niche environment (Figure 22). Here, in response to uncontrolled stress, the HSCs undergo apoptosis (Figure 22). This also indicates, as stated also by the authors [208], that the wiring in the aged context might not completely be cell-autonomous, but rather likely controlled by the niche environment. These results might also explain the rather debated role of cellular senescence in the HSC ageing [122]. Since generally the niche and HSCs are assumed to age in a coordinated manner, this crosstalk might limit the loss of HSCs by stimulating their expansion, as sustained also by niche-driven model simulations (Figure 22). In this scenario, the risk of uncontrolled HSC expansion and consequent potential insurgence of

leukemia would be considered the price to be paid not to loose the HSC compartment. Hence the amount of actually senescent HSCs would be rather limited, as shown by some studies [24, 269].
While sustaining a general hypothesis of co-adaptation of HSC and niche signals during ageing, the different model perturbations setups can be also considered as potentially plausible conditions describing the heterogenous behaviour of aged HSCs. In this context, a set of different perturbations might capture the heterogeneous activity of aged HSCs, thus providing a systems perspective in which niche and HSCs rewind in different scnarios. This process would ultimately give rise to the complexity of the ageing activities in HSCs.

3.1.3 *The NF-κB signalling during HSCs ageing*

Inflammation plays a central role in the ageing process of HSCs [122, 170, 420] and the NF-κB signalling pathway is pivotal in the cellular response to this process [229, 495]. During the immune system ageing, NF-κB increases and influences the differentiation process of HSCs [229, 495]. Here, extended inflammatory signalling causes the massive activation of the NF-κB signalling pathway, priming differentiating cells to the myeloid fate [229, 495]. Nevertheless, little is known about the role of this pathway in the HSCs population [122, 229]. As already shown in the HSC maintenance model (Results Section 3.1.1), the ageing process of HSCs is heterogeneous and complex. While common effects of ageing-related dysfunctions have been identified, not all HSCs are thought to present this loss of function during ageing, which results in a likely heterogeneity of individual aged HSCs in single-cell expression data. For this reason, the NF-κB pathway was further studied using human HSC single-cell expression data [507]. Likely reflecting this heterogeneity, hierarchical clustering and t-SNE procedures on the utilised dataset [507] did not show relevant clustering between young and aged cells (data not shown, reported in Schwab, Ikonomi et al. [570]). Hence, to capture the heterogeneity of the ageing process, the NF-κB pathway alterations during human HSC ageing were investigated with a newly established tailored network reconstruction approach based on human HSC single-cell expression data [507].

3.1.3.1 *A strategy to reconstruct Boolean network ensembles from time series of single-cell data*

Generally, all data-based reconstruction algorithms suffer from the limited number of time points and samples available for network reconstruction typical of biological data [245]. However, in single-cell sequencing data, each sample is described by a potentially large set of single-cell measurements. In the context of HSCs, each sequenced stem cell represents an activation state within the same population. Normally HSCs are divided into quiescent LT-HSCs and activated ST-HSC via fluorescence-activated cell sorting (FACS) analyses based on their membrane markers [613, 162, 309, 4, 77]. As largely shown in the previous sections, these populations of HSCs show different activities in terms of cell cycle, metabolism, and survival statuses. Nevertheless, experimental results, actually show that also within LT- and ST-HSC there is a continuous gradient of activities, showing parts of dormant LT-HSC to be also activated, resembling ST-HSCs [63, 696]. Thus, while FACS strategies support the selection of specific populations of HSCs with an abundance of certain activities, it is likely that HSCs transit from one activation state to the other continuously and reversibly [63, 696]. This is further sustained

by many previous results showing that also HSCs that have undergone multiple cycles of activation can revert to a quiescent state [631, 333]. This concept is applied in the present work to model pseudo-time points. By assuming that within a population of LT-HSC each cell dynamically transits from one activity level to the other, each single cell measurement becomes a potential time point for network reconstruction. Consequently, under this assumption, it is possible to form a large number of tuples of predecessor and successor time steps $X(t)$ and $X(t+1)$ by a combination of random single-cell measurements (Figure 24 and Methods Section 2.2.2.3).

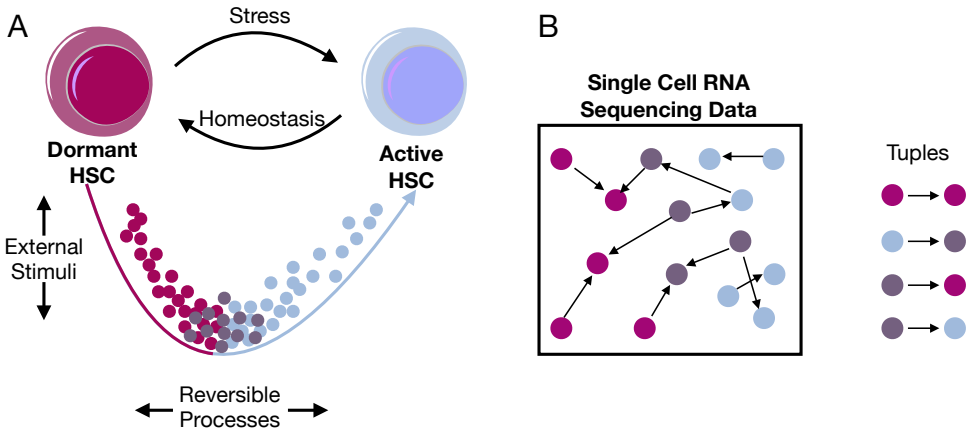


Figure 24: **Heterogeneity of activity levels in the LT-HSC population.** (A) Biological concept: within the LT-HSC population, stem cells can reversely transit between more dormant or activated states without changing their stemness. The heterogeneity of this population is influenced by environmental stimulation. (B) Generation of tuples from single-cell RNA sequencing data exploit the heterogeneity of the LT-HSC population. Pseudo-time-points assume the possibility for each cell of the pool to switch to any of the other cell expression profiles. This implies that trajectories can be randomly selected within the population. The figure has been modified from Schwab, Ikonomi et al. [570], licensed under CC BY 4.0, https://creativecommons.org/licenses/by/4.0/.

The introduction of this conceptualisation of pseudo-time points from single cells and the consequent increase of time-points for network reconstruction challenges the currently available reconstruction algorithms in terms of time computation. Hence, an adaptation of Boolean network reconstruction approaches is proposed in a newly-established pipeline for the reconstruction of Boolean models. The method combines the search for potential regulatory inputs proposed by Maucher et al. [412], which serves now as a preprocessing step, with the exact Best-Fit-Extension proposed by Lähdismäki et al. [341]. The preprocessing phase serves as a filtering

step to select input candidates that are then fed to the reconstruction algorithm, which does not have to test all potential combinations of input candidates anymore. Based on the reconstruction results, an ensemble of Boolean networks can be generated by randomly sampling one regulatory function from the reconstructed set of potential functions for each compound of the modelled system. The pipeline, named "filtered best-fit" approach, was shown to outperform Best-Fit-Extension in terms of computation time and sensitivity in network reconstruction, especially in the context of noisy data (data not shown, reported in Schwab, Ikonomi et al. [570]).
The introduced approach was applied to reconstructed ensembles of Boolean networks modelling the NF-κB signalling pathway for each of the eight LT-HSCs single-cell expression samples reported in the data of Ratliff et al. [507] (See also Methods Section 2.2.2). The reconstruction started from selecting the genes belonging to the NF-κB according to the KEGG database [288]. Of these 101 genes, 96 were significantly binarisable (p-value$<$ 0.05), and were fed to the described reconstruction pipeline. This revealed eight ensembles of Boolean networks. Each reconstructed ensemble refers to a human sample of single-cell HSC expression data of a certain age. In the following sections, each ensemble of models that were analysed in terms of topological and dynamic properties is composed of a total amount of 2000 reconstructed models. The eight human donors from which the LT-HSC populations are retrieved are distributed as follows: 19, 21,37, 40 years old (young group) and 61, 66, 68, 70 years old (aged group).

3.1.3.2 *Network ensembles from aged individuals show reduced topological properties and network motifs*

By applying the above-described pipeline, eight ensembles of networks were obtained starting from the single-cell expression data from Ratliff et al. [507]. The reconstructed networks comprise up to 950 potential Boolean functions for one regulatory compound. The mean number of reconstructed Boolean functions per compound was between 1.06 and 16.50 across the different individuals and the 20 repeated runs. Reconstructed Boolean functions had between 1 and 5 regulatory inputs (Figure 25).
As a first validation of the reconstructed Boolean functions, the obtained interactions were compared to the ones found in the STRING-DB [627] (data not shown, refer to Schwab, Ikonomi et al. [570]). Considering all interactions retrievable from the database, 94.1% of the reconstructed regulations for the young phenotypes and 94.0% for the aged ones (across all individuals for the two groups) could be validated. By applying a stricter constraint including only STRING-DB regulations coming from experimental evidence and database curation, still, 66.1% of recon-

structed regulations for the young phenotype and 65.1% for the aged phenotype could be validated. Some reconstructed regulations were not found in STRING-DB. These could point to unknown interactions, which are open for further validation in experimental setups.

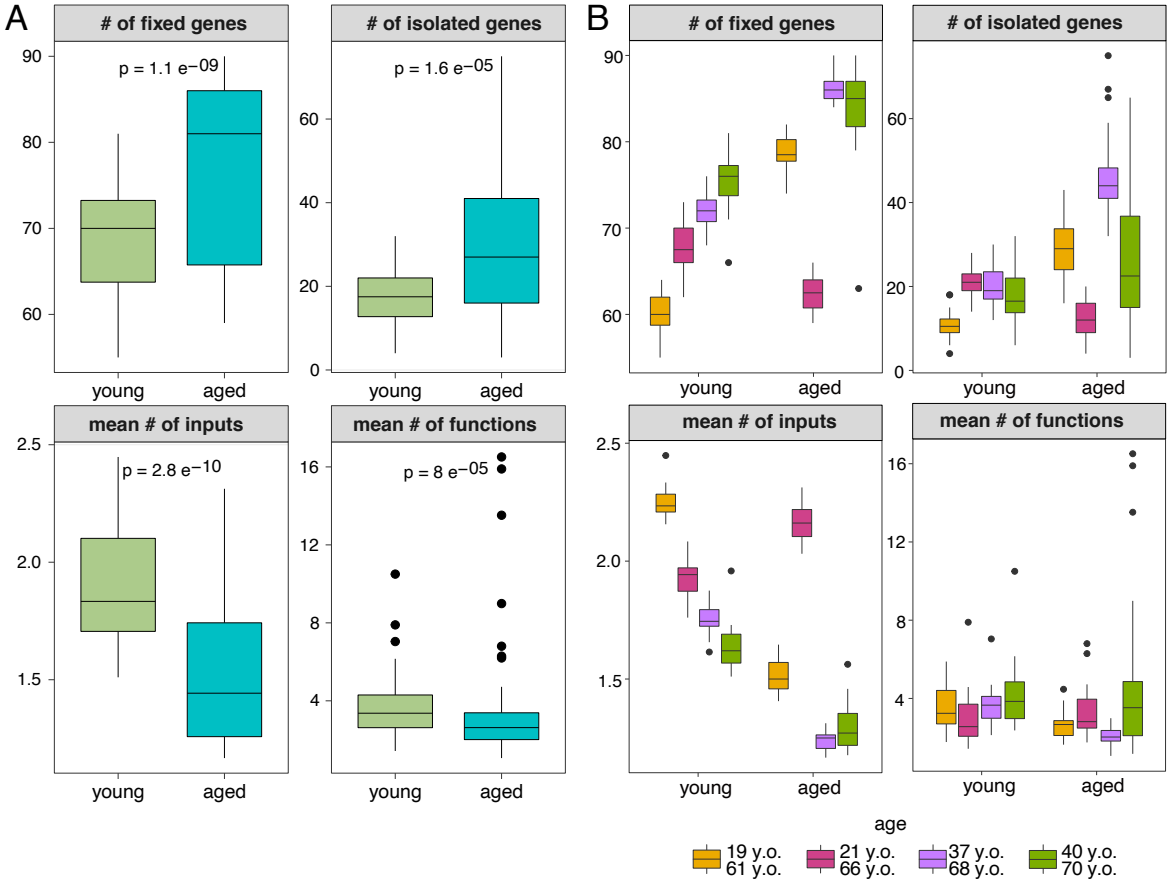


Figure 25: **Structural properties of reconstructed ensembles.** Static properties across reconstructed ensembles were compared by young (19-40 years old) and aged groups (61-70 years old) (A), as well as individual-wise (B). Measured features are reported on top of the plots. Wilcoxon signed-rank test was applied to evaluate differences between age groups. Results were considered significant for $p < 0.05$. The figure has been modified from Schwab, Ikonomi et al. [570], licensed under CC BY 4.0, https://creativecommons.org/licenses/by/4.0/.

By comparing the reconstructed functions among young (19-40 years old) and aged (61-70 years old) individuals, it could be shown an increase in the mean functions and regulatory inputs in the young phenotypes compared to aged ones (Figure 25). On the contrary, fixed genes and isolated ones were significantly lower in the young reconstructed networks (Figure 25). Observing the trends by single individual re-

construction, it could be shown that the aged individual of 66 years old had similar interaction graph-based features as the networks from the young ones (Figure 25).

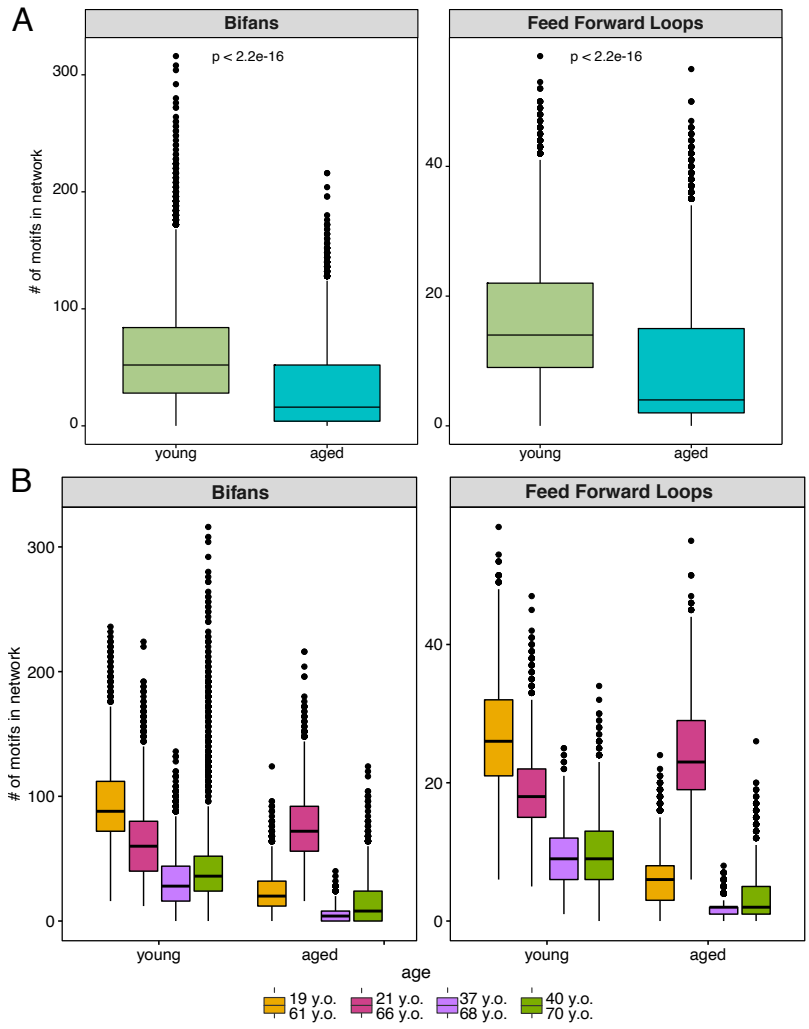


Figure 26: **Network motifs evaluation.** Network motifs (bifans and feed forward loops) were evaluated and compared in young (19-40 years old) and aged groups (61-70 years old) (A), as well as individual-wise (B). Measured features are reported on top of the plots. Wilcoxon signed-rank test was applied to evaluate differences between age groups. Results were considered significant for $p < 0.05$.The figure has been modified from Schwab, Ikonomi et al. [570], licensed under CC BY 4.0, https://creativecommons.org/licenses/by/4.0/.

As a second analysis, it was investigated whether the observed reduction in regulatory functions and regulatory inputs during ageing was also connected to an alteration of network motifs, thus resulting in a reduction of functional structures in

the models. Hence, the abundance of bifans and feed-forward loops was screened in the reconstructed ensembles (Figure 26).
Results show that the number of both motifs significantly decreases moving from young to aged groups. Again, individual-wise, the reconstruction belonging to the 66 years old individual showed similar number of motifs compared to the young reconstructed networks.

3.1.3.3 *Analysis of the ensembles'dynamics highlights new alterations during ageing*

The human HSCs ageing process remains widely unexplored [122, 362]. The dynamic analysis aims to get an initial understanding of the general dynamics governing HSCs ageing in the NF-κB pathway. To this end, the computation of the attractor landscape of the reconstructed ensembles was performed.
First, the long-term behaviour of the system was studied in terms of attractor properties, namely number and type of retrieved attractors (Figure 27). While a general tendency towards having few attractors was observed, among young and aged networks, still a significant increase in the number of attractors and their length is shown in the young reconstructed networks (Figure 27). Together with the results from the structural analysis (Figure 25), the reconstructed networks of young HSCs show increased connections and attractors, hinting at a potentially increased response to sudden changes in external stimuli. Observing these alterations already in the quiescent LT-HSC population also sustains the hypothesis that major changes in hematopoiesis during ageing arise from differentially prompted and reactive HSCs [122, 362]. Following the hypothesis of a different intrinsic rewinding of quiescent HSC which is responsible for their differential responses without induing *per se* a direct activation, the dynamic analysis of the retrieved phenotypical landscape was deepened. To do so, the general tendencies of attractors´ activties were analysed between the young and aged individuals as well as individual-wise. Here, both stable and changing activities between young and aged attractor landscapes were analysed and validated by literature screening. In both scenarios, attractor activities were matched with expected alterations during HSC ageing or general characteristics of quiescent HSCs. A first literature search revealed that over the complete 96 genes comprised in in the reconstructed networks, 78.73% could be validated by literature search in HSCs, while 12.5% had no described function in HSCs. Only 6.25% of the genes had an activity in the attractor landscapes that did not match behaviours expected for HSCs from literature (details provided in Schwab, Ikonomi et al. [570]).
First, stably inactive genes within the attractor landscapes of both young and aged reconstructed ensembles were analysed (detailed list provided in Schwab, Ikonomi et al. [570]). As a general observation, the activation of these genes was either related to leukemic transformation, blood cell differentiation, specific differentiated

immune cells, or niche-specific secreted factors [19, 363, 414, 718, 635]. Therefore, these genes are not considered to influence the quiescent HSC compartment, and thus are correctly found inactive across young and aged attractor landscapes.

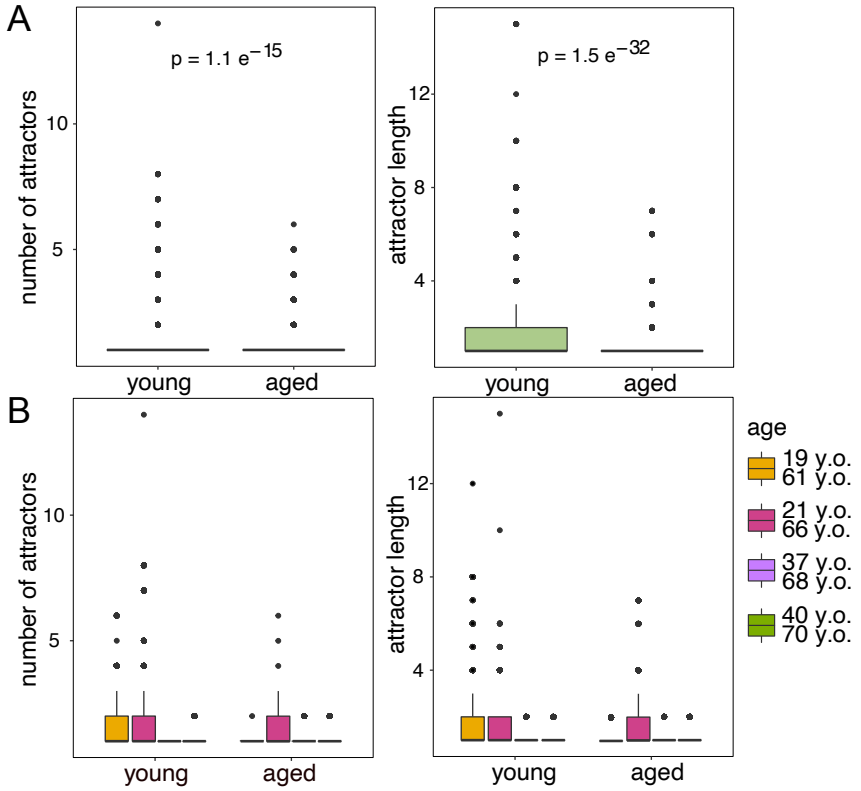


Figure 27: **Evaluation of the attractors landscape.** The number of attractors and their length were evaluated and compared in young (19-40 years old) and aged groups (61-70 years old) (A), as well as individual-wise (B). Wilcoxon signed-rank test was applied to evaluate differences between age groups. Results were considered significant for $p < 0.05$. The figure has been modified from Schwab, Ikonomi et al. [570], licensed under CC BY 4.0, https://creativecommons.org/licenses/by/4.0/.

Next, genes changing their activities during ageing were analysed (Figure 28, Table 3). Observing the attractors patterns, a general trend in reducing activities during ageing is observed. This tendency was observed in both the overall averaged young and aged groups and individual-wise. Interestingly, while this decrease in activity levels is preserved during ageing, still a certain heterogeneity among individuals is observed, pointing again at an increased activity in the reconstructed ensembles of the 66 years old individual (Figure 28). Along with the attractor patterns, the gene activities were divided into three subgroups: decreasing, increasing,

and stable activities during ageing. In the following, the three subgroups will be analysed in detail, and a summary of the activities validation is provided in Table 3. Note that, only nodes with an activity greater than 1% were considered to be active.

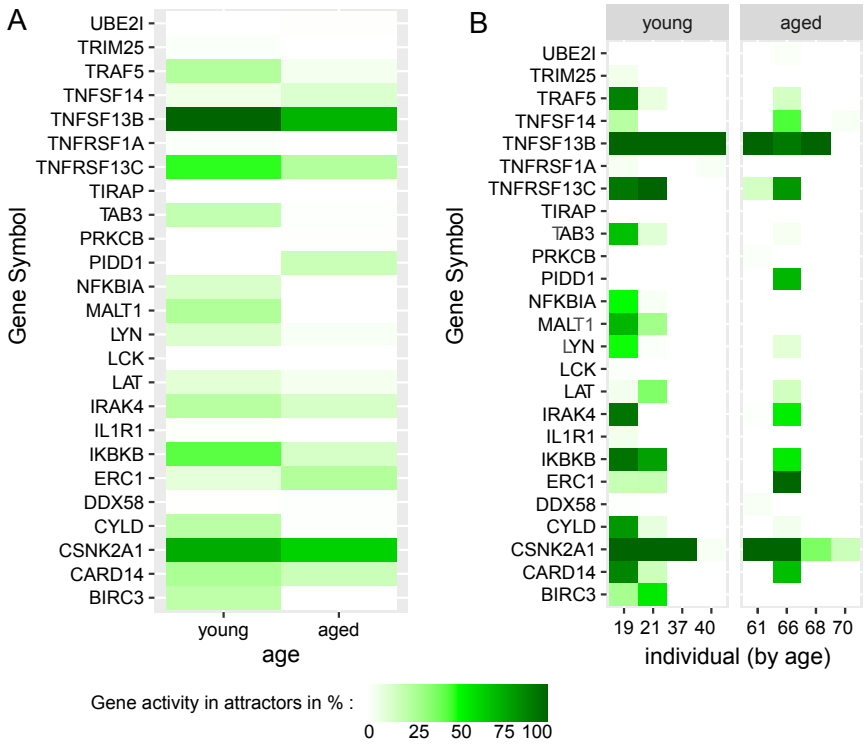


Figure 28: **Changing activities levels during ageing.** (A) The average activity of all non-zero genes over all ensembles of the young phenotype group (left column) and the aged phenotype group (right column) is depicted respectively. (B) The gene activity in the attractors of the ensembles averaged for each individual is shown. The individuals are sorted by increasing age (see x-axis). The color of the heatmap indicates the activity of a gene, ranging from 0% (white) to 100% (dark green). The figure has been taken from Schwab, Ikonomi et al. [570], licensed under CC BY 4.0, https://creativecommons.org/licenses/by/4.0/.

The genes decreasing their activity during ageing represent the largest among the three subsets (Figure 28, Table 3). TNF receptor superfamily member 13C (TNFRSF13C) was shown to be also decreased during HSCs ageing [532, 531]. The other genes, instead, were mainly studied in the context of HSC loss of function, but dysregulations of their activities are yet to be reported in ageing. In addition, others, like ELKS/RAB6-interacting/CAST family member 1 (ERC1), were still not studied in HSCs. Baculoviral IAP Repeat Containing 3 (BIRC3) and interleukin-1 receptor-associated Kinase 4 (IRAK4) are connected to the loss of rescue mechanisms for apoptosis, leading to a final impaired survival [513, 718, 651]. A general

increase of apoptosis-related genes is also observed in aged HSCs [484], together with a decision switching towards cell death during stress conditions [272, 280, 281]. In addition loss of IRAK4 in humans leads to a deficiency in innate immune response [121]. Loss of IKBKB, and CYLD Lysine 63 Deubiquitinase (CYLD) has instead been connected to HSC loss or impairment of quiescence [635, 749]. A hallmark of HSC ageing is indeed related to a more active and expanded population of HSCs, with impaired maintenance of quiescence that results in an impaired HSC activity [484]. Caspase recruitment domain family member 14 (CARD14) is also implicated in the alteration of HSC quiescence and activation. While mainly studied in epithelial-related disease, CARD14 is induced by interleukin 17 (IL17), which is reported to inhibit HSC colony formation [53, 260, 411, 421, 437]. Mucosa-associated lymphoid tissue lymphoma translocation protein 1 (MALT1) was also observed to decrease with ageing in the attractor landscape. This reduced activity would lead to a double-edged effect: on the one side, loss of MALT1 promotes HSC quiescence [308]. On the other side, it skews hematopoiesis towards myeloid cells [537]. As MALT1 is an inhibitor of NF-κB, its loss induces the increase of the latter. Nevertheless, MALT1 loss also has a positive effect on quiescence [308]. This might counteract the increased stress-response induced by NF-κB that normally leads to cell cycle entry [537]. Also, TNF receptor associated factor 5 (TRAF5) and linker for activation of T-Cells (LAT) loss were connected to myeloid skewing, which is a phenotypical hallmark of aged HSCs [122, 362]. This effect is potentially boosted by the decrease of TNFRSF13C in the attractor landscape. The loss of this gene activity is in fact connected to impaired lymphoid specification during HSC ageing [532, 531]. Loss of NFKB Inhibitor Alpha (NFKBIA) increases the propensity towards an inflammatory response by controlling the NF-κB pathway [498, 456], in accordance with the increased inflammatory signals reported during ageing [170]. LYN proto-oncogene (LYN) also decreases in the attractor landscape. The decrease of LYN causes increased numbers and impaired repopulation potential of HSCs [344, 480, 480]. The loss of ERC1 instead is described to be involved in cellular polarity maintenance. Specifically, the loss of ERC1 reduces motility by altering the turnover of focal adhesions. Aged HSCs are reported to have a reduced homing ability to the bone marrow [364, 280]. This directly connects to altered polarity and cytoskeleton organisation. High cell division control protein 42 homolog (CDC42) activity was reported in aged HSCs and showed to be involved in reduced adhesion to niche cells and engraftment abilities. Jung et al. [280] also connected this reduction of engraftment observed in aged HSCs with the increase of stress signals and p38 activity. The model suggested activities that are potential new targets to investigate in HSC ageing.

Two genes showed a stable activity in the all attractor patterns: TNF superfamily member 13B (TNFSF13B) and casein kinase 2 alpha 1 (CSNK2A1) (Figure 28, Ta-

ble 3). The first is linked to a stable immune response being involved in survival and development of B-cells [107, 156, 549, 753]. In particular, TNFSF13B is already expressed in the HSC compartment [107, 156, 549, 753]. Interestingly, loss of other genes for B-cell differentiation such as myeloid differentiation primary response 88 (MyD88) already show effects on the activity of LT-HSC and not only on differentiated progeny [156]. CSNK2A1 was found to be implied in resistance to senescence [540]. Its down-regulation leads to the insurgence of senescence in fibroblast cells, and it is associated with rat liver and testis ageing [540]. Thus, these genes could be considered as gatekeepers also in the context of HSC activity through ageing.
Finally, genes showed increased activity in the attractors' landscapes: TNF Superfamily Member 14 (TNFSF14) and P53-induced death domain protein 1 (PIDD1) (Figure 28, Table 3). TNFSF14 increase is related to cycling and proliferation of mesenchymal stem cells, while in HSCs is also reported to drive myeloid differentiation [234, 86]. PIDD1 activity is uniquely reported to the 66 years old individual networks (Figure 27) and in none of the other individuals. Interestingly, this individual also showed more similarity to the young individuals in terms of topological and general dynamic features (Figure 25, Figure 26, Figure 27). In addition, this ensemble of networks is specifically responsible for the majority of residual activities in the ageing group, strongly resembling the attractor patterns of ensembles retrieved from the youngest individuals (19 and 21 years old). Hence, the activity of PIDD1 is of particular interest giving its uniqueness and relation to this precise ensemble of networks. PIDD1 activity is related to DNA damage response [118, 268, 706]. In particular, PIDD1 is suggested to act as a switch between DNA damage response and apoptosis by regulating the activation of first damage response via NF-κB, and apoptosis via Caspase-2 [118, 268, 706]. The loss of PIDD1 is not able to block apoptosis. Nevertheless, the apoptotic process happens faster. Probably this is due to the lack of the initial NF-κB activation as a first attempt to contain and correct DNA damage [268, 118, 706]. While PIDD1 activity has still not been investigated in HSCs, the HSC phenotype of Caspase-2-deficient cells is known [268, 118, 706]. Caspase-2 deficient mice develop normally but show age-related dysfunctions. In addition, when challenged by oncogenic stimuli or stress, Caspase-2 deficient mice show enhanced tumour development [268, 118, 706]. Overall, this supports the idea that reactivation of PIDD1 could contribute to a delayed ageing process, by promoting the resolution of DNA damage, which is a huge player in HSC ageing and stress [122, 170, 420].

Table 3: **Analysis of altered attractor activities in the young and aged ensembles.** The attractor activities analysed in the text are reported and grouped by decreasing, stable, or increasing activities. The activities are evaluated based on the averaged attractor activities among all young and all aged individuals. Only activities above 1% were considered. The table has been modified from Schwab, Ikonomi et al. [570], licensed under CC BY 4.0, https://creativecommons.org/licenses/by/4.0/.

Activity	Altered compound in the ensembles	Experimentally matched impact	References
Decreasing	BIRC3, IRAK4	Loss of rescue mechanisms for apoptosis causing impaired survival.	[513, 718]
	CARD14, IKBKB, CYLD	Loss/impaired quiescence.	[53, 260, 411, 421, 437, 635, 749]
	TRAF5, LAT	Myeloid skewing/loss of lymphoid cell lineages	[76, 441, 457, 458]
	MALT1	Compensatory inhibition of NF-κB activation via induction of quiescence. Loss of direct NF-κB inhibition.	[308, 537]
	NFKBIA	Propensity to increased inflammatory response via NF-κB activation.	[498, 456]
	LYN	Impaired repopulation potential and increased number of HSCs.	[344, 480]
	ERC1	Cellular polarity alteration causing reduced motility. The presence of ERC1 promotes the turnover of focal adhesions.	[23, 599, 190, 345, 740]
	TNFRSF13C	Impaired lymphoid specification. Already shown in HSC ageing.	[532, 531]
Stable	TNFSF13B	Stable immune response. Responsible for B-cell development and survival, expressed in HSCs.	[107, 156, 549, 753]
	CSNK2A1	Resistance to senescence. Loss of CSNK2A1 promotes cellular senescence. It is downregulated in rat liver and testis during ageing.	[540]
Increasing	PIDD1	Control of balance between repair and apoptosis after DNA-damage.	[268, 118, 706]
	TNFSF14	Loss of quiescence due to increase input to enter cycling/Myeloid differentiation.	[234, 86, 747]

3.1.4 *Discussion – Modelling the Nf-κB pathway in human HSC ageing via network ensembles*

3.1.4.1 *Interaction-graph based and dynamic changes during ageing*

The ensembles of networks reconstructed from single-cell expression data from human LT-HSCs samples (four young and four aged human individuals) showed distinct changes in network topology during ageing. On the one hand, results showed a significant decrease of regulatory inputs and mean reconstructed functions during ageing (Figure 25). On the other hand, the number of isolated and fixed genes increases during ageing (Figure 25). These findings hint that, in aged HSCs, regulatory interactions are muted, which would be consistent with a reduced response to stimuli as described by Schwab et al. [573] in the context of network reconstructions in muscle stem cells. Additionally, it was shown that the observed decrease in regulatory connections is coincident with a decrease in network motifs during ageing. Previous work also associated alteration of motifs distributions with neurological disorders and cancer [10, 167]. Altogether, this suggests a link between the dysregulated phenotypes and the structural alterations in the networks, hinting at a loss of regulatory structures during ageing. Also, the attractor landscape of the network ensembles was shown to be altered. In general, most of the retrieved attractors in both young and aged ensembles were single-state ones. Single state attractors are considered to be more stable and less likely disturbed by noise [572, 321]. This is also consistent with a deep dormant state of HSCs. In accordance, also the retrived attractor of the physiological maintenance model of HSCs are single state ones (Figure 15). However, ensembles from young individuals showed an increased number of attractors, specifically in cycling ones. This increase might also be interpreted as an increase of available phenotypes or states that might confer to the HSCs a prompt response to external stimulation. In accordance, a decrease in the ability to respond adaptively to environmental stimuli is a common event in ageing and it also further affects HSCs [3, 18, 650].

3.1.4.2 *Capturing altered activities in HSC ageing*

The averaged attractor patterns across all of the reconstructed networks in the young and aged ensembles of the NF-κB pathway were analysed. In general, a tendency in having decreased activity of genes from young to old attractor landscapes was observed (Figure 28). In accordance, it is shown that silencing of genes by DNA methylation is associated with progressive ageing [60, 378]. This silencing phenomenon affects principally cell cycle regulators, as well as tumour suppressors or inflammatory regulators [60, 378]. This epigenetic-driven phenomenon is also observed in HSCs [78]. Thus, it is not surprising that the decreased activi-

ties are observed in the attractor landscapes describing the NF-κB pathway. Based on the attractor pattern analysis of the young and aged ensembles of the NF-κB pathway, this down-regulation seems to prompt HSCs to higher cycling, inflammatory response, and damage response impairment (Figure 28, Table 3). Following the same direction, the dynamic analysis of the literature-based HSC maintenance model also indicates a loss of cell cycle regulators, which leads to priming of HSCs to active states in ageing simulating conditions (Figure 22). The observed loss of regulators in both modelling approaches shows priming of HSCs to a different activation propensity during ageing. In the specific case, the ensemble dynamic analysis shows a tendency to a general loss of quiescence, myeloid skewing and impaired homing.
Together, the two described modelling approaches capturing HSCs dynamic behaviour cover most of the described hallmarks of ageing [122].

3.1.4.3 *Capturing the heterogeneity of the ageing process*

The HSC ageing process is a highly heterogeneous and complex process [394, 448, 664]. In this conception of ageing, the HSC compartment consists of several subpopulations of HSCs each with distinct differentiation and proliferation behaviours [394, 448, 664]. Capturing this heterogeneity and understanding its underlying mechanisms is an open research challenge. Besides, the challenging maintenance and isolation of HSCs in culture systems adds a layer of complexity to this issue [77, 168, 274, 323, 489, 534, 690]. For this reason, mathematic modelling approaches attempting to dissect and investigate mechanisms behind the ageing process of HSCs are of great interest. The ageing related simulation of the HSC maintenance model already showed different potential scenarios in HSC ageing. Ideally, this leads to the idea that all of these conditions could coexist and generate differential behaviours in the entire aged HSC population (Figure 22). In accordance, Zeng et al. [747] also individuated markers for different enriched subpopulations of aged HSCs. The advantage of the modelling approach in this context is the dynamic investigation that allows characterising the behaviour of these subpopulations.
In general terms, to the intrinsic HSC population heterogeneity, intra-individual heterogeneity is added. Is well known that chronological and biological ageing may not match [124]. A striking example of this is shown in the single-cell-based network ensemble reconstructions of the NF-κB pathway. Here, the ensemble for the aged individual of 66 years showed similar interaction graph-based and dynamic properties to the ensembles of the youngest ones. Interestingly, this particular ensemble is the one retaining also most of the attractor activities that are shown to be declined with age (Figure 28). Also, it shows that the activity of PIDD1. While very little is known about the activity of PIDD1 in HSCs or ageing [602], its

role is more established in the context of liver regeneration [602]. Here, Caspase-2 and PIDD1 are involved in controlling liver formation during embryogenesis and regeneration, by limiting excessive proliferative activities [602]. Transferring this knowledge in the HSC context together with the general role of PIDD1 in DNA damage response [268, 706], the limitation of HSC cycling activity would counteract the activation of HSCs reported during ageing [484]. Strengthening this hypothesis, the loss of Caspase-2 in HSCs, a downstream effector of PIDD1, leads to premature ageing [118]. In addition, Caspase-2 deficiency in mouse aged liver cells results by a yet unknown mechanism in the reduced expression of FOXOs and their transcriptional targets, thus correlating it to oxidative stress response [581]. Altogether, the detected activity of PIDD1 only in the attractor landscape of the 66 years old reconstructed ensemble might lead to a new marker for HSC rejuvenation, that will require further future experimental validations.

3.2 Modelling pNETs' progression and targeted interventions

pNETs are the second most common epithelial neoplasms in the pancreas, after pancreatic ductal adenocarcinoma (PDAC) [58, 415, 445]. These tumour entities are considered indolent and slow-growing, however preserving a malignant potential that results in a moderate malignancy in the vast majority of cases [519]. More in detail, there is high heterogeneity in tumuor behaviours, ranging from nearly benign to extremely aggressive ones [58]. Most pNETs grow and eventually metastasise in the liver with mostly unpredictable progression time-spans, making this aggressive progression the most common cause of death for these tumours [415, 519]. Hence, the biological behaviour of pNETs is still largely unpredictable [519].
As for their progression, also the pathogenesis of pNETs is largely unexplored [519]. Around 10% of pNETs are part of familiar endocrine tumour syndromes and are therefore generated by germline mutations. Of these, the most frequent germline mutation is MEN1 [519]. Sporadic pNETs arise instead from somatic mutations. Here, 44% of cases harbour a MEN1 mutation, 43% DAXX/ATRX mutation, and 14% report mutations in the mTOR pathway (e.g. tuberous sclerosis protein (TSC)) [415, 519, 719]. Overall, the hyperactivation of the mTOR pathway is a common hallmark of pNETs, while MEN1 mutations are the best known common drivers of tumour formation [169, 719].
Altogether, pNETs pathogenesis and progression is mechanistically largely unknown. This directly reflects the difficulties in the diagnosis and treatment of these types of tumours [519]. As a result, nearly 60% of patients are diagnosed at later stages when the tumours are already metastatic [58, 415, 527]. For what concerns the therapeutic handling of these tumours, most of the pNETs are addressed with a "wait and see" strategy that attempts to understand the specific tumour progression before starting treatment strategies [519]. A more aggressive approach involves surgical resection [519]. As for targeted therapies, mTOR inhibitors have shown prolonged progression-free survival in clinical trials granting them a food and drug administration U.S. (FDA) approval [741]. However, the administration of these inhibitors has also been reported to evoke resistant phenotypes, adding further challenges to the therapeutic handling of these tumours [80, 163, 351, 741].

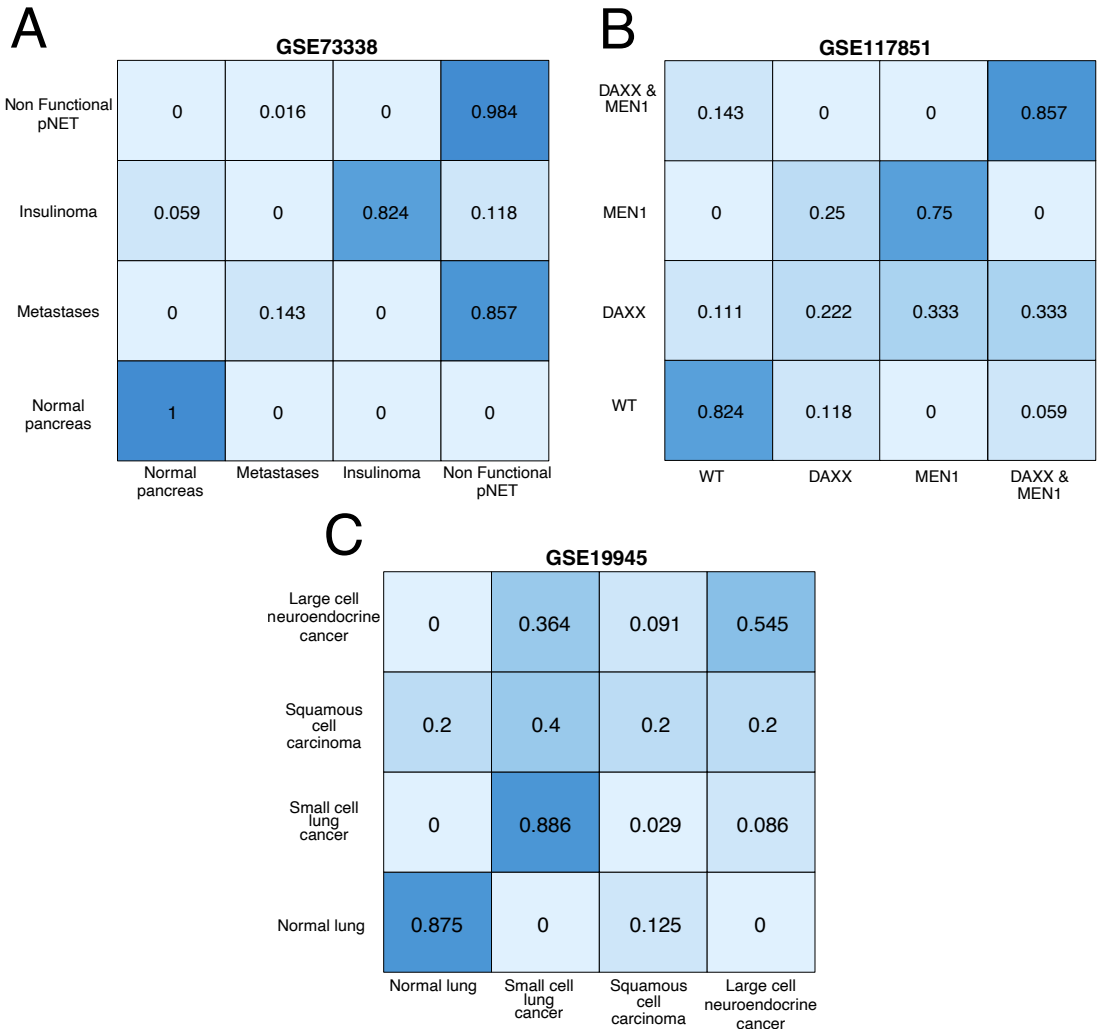


Figure 29: **Multi class classifier experiments on NETs human expression datasets** The figure depicts the results of a multi class classfier experiment performed on two pNETs human expression profiles (GSE73338, GSE117851) (A,B) and on lung tumour expression profiles including squamous cell carcinomas and known neuroendocrine lung malignancies(GSE19945) (C). Results are depicted in form of a confusion matrix. Each cell of the matrix reports the probability of that group to be assigned to the corresponding one in the matrix. Colour intensities reflect these probabilities, where the higher the probability the more intense the colour.

A molecular mechanistic understanding of pNETs´ development and progression is paramount to both an early diagnosis and efficient treatment. To gain some initial insights about the features of pNETs a first multi class classfier experiment was performed and results were visualised in form on a confusion matrix (see Methods Section and Figure 29A and Figure 29B). Within the confusion matrix, each cell reports the probability of that specific group of class to be classified to the correspond-

ing one in the matrix. Hence, if the multi class classifier would perfectly separate the different groups, a matrix with diagonal of ones would be expected, meaning that each group is perfectly distinguished from the others in the system (see also Methods 2.3.2.2). In the specific case, the two datasets GSE73338 and GSE117851 reporting pNETs patients expression profiles, grouped respectively by functionality and metastatic status, or by reported mutations were utilised. In both cases, it could be observed that the multi classification experiment generally failed to correctly classify all the different groups in a reliable manner, independently from considering driving mutations or tumour histo-pathological features. However, some groups were more reliably classified than others (e.g. Insulinomas or WT tumours) and some assignements could be excluded (e.g. metastases are never classified as normal tissue) (Figure 29A and B). Interestingly, only normal pancreas could be always correctly classified, while for example metastases are mostly classified as non functional tumours (Figure 29A). In a similar fashion DAXX mutated pNETs show an almost evenly distributed probability to be classified as either any of the other groups (Figure 29A). Lung neuroendocrine malignancies are the second most common type of neuroendocrine tumour after pNETs [152, 293, 379, 754]. Similar results were also achieved by when performing the same experiment on different lung malignancies including neuroendocrine characteristics (GSE19945) (Figure 29C).
Despite excluding the incorrect classification for some classes, the multi classification experiment could not obtain a reliable classification of all the involved tumour entities (Figure 29).These results are in accordance with the high heterogeneity observed in neuroendocrine malignancies and difficult to predict tumour aggresivity potential. In this scenario, static modelling approaches, such as classification systems, only considering expression profiles might need the integration of information from dynamic models to further understand these tumour entities. Hence, a Boolean model describing the main altered pathways in pNETs and their crosstalk was established. Based on the established model, the aim is to deepen the understanding of mechanisms involved in tumour progression, new tumour drivers, and new targeted therapeutic interventions.

3.2.1 *A Boolean network model of pNETs initiation and progression*

The pNET Boolean model is based on intensive literature search and database screening. Nodes (genes/proteins) which were found to be mutated in pNETs were included, together with their involved pathways and crosstalks. In particular, regulations involving the mTOR, PI3K/AKT pathway, as well as MEN1, and DAXX/ATRX signalling were included. Given that pNETs are related to angiogenesis and insulin growth factor (IGF) signalling [415], regulatory dependencies involving VEGF, IGF, and mitogen-activated protein kinase (MAPK) signalling were considered. Fi-

nally, given that the established model aims to understand the mechanistic manner of pNETs progression and invasion, cell cycle progression from G1- to S - phase and cell adhesion were integrated (Figure 30, Table 4). The final Boolean model consists of 56 nodes and 198 regulatory interactions including the above-mentioned pathways and their effects on proliferation and invasion (Figure 30, Table 4).

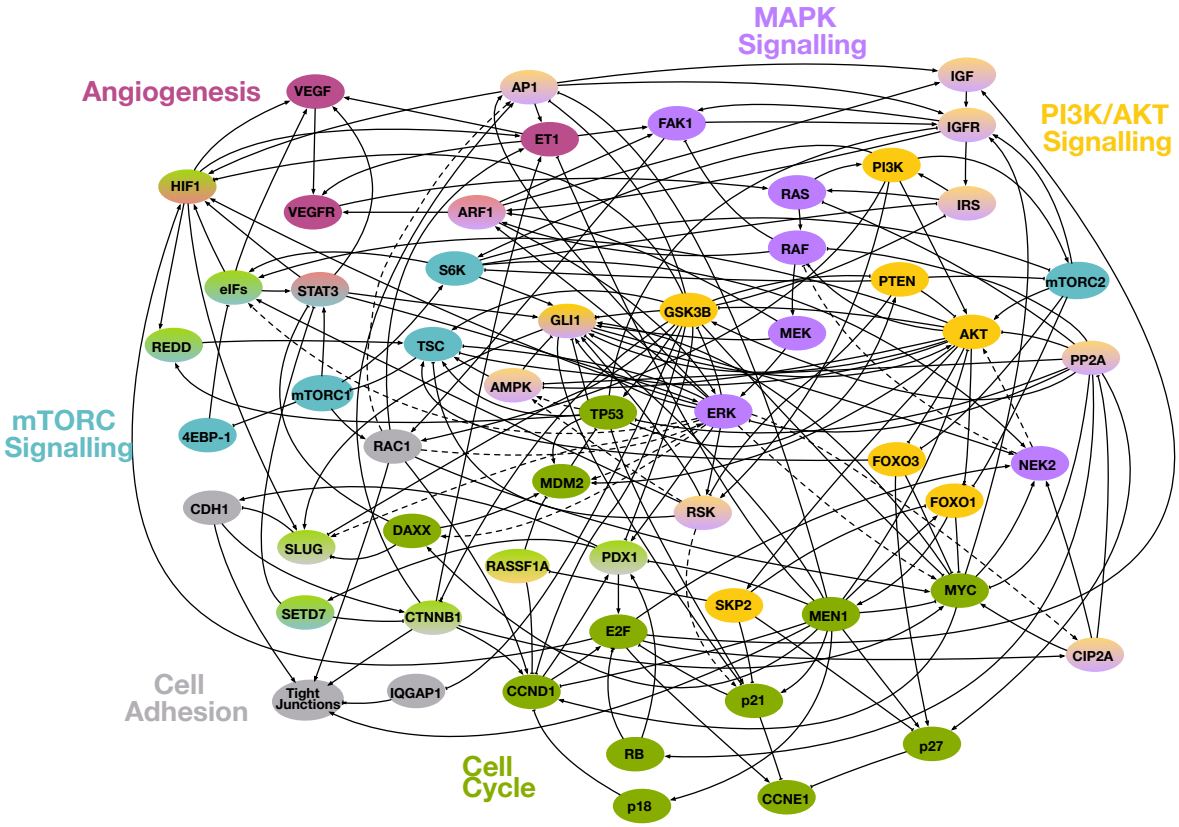


Figure 30: **Interaction graph of the pNET Boolean model.** The 198 directed edges in the static interaction graph depicts the regulatory dependencies between the 56 nodes (genes/proteins). Here, arrows show activating regulations while bar-haded lines depict inhibitory interactions. Linear cascades of interactions are represented by dashed lines between the starting and the end node. The colour of each node depicts its association to a specific pathway.

Table 4: Boolean functions of the pNET model. Regulatory interactions of the model are summarised by logic connectives AND ($\wedge$), OR ($\vee$), and NOT ($\neg$). To reduce the complexity of the model, linear interactions are depicted by time delays ([−2]). A detailed biological description of the Boolean functions is reported with references.

	Node; $t+1$	**Boolean function;** t	**Description**
Angiogenesis	VEGF	(STAT3 $\vee$ HIF1 $\vee$ ET1) $\wedge$ eIFs	Eukaryotic initiation factors (eIFs) allow selective translation of VEGF [426]. Signal transducer and activator of transcription 3 (STAT3), Hypoxia-inducible factor 1 (HIF1), and Endothelin 1 (ET1) increase VEGF transcription [287, 418, 529].
	VEGFR	VEGF $\wedge$ ARF1 $\wedge$ ET1	VEGF is the ligand of VEGFR and responsible for receptor activation [45]. ADP-ribosylation factor 1 (ARF1)-dependent regulates cellular exit of VEGFR [449]. ET1 can up-regulate the transcription of VEGFR [529].
	ARF1	IGFR $\vee$ MEK $\vee$ ERK $\vee$ RAF	Activation of ARF1 is downstream of the MAPK signalling cascade. Here, ARF1 activation depends on IGFR, mitogen-activated protein kinase kinase (MEK), RAF proto-oncogene (RAF), or mitogen-Activated Protein Kinase (ERK) [71, 117, 211, 449, 594].
	ET1	(HIF1 $\wedge$ AP1) $\vee$ (CTNNB1 $\wedge$ RAC1 $\wedge \neg$MEN1)	HIF1 and AP1 induce together ET1 [529, 717]. β-catenin (CTNNB1) can induce the expression of ET1 [312, 624]. CTNNB1 presence in the nucleus is controlled by Ras-related C3 botulinum toxin substrate 1 (RAC1) [704]. On the opposite way, MEN1 shuffles CTNNB1 from the nucleus to the cytosol [67, 276, 319].

Table 4: Boolean functions of the pNET model. Regulatory interactions of the model are summarised by logic connectives AND ($\wedge$), OR ($\vee$), and NOT ($\neg$). To reduce the complexity of the model, linear interactions are depicted by time delays ([−2]). A detailed biological description of the Boolean functions is reported with references.

	Node; $t+1$	**Boolean function;** t	**Description**
	HIF1	$(STAT3 \vee E2F) \wedge ERK \wedge eIFs \wedge (\neg GSK3\beta \vee (GSK3\beta \wedge AP1))$	STAT3 enhances HIF1 transcription and increases HIF1 protein level [125, 126]. E2F activity directly regulates and is required for induction of HIF1 [574]. eIFs mediate the translation of HIF1 [367]. Phosphorylation from ERK increases HIF1 activity [243, 250, 504]. GSK3β phosphorylates HIF1 and primes it for ubiquitination. cJUN a component of the AP1 complex, can bind HIF1 at its ubiquitination sites and prevent its proteaosomal degradation [160, 736].
MAPK signalling	IGF	$(E2F \vee AP1) \wedge ARF1$	AP1 is responsible of inducing IGF expression. E2F binds to the promotor of IGF and induces IGF expression [739]. ARF1 is involved in neuorendocrine secretion and release IGF [449].
	IGFR	$(\neg TP53 \wedge (AP1 \vee MYC)) \wedge (IGF \vee mTORC2 \vee FAK1)$	IGF binds to its receptor and activates the Insulin growth factor receptor (IGFR) [153, 133, 707]. Focal adhesion kinase (FAK1) stabilises via phosphorylation IGFR [20]. mTORC2 promotes the activation of IGFR [729]. TP53 suppresses the IGFR promoter [693]. TP53 inhibits IGFR through induction of IGF-BP3 expression, preventing its binding of IGF [153]. MYC promotes the expression of IGFR [622]. Also, cJUN, which is part of AP1, activates the transcription of IGFR [518, 554, 561].

Table 4: Boolean functions of the pNET model. Regulatory interactions of the model are summarised by logic connectives AND ($\wedge$), OR ($\vee$), and NOT ($\neg$). To reduce the complexity of the model, linear interactions are depicted by time delays ([−2]). A detailed biological description of the Boolean functions is reported with references.

	Node; $t+1$	**Boolean function;** t	**Description**
MAPK signalling	IRS	IGFR $\wedge$ $\neg$S6K $\wedge$ $\neg$GSK3β	Protein S6 kinase beta-1 (S6K) regulates Insulin receptor substrate (IRS) on transcriptional and translational level, thereby impairing IRS adaptor fusion [707, 418, 425]. Phosphorylation by S6K targets IRS to proteasomal degradation [418]. GSK3β phosphorylates IRS, thereby reducing the insulin-stimulated activation [235]. IRS is the major substrate of IGFR [670].
	RAS	(IRS $\vee$ VEGFR) $\wedge$ $\neg$PP2A	IGF/IGFR axis induces activation of MAPK signalling by IRS [133, 728]. VEGFR activates RAS [728]. Protein phosphatase 2A (PP2A) inhibits RAS [654].
	RAF1	RAS $\wedge$ $\neg$PP2A $\wedge$ ($\neg$AKT $\vee$ (AKT $\wedge\neg$NEK2[-2]))	RAS activates the RAF-MEK-ERK cascade [658, 707, 744]. PP2A dephosphorylates RAF1 [418]. Inhibitory phosphorylations by AKT on RAF1 are removed by PP1 and/or PP2A during mitogen-stimulated RAF activation [425]. PP1 activity toward AKT-S473 is inhibited by NIMA related kinase 2 (NEK2) (therefore included as delay) [654].
	MEK	RAF	RAF1 activates MEK via phosphorylation [418, 658, 744].

Table 4: Boolean functions of the pNET model. Regulatory interactions of the model are summarised by logic connectives AND ($\wedge$), OR ($\vee$), and NOT ($\neg$). To reduce the complexity of the model, linear interactions are depicted by time delays ([−2]). A detailed biological description of the Boolean functions is reported with references.

	Node; $t+1$	**Boolean function;** t	**Description**
MAPK signalling	ERK	STAT3 $\wedge$ (MEK $\vee$ RAC1[-2] $\vee$ ARF1)$\wedge \neg$PP2A	STAT3 activates ERK promoter [287]. MEK activates ERK via phosphorylation [418, 658, 707, 744]. Alternatively, Serine threonine protein kinase (PAK4), a downstream target of RAC1, can also activate ERK [444]. Expression of ARF1 induces the activation of ERK [117]. PP2A inhibits ERK [654].
	RSK	ERK $\wedge$ PI3K $\wedge \neg$PTEN	Activated ERK phosphorylates and activates RSK [707, 418, 580]. PI3K also activates RSK via phosphorylation [580]. Full activation of RSK requires phosphorylation by both ERK and PI3K pathway constituent [105, 528]. PI3K receives a feedback inhibition from Phosphatase and tensin homolog (PTEN), prohibiting its activity [70].
	CIP2A	ERK[-2] $\vee$ E2F	Treatment of cells with phorbolester TPA, a well-characterised activator of MEK-ERK signalling pathway, increased cellular inhibitor of PP2A (CIP2A) mRNA expression more than threefold probably via ETS1, a transcription factor downstream of ERK signalling (included as delay) [305]. E2F induces CIP2A expression [612].
	PP2A	$\neg$CIP2A	CIP2A binds to PP2A and inhibits its phosphatase functions resulting in tumorgenic transformation of cells [119, 305, 612, 654].

Table 4: Boolean functions of the pNET model. Regulatory interactions of the model are summarised by logic connectives AND ($\wedge$), OR ($\vee$), and NOT ($\neg$). To reduce the complexity of the model, linear interactions are depicted by time delays ([−2]). A detailed biological description of the Boolean functions is reported with references.

	Node; $t+1$	**Boolean function;** t	**Description**
MAPK signalling	NEK2	(GLI1 $\vee$ MYC $\vee$ E2F) $\wedge$ (CIP2A $\vee$ S6K)	Glioma-associated oncogene homolog 1 (GLI1) induces the transcription of NEK2 [761]. Also MYC can transcriptionally activate NEK2 [198]. Similarly, E2F is also a transcriptional regulator of NEK2 [352]. CIP2A enhances NEK2 kinase activity independent from PP2A-PP1 activity [119, 270]. S6K can phophorylate NEK2 and thereby enhancing its activity [128]
	AP1	(ERK $\vee$ (CTNNB1 $\wedge$ $\neg$GSK3β $\wedge$ $\neg$MEN1)) $\wedge$ RAC1[-2]	ERK increases the expression of AP1 transcription factor [140, 295, 705]. CTNNB1 can also transcriptionally induce AP1 [393, 676, 755]. MEN1 shuffles CTNNB1 from the nucleus to the cytosol [67, 276, 319]. GSK3β-triggered c-JUN phosphorylation inhibits AP1 [744]. c-Jun-N-terminal kinase (JNK) mediates the activation of AP1 via its phosphorylation (here RAC1[-2]) [73, 112, 291].
	FAK1	(ET1 $\vee$ (IGFR $\wedge$ ARF)) $\wedge$ $\neg$RAF1	ARF1 is essential for the IGF-mediated activation FAK1 [562, 71]. ET1 signalling increases the activation of FAK1 [529, 655]. SRC-dependent association of FAK subunits of IGFR are both required for its activity [511]. Over expressed RAF increases phosphorylation of FAK1 at the site of Tyr407, down-regulating its activity [368, 463].

Table 4: Boolean functions of the pNET model. Regulatory interactions of the model are summarised by logic connectives AND ($\wedge$), OR ($\vee$), and NOT ($\neg$). To reduce the complexity of the model, linear interactions are depicted by time delays ([−2]). A detailed biological description of the Boolean functions is reported with references.

	Node; $t+1$	**Boolean function;** t	**Description**
PI3K/AKT signalling	PI3K	RAS $\vee$ IRS	RAS activates PI3K [658, 728]. PI3K bound to IRS converts PIP2 into PIP3 [133, 425, 658, 707].
	PTEN	TP53 $\wedge \neg$GSK3β	TP53 induces the expression of PTEN [153]. GSK3β inhibits PTEN via phosphorylation [235, 385].
	GSK3β	PP2A $\wedge \neg$AKT $\wedge \neg$ERK	PP2A activates GSK3β [654]. AKT inactivates GSK3β by phosphorylation at Ser9 [153, 418, 500]. ERK phsophorylates GSK3β at Thr43 which primes GSK3β for subsequent phosphorylation and inactivation by RSK [425]. Furthermore, ERK phosphorylates PP2A at Ser9 [744].
	AKT	GLI1 $\wedge$ ((PI3K $\wedge \neg$PTEN) $\vee$ mTORC2 $\vee$ NEK2[-2]) $\wedge \neg$PP2A $\wedge \neg$MEN1	GLI1 induces AKT transcription [5]. PTEN acts as a negative regulator of PI3K/AKT signalling by reverting PI3K [418, 500, 658]. PI3K activates AKT [153, 133, 418, 425, 584, 658, 707]. Phosphorylation of AKT by mTORC2 on Ser473 leads to full activation of AKT [153, 133, 418, 425, 584, 658, 707]. PP2A dephosphorylates and inhibits AKT [654]. PP1 also dephosphorylates AKT [654]. PP1 activity toward AKT-S473 is inhibited by NEK2 [654]. This is thus included as a delayed regulation. MEN1 inhibits AKT activity by controling its subcellular localisation [678].

Table 4: Boolean functions of the pNET model. Regulatory interactions of the model are summarised by logic connectives AND ($\wedge$), OR ($\vee$), and NOT ($\neg$). To reduce the complexity of the model, linear interactions are depicted by time delays ([−2]). A detailed biological description of the Boolean functions is reported with references.

	Node; $t+1$	**Boolean function;** t	**Description**
PI3K/AKT signalling	SKP2	AKT	Inactivation of AKT1 decreases S-phase kinase associated protein 2 (SKP2) mRNA levels [175].
	FOXO1	((¬AKT ∧ ¬SKP2) ∨ (AKT ∧ MEN1) ∨ (SKP2 ∧ MEN1)) ∧ ¬mTORC2	AKT phosphorylates FOXO1 causing its export from the nucleus and thus its inactivation [154, 227, 401, 654, 668]. SKP2 inhibits FOXO1 through induction of its degradation [685]. MEN1 represses ubiquitination of FOXO1 and AKT phosphorylation. MEN1 also stabilises FOXO1 by repressing its degradation mediated by S-phase kinase-associated protein 2 (SKP2), an E3 ubiquitin ligase [276]. mTORC2 inhibits FOXO1 via control of its acetylation [406].
	FOXO3	¬AKT ∧ ¬mTORC2	AKT phosphorylates FOXO3 [654, 227]. mTORC2 inhibits FOXO3 via controlling its acetylation [406].
	AMPK	(RSK[-2] ∨ TP53[-2]) ∧ ¬PP2A ∧ ¬AKT	Liver kinase B1 (LKB1) activates AMP-activated protein kinase (AMPK) via phosphorylation [153, 418, 584, 707]. Given that LKB is phosphorylated and activated by RSK, it was included as a dealy node [553]. Overexpression of Sestrin1 leads to increases in AMPK activation [584]. TP53 induces expression of Sestrin1/2 [153]. Again, it is included as a delay node. PP2A inhibits AMPK [178, 303]. AKT inhibits AMPK via phosphorylation [37, 210, 246, 332, 547, 604].

Table 4: Boolean functions of the pNET model. Regulatory interactions of the model are summarised by logic connectives AND ($\wedge$), OR ($\vee$), and NOT ($\neg$). To reduce the complexity of the model, linear interactions are depicted by time delays ($[-2]$). A detailed biological description of the Boolean functions is reported with references.

	Node; $t+1$	**Boolean function;** t	**Description**
PI3K/AKT signalling	GLI1	$((MYC \vee STAT3) \wedge \neg MEN1 \wedge \neg TP53) \wedge ((MEK \vee AKT \vee ERK \vee RSK) \wedge (\neg AMPK \wedge (\neg GSK3\beta \vee (GSK3\beta \wedge S6K))))$	MYC transcriptionally activates GLI1 [375, 497, 661, 731]. Similarly, STAT3 can induce GLI1 transcription [52, 69, 601]. MEN1 represses GLI1 expression [207]. TP53 inhibits the transcription, nuclear translocation and protein stability of GLI1 [497]. MEK and ERK increase the transcriptional activity of GLI1 [497]. MEK and RSK also promote GLI1 nuclear localisation and stabilisation [497]. AKT also increases the transcriptional activity, nuclear localisation and protein stability of GLI1 [497]. GSK3β induces degradation of GLI1 [497]. AMPK inhibits GLI1 via direct binding [711, 752]. S6K enhances activation of GLI by preventing its GSK3β mediated degradation [497].
	REDD	$(HIF1 \vee TP53)$	HIF1 induces the expression of REDD [153, 707]. TP53 also induces REDD expression [153].

Table 4: Boolean functions of the pNET model. Regulatory interactions of the model are summarised by logic connectives AND ($\wedge$), OR ($\vee$), and NOT ($\neg$). To reduce the complexity of the model, linear interactions are depicted by time delays ($[-2]$). A detailed biological description of the Boolean functions is reported with references.

	Node; $t+1$	**Boolean function;** t	**Description**
mTOR signalling	TSC	$(TP53 \vee FOXO3) \wedge (AMPK \vee GSK3\beta \vee REDD) \wedge \neg AKT \wedge \neg ERK \wedge \neg RSK$	TP53 induces the expression of TSC [153]. Similarly, FOXO3 can induce the expression of TSC [306]. Activated AMPK phosphorylates and activates TSC [153, 425, 426, 584, 707]. GSK3β activates TSC via phosphorylation [425, 257]. AKT phosphorylates and inhibits TSC [153, 235, 418, 425, 500, 707]. REDD releases TSC2 from the association with inhibitory 14-3-3 proteins, which act independently from AKT phoshorylation activity and AMPK [153, 418, 584, 595, 658]. ERK inhibits TSC in independent sites from AKT [418, 584, 658, 707]. RSK also inhibits TSC by phosphorylation [584, 707].
	mTORC1	$\neg TSC$	TSC exerts guanosine triphosphate (GTP)ase activity to negatively regulate GTP-binding protein Ras homolog enriched in brain (RHEB), part of the mTORC1 complex [153, 425, 500, 584].
	S6K	$mTORC1 \wedge PI3K \wedge \neg PTEN$	Both the phosphorylation of mTORC1 and PI3K are required for the activation of S6K [153, 580, 654, 658, 670, 707]. PI3K can be active only in absence of PTEN [70].
	mTORC2	$PI3K \wedge \neg PTEN \wedge \neg S6K$	PI3K, active only in absence of PTEN, activates mTORC2 [153, 70]. S6K inhibits mTORC2 [708].
	4E-BP1	$\neg mTORC1$	mTORC1 phosphorylates Eukaryotic translation initiation factor 4E-binding protein 1 (4E-BP1) [346, 425, 708].

Table 4: Boolean functions of the pNET model. Regulatory interactions of the model are summarised by logic connectives AND ($\wedge$), OR ($\vee$), and NOT ($\neg$). To reduce the complexity of the model, linear interactions are depicted by time delays ([−2]). A detailed biological description of the Boolean functions is reported with references.

	Node; $t+1$	**Boolean function;** t	**Description**
mTOR signalling	eIFs	(RSK $\vee$ AKT $\vee$ S6K $\vee$ ERK[-2]) $\wedge$ $\neg$4EBP1	RSK, AKT, and S6K phosphorylate and activates eIFs [425]. ERK inderictly activates eukaryotic initiation factors (eIFs) via MAP kinase interacting serine/threonine kinase 1 (MNK) (here as delay node) [535]. 4E-BP1 inhibits eIFs [153, 346, 418, 707].
	STAT3	eIFs $\wedge$ mTORC1 $\wedge$ $\neg$SETD7 $\wedge$ $\neg$DAXX	eIFs are required for the translation of STAT3 [418]. mTORC1 phosphorylate and activates STAT3 [346]. STAT3 transcriptional function is inhibited by SET domain-containing 7 histone lysine methyltransferase (SETD7), preventing STAT3 binding to DNA promoters [32, 328, 618]. DAXX supresses STAT3 transcription [409, 450].
	DAXX	MEN1 $\wedge$ ERK[-2]	MEN1 binds and up-regulates DAXX activity at gene promoters [154, 155]. DAXX expression can be induced by ETS1 a transcription factor downstream of ERK (here as delay node) [356].
	TP53	GSK3β $\wedge$ $\neg$PP2A $\wedge$ $\neg$MDM2	Phosphorylation by GSK3β derepresses TP53 translation [235]. PP2A dephosphorylates TP53, thereby inactivating it [153, 327]. MDM2 inhibits TP53 [153, 500].

Table 4: Boolean functions of the pNET model. Regulatory interactions of the model are summarised by logic connectives AND ($\wedge$), OR ($\vee$), and NOT ($\neg$). To reduce the complexity of the model, linear interactions are depicted by time delays ($[-2]$). A detailed biological description of the Boolean functions is reported with references.

	Node; $t+1$	**Boolean function;** t	**Description**
Cell cycle	MDM2	(ERK[-2] $\vee$ TP53) $\wedge$ (AKT $\vee$ (DAXX $\wedge \neg$ RASSF1A))	TP53 can transcriptionally activate MDM2 [153, 500]. AKT inhibits MDM2 via phosphorylation [153, 418]. MEF, activated by ERK can transcriptionally regulate MDM2 [555]. DAXX binds to MDM2 and is required for MDM2 activity. Also, DAXX associates with Ras association domain family 1 isoform A (RASSF1A). Mechanistically, RASSF1A increases MDM2 self-ubiquitination by disrupting MDM2–DAXX interactions [608].
	SETD7	PDX1	SETD7 is activated at transcription level by Pancreatic and duodenal homeobox 1 (PDX1) [469].
	MEN1	FOXO1	MEN1 expression is induced by FOXO1 [154, 276, 678].
	RASSF1A	$\neg$SKP2	RASSF1A undergoes ubiquitin-mediated degradation by SKP2 [607, 608].
	CTNNB1	$\neg$GSK3β $\vee$ (GSK3β $\wedge \neg$SETD7) $\vee$ (GSK3β $\wedge$ CDH1)	GSK3β phosphorylates CTNNB1 inducing its proteaosomal degradation [386, 656]. SETD7 methylates CTNNB1 strengthening its interaction with GSK3β [32]. CTNNB1 can be sheltered from GSK3β degradation activity when it is bound to E-cadherin (CDH1) at the cellular membrane [641].

Table 4: Boolean functions of the pNET model. Regulatory interactions of the model are summarised by logic connectives AND ($\wedge$), OR ($\vee$), and NOT ($\neg$). To reduce the complexity of the model, linear interactions are depicted by time delays ([−2]). A detailed biological description of the Boolean functions is reported with references.

	Node; $t+1$	**Boolean function;** t	**Description**
Cell cycle	MYC	(ERK[-2] $\vee$ (CTNNB1 $\wedge$ RAC1)) $\wedge$ $\neg$FOXO3 $\wedge$ $\neg$FOXO1 $\wedge$ $\neg$MEN1 $\wedge$ $\neg$GSK3β $\wedge$ ($\neg$PP2A $\vee$ CIP2A)	ERK transcriptionally controls the activation of MYC [96, 451]. GSK3β inhibits MYC via phosphotylation [195, 331]. CTNNB1 presence in the nucleus, where it can induce MYC expression, is controlled by C3 botulinum toxin substrate 1 (RAC1) [704]. On the opposite way, MEN1 shuffles CTNNB1 from the nucleus to the cytosol [67, 276, 319]. MEN1 can also control expression of MYC [207]. FOXO1 and FOXO3 repress the expression of MYC [406]. If not bound to cancerous CIP2A, PP2A degradates MYC [119, 695].
	p27	(MEN1 $\vee$ FOXO3 $\vee$ PP2A) $\wedge$ $\neg$ SKP2	p27 can be transcriptionally induced by MEN1 [259, 292, 408, 430, 564, 629, 703]. Also FOXO3 can transcriptionally induce p27 [192, 290]. PP2A can also induce accumulation of p27 independently from the AKT pathway [273, 311]. SKP2 induces p27 degradation [758].
	p18	MEN1	MEN1-dependent histone methylation maintains the expression of Cyclin Dependent Kinase Inhibitor 2C (p18) [292, 408, 430, 564, 629, 702, 703].

Table 4: Boolean functions of the pNET model. Regulatory interactions of the model are summarised by logic connectives AND ($\wedge$), OR ($\vee$), and NOT ($\neg$). To reduce the complexity of the model, linear interactions are depicted by time delays ([−2]). A detailed biological description of the Boolean functions is reported with references.

	Node; $t+1$	**Boolean function;** t	**Description**
Cell cycle	p21	(TP53 $\vee$ RSK[-2] $\vee$ MEN1) $\wedge$ $\neg$ SKP2 $\wedge$ $\neg$GLI1	LKB1, directly downstream of RSK, can transcriptionally induce the expression of p21 [640, 746]. TP53 induces p21 expression [59, 608]. MEN1 can also induce p21 expression [34]. SKP2 phosphorylates p21 and prompts it for degradation [686]. p21 expression is up-regulated when GLI1 is down-regulated [471].
	CCND1	(MYC $\vee$ (CTNNB1 $\wedge$ RAC1 $\wedge$ $\neg$MEN1)) $\wedge$ $\neg$p18 $\wedge$ $\neg$RASSF1A $\wedge$ $\neg$GSK3β	MYC can induce the expression of CCND1 [114, 157, 174]. CTNNB1 presence in the nucleus, where it can induce CCND1 expression, is controlled by RAC1 [704]. On the opposite way, MEN1 shuffles CTNNB1 from the nucleus to the cytosol [67, 276, 319]. p18 inhibits CCND1 activity by inhibiting binding to CDK4 and CDK6 [238]. GSK3β has been shown to phosphorylate and inhibit CCND1 [129]. RASSF1A inhibits the accumulation of CCND1 [591].
	RB	PP2A	PP2A dephosphorylates RB, leading to its activation [14, 97, 326, 383, 645].
	E2F	($\neg$RB $\vee$ (RB $\wedge$ CCND1) $\vee$ (RB $\wedge$ PDX1)) $\wedge$ $\neg$p21	Phosphorylation of RB by CCND1 releases E2F [51, 101, 237, 472]. RB can also stabilise via binding PDX1 at the same site of E2F, thus creating a binding competition [313]. p21 suppresses the activity of E2F-responsive promoters [130].

Table 4: Boolean functions of the pNET model. Regulatory interactions of the model are summarised by logic connectives AND ($\wedge$), OR ($\vee$), and NOT ($\neg$). To reduce the complexity of the model, linear interactions are depicted by time delays ([−2]). A detailed biological description of the Boolean functions is reported with references.

	Node; $t+1$	**Boolean function;** t	**Description**
	CCNE1	E2F $\wedge$ ¬p21 $\wedge$ ¬p27	E2F promotes CCNE1 transcription and progression from the G1 to S phase of the cell cycle [51, 101, 472]. p27 can inhibit CCNE1 by binding CDK4 [508, 648]. p21 inhibits CCNE1 [264].
Cell adhesion	SLUG1	¬GSK3β $\wedge$ (ERK[-2] $\vee$ GLI1) $\wedge$ (¬DAXX $\vee$ (DAXX $\wedge$ HIF1))	Snail family transcriptional repressor 2 (SLUG1) bound to DAXX cannot inhibit the CDH1 promotor anymore, thus is inactive; when HIF1 is present instead, it can bind DAXX and prevent SLUG1 inhibition of CDH1 activity [369]. GSK3β induces the degradation of SLUG1 [289]. ERK can control the expression of SLUG1, putatively via Sp1 transcription factor (SP1) [93, 200]. GLI1 can induce transcription of SLUG1 in BON-1 cells [151, 360, 361].
	RAC1	(FAK1 $\vee$ PI3K $\vee$ mTORC1)	RAC1 is activated by PI3K [120, 724]. FAK1 activates and translocates RAC1 for focal adhesion [82, 286]. mTORC1 inhibits RAC1 activity and translation [203, 373].
	IQGAP1	¬GSK3β	Inhibition of GSK3β frees IQ motif-containing GTPase-activating protein 1 (IQGAP1) to regulate and activate RAC1 [625].

Table 4: Boolean functions of the pNET model. Regulatory interactions of the model are summarised by logic connectives AND ($\wedge$), OR ($\vee$), and NOT ($\neg$). To reduce the complexity of the model, linear interactions are depicted by time delays ($[-2]$). A detailed biological description of the Boolean functions is reported with references.

	Node; $t+1$	**Boolean function;** t	**Description**
Cell adhesion	PDX1	$((RB \wedge CCND1) \vee RB \vee ERK) \wedge \neg GSK3\beta \wedge \neg MEN1$	ERK activates PDX1 via phosphorlylation [307]. RB stabilises PDX1 [313]. Besides, PDX1 preferentially interacts with phosphorylated forms of RB (here RB and CCND1) [307]. GSK3β phosphorylates PDX1 prompting it to proteosomal degradation [46, 251]. MEN1 can repress the expression of PDX1 [275].
	CDH1	$\neg SLUG1 \vee PDX1$	SLUG1 inhibits the CDH1 promoter [151, 730]. PDX1 directly binds and activates CDH1 transcription [403].
	Tight Junctions (TJ)	$CDH1 \wedge CTNNB1 \wedge (\neg IQGAP1 \vee ((IQGAP1 \wedge (RAC1 \vee MEN1)))$	CDH1 and CTNNB1 are essential components of tight junctions [466, 723]. RAC1 promotes CTNNB1 shuffling to the nuclei, while MEN1 promotes its presence in the cytoplasm where it can partecipate to tight junctions [67, 276, 319, 704]. The binding of IQGAP1 to CTNNB1 abrogates the binding of the CTNNB1/CDH1 complex to α-catenin and thus, leads to decreased adhesion [466, 723]. IQGAP1-mediated inhibition of adhesion can be relieved by binding of RAC1–GTP to IQGAP1, which displaces IQGAP1 from CTNNB1 [337, 466, 723]. Also, MEN1 can cause a similar effect to RAC1 by competitively binding IQGAP1 [723].

3.2.2 *Simulating pNET mutations reveals a heterogeneous phenotypical behaviour*

Once established, the dynamic behaviour of the pNET model was investigated. From literature, it is known that the most frequently reported mutations for pNETs are alterations in MEN1, DAXX, and TSC [163]. Hence, this mutational landscape was reproduced by simulating in *in silico* knockouts for these genes. In addition to the mutations, a wildtype (WT) condition was simulated by applying an unperturbed simulation setup (Figure 31, and Appendix Figures A3-A6). For each condition, the attractor landscapes and corresponfing basin distributions were estimated based on 10,000 randomly drawn starting states (see Methods Section 2.1.1).
To evaluate and compare the obtained attractor patterns to the experimental phenotypical data available for these mutations, the activity of certain nodes in the attractors were used to assign a given phenotype. To do so, phenotypes that are also described in experimental results such as proliferation, quiescence, Go-alert, detachment, and angiogenesis were considered. To evaluate the proliferation status, the activities of CCNE1 and E2F were considered. The activation of these two proteins marks the entry to the S-phase. As a result, their absence of activity in the attractor pattern was assigned to a quiescent phenotype. Attractors with no CCNE1 and E2F activity, but presenting mTORC1 activity were assigned to a Go-alert phenotype. This particular state was first described in stem cells and related the activity of mTORC1 to an "alert" state priming cells to enter the cell cycle [523, 539]. The presence of this combination of attractor states was interpreted as priming to proliferation, and therefore this state was differentiated from complete quiescence. The detachment was evaluated based on the activity of the node "tight junctions". Instead, angiogenesis was considered present when both VEGF and VEGFR were active in the attractor landscape. Finally, the dominance of these phenotypes (or their combination) in the attractor landscape was evaluated based on the corresponding estimated basin of attraction (see also Methods Section 2.3.1.1). Please note that the larger the basin, the more the attractor is preponderant in the landscape, and the more the corresponding phenotype is considered relevant [709]. A visual summary of the attractor pattern matching to phenotypes is presented in Figure 31A.

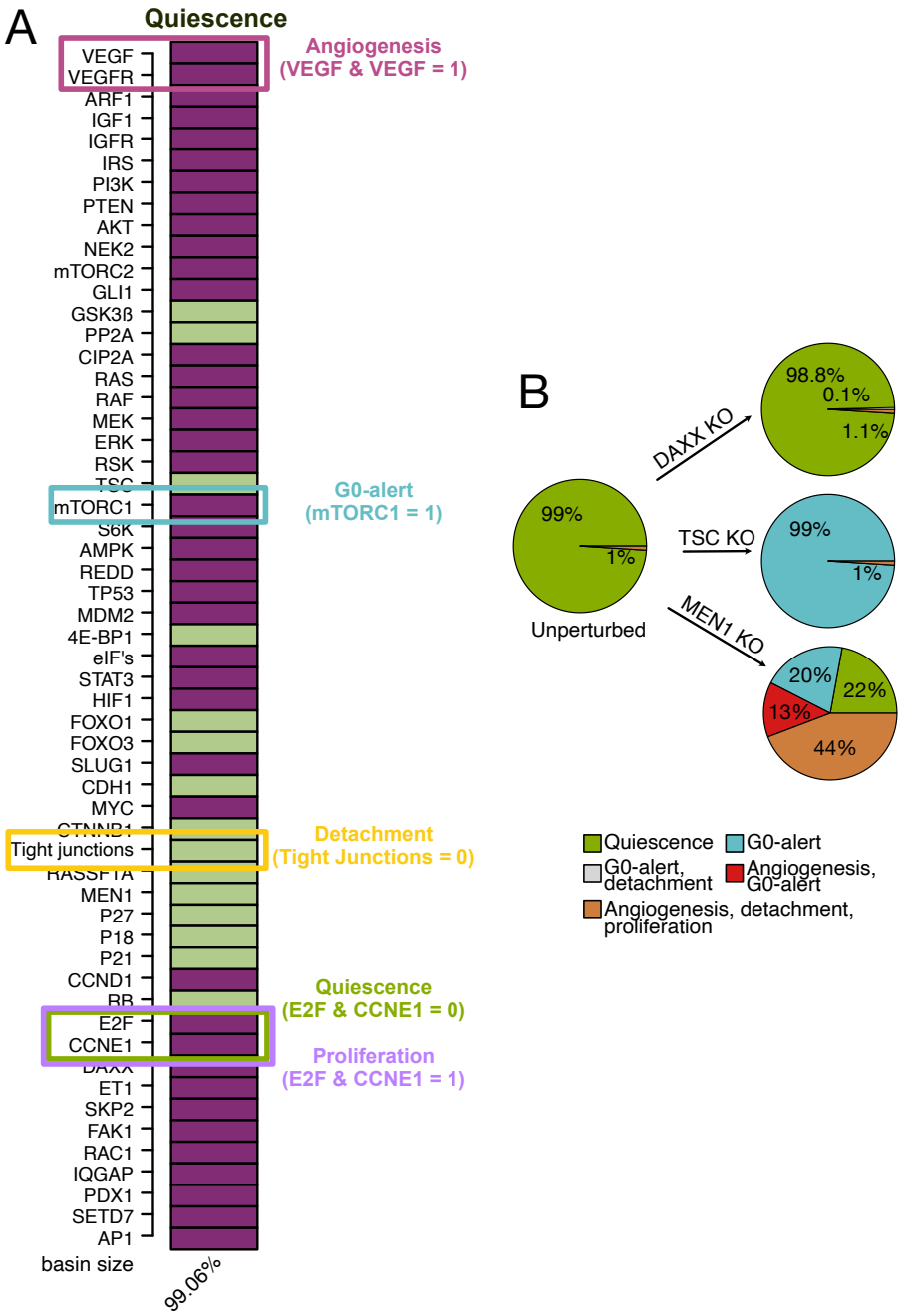


Figure 31: **Attractor landscape evaluation of the PNET model.** The attractor patterns of the pNET model simulations were matched to cell related phenotypes (A). Nodes whose activities were evaluated for phenotype matching are highlighted and the criteria for each phenotype is depicted. Exemplarily, the attractor pattern of the unperturbed condition matching to quiescence was depicted. Basin percentage distributions of pNET phenotypes in the wild type (unperturbed) as well as after introducing common mutations like DAXX, TSC, or MEN1 knockout (KO) are shown (B). Here, phenotypes are presented in their abundance and the legends reports the colour-code interpretation. The complete phenotypical landscape with the activity of each node can be found in the Appendix Figures A3-A6.

The simulations indicate that unperturbed (=WT) and DAXX knockouts were the ones with the largest percentage of the quiescent phenotype (Figure 31B). In addition, they resulted in respectively in three and four attractors, one single state and two/three cyclic ones (Appendix Figure A3 - A4). In both simulation scenarios, around 99% of the estimated basin of attraction is covered by quiescent activities. In around 1% of cases instead, the attractor landscape reports a combination of angiogenesis, detachment, and proliferation activities (Figure 31, Appendix Figure A3- A4). For the DAXX knockout specific simulation, a small percentage of the estimated basin of attraction (0.1%) showing Go-alert and detachment was found, represented by a cyclic attractor and indicating a potentially more severe condition compared to the WT (Figure 31B, Appendix Figure A4). These results are in line with the known indolent behaviour of pNETs, which are known to be slow-growing tumours [415]. Interestingly, a certain percentage of proliferating and invading phenotypes is still found, that might account for the malignant potential observed in these tumours could be retrieved (Figure 31, Appendix Figure A3- A4). In line with this, different authors could show that staining for Ki-67 with an amount greater than 2-10% correlates with metastatic behaviour and malignancy grade [266]. In the specific context of DAXX loss, the effects of its dysregulation remain extremely poorly understood in patients and *in vivo* models [389]. A recently published study of a mouse model with conditional Pdx1-cre driven DAXX inactivation indicated that DAXX alone has no effect on pancreatic development and function, which remained predominantly normal [683]. On the other hand, DAXX loss altered the transcriptome in association with derepression of endogenous retroviral elements (ERV), mirroring the human pNETs condition [683]. This potentially creates permissive chromatin states that, in response to stress or other mutations, could promote tumour development [683]. Also, human studies showed that DAXX mutations had better overall survival when compared to other types of mutations [277]. The results on the DAXX mutational landscape, suggest a rather limited role of DAXX as a driver mutation in inducing aggressive tumour phenotypes, thus corroborating the results observed in mouse and human cohorts. Nevertheless, the impact on patients´ phenotypes of DAXX mutations is still far from being fully elucidated, showing heterogeneous results in different patient cohorts [396].
Also the TSC *in silico* knockout resulted in three attractors, one single state and two cycling ones (Appendix Figure A5). In the simulation, a 1% of the estimated basin of attraction reporting angiogenesis, detachment, and invasion. Instead, the 99% of the estimated basin shows a Go-alert associated phenotype, connected to the activation of mTORC1 in the attractor pattern (Figure 31B, Appendix Figure A5). The activation of the mTOR pathway is a commonly reported event after TSC loss in patients [347]. In addition, the loss of TSC in most of the cases does not correlate with aggressive pNETs [347], following the *in silico* simulation results. However, due to

the scarce number of patients identified with this mutation, it is rather difficult to formulate reliable predictions based on the currently available clinical data [347]. The MEN1 *in silico* knockout showed the highest number of attractors, 12 in total, with only one single state attractor (Appendix Figure A6). Interestingly, together with the increase of attractors, also the combination of phenotypes became more heterogenous (Figure 31B, Appendix Figure A6). In particular, 44% of the basin of attraction resulted in attractors showing angiogenesis, detachment, and proliferation. The rest of the attractor landscape showed either complete quiescence (22%) or Go-alert alone or in combination with angiogenesis (respectively 20% and 13%). MEN1 mutations are among the most studied mutations in pNETs. In the case of MEN1 germline mutations, patients develop in 70% of cases NETs with predominance to the pancreas [347]. Distal metastases from pNETs are the major cause of MEN1-specific mortality [347]. Additionally, pNETs in MEN1 germline mutations occur at a younger age and in multiple sites of the pancreas [347]. For what concerns sporadic pNETs, MEN1 loss is still the most frequent alteration present in 44% of cases [277]. 40% of sporadic pNETs display abnormally low nuclear staining from MEN1 [102]. Altogether these data provide strong evidence that MEN1 has a crucial role in the tumorigenesis of pNETs. Accordingly, mouse models with heterogeneous loss of MEN1 develop multiple endocrine tumours [748]. Interestingly, these mice do not develop poorly differentiated and highly metastatic NECs, suggesting that additional mutations might be needed for the formation of high-grade tumours [748]. In accordance with experimental data, the *in silico* knockout for MEN1 shows a more prominent proliferation and invasion potential compared to the other simulation conditions (Figure 31B). However, also, in this case, most of the basin of attraction still indicates overall a non proliferating, non proliferating tumour (55% of the estimated basin). This result enforces the ideas of both the crucial role of MEN1 in pNETs tumourigenesis and the further need for additional mutations for the insurgence of a highly aggressive pNET.

3.2.3 *Integration of model prediction and foreign feartures classification experiments in defining similarities in WT, MEN1, DAXX loss phenotypes*

As described above, correlating pNETs mutations with patients outcome and tumour severity might be a rather difficult task, especially in case of mutations such as DAXX or TSC. For this reason, based on the availability of expression data from tumour specimens, a further strategy to evaluate similarities between alterations in pNETs was set up in order to support the elucidation of mutation severity (see also Methods 2.3.2.2). The GSE117851 dataset, reporting expression profiles for DAXX, MEN1, double mutated and WT patients, was utilised for the set up of series foreign features classification experiments (Figure 32A, see also Methods 2.3.2.2).

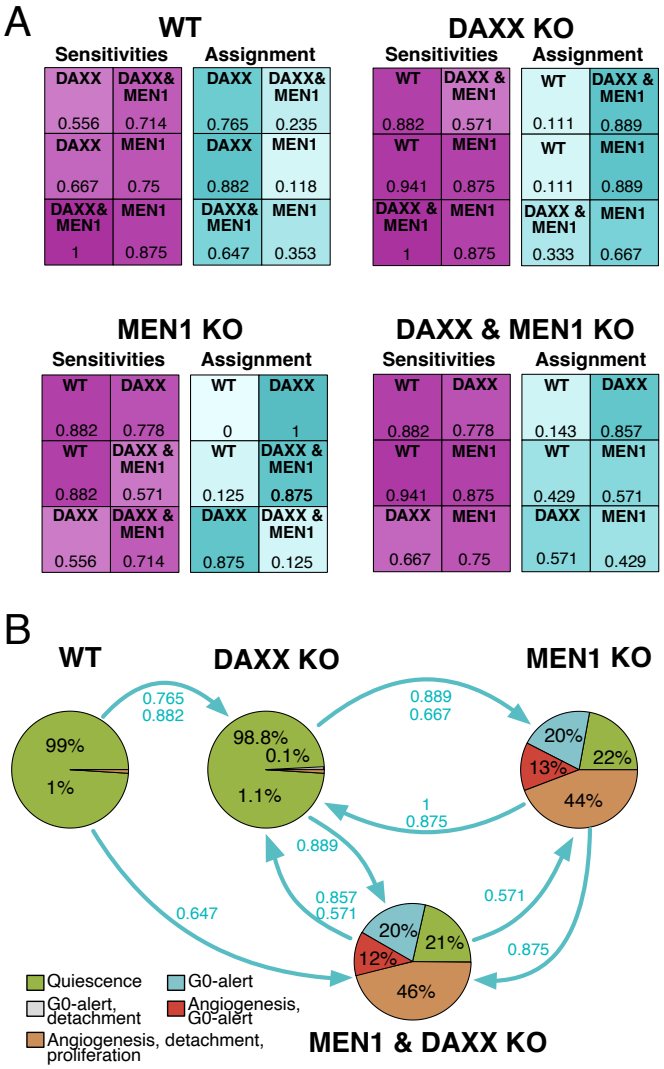


Figure 32: **Integration of model simulation with patients expression data via foreign classifier experiments.** The foreign classifier experiments were performed on the GSE117851 dataset for each mutated pNETs cohort of patients (A). For each mutated group the sensitivities of the binary classifications are reported in the tables in purple on the left. On the right side in the blue tables, instead, the assignment of the foreign class within the binary classification experiments is reported. Colour intensities follow the increasing sensitivities and assignment frequencies. The results of the foreign classifier experiments are integrated in the attractor landscapes of the pNETs model (B). Attractor phenotypical landscapes are depicted in order of similarities one to the other. The light blue arrows indicate the assignments from the foreign classifier experiments and the directions suggest which group was assigned as a foreign one into the other. E.g. WT is always more frequently assigned to DAXX mutated tumours and the assignment frequencies for each experiment are reported in the corresponding arrows. Finally frequencies of assignment for all foreign classification experiment are reported in proximity of each arrow.

The aim was not only to compare similarities retrievable from expression profiles and dynamic landscapes but also to potentially integrate results inferred from both approaches. Within the foreign classifier approach, binary classification experiments are performed for classes present in the dataset excluding one. Afterwards, the group initially left out is classified as a foreign class within all performed binary classification tasks and the percentage of assignments to one of the two original classes is calculated. Based on the percentage of assignments in the foreign class it is possible to deduce similarities among groups. The results of this approach are depicted in Figure 32A. When the WT group is considered as a foreign class, it is always preferentially assigned to DAXX mutated samples compared to MEN1 and double mutated ones, suggesting that the WT tumours share similarities in their expression profiles preferentially with DAXX mutated ones. The only assignment where the double mutated tumour is preferred is in the classification with MEN1. This suggests that a DAXX mutated condition a(s in the double mutated group) is still preferred to MEN1 alone. Interestingly, when the DAXX mutated group is considered as a foreign class, it got assigned with higher frequency to MEN1 tumours or double mutated ones when in the binary classification with the WT group. Instead, within the binary classification of MEN1 and double mutated tumours, the first received a more frequent assignment of the DAXX mutated group. Hence, DAXX mutated tumours seem to be rather more frequently assigned to MEN1 mutated ones rather than WT. Considering MEN1 mutated tumours as a foreign class, instead, in most classification results it got more frequently assigned to DAXX or double mutated tumours, interestingly avoiding WT ones with very low or zero frequency of assignment. Finally, the double mutated tumours have rather higher assignments to DAXX or MEN1 groups. Interestingly, in the binary classification of DAXX and MEN1 groups, double mutated ones are almost equally assigned as a foreign class. Thus suggesting that common features might be shared on the molecular profile of double mutated tumours.
The results of the foreign classifier strategy were further compared with attractor landscapes. Figure 32B depicts attractor landscapes ordered by similarities and connected by arrows referring to the higher assignment of the corresponding class in the foreign classifier experiments. To fully compare the two approaches, also the attractor landscape of the double mutation of DAXX and MEN1 was computed (see also Appendix Figure A7). Interestingly, the double mutated attractor landscape does show high similarity with the MEN1 loss landscape, with a small increase of the aggressive phenotype when including the DAXX loss mutation. In accordance, with the foreign classifier approach, the double mutated expression profiles are more frequently assigned to either the MEN1 or the DAXX mutated groups, while having fewer assignment frequencies to the WT one. The attractor landscape and phenotype distribution of WT tumours, instead, shows the largest similarity to the

DAXX loss one, again following the assignment frequencies of the foreign classifier approach. The MEN1 attractor landscape, instead, is the most severe in terms of tumour aggressive traits, comparable to the double mutated one. In accordance, the MEN1 mutated group is less frequently assigned to WT group, which is also less severe in terms of attractor landscapes. The DAXX attractor landscape shows a phenotype distribution similar to the WT, while still reporting an extra phenotype showing more severe and non-quiescent trades. However, when the DAXX mutated group of patients' molecular profiles is applied as a foreign class, it gets higher frequencies of assignment with MEN1 mutated samples or double mutated ones, rather than the WT group. Vice versa, the WT group is highly assigned as a foreign class to the DAXX mutated group when classified against MEN1 or double mutations. Hence, it seems that the DAXX mutated group of patients' expression profiles is somehow more heterogenous sharing common features with both WT and MEN1 or double mutated tumours. A hint of this potential similarity observed in the expression profile is the persistent DAXX-related phenotype observed in the attractor landscapes, potentially influencing also the distribution of the double mutated landscapes. Interestingly, as a support to this theory, also the multi class classification approach showed an almost evenly distributed assignment of the DAXX mutated group to the other ones (Figure 29B). A potential explanation for this level of heterogeneity in DAXX mutated pNETs expression profiles might reside in its effects on chromosomal instability [397]. This possibility would explain the heterogeneity of DAXX expression profiles. While chromosomal instability might be difficult to capture at a molecular crosstalk level, the pNETs model still captures a difference between DAXX and WT tumours. Furthermore, the integration of information from the foreign classifier approach was able to detect this enhanced heterogeneity that might be the basis of the heterogenous effects of DAXX mutation in patient cohorts [396]. In fact, while at a pathway crosstalk level DAXX loss might have a rather small impact, as also shown in mouse models [683], in the patients' cohort the presence of chromosomal instability induced by the loss of DAXX might, on the long run, induce further unpredictable mutations, outputting a variety of potential phenotypes independent from the effect of DAXX loss on the molecular crosstalks. Altogether, especially in light of the high heterogeneity of pNETs, model dynamic simulation and foreign classification results based on patients' expression profiles could show general accordance when comparing similarities among molecular profiles and attractor landscapes.

3.2.4 *Attractor-specific activities validation based on known expression patterns of pNETs*

After investigating the mutation-specific tumoral phenotypes, the attractor pattern connected to the combined phenotype showing angiogenesis, detachment, and pro-

liferation was further investigated. While the distribution of this phenotype varies among different *in silico* knockout simulations (WT, MEN1 loss, TSC loss, DAXX loss), the attractor pattern related to its behaviour remains highly conserved (Appendix Figures A3 - A6). Considering this attractor pattern as a progressed pNET, it was further validated by matching its activities to the ones experimentally observed suring pNETs progression (Figure 33, Table 5).

Table 5: **Validation of attractor patterns for pNETs progression.** The attractor activities for pNET progression described in the text are listed and divided by analysed signalling pathway. For each node, the activity in the aggressive pNET attractor landscape compared to the quiescent one is indicated. For each attractor-inferred activity, experimental evidence was matched as referenced.

Pathway	Attractor activity	Experimentally matched activity
Angiogenesis	VEGFR (increased)	[563, 575]
	VEGF (increased)	[563, 575]
	HIF1 (increased)	[563]
MAPK signalling	ERK (partially increased)	[205]
	CIP2A (increased)	Figure 33
	IGF1 (increased)	Figure 33
	FAK1 (increased)	[163, 368, 463]
PI3K/AKT signalling	AKT (increased)	[185, 205, 638]
	FOXO3 (decreased)	Not yet investigated, but lowly expressed in β-cells [192]
	FOXO1 (decreased)	[72]
	PTEN (decreased)	[432]
mTORC signalling	TSC (decreased)	[432]
	mTORC1 (increased)	[98]
Cell cycle	CCND1 (increased)	[94, 205]
	E2F (increased)	Figure 33
	CCNE1 (increased)	Figure 33
	MYC (increased)	[83, 674]
	MEN1 (decreased)	[616, 658]
Cell adhesion	CDH1 (decreased)	Figure 33

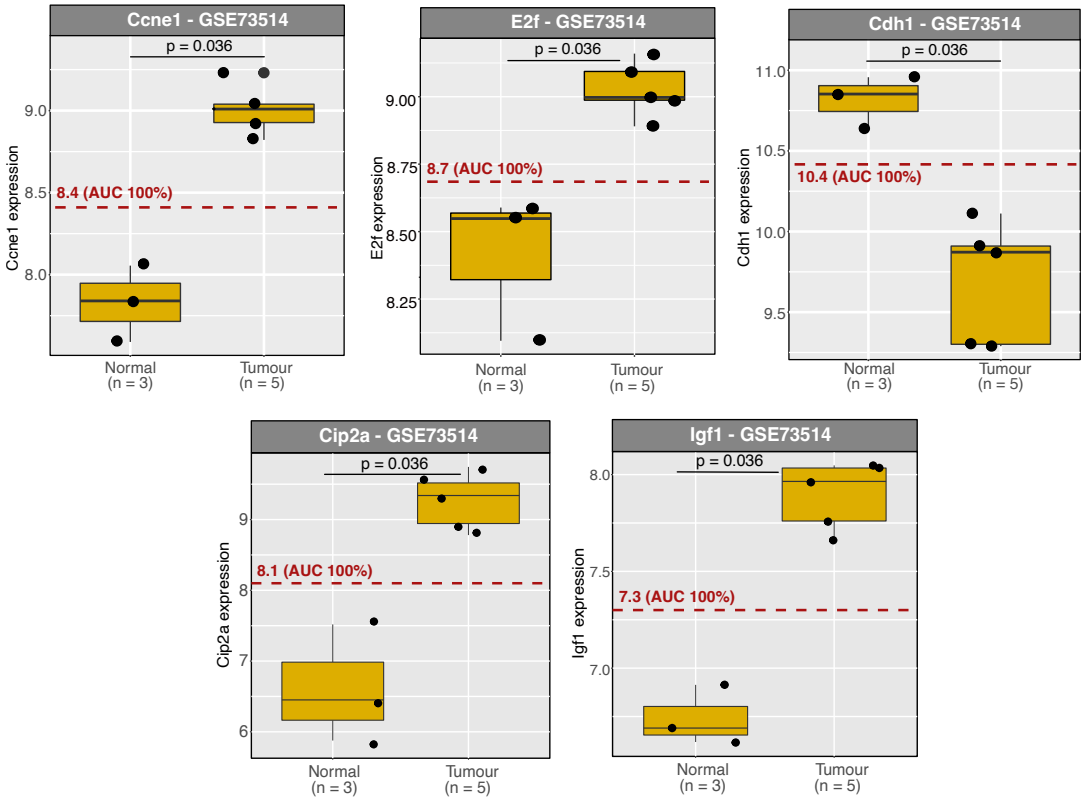


Figure 33: **Model validation via the GSE73514 dataset.** The gene expression level of normal and tumoural tissues derived from RIP-TAG2 mice in the dataset GSE73514 [546] is depicted in box plots. A Wilcoxon test was applied and significant values were considered for $p<0.05$. The dashed-lines depict the binarisation threshold, defining the value which separates normal and tumour tissue with simultaneously the highest sensitivity and highest specificity. The area under the curve (AUC) indicates the performance of the classifier. In all the depicted binarised expression values, an AUC of 100% was measured. Ccne1, E2f, Cip2a, and Ifg1 were significantly up-regulated in tumours, while Cdh1 was significantly down-regulated. These results matched the activities observed in the attractors (Appendix Figures A3-A6).

The validation was performed via both literature screening and analysis of a dataset from the RIP-TAG2 mouse model, which is tumour progression model of pNETS in mouse with a characterised progression [546]. In the latter, the attractor specific activities were compared to the binarised expression values for the corresponding investigated genes (for details on the procedure, See Methods Section 2.3.2.1). Activities of experimentally investigated regulators of the described signalling pathways and processes could be successfully validated (Figure 33, Table 5). Crucial proteins activities involved in the progression of pNETs such as AKT, mTORC1, and TSC, all belonging to the PI3K/AKT and mTOR signalling pathways were suc-

cessfully matched between attractor landscapes and experimental results (Table 5). Additionally, Focal adhesion kinase 1 (FAK1) and Extra-cellular signal-regulated kinase (ERK) activities were also matched as members of the MAPK signalling pathway (Table 5). Activation of receptors and secretion of ligands such as VEGF/VEGFR and IGF/insulin growth factor receptor (IGFR) are primary causes of aberrant activation of downstream signalling cascades [415]. These activations were accordingly observed in the attractor landscapes matching with proliferation and invasion. S-phase entry markers such as CCND1, CCNE1, and E2F in the attractor landscape were also shown to match the experimentally observed activities (Figure 33 and Table 5). CDH1 was down-regulated at the tumour stage in RIP-TAG2 mice (Figure 33), in accordance with the decrease observed in the attractor patterns (progressed versus quiescent patterns), with a consecutive loss of tight junctions (Appendix Figures A3-A6). Altogether, the attractor pattern describing aggressive behaviour in pNETs agrees with experimental data collecting tumour related activities of the same compounds. This result also further sustains the interpretation of the attractor landscapes into phenotypical readouts.

3.2.5 *Analyses of model dynamics suggest potential tumour drivers in pNETs*

Predicting the progression of pNETs is often a difficult task. While these tumours are mostly indolent, they preserve a malignant potential together with a highly heterogeneous behaviour [519]. In addition, while mutations such as MEN1 are known to be crucial for tumour development, they are frequently not sufficient to lead to predominantly aggressive phenotypes [748]. These results eventually lead to the hypothesis that a cumulative set of mutations might be required for pNET to progress into aggressive highly invasive tumours. On these grounds, it was further investigated whether the established pNETs model could support the prediction of tumour drivers. Thus, a tumour driver screening was set up by evaluating the activity of nodes in the 100 million initial states of the basin of attraction leading to the aggressive related attractor pattern in both WT and MEN1 simulation setups (Figure 34). The WT setup was selected to investigate first-hit mutations, while the MEN1 loss condition was selected to investigate potential second-hit alterations.
Given that the start states are randomly sampled, the mean activity of 0.5 is expected for nodes having no impact on the attractor pattern. Consequently, activities exceeding one standard deviation from this mean in both directions were considered as potentially relevant to the final attractor pattern. Hence, if a node has a low probability to be active in the start states leading to the severe attractor pattern, this will be considered as a hint for that node being lost or inactivated during tumour progression (See also Methods Section 2.1.3). From the set of identified drivers, nodes presenting a high or low probability of activation in the basin resulting in

a constant matched activity in quiescent and aggressive attractors were excluded. This means, that even if a node is biased towards a certain activation state in the basin, its regulatory function would lead to the same activity in both quiescent and aggressive phenotypes (namely AMPK and TP53 in the WT condition). Hence, the perturbation of that node according to the basin bias would not influence the dynamic behaviour of the system (See also Methods Section 2.1.3). Please note, that TP53 was simulated also in the WT as a comparison to the MEN1 condition, where its activity is altered in the quiescent and aggressive attractors.

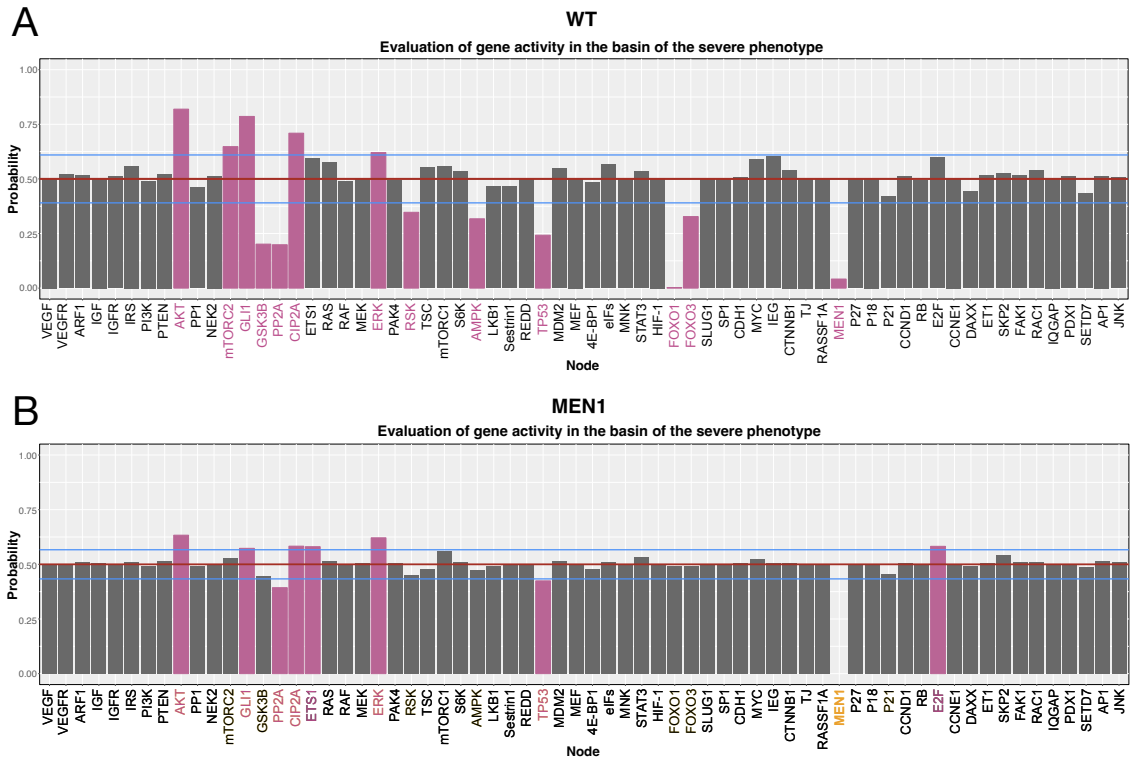


Figure 34: **Distribution of node activities in basin states leading to the severe attractor phenotype**. Probability of a certain node in the network to be active or inactive in the basin of the severe pNET related phenotype was computed by considering the times the node of interest was found active in 100 million examined states. The analysis was performed in both WT (A) and MEN1 knockout (B) simulations. Nodes highlighted in purple are the ones whose activities exceeded one standard deviation (light blue line) from the mean (dark red line) in both directions.

Following these criteria, genes selected as tumour drivers were further analysed by performing *in silico* knockins and knockouts, matching their biased activities within the basins (Figure 34). Attractor simulations and basin estimations were performed by randomly sampling 10,000 starting states (See also Methods Section 2.1.1). The

resulting attractor landscape was then analysed and matched to the previously described phenotypes for quiescence, proliferation, detachment, and angiogenesis (Figure 35). In this case, each phenotype was considered independently from the others in the overall attractor landscape (for details see Methods Section 2.3.1.1), and for each condition the total number of combined phenotypes (as previously estimated for the mutation landscapes in Figure 31B) and attractors was estimated.

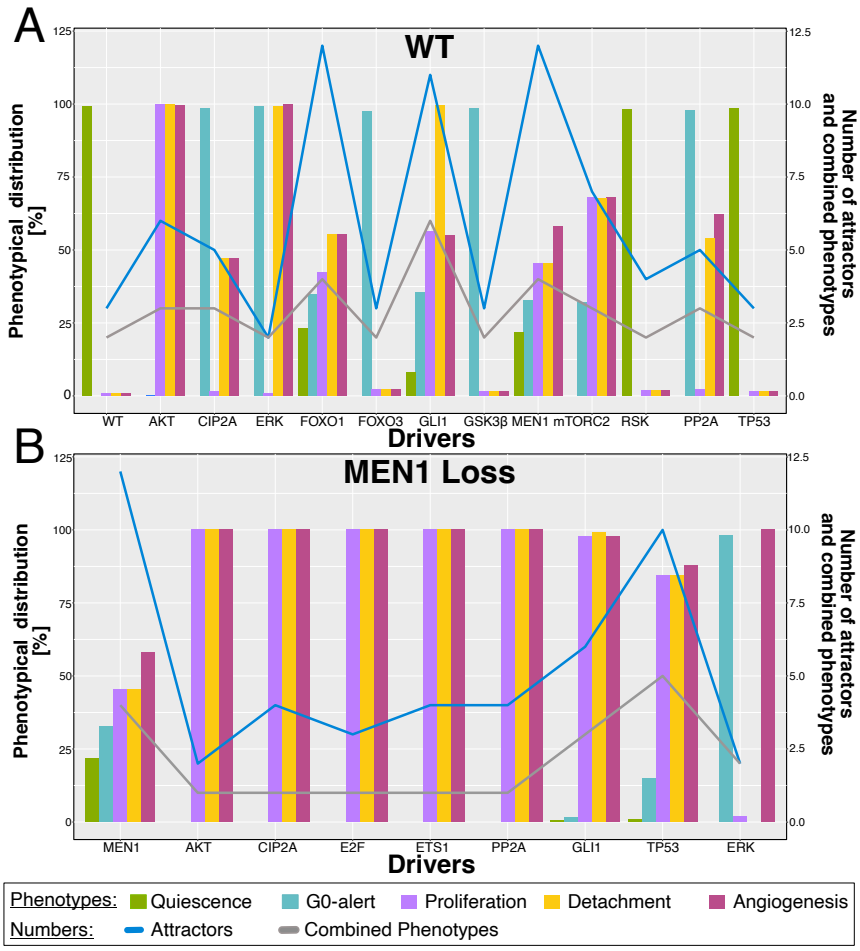


Figure 35: **Attractor landscape of pNETs drivers for WT and MEN1 loss tumours**. The attractor related phenotypes for the pNETs drivers identified via *in silico* analyses are reported for WT (A) and MEN1 loss (B) simulations. Single phenotypes are reported in the barplots as percentages of the estimated basin of attraction and colour coded as shown in the legend. The number of attractors and total number of combined phenotypes is also reported below and depicted in the lines. As comparison, the WT MEN1 loss condition are reported on the left of each subgraph.

In general, a greater heterogeneity of node activities in the WT simulation compared to the MEN1 loss was observed (Figure 34A and B). This result is concomitant with a larger set of selected drivers in the WT simulation (N=13) compared to the MEN1 loss (N=8). Looking at the attractor landscapes, the drivers of the MEN1 loss condition leads in most cases to a severe phenotype, concomitant with a decrease in the number of attractors and combined phenotypes (Figure 35A and B). On the contrary, WT-related drivers generally lead to more heterogeneous and less severe phenotypes (Figure 35A and B), supporting the hypothesis of the requirement of additional mutations to induce tumour progression [748, 163].
In the WT driver set, no driver except for AKT knockin was able to induce the severe cancer phenotype connected to full induction of proliferation, detachment, and angiogenesis (Figure 35A). The activation of AKT and the mTOR pathway is a hallmark of pNETs [163, 185, 205, 638]. Thus this result corroborates the correctness of the simulations. In the same line, also mTORC2 was selected as a driver [342, 588]. MEN1 and the FOXOs proteins 1 and 3 were also included in the driver set. MEN1 loss is the most common mutation in pNETs and has been connected to tumour initiation and progression [102, 277, 347]. Interestingly, FOXO1 is a direct and main regulator of MEN1 [68]. Hence, its loss mimics the loss of MEN1 (Figure 35A). CIP2A was shown to be up-regulated in pNETs based on the expression data analysis (Figure 33), and PP2A is its direct target [284]. GLI1 was shown to be highly expressed in BON1 cells and NETs of the ileum, supporting its identification as a knock-in tumour driver in the pNET model [151]. In general, the MEN1 loss driver set showed less drivers related to a more severe effect on the attractor landscape compared to the WT driver set (Figure 34B and Figure 35B). Most of the nodes in the MEN1 loss driver set overlap with the WT one, with the exception of ETS1 and E2F (Figure 34A and B). In general, nodes which the two sets have in common show a more severe phenotype when coupled with MEN1 mutation (Figure 35A and B). A striking example of this is TP53, which has hardly any influence on the landscape of the WT simulation. In MEN1 loss conditions, however, the loss of TP53 causes a sensible worsening of the attractor landscape, suggesting that TP53 might relate as a second-hit mutation. E2F and ETS1 were only found as drivers in the MEN1 loss condition. While E2F is directly connected to an increase in proliferation [633], ETS1 is still poorly studied in pNETs. Altogether it could be shown that the model was able to predict driver genes whose alteration in activities could worsen both the WT and the MEN1 loss *in silico* conditions. These drivers could be further investigated and validated in future laboratory experiments, unravelling potentially new markers for tumour progression.

3.2.6 *Model-based simulations identify a potential mechanism involved in mTORC1 inhibitors resistance*

After investigating potential tumour drivers, the model-based dynamic analyses were applied for screening of therapeutic targets. Given the relevance of the PI3K/AKT and mTOR pathways in the progression of pNETs, different studies and clinical trials have pointed to the potential relevance of the therapeutically targeting mTORC1 [350, 741]. These results have led to the approval by the FDA of the mTORC1 specific inhibitor everolimus for the treatment of pNETs [479]. The *in silico* targeting of mTORC1 was also investigated in the pNET model (Figure 36 and Appendix Figures A8-A11). The knockout simulation was performed on both the WT and the other previously investigated alterations frequently reported in pNETs, namely DAXX, TSC, and MEN1 loss conditions (Figure 36A). The distribution of the basins of attraction in each condition was estimated simulating 10,000 randomly drawn starting states (see Methods Section 2.1.1). In the WT simulation, the mTORC1 intervention caused an increase from 1% to 4% of the combined phenotype connected to proliferation and detachment. The same scenario regarding the proliferating and detaching phenotypes was shown also in DAXX and TSC loss conditions (Figure 36 and Appendix Figures A8-A10). However, in the TSC loss condition, an improvement of the phenotypical landscape by reversion of the Go-alert phenotypes to a quiescent one was observed after mTORC1 intervention (Figure 36A and Appendix Figure A10). For what concerns the MEN1 knockout, it could be observed a beneficial effect via the increasing of the quiescent phenotype (from 22% to 69%), concomitant with the loss of the Go-alert related phenotype. Still, a remaining 17% of states in the basin of attraction lead to a detaching and proliferating phenotype. In all mTORC1 interventions the angiogenic phenotype was not found (Figure 36A).

This persistance of proliferating and detaching phenotypes after mTORC1 inhibition in all simulated conditions was interpreted as an insurgence of resistance to the intervention. In accordance with these results, it was experimentally observed that mTORC1 inhibitors frequently induce resistance via the reactivation of AKT, thus preventing tumour regression and further reactivating tumour progression [80, 163, 350]. The potential mechanism leading to the insurgence of resistance after mTORC1 inhibition was further investigated. To do so, the molecular cascade leading to the resistant mTORC1 phenotype, starting from the aggressive pNET tumour attractor was studied (Figure 36B). The cascade was simulated and gave identical results starting from any state of the cyclic attractors depicting aggressive tumour trades for all investigated conditions (cyclic attractors reported in Appendix Figures A3 and A6). In Figure 36B, the cascade starting from the first state of the aggressive cancer phenotype of the WT condition was reported as an

example. Based on this simulation, it was possible to follow the molecular cascade connecting the two attractors and thus reconstruct the underlying molecular mechanism (Figure 36C). The results indicate that after mTORC1 inhibition, there is the concomitant inactivation of S6K and the reactivation IRS, which further activates AKT. The inactivation of S6K also affects mTORC2, leading to its activation and further enforcing the positive feedback on AKT. The latter shows downstream effects that affect both tumour proliferation and invasiveness (Figure 36B and C). Thus, the pNET model supports the hypothesis that mTORC1 resistance arises from a synergistic reactivation of mTORC2 and IRS. In addition, based on model simulations, this mechanism can be extended to its downstream effects on cell cycle and invasion (Figure 36B and C). In particular, the reactivation of the IRS/PI3K/AKT axis inhibits FOXOs and GSK3β, further causing the activation of CTNNB1 and MYC, and inducing the maintenance of active cyclins (CCND1 and CCNE1) (Figure 36B and C). The same axis also causes the sustained activation of RAC1 and IQGAP1 which involved the complete loss of tight junctions. The loss of STAT3 after mTORC1 inhibition further sustained the inactivation of tight junctions via the loss of PDX1 (Figure 36B and C).
This general regulatory mechanism is further sustained by the efficacy in decreasing pNET progression when using double mTOR inhibitors that target both mTORC1 and mTORC2 [479]. Orr-Asman and colleagues could show in mice that pNETs resistant to everolimus could reduce progression via switching to a double mTOR inhibitor [479]. In accordance with the hypothesised mechanism and with the experimental evidence, also the *in silico* double inhibition of mTORC1 and mTORC2 showed a decrease of the resistant phenotype in all simulated conditions (Figure 36A and Appendix Figures A12-A15).

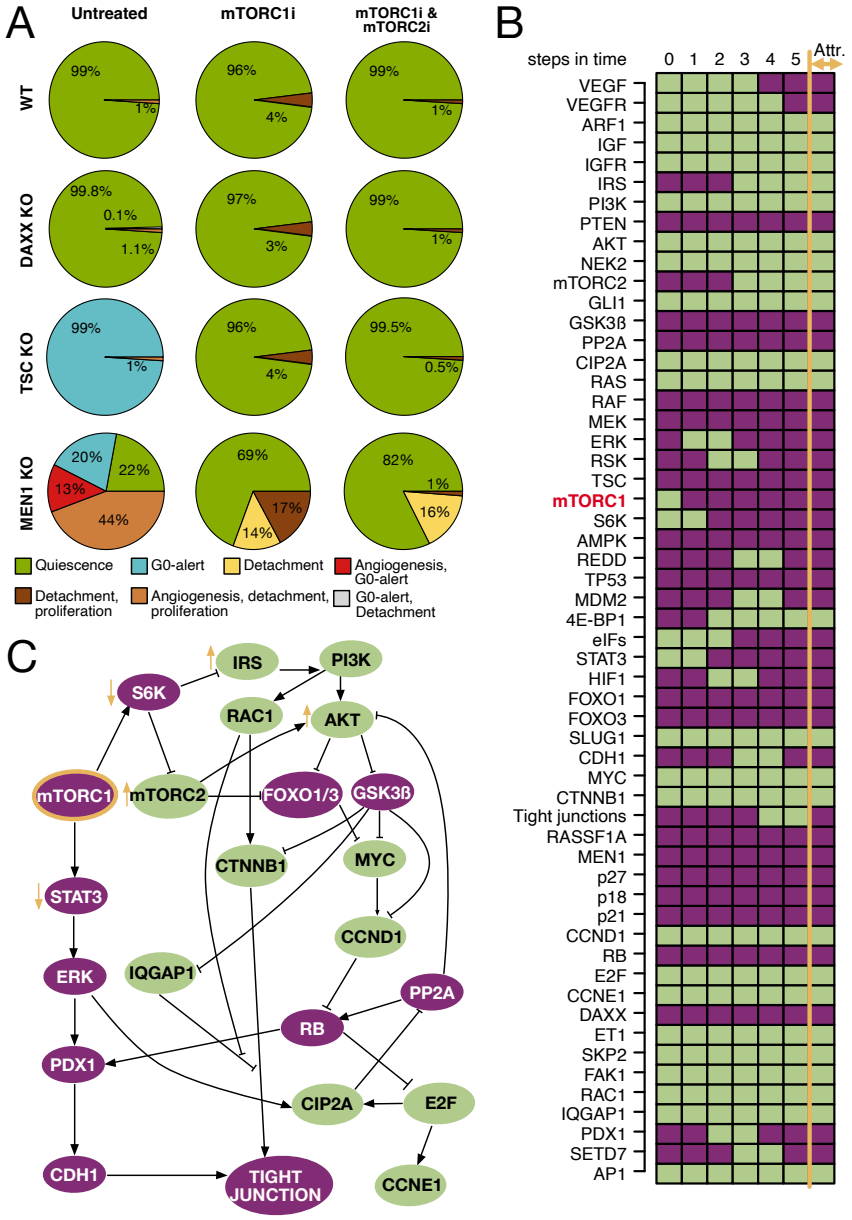


Figure 36: **mTOR targeting in pNETs**. mTORC1 knockout and its combination with mTORC2 knockout was simulated and evaluated in WT and DAXX, TSC, and MEN1 loss conditions (A). The cascade from the most severe cancer phenotype to the mTORC1 resistant phenotype was studied to infer its mechanistic behaviour (B). Genes are listed on the side and mTORC1 is highlighted in red. Node activities are depicted via coloured boxes. Green indicates active while dark purple indicates inactive nodes. A summary of the hypothesised mechanism of mTORC1 resistance is represented in an interaction graph (C). Activities of nodes directly downstream of mTORC1 are depicted with orange arrows pointing upwards (activated during resistance) or downwards (inhibited during resistance). The colour of the nodes in the interaction reflects the activities in the attractor.

3.2.7 *Automatic screening to predict potential targets in pNETs*

The insurgence of resistance in mTORC1 treated pNETs has further highlighted the need for therapeutic options in progressed pNETs [479]. To unravel new potential intervention targets, an automatic drug intervention screening was set up. Here, the aim was to identify single and double interventions able to remove the aggressive cancer attractor showing angiogenesis, proliferation, and detachment from the attractor landscape (See also Methods Section 2.1.3). For the less progressed pNETs, the normal therapeutic approach involves a "wait and see" strategy with a potential evaluation of surgical resection [519]. This condition resembles what was observed for the WT, DAXX, and TSC simulations (Figure 31B). Based on this evidence, the focus of the perturbation screening was set on the MEN1 loss condition (Figure 37), which leads to a more severe cancer phenotype and thus potentially more interesting in the perspective of potential targeted interventions.

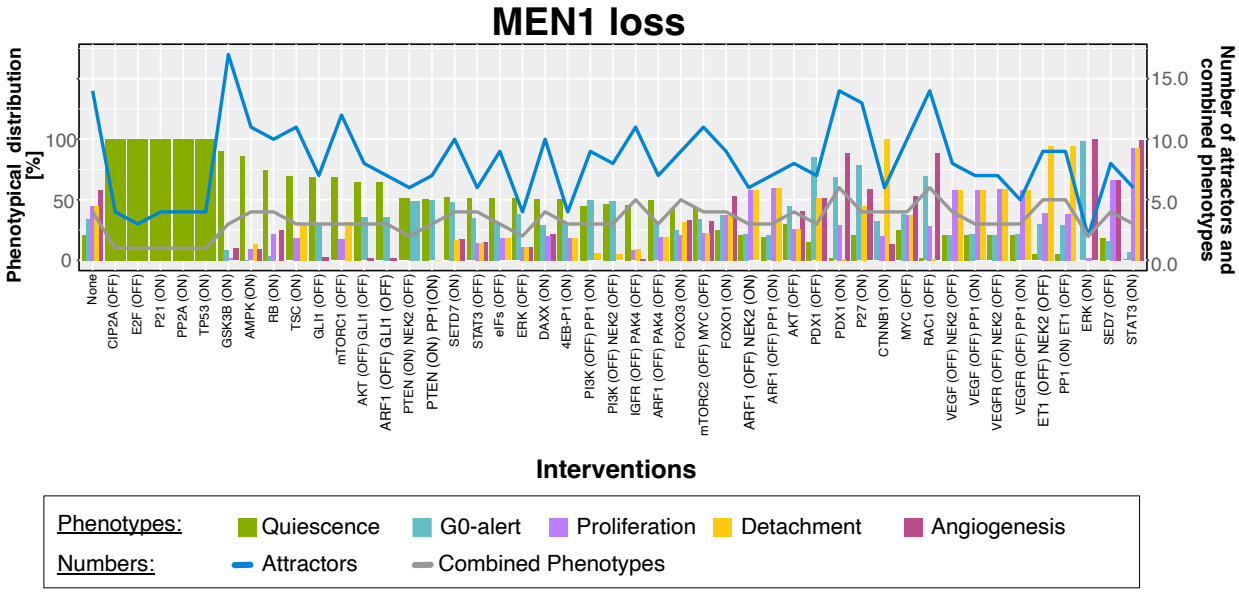


Figure 37: **Attractor landscapes of the targeted perturbation screening in MEN1 loss.** The phenotypical landscape of the obtained intervention targets from the perturbation screening are listed. Both single and double perturbation are reported. As comparison, the MEN1 loss condition is reported on the left. Perturbations that correspond to molecular knockins are reported as (ON), while knockouts are reported as (OFF). Single readout phenotypes are reported as percentages of the estimated basin of attraction in the barplots and colour coded as shown in the legend. The number of attractors and total number of retrieved combined phenotypes is also reported in the legend and depicted in the figure by the coloured lines.

Given the size of the pNET model, an automatic screening for perturbations was performed via the tool ViSiBooL [569]. After obtaining a set of single and double interventions, the corresponding basins of attraction were computed for each of them from an initial randomly drawn set of 10,000 starting states (Figure 37, Methods Section 2.1.1). The complete set of identified targets together with their phenotypical characterisation is displayed on Figure 37, including both single and combined interventions. While the identified interventions had, in general, a beneficial effect on the MEN1 loss attractor landscape, five single interventions could successfully restore a complete quiescent phenotype, namely CIP2A (OFF), E2F (OFF), p21 (ON), PP2A (ON), and TP53 (ON) (Figure 37). Interestingly, these interventions were also the ones reporting also a smaller number of combined phenotypes and attractors in the analysed attractor landscapes (Figure 37). The reduced number of attractors might relate to the network stability, indicating that the perturbation is evoking a few homogenous phenotypes connected to quiescence.
To evaluate their potential application in the case of pNETs, a literature search was performed focusing on the availability of small molecules, mechanism of action, application in clinical trials of the compounds, and application of the compounds to pNETs (Table 6). The focus on small molecules and the availability of clinical data, besides the novelty for pNETs, is aimed to highlight the potential direct transferability of our targets to a reasonable clinical setting. For all the identified intervention targets at least one small molecule was available for specific targeting (Table 6). Among the found small molecules, only Bortezomib has unidentified mechanisms of action, with the only phenotypical description of alteration of CIP2A concomitant with apoptosis induction [486]. Clinical trials were available for small molecules targeting CIP2A, p21, and TP53 (Table 6). Only Bortezomib was previously applied to pNETs and withdrawn in clinical trials [579].

Table 6: **Evaluation intervention targets** The suggested targeted interventions were analysed based on the availability of small molecules, mechanism of action, and information on clinical trials in general, or in pNETs. The screening on the clinical trial numbers was evaluated on the 30th July, 2021.

Intervention	Available small molecule	Mechanism	Clinical trials	Clinical trials (pNETs)
CIP2A (OFF)	TD52, an Erlotinib derivative [737] and Bortezombib [486].	Elk1 binding to the CIP2A promoter is blocked by TD52 and thus CIP2A transcription [371, 737]. The mechanism of action for Bortezomib is unclear.	949 clinical trials with Bortezomib (clinicalTrials.gov)	NCT00017199, Bortezomib (the study was withdrawn) [579].
PP2A (ON)	SMAPs like RTC-5 (TRC-382), DT-061, or SMAP-2 (DT-1154), derived from anti-psychotic phenothiazines.	The drug binds to inter subunits of PP2A thereby preventing the dissociation of the active enzyme [353].	–	–
E2F (OFF)	HLM006474 [434]	Loss of E2F DNA-binding [434].	–	–
p21 (ON)	Alkylphospholipids like perifosine or miltefosine [123].	They increase the phosphorylation of SP1 and consequently its binding to the p21 promoter [123].	42 clinical trials with perifosine (e.g. NCT00873457 [166], NCT00590954, NCT00058214) and 42 clinical trials with miltefosine (e.g. NCT00471705 [377]) (clinicalTrials.gov).	–
TP53 (ON)	RB7112, RG7338, MK-8242, RO6839921, APR-246, etc (see Nguyen et al. [461]).	MDM2: p53 antagonists, MDM2 inhibitors, mutant p53-WT reactivation, inhibition of MDM2-p53 proteasomal interaction [461].	More than 350 clinical trials (clinicalTrials.gov).	–

3.2.8 *Discussion – Modelling pNETs*

3.2.8.1 *Capturing the heterogeneity of pNETs*

Most of the pNETs are indolent and slow-growing tumours, which however preserve a malignant potential [415, 519]. There is high heterogeneity in tumoural behaviours, ranging from nearly benign to extremely aggressive ones [415, 519]. This heterogeneity, together with the lack of knowledge on tumour drivers and molecular mechanisms, makes the biological behaviour of pNETs largely unpredictable [415, 519]. This issue also reflects the struggle of setting experimental models able to capture this high heterogeneity. BON1 and QGP cell lines have been widely applied to study pNETs *in vitro*. However, different questions have been raised regarding their relevance as models, especially due to the absence of MEN1 mutations [384]. Nevertheless, a down-regulation of MEN1 was still observed in BON1 cells [616]. In the RIP-TAG2 mouse model, pNETs are induced by expression of the SV40 T-antigen oncogenes in insulin-producing islet α-cells [215, 216]. This model is a valuable prototype for studying the stepwise progression of multistage tumourigenesis, displaying different similarities with the progression and classification of human pNETs [546]. Nevertheless, a major limitation in the understanding of pNETs´ development and progression is the largely unknown mechanisms and drivers that lead to the developments of these heterogeneous tumours [415, 519]. For this reason, the established Boolean model aims to understand and unravel the molecular mechanisms and predict phenotypes causing pNETs insurgence, progression and resistance to treatments. The presented mathematical modelling approach allows studying independently and in combination different mutational landscapes and intervention targets. Hence, this approach complements and integrates the already available phenotypical description of pNETs from experimental data.
The heterogeneity of pNETs was captured also in the model simulations. Different mutational landscapes involved in the progression of pNETs (Figure 31) were simulated and characterised. These simulation results were also compared with foreign features selection experiments that could recapitulate the similarity observed in the dynamic model. Additionally model based and foreign features classification results could show different aspects of the heterogeneity observed in DAXX mutated patient cohorts and models. All in all, the corroborated results between patients expression profiles and the pNET model simulations highlighted the prediction power of the dynamic model, especially in light of the scarse information available on these mutation in influencing tumour phenotypes. Additionally, the model could show the potentiality to capture mutational landscapes in the direction of a personalised fashion. In addition, also in the most severe attractor landscape corresponding to the MEN1 loss simulation, it could not be possible to reach a completely aggressive phenotype (Figure 31). Instead, a heterogeneous set of pheno-

types combining quiescence, proliferation, detachment, and angiogenesis could be observed. This reflects the experimental observations on the heterogeneity of these tumours [546]. In contrast to pNETs, pancreatic ductal adenocarcinomas (PDACs) are very aggressive tumours characterised by a predominance of KRAS mutations observed in 90% of cases [692]. Dynamic models describing PDACs progression also reflect this highly aggressive behaviour [692]. Exemplarily, the model of Werle and colleagues describing Cofilin1 (CFL1) hyperactivation in PDAC shows a stable cancer attractor with aggressive traits after the activation of KRAS. In contrast, KRAS mutations are rarely observed as driving in the case of pNET patients, [189]. Accordingly, when screening for tumour drivers (Figure 34 and Figure 35), RAS was also not identified as a tumour driver. This result supports the hypothesis that different crosstalk affects the development of these two tumour entities, resulting in different progressions.

3.2.8.2 *Identifying new tumour drivers in pNETs: first and second hit alterations*

The cancer drivers screening also highlighted general differences in the attractor landscapes when investigating WT and MEN1 loss conditions (Figure 35). This *in silico* screening has been established in the present work. In particular, the approach is aimed to identify nodes, whose activities in start states is biased towards a one or a zero. The more a node is fixed in its start state towards a certain activity the higher is assumed to be its potential influence towards the transition to a certain attractor. The most intuitive example of such nodes are input nodes, whose initial states determine a split in the basin of attraction towards different attractors [255]. On the contrary of the targeted intervention screening that intends to eliminate certain attractor, the presented strategy tries to better understand a certain attractor pattern. In addition, analysing the basin sizes and compositions is a rather common practice when evaluating attractor-related phenotypes and individuating drivers in systems biology cancer research [92, 254, 692]. Tumour drivers identified from the WT condition showed more heterogeneous phenotype distributions (Figure 35). This was concomitant with the presence of multiple combinations of phenotypes and high attractor numbers. On the contrary, MEN1 loss-derived drivers showed more homogenous phenotypes and low attractor numbers. These results reflect the experimental evidence depicting WT tumours as more heterogeneous in their gene expression [546]. They also support the hypothesis of multiple-hit tumour development, leading to more severe and stable cancer phenotypes with the increase of mutations [163]. MEN1 was identified as a driver from the WT condition confirming its experimentally established role as pNET driver [163], and also highlighting the validity of the screening approach. In contrast, neither DAXX nor TSC were identified as drivers from the *in silico* screening (Figure 35). This result is explainable via the structure of the tumour driver search. The cancer driver screening

searches for biased activities of nodes that are represented in the basin of attractors showing an aggressive cancer phenotype. Hence, not identifying DAXX or TSC as drivers might be interpreted in the context of these nodes' activities not being highly effective at inducing an aggressive phenotype. This hypothesis is also following the phenotypical landscape of DAXX and TSC loss simulations, which showed less severe behaviours (Figure 31). TP53 was identified as a driver both in WT and MEN1 loss simulation conditions. However, when combined with MEN1, the loss of TP53 shows a more severe phenotype, indicating that this gene could be a good candidate as a second hit mutation in pNETs. In accordance, Yamauchi and colleagues [719] could show that a TP53 mutation alone did not affect pancreatic endocrine and exocrine tissues in mouse. In contrast, when coupled with an RB mutation, mice developed aggressive pNET with a Ki-67 labelling index of almost 30% [719]. Additionally, TP53 alterations were predominantly found in more aggressive types of neuroendocrine tumors, highlighting their potential role in the late tumourigenesis [713, 719, 277].

3.2.8.3 *Studying mechanisms of resistance to mTORC1 inhibitors in pNETs*

After studying the potential drivers leading to tumour progression, the focus was shifted to intervention targets. Results on simulations targeting mTORC1, one of the largely suggested molecular target in pNETs [350, 741, 479], confirmed the presence of resistant phenotypes still inducing tumour proliferation and invasion in all simulated pNETs mutational conditions (Figure 36). The resistant phenotypes did not show angiogenesis (Figure 36). The absence of angiogenesis is following the anti-angiogenic effect observed in experimental setups for the mTORC1 inhibitor everolimus [343, 479, 743]. In addition, the persistence of the anti-angiogenic effect might relate to the central effect of mTORC1 in regulating angiogenesis via multiple regulatory dependencies [134]. Besides the presence of the resistant phenotype, a beneficial effect of mTORC1 knockout was observed in MEN1 and TSC loss conditions (Figure 36A). Whether MEN1 mutations may be associated with any differential responses to mTOR inhibitor therapy remains still to be definitively established [395]. Nevertheless, a recent study on 31 patients with advanced pNETs could show a higher disease control rate, progression free survival, and time to treatment failure in MEN1 (germline) mutated pNETs after treatment with everolimus [467]. However, the study included only 6 patients with MEN1 germline mutations and thus the results should be considered rather preliminary hints to the potential beneficial effect of everolimus on MEN1 mutated pNETs [467]. The loss of TSC induces the hyperactivation of mTORC1 [110]. Thus, the beneficial effect of further suppressing mTORC1 in TSC loss pNETs is not surprising. In accordance, mTORC1 inhibition has been suggested in TSC mutated pNETs [110]. Again, the low number of cases reported for this mutation in pNETs impairs an extensive eval-

uation of treatment options. However, Schrader et al. [566] could show beneficial effects of everolimus treatment on a patient harbouring a TSC mutated pNET.
Based on the simulation of cascades following mTORC1 intervention and leading to the resistant attractor patterns, a general mechanism of resistance to mTORC1 inhibitors was formulated (Figure 36B and C). The direct effects of mTORC1 inhibition showed reactivation of AKT based on IRS and mTORC2 combined reaction. This mechanism of AKT reactivation was hypothesised and observed experimentally in different tumour models [475]. In addition, the reactivation of AKT after mTORC1 loss was connected to both cellular proliferation and invasion. In particular, the reactivation of the IRS/PI3K/AKT axis inhibits FOXOs and GSK3β, further maintaining CTNNB1 and MYC, and causing the sustained activity of cyclins (CCND1 and CCNE1) (Figure 36B and C). Interestingly, maintenance of MYC activity was also observed in the resistance to mTORC1 inhibitors in colorectal cancer [322]. The same axis also causes the sustained activation of RAC1 and IQGAP1 which involved the complete loss of tight junctions. The loss of STAT3 after mTORC1 inhibition further sustained the inactivation of tight junctions via the loss of PDX1 (Figure 36B and C). Breast cancer cells harbouring PI3K mutations were most sensitive to RAC inhibition, confirming the link between RAC activity and the PI3K/AKT/mTORC1 signalling [213]. In addition, the regulatory effect of mTORC1 on STAT3 was further confirmed in osteosarcomas and renal cystadenoma cells [679, 134]. The downstream effect of the STAT3 inhibition affects PDX1, whose role in maintaining CDH1 expression in the development of pancreatic tissues is well characterised [403]. Furthermore, differential expression of PDX1 is paramount in the identity maintenance of neuroendocrine pancreatic α and β-cells, being expressed mostly in β-cells [42]. In pNETs, higher levels of methylation of the PDX1 promoter, and thus lower PDX1 expression, correlated with the presence of distant metastasis at diagnosis [42]. Accordingly, in PDACs, subsets of malignant cells lose PDX1 expression while undergoing epithelial-to-mesenchymal transition, thus sustaining the hypothesised mechanism after complete loss of PDX1 [536]. These results corroborate the model-based hypothesised mechanism involving a worsening of the tumour behaviour also via a PDX1-dependent loss of tight junctions after mTORC1 inhibition.

3.2.8.4 *Automatic intervention screening shows five new therapeutic targets in pNETs*

In addition to the tumour driver screening, an automatic targeted perturbation screening based on the MEN1 mutational landscape was performed with the aim of identifying new therapeutic interventions. Different treatment therapies against pNETs have been approved by the FDA [389]. Surgical resection is still the only curative treatment in case of focalised tumours [7]. However, almost half of the patients present already with advanced, metastatic disease, requiring a systemic

pharmacological or radiation-based therapy [115]. Approved targeted therapies include mTOR inhibitor everolimus, somatostatin analogs, and multi-targeted tyrosine kinase inhibitor sunitinib [389]. Despite these therapeutic options, a significant percentage of pNET patients are still non-responsive to existing anti-tumour therapies or develop acquired drug resistance [389]. This highlights an urgent need to set up more effective therapeutic strategies, achievable only through a better understanding of pNETs pathogenesis and molecular mechanisms [389]. Exemplarily, a phase II (PALBONET) study for the single agent palbociclib, a cyclin dependent kinase 4/6 (CDK4/6) inhibitor, failed to show beneficial outcomes in patients with metastatic grade 1 and 2 pNETs [194]. However, patients of this study were not selected for molecular alterations and developed resistance to treatment linked to high levels of CCNE1 and RB1 inactivating mutations [194]. Deepening the study of pNETs molecular profiles before treatment might be paramount in preventing such inefficient response to therapies. Indeed, Keutgen and colleagues [302] showed that MEN1 and Von Hippel-Lindau (VHL) syndromes have highly up-regulated CDK4/6, proofing a rationale for selecting molecular targets for therapy based on the pNET subtype. In the present work, this mutation-specific investigation of therapeutic targets was addressed by performing the drug screening in MEN1 loss conditions. Hence, the targeted approach considers the underlying mutational landscape and altered phenotypical traits in the dynamic analysis.

For the MEN1 loss condition, five intervention targets able to completely revert the attractor landscape to a quiescent phenotype were individuated (Figure 37). Interestingly, four out of five of these individuated interventions were also found as tumour drivers. Thus, these results highlight their relevance in the crosstalk inducing the progression of pNETs. P21 was the only drug target not found also as a driver. High levels of P21 are detected in 34% of GEPs [374]. Ubiquitin carboxyl-terminal hydrolase isozyme L1 (UCHL1) down-regulation was observed in BON1 and QGP1 cells [158]. Its re-expression correlated with a significant increase of P21 in these cells and a higher percentage of cells in the Go-phase [158]. Similarly, UCHL1 expression was shown to increase TP53 and P21 expression in nasopharyngeal cancers phase [158]. Hence, these results highlight its potential benefit as a therapeutic target in pNETs.

The use of small molecules, especially the ones already in clinical trials or approved for other tumours, could speed up consistently the potential transfer from bench to bedside of the suggested targets, thus justifying their choice in light of drug repurposing possibilities [131, 756]. Small molecules were available for all the identified five intervention targets (Table 6). Only Bortezomib was previously applied to pNETs and withdrawn in clinical trial due to lack of efficacy [579]. Bortezomib has been shown to alter the activity of CIP2A [486]. However, the mechanism of this influence, and more in general the mechanisms of action of this drug is still

unclear [446]. Yamaguchi et al. [716] studied the factors influencing the approval success rates of 3999 drug candidates, developed in the United States, the European Union, or Japan. Interestingly, they could show that drugs with unknown targets or unknown mechanisms tend have a lower success rate compared to drugs with using targeted approaches [716]. Additionally, in the clinical study of Bortezomib, only a small cohort of patients was evaluated, and the drug was majorly considered for its pro-apoptotic effects [579]. On these grounds, it is possible that a targeted approach with a defined mechanism of action on CIP2A, like TD52, would still yield beneficial results in pNETs. TD52 is a derivative of an already approved small molecule for lung tumour treatment [371, 737]. More in general, TD52 is a quinzoline derivative, which are a very successful class of compounds with many clinically approved targets for cancer therapy [252, 400]. In summary, the automatic perturbation screening could identify five promising single interventions effectively reverting the aggressiveness of MEN1 loss phenotypes, for which small molecules with defined mechanism of action are available.

3.3 Predicting dynamic relevance via graph theoretical measures

The simulation of Boolean models can predict dynamic behaviours and further biologically related phenotypes. However, given the exponential growth of the state space, its exhaustive exploration in reasonable time eventually becomes unfeasible for models with a high number of nodes [244]. Additionally, as in the case of the previously presented HSC and pNET networks, modellers might most likely need to perform multiple simulations in the attempt of unravelling intervention targets, disease drivers, or validating molecular mechanisms, thus further increasing simulation demands. Methods to circumvent this complexity issue are of growing interest, especially if they focus on absolving the task of predicting dynamically relevant nodes at lower computational costs. This research question has been addressed via both dynamic and interaction graph-based approaches. In particular, unlike the state transition graph, the interaction graph does not scale exponentially with network size. This has brought the attention to the possibility of using interaction graph-based measures, referred in the present work also as static measures, as predictors of dynamic influencing nodes [407, 572, 763]. Multiple static measures have been suggested [164, 231, 407], which however miss analyses on their potential impact in predicting alterations in dynamics. The lack of this link to network dynamics in the prediction of relevant nodes has been shown to lead to undershoot or overshoot the prediction of sets of dynamic influencing nodes [180]. In the following, this gap between interaction graph and dynamic analyses is filled by setting up a method to identify static measures that alone, or in combination, select for highly relevant nodes for network dynamics.

3.3.1 *A combination of static measures captures dynamic influencing compounds in biologically motivated Boolean models*

The study on the determination of static measures able to predict dynamic relevance was performed on 35 previously published Boolean models, describing a wide variety of biological processes (Table 7). The set of selected models ranges in size from 5 to 51 genes, with an average of 20 nodes. The median number of nodes in networks is 18, with an interquartile range of 10.5 (from 12.5 to 23). The number of regulations ranged from 12 in a network of 7 nodes to 158 in a network of 32 nodes, with an average of 48 connections for an overall number of 684 nodes. Thus a variety of network sizes and described biological processes was selected.

Table 7: **Boolean network models taken from literature.** The list of the Boolean models used for the presented method is reported below. Here for each model, the organism and the modelled process are reported.

Network	Organism	Process
Azpeitia et al. 2013 [25]	*Arabidopsis thaliana*	Root stem cell niche
Brandon et al. 2015 [49]	*Aspergillus fumigatus*	Oxidative stress response
Calzone et al. 2010 [65]	*Homo sapiens*	Cell-fate decision
Cohen et al. 2015 [100]	*Homo sapiens*	Epithelial-to-mesenchymal transition (EMT)
Dahlhaus et al. 2016 [113]	*Homo sapiens*	Cancer signalling in neuroblastoma
Davila-Velderrain et al. 2015 [116]	*Arabidopsis thaliana*	Early flower development
Enciso et al. 2016 [146]	*Homo sapiens*	Lineage fate decision of haemopoietic cells
Fauré et al. 2006 [148]	*Homo sapiens*	Mammalian cell cycle
Garciá - Gómez et al. 2017 [179]	*Arabidopsis thaliana*	Root apical meristem
Giacomantonio et al. 2010 [187]	*Homo sapiens*	Cortical area development
Gupta et al. 2007 [206]	*Homo sapiens*	Neurotransmitter signalling
Herrmann et al. 2012 [236]	*Homo sapiens*	Cardiac development
Irons 2009 [258]	*Saccharomyces cerevisiae*	Cell cycle
Klamt et al. 2006 [318]	*Homo sapiens*	T-cell receptor signalling
Krumsiek et al. 2011 [334]	*Homo sapiens*	Haematopoiesis
MacLean et al. 2010 [387]	*Pseudomonas syringae*	Type III secretion system
Mai et al. 2009 [390]	*Homo sapiens*	Apoptosis
Marques-Pita et al. 2013 [398]	*Drosophila melanogaster*	Body segmentation
Martinez-Sanchez et al. 2015 [402]	*Homo sapiens*	CD4+ T-cell fate
Méndez et al. 2016 [422]	*Homo sapiens*	B-cell differentiation
Méndez-López et al. 2017 [423]	*Homo sapiens*	Immortalisation of epithelial cells
Mendoza et al. 2006 [424]	*Homo sapiens*	T-cell signalling

Table 7: **Boolean network models taken from literature.** The list of the Boolean models used for the presented method is reported below. Here for each model, the organism and the modelled process are reported.

Network	Organism	Process
Meyer et al. 2017 [428]	*Homo sapiens*	Senescence-associated secretory phenotype
Orlando et al. 2008 [478]	*Saccharomyces cerevisiae*	Cell cycle
Ortiz-Gutiérrez et al. 2015 [481]	*Arabidopsis thaliana*	Cell cycle
Ríos et al. 2015 [515]	*Homo sapiens*	Gonadal sex determination
Saadatpour et al. 2011 [544]	*Homo sapiens*	T-cell large granular lymphocyte survival
Sahin et al. 2009 [548]	*Homo sapiens*	Cell cycle
Sankar et al. 2011 [552]	*Arabidopsis thaliana*	Hormone crosstalk
Siegle et al. 2018 [598]	*Homo sapiens*	Ageing of satellite cells
Sridharan et al. 2012 [615]	*Homo sapiens*	Oxidative stress
Sun et al. 2014 [623]	*Sea urchin*	Endomesoderm tissue specification
Thakar et al. 2012 [637]	*Homo sapiens*	Immune response against infection
Todd et al. 2012 [642]	*Saccharomyces cerevisiae*	Cell cycle
Yousefi et al. 2013 [734]	*Homo sapiens*	Metastatic melanoma

To evaluate the prediction power of static measures on dynamics, a range of eight commonly described static measures, namely VB [164], DP [231, 407], connectivity [201], resistance distance [320], coreness [188], eigenvector centrality [460], eccentricity [209], and shimbel index [524, 589, 590] was evaluated. By applying feature selection, their performance in predicting the dynamic characteristics was further investigated (as defined in Methods Section 2.4.2). By training the selected 35 Boolean models, VB and DP performed best in predicting dynamic relevant compounds (data not shown, refer to Weidner, Schwab, Kühlwein, Ikonomi et al. [688]). Next, the possibility that combinations of these two measures might improve the prediction power of dynamic features was evaluated. Hence, selected nodes by VB, DP, their intersection, and their union were considered, and their specificity and sensitivity was evaluated at different thresholds T ($\mathbf{VB}_T \cap \mathbf{DP}_T$). Among the static

measures, $\mathbf{VB}_T \cap \mathbf{DP}_T$ yielded the best results considering both single dynamic measures and their average (data not shown, refer to Weidner, Schwab, Kühlwein, Ikonomi et al. [688]). Here, a sensitivity of 0.756 at a threshold of 73% with an accuracy of 0.756 ± 0.136 for all 35 networks was observed. This result was also shown to have a stable threshold selection and was independent from network size (data not shown, refer to Weidner, Schwab, Kühlwein, Ikonomi et al. [688]). These results confirm that a combination of static measures able to faithfully capture changes in dynamic behaviours actually exists and consequently their drivers.

3.3.2 *The characterisation of the selected nodes reveals a new class of dynamic drivers*

As described in Weidner, Schwab, Kühlwein, Ikonomi et al. [688], the resulting class of nodes was further studies, based on further properties. Highly connected compounds are thought to strongly influence the dynamic behaviour of biologically motivated networks [271]. Thus, the first focus in characterising the set of nodes included the selection given by the $\mathbf{VB}_T \cap \mathbf{DP}_T$ was on studying the relationship between connectivity and dynamic influence. First, it was observed that highly connected nodes (hubs) were all selected by the presented method, further corroborating its correctness. However, according to the definition of hub nodes [201] only 21 compounds (3.1% of the $\mathbf{VB}_T \cap \mathbf{DP}_T$) were classified as highly connected. As a result, it was further considered that within the selected nodes other statically definable classes of dynamic influencing nodes might exist. To address this possibility, the characterisation of the selected set was deepened by measuring mismatches between the impacts regarding connectivity and the nodes selected by the presented approach.
The set of nodes given by the $\mathbf{VB}_T \cap \mathbf{DP}_T$ at $T = 73\%$ selected 424 nodes out of 684 nodes in total present in the 35 analysed networks. Nodes excluded from this first selection are 260 (38.0%). This group was named non-selected (NS). To further investigate the set of selected nodes, they were ranked by a) their static impact according to VB and DP as an average, and b) their connectivity. For all nodes in $\mathbf{VB}_T \cap \mathbf{DP}_T$ at $T = 73\%$, mismatches between these two rankings were considered. Therefore, the selected nodes were divided as follows: positive mismatches (PM) are nodes that show a higher average ranking in DP and VB than in connectivity. Negative mismatches (NM) instead are nodes with lower or equal average ranking of VB and DP compared to connectivity. As a result, the aim of the analysis is to investigate whether it is possible to identify nodes with high static and dynamic impact, which are also not highly connected.
Out of all 684 nodes across all networks, 227 (33.2%) were classified as positive mismatch. The remaining 197 (28.8%) selected nodes were classified as negative mismatches (data not shown, refer to Weidner, Schwab, Kühlwein, Ikonomi et al.

[688]). Positive mismatch nodes have a lower score in static impact ($p < 1 \cdot 10^{-5}$), if compared to hub nodes. However, this group of nodes showed a dynamic impact comparable to the one of hubs ($p > 0.99$) and a significantly higher one compared to other groups ($p < 0.0001$) (data not shown, refer to Weidner, Schwab, Kühlwein, Ikonomi et al. [688]). Accordingly, for hubs, the median for the dynamic impact is at 0.667, whereas for positive mismatch nodes the median is 0.696. Negative mismatch nodes have a median of 0.546. Positive mismatch nodes show significantly lower connectivity if compared to hubs and negative mismatching nodes ($p < 1 \cdot 10^{-5}$; data not shown, refer to Weidner, Schwab, Kühlwein, Ikonomi et al. [688]). Considering that Boolean network models describe parts of complex biological regulations, input nodes are often used to trigger activation or inhibition of cascades. However, these nodes are considered as external inputs and not regulated within the network. Hence, it would not be expected for input nodes to have a major impact in the performed analysis. In fact, the majority of input nodes across networks fall into the low-impact group of non-selected genes. For a total of 53 input nodes, 44 (83.0%) are classified as non-selected, while 7 (13.2%) are assigned to the positive-mismatch group and 2 (3.8%) to the negative mismatch group.
The presented results unraveled the existence of a group of nodes characterised by low connectivity and high dynamic impact. Interestingly, this group can be identified only based on topological measures. Additionally this set of nodes was also showed to not be identified by applying other interaction graph-based methods (Feedback vertex set (FVS)), considering an enrichment of canalysing nodes in the set, or an enrichment of network motifs (data not shown, refer to Weidner, Schwab, Kühlwein, Ikonomi et al. [688]).

3.3.3 *Higher mutual information characterises positive mismatches nodes as gatekeepers of hubs*

Given that positive mismatches show the unique feature of being not highly connected and still preserving a highly impacting dynamic behaviour, it was investigated whether this new class of nodes is somehow related to hub nodes. Combining the idea of hubs as master regulators of biological processes, together with the possibility of new groups of dynamic drivers arising, it was hypothesised that the positive mismatch class is affecting dynamics by acting through hubs. To evaluate this concept, the reliability with which signals are passed among these nodes was evaluated. All simple paths (i.e. paths in which no vertex is visited twice) across networks starting at a non-hub and ending at a hub node were calculated and compared depending on the classification of the start node. The mutual information (MI) was calculated for every edge along these paths and normalised by the number of edges. Every path P is thus assigned a value $MI_P \in [0, 1]$. Across all

pairs of non-hub starting nodes and hub end nodes, the maximal MI values among their connecting paths were compared. As reported in Weidner, Schwab, Kühlwein, Ikonomi et al. [688], it was shown that channels of information flow beginning at positive mismatch nodes and more reliably affecting hub nodes exist, indicating a special gatekeeper role of these positive mismatch nodes. For this reason, this new group of nodes was named gatekeepers.
Having shown that there is an information flow between gatekeepers and hubs, the potential nature of this relationship was further investigated. One hypothesis in this sense, could be that these two classes of nodes are co-expressed. To address this idea, a co-expression analysis available in STRING was performed [628]. The obtained results show that gatekeepers and hubs seem not to be significantly co-expressed (Appendix Table A1). Another important relationship between compounds is mutual exclusivity, which is relevant especially in disease development and treatment [669]. Exemplarily, in cancer progression, mutually exclusive gene alterations mark different cohorts of patients, potentially occuring with different disease development and treatment sensibilities [127]. In fact, more than one quarter of well-known cancer genes are involved in mutual exclusivity, covering a broad spectrum of cancer pathways [171]. Therefore, mutually exclusive pairs of hubs and gatekeepers for human networks using cBioPortal [176] were investigated (Appendix Table A2). In this context, only human networks (in total 22) were selected for the analysis. Again, any enrichment of significantly mutually exclusive couples of hubs and gatekeepers was detected (Appendix Table A2).

3.3.4 *Perturbation of gatekeepers impacts biological phenotypes*

In the previous sections, gatekeeper nodes were identified and characterised. In particular, it was also shown that they also impact the attractor landscape when perturbed in a significant manner. Next, it is evaluated whether the perturbation of gatekeeper nodes not only alters the attractor landscape, but also that it does so with a biologically relevant impact. For this purpose, interventions on gatekeepers were compared with experimental results in three case studies extracted from the selection of Boolean models.
The Boolean network by Cohen and colleagues [100] depicts pathways involved in tumour development involved in invasion and the metastatic process. In the network one gatekeeper node, twist-related protein 1 (TWIST1), is of particular interest (Appendix Table A3). *In silico* knockout of TWIST1 impairs tumor-associated activities. In accordance, TWIST1 knockout in breast cancer cells inhibits the expression of epithelial to mesenchymal transition (EMT) markers, preventing metastases formation in immune-deficient mice [359, 712]. Further, a similar effect of TWIST1 on invasion potential has also been observed in other types of tumours, such as

prostate cancer, melanoma, and glioblastoma [91, 429, 689].
Another example of the biological impact of not highly connected gatekeepers is the network of Méndez-López and colleagues [423] (Appendix Table A3). Also here, the network describes the EMT process. Again, individuated gatekeepers (E74 like ETS transcription factor 5 (ESE2) and p16) are not hub nodes. The unperturbed network simulation leads to three single state attractors describing epithelial, senescent, and mesenchymal characteristics [423]. The highest impact on attractor alterations after perturbation can be observed in the context of ESE2 loss of function, leading to an attractor with only mesenchymal characteristics. In accordance, experimental results in ESE2 conditional knockout mice show induction of EMT by up-regulation of Snail Family Transcriptional Repressor 2 (Snail2) [75]. Comparable results have been shown for loss of ESE2 in both breast and prostate cancer, identifying also a prognostic value linked to its expression in cancer tissues [150, 357, 725, 684].
Besides tumour associated phenotypes, it was also investigated the effect of gatekeepers in homeostatic and physiologic conditions. In this context the network of Krumsiek et al. [334] describes the differentiation process in hematopoiesis. In this context, the authors described the loss of hematopoietic differentiated populations concomitant with knockout of identified gatekeepers such as GATA binding protein 2 (GATA2), friend leukemia integration 1 (FLI1), CCAAT enhancer binding protein alpha (CEBPα), PU.1, and GFI1 (Appendix Table A3).
Altogether, besides the general effect on the attractor landscapes, the perturbation of gatekeeper nodes extensively affects biological phenotypes in both disease and physiological conditions.

3.3.5 *Gatekeepers capture both tumour drivers and interventions targets of the pNET model*

The ultimate goal of the established method, is to allow for a fast and effective screening of potential dynamic impacting nodes only based on interaction graph-based properties. To this end, the method was applied to the previously presented pNET network (Result section 3.2). This network, besides being large, also recapitulates the scenario in which very little is known on the potential interesting drivers and interventions from experimental evidence. Hence, the gatekeepers individuated for the pNET model were compared to the dynamic-based results from the tumour drivers and targeted perturbation screening (Result sections 3.2.5 and 3.2.7). From the pNET model, 29 (44%) nodes were selected as gatekeepers, 12 (18%) nodes were identified as negative mismatch, and finally 26 (39%) nodes as non-selected. The complete list divided into the three classes of nodes is depicted in the Appendix Table A4. Gatekeepers are also ranked according to their mismatch between connectivity and static score.

Nodes selected by dynamic-based screening approaches as tumour drivers or targeted interventions were also highly represented in the $\mathbf{VB}_T \cap \mathbf{DP}_T$ (gatekeepers and negative mismatch), and in particular in its sub-class of the gatekeepers (Figure 38A and Appendix Table A4). While gatekeepers still represent a larger set compared to the set of tumour drivers or targeted interventions, their selection does not include any previous knowledge on the dynamic behaviour of the system. Thus, the larger set might also contain nodes relevant in other perturbation conditions outside of the ones considered in the targeted screening. In addition, the class of non-selected nodes is particularly poor in nodes selected by the dynamic screenings (Figure 38A and Appendix Table A4). This result highlights the relevance of the interaction graph-based approach, since the dynamic features taken into account for this comparison are different from the ones previously described for the setup of the interaction graph-based method.

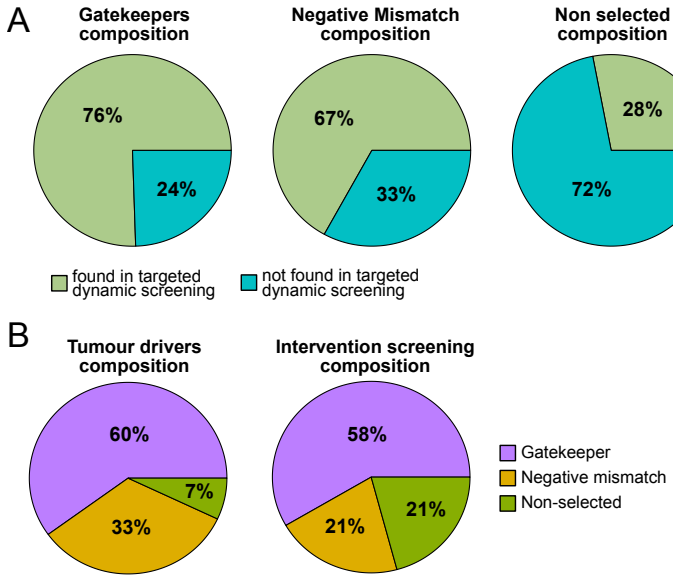


Figure 38: **Distribution of nodes among static and dynamic selection methods.** The distribution of nodes selected from the dynamic-based screening is shown in the three interaction graph inferred classes (A). Vice versa, the distribution of nodes selected as one of the three interaction graph-based classes is also shown within nodes selected from dynamic-based screenings (B). In both scenarios, gatekeepers are enriched in of nodes selected also by dynamic-based screenings.

Vice versa, considering now independently the nodes selected by the tumour driver (both MEN1 and WT simulation condition) and the targeted perturbation screening, these are again enriched for nodes in the in the $\mathbf{VB}_T \cap \mathbf{DP}_T$, and especially for gatekeepers (Figure 38B and Appendix Table A4). In particular, for what concerns tumour drivers, only FOXO3 was classified as non-selected for the interaction

graph-based method (Appendix Table A4). For what concerns the automatic perturbation screening for therapeutic targets (Figure 37), instead, the $\mathbf{VB}_T \cap \mathbf{DP}_T$ contains 79% of suggested intervention targets. In addition, 58% of the suggested targeted interventions from the dynamic based approach were also selected as gatekeepers (Figure 38B and Appendix Table A4). Additionally, all five interventions yielding a complete quiescent phenotype for the targeted intervention screening (Figure 37) were all also selected as gatekeepers (Appendix Table A4). Interestingly, the two gatekeepers with a higher mismatch score were CIP2A and mTORC1 (Appendix Table A4). CIP2A was individuated as both a tumour driver and a targeted intervention from dynamic based analyses (Figure 35 and Figure 37). mTORC1, instead, is one of the gold standard interventions described by literature evidence in pNETs [350, 741]. Thus, the interaction graph-based screening actually resulted in intervention candidates highly influencing the dynamic behaviour of the system, as confirmed by the comparison to the dynamic-based screening approaches. In addition, given that the interaction graph-based methods does not require any previous knowledge on the dynamic of the system, the gatekeepers not selected from any dynamic based targeted screening might still be of interest for further perturbed conditions not yet elucidated in literature.

3.3.6 *Discussion – Predicting dynamic relevance via static measures*

3.3.6.1 *Comparing to other strategies for selecting dynamic relevant nodes*

There is a variety of proven approaches to identify nodes with high impact on the dynamics of regulatory networks [193, 316, 317, 569, 757, 490, 691]. Each of the mentioned approaches relies on the determination of intervention targets by calculation of the networks' dynamics. In contrast, the presented method is highly relies on static properties, making the method scaling more scalable to larger networks. In particular, the presented method was set up by studying the dynamic and static features of 35 published Boolean Networks. It could be shown that the intersection of two static measures, VB and DP at a certain threshold T, can faithfully capture dynamic influencing nodes. On the one hand, by comparing the selected set of nodes from the presented approach to the ones of other static measures [431, 453, 742], a wide overlap of nodes compared to each of the other approaches could be found. This indicates that the intersection of VB and DP is actually selecting a relevant subset of nodes. On the other hand, results show the method uncovers additional relevant nodes. Furthermore, applying the presented method provides a series of advantages. First, the static selection according to VB and DP can be applied very broadly. Methods based on detecting canalysing nodes, instead, require canalysing functions [453]. Methods like FVS provide sets of nodes for control of networks. However, the whole set needs to be controlled in order to shift the dynamic behaviour. This is not the case here: each of the nodes selected by the static intersection can yield a dynamic shift when perturbed and does not *per se* to be applied in combination to others. Due to this fact, the method can also be applied for e.g. drug targeting purposes, or to detect dynamic drivers. In this context the method can have multiple benefits. On the one side, a limited amount of druggable targets is desirable in clinical settings [483]. On the other, it has been shown that disease drivers are single or combined alterations that then cause disrupted cellular signalling [669].

3.3.6.2 *Gatekeeper as new class of dynamic influencing nodes*

The static-based inferred selection can be further subdivided into two subgroups: positive and negative mismatches. In particular, the positive-mismatch subgroup of the selection provides a new set of compounds with not high connectivity and high dynamic impact. This group of nodes was named gatekeeper for their property of transferring information reliably to hub nodes. Gatekeepers cannot be detected univocally by any previously published method (data not shown, refer to Weidner, Schwab, Kühlwein, Ikonomi et al. [688]). Instead, other methods [431, 453, 742] tend to select the class of negative mismatch compounds. This means, these meth-

ods tend to select highly connected nodes with high dynamic impact. Hence, the selection captures two types of compounds based on static properties. First, the well known and detectable highly connected dynamic influencing drivers. Second, a new set dynamic drivers, the gatekeepers, with high dynamic relevance but not high connectivity. Based on the presented results, it was hypothesised that the high dynamic impact of a new class of gatekeeper nodes may arise due to the perturbations of these nodes being more reliably passed on to downstream hubs. This hypothesis would be corroborated by the implications of nodes having a disproportionately high DP or VB. A node ranking high in DP indicates a higher likelihood that the effect of modifications will influence a nodes' direct outputs and will not be outweighed by the influence of other inputs of these target genes. The existence of paths from gatekeeper nodes to hubs having a higher maximal mutual information than those of other classes further demonstrates that this principle extends to longer paths, that is there exist channels of information flow which are more stable carriers of signals. High values of VB further suggest that a node represents a bottleneck in the communication between various modular subnetworks [738]. A perturbation of a high-VB node should, therefore, have a disproportionate impact on the dynamic behaviour of genes in a given subnetwork. Besides theoretical hypotheses, the biological co-expression, co-occurance, and mutual exclusivity between gatekeepers and hubs (Appendix Tables A1 and A2). Here, enriched pairs were not found in any scenario. This finding may be correlated with time and localisation effects of hub interactions. Relating to this, Han et al. [214] subdivided the class of hubs into 'party' hubs which interact with most of their partners simultaneously and 'date' hubs, which bind their different partners at different times or localisations. This would indicate that also interactions are process and context-dependent, and may not be detected by analyses based on overall expression data.

3.3.6.3 *Gatekeeper in the pNET model: tumour drivers and targeted intervention screening*

The interaction graph-based method for screening dynamic relevant nodes was applied to the pNET model as case study. Here, it could be shown that gatekeepers were particularly enriched for nodes individuated by dynamic-based targeted screening for both tumour drivers and intervention targets. Interestingly, for the targeted interventions, all five previously suggested new therapeutic interventions able to completely revert to quiescence the pNET model aggressive phenotypical landscape were also selected as gatekeepers (Figure 37, Figure 38, and Appendix Table A4). This result is of particular interest in light of gatekepeers being not highly connected. In fact, this characteristic is of fundamental interest in the context of selecting potential intervention targets. Besides being generally difficult to target [139, 381, 609], hub node tend to yield lethal phenotypes when removed

[43, 230, 271] Thus, the belonging to the gatekeepers class, highlights even more the relevance of the new suggested therapeutic targets for the pNET model. Looking also at the mismatch score, that ranks gatekeepers based on the mismatch between static score and connectivity, CIP2A and mTORC1 were the gatekeepers with the highest ranking (Appendix Table A4). While CIP2A is one of the five suggested new therapeutic targets for pNETs, mTORC1, instead, is one of the most frequently applied interventions described by literature evidence in pNETs [350, 741]. However, as previously shown, the targeting of mTORC1, while causing actually a dynamic shift, also causes the insurgence of resistance phenotypes (Figure 36). This potentially undesired effect of the perturbation is not considered by the interaction graph-based method, therefore mTORC1 is still listed as a gatekeeper. Also, PI3K is selected as a gatekeeper with a rather high mismatch score (Appendix Table A4). Interestingly, PI3K has been experimentally suggested as a target to be coupled to mTORC1 inhibition in pNETs [658].
In conclusion, the presented interaction graph-based approach was shown to be a fast and effective screening method for identifying dynamic influencing nodes that could be applied as both tumour drivers or targeted interventions. The pNET case study could further confirm that the method can individuate highly dynamic influencing nodes with no previous knowledge on the dynamic of the system. Finally, the method could be successfully applied as an initial screening to scale down the number of candidate nodes to be further investigated via dynamic simulations.

4

GENERAL DISCUSSION

4.1 Biological complexity: is less more in defining phenotypical landscapes?

Regardless of being an applied or *in silico* approach, all models have to deal with describing the complexity of biological systems. Hence, model organisms like *Mus musculus*, *Drosophila melanogaster*, and *Caenorhabditis elegans* as well as *in vitro* studies based on cell lines tend to tackle complex biological questions by using a controllable and simplified system. Each model, in general, will capture certain aspects of the biological question to characterise [582]. However, each of these models alone is often not able to capture the final complexity of the human scenario [582]. Hence, when choosing a certain model, the underlying biological question it should answer has to be clear. The variety of information derived by experimental data is integrated into dynamic models to reconstruct complex biological phenotypical landscapes. The final goal of these predictions is to apply these models to reduce experimental costs via targeted *in silico* suggestions [760].
Given the variegated availability of dynamic modelling approaches, also here the question on the most suitable modelling approach to apply under different biological questions remains. In particular, mathematical models of GRN differ in their complexity and thus in parameter requirements and model sizes [542]. In the present work, Boolean networks were applied to study large cellular crosstalks. From a mathematical perspective, Boolean networks are rather simple models, with the great advantage of integrating qualitative information on regulation, and thus scaling up model sizes. Cantone and colleagues [66] reviewed this gain in network size in the context of bacterial lung infection. Here, they showed that ODE models describing bacterial lung infections scale up to 20 nodes, whereas the scalability of Boolean models goes up to 100 nodes. The scalability of logic-based approaches makes also them suitable for targeting a potentially larger set of biological questions where also complex crosstalks are involved [66]. In accordance, the two HSC models and the pNET model presented in the current work accounted respectively for: 37, 96, and 56 nodes.
The simplicity of Boolean networks, however, might also raise the issue of whether

these models rely on a too extensive simplification of the complex underlying dependencies. In this direction, different authors have shown that Boolean models can capture the key dynamics of ODE models describing the same biological process [348, 663]. In addition, recently established extensions of the Boolean modelling paradigm showed the potentiality to reconcile dynamic behaviours also of ODE models [491]. This simplification into ON/OFF and logical relationships is not so uncommon also to the experimental investigator. When applying statistical testing to observe a significant change of expression or protein levels in certain conditions, what is performed is actually a sort of binarisation of the problem. This would lead to the conclusion that a certain gene or protein is significantly more or less represented in one of the two conditions, again recalling a 0/1, or ON/OFF, status.
On these grounds, given that this work aimed to investigate rather large molecular crosstalks, Boolean networks result indeed the potentially most suitable modelling approach. All the presented models captured crosstalks on a rather large scale and could successfully recapitulate a variety of experimentally observed phenotypes. In addition, the presented models could also suggest new regulatory mechanisms, markers, and therapeutic interventions. The successful application of this modelling approach and its ability to recapitulate phenotypical landscapes highlights the potential success of a "less is more" approach to dynamic modelling of complex GRNs [44].

4.2 Modelling strategies and challenges in Boolean networks

In the presented work, three Boolean models dealing with physiological maintenance and ageing of HSCs and the progression of pNETs were established. In particular, two models, the HSC and the pNET one, were manually curated, while the HSC ensembles describing the NF-κB pathway during ageing was based on automatic reconstruction from human scRNA-seq data.
When curating manually a model, every interaction is evaluated by the modeller. This allows for precise evidence connected to every edge included in the final network. However, this modelling approach is exposed to potential subjective presumptions by the modeller. Besides, interactions are often described controversially in literature [16, 605]. This limitation can be overcome by simulating different hypotheses and selecting the one best fitting the expected phenotype. Even when an obvious solution is not found, it is still possible to experimentally investigate the best hypothesis. In the context of automatically driven models, instead, the Boolean rules are inferred via algorithms. Here, found interactions are not corroborated by literature evidence. Nevertheless, the validity of the established rules can be addressed via comparison to interaction databases. In the case of the HSC ensembles, found interactions were validated via STRING-DB [627]. Nevertheless, the issue

of the reliability of Boolean models is still open, with some authors discussing a potential poor consistency between models describing similar processes, such as cell cycle regulation, in different biological contexts [132, 632]. Also, the manually curated HSC model describes general processes as cell cycle regulation. Here, dynamic simulations lead to a single state attractor depicting cycling HSCs. However, previously published cell cycle models showed cycling cells to be depicted in cyclic attractors [132, 148, 632]. This results, at a first glance, might contradict the conclusions of the different models. Focusing now on the modelling strategy of the HSC model, here only the exit from the Go-phase and the entering of the S-phase was described. Hence, cell cycle regulators involved in this switch were selected. If considering only this cell cycle progression point, also previously published models show a single state attractor [132, 632]. Moreover, by inserting as start states the attractor activities of cell cycle regulators of the HSC model in the Fauré et al. [148] one, which describes the mammalian cell cycle, a cyclic attractor is obtained (Appendix Figure A16). As a result, even if the two models describe cell cycle regulations in different biological contexts, the ground attractor phenotypical landscape of cell cycle regulators can be reproduced and is coherent between them.
Another relevant decision when approaching the dynamic modelling of Boolean networks, is the choice of the update scheme to be applied. In all modelling approaches presented in the current work, a synchronous update scheme was applied. Again, the choice of the update scheme is also influenced by the modelled system. The synchronous update scheme updates at every step in time t the Boolean rule of each node of the network [572]. While this update scheme might seem an oversimplification of the time scales of the biological processes, it comes with an advantage when modelling signalling pathways. It ensures that consequentiality is maintained during signal transduction. Exemplarily, it would be expected that a transcription factor is activated before the expression of its regulated genes, independently from the different time scales of the two regulations. Hence, the choice of synchronous update for the presented models all dealing with pathway signalling transductions is justified. Instead, asynchronous updating, where only one function is randomly updated at each step in time t, can be exploited in other modelling contexts. An example of this is when only one regulatory level is considered, as in the case of transcription factor networks, such as differentiation models [334]. Here, transcription factors compete for binding sites of promoters, with a certain stochasticity in deciding which one will lead the final regulatory decision [334]. Hence, in this case, asynchronous updating better suits the process under analysis. As a result, the update scheme chosen for simulations can also be interpreted and suited to the modelled system, becoming an active part of the modelling strategy.

4.3 Capturing heterogeneity: towards personalised modelling

In general, modellers aim to tailor dynamic models to the specific modelled system. For this reason, models presented in this work were also tailored to the described biological context, preferentially including regulations in the defined tissue context, such as pancreas or HSCs niche. Regulations from different regulatory contexts were evaluated in case specific manner, where there were grounds for assuming a similar regulatory dependency (see also Methods 2.2.1). This choice is enforced given the potential presence of tissue- or context-specific regulations, present in certain regulatory scenarios and not in others [605]. Additionally, many biological processes, such as the described ageing of HSCs or progression of pNETs, are governed by a high level of heterogeneity. These heterogeneous behaviours finally lead to different phenotypical landscapes in potentially each individual. A striking example of this is the attractor pattern retrieved from the HSC ensemble from the 66 years old individual resembling the youngest reconstructed ensembles (Figure 28). As a result, strategies to capture heterogeneity and thus get closer to more personalised models types are more and more of interest.
One way to capture heterogeneity is to represent the variety of specific alterations of the analysed system. In the presented work, this concept was addressed in both physiological and oncological contexts. In the case of the HSC manually curated model, ageing simulations were performed by capturing different intrinsic- and niche-related alterations during ageing. By simulating these perturbations independently, it was possible to capture different hypothesised phenotypes reported for aged HSCs. Thus, the heterogeneity of cellular intrinsic status and niche inputs was captured, and simulation results could lead to a general hypothesis of co-adaptation of niche and HSC ageing. In the oncological context, the heterogeneity typical of pNETs was captured via simulation of different mutational landscapes. Ideally, each mutation applied as a permanent perturbation to the model represents, with its phenotypical landscape, the cohort of patients reporting the same alteration. Grouping and characterising patients based on their mutation pattern might be also advantageous in light of the economic challenge for laboratories and companies to pursue true patient-specific treatments [109]. Instead, a grouping via mutational landscape-based tumour phenotypes might also advantage the set up of future clinical trials for validating new intervention targets [109]. To get even closer to a patient scenario, model results on pNETs mutations were integrated and validated by analysing corresponding mutations in patients' expression profiles via a newly designed foreign classification strategy. By this further integration, additionally, hypotheses could be generated in particular on the heterogeneity of DAXX mutated pNETs Figure 32. The combination of these strategies helped also elucidate tumour behaviours observed in patients and different models, reconciling

again the diversity of reported results. Especially in light of the scarce knowledge on the prediction of the progression and malignity of pNETs, model-based simulations and further integration of classification results could help in formulating new predictions and hypotheses on pNETs alterations and their impact.
Another approach to capture and combine heterogeneity with model personalisation was implemented in the ensembles automatically reconstructed from human scRNA-seq data in the context of HSC ageing. Here, the heterogeneous activity of HSCs was exploited to reconstruct pseudo-time series from scRNA-seq data. Hence, from a population of cells, it was possible to reconstruct an ensemble of networks in a personalised manner. Previous approaches have also integrated scRNA-seq profiles, or expression profiles in general, into dynamic models. Exemplarily, some authors have used patient expression profiles to either match attractor patterns or as biologically meaningful starting states for attractor searches [482, 578]. Béal and colleagues, instead, included patient specific-omic profiles into manually curated models. Here, the authors proposed a hybrid modelling framework (continuous and Boolean models), where expression profiles (or other omic data) were applied to alter the node initial states statuses or the transition rates of nodes [35, 36]. Analogously, Montagud and colleagues [439] applied the same framework to personalise a manually curated model by integrating patients omics profiles. Here, the authors focused on personalising models via tuning the dynamic behaviour of the same manually curated model. In the presented work instead, it was possible to directly address the intra-individual heterogeneity via scRNA-seq and exploit it to directly generate ensembles of models.
In conclusion, modern modelling strategies are moving forward to capture in a more and more precise and personalised manner, via capturing at different levels the heterogeneity of biological processes. The presented models tackle in different ways this point, also suggesting new frameworks for how to generate personalised models.

5

SUMMARY

Systems biology investigates the understanding of complex biological processes, such as ageing or cancer, by integrating a holistic view, which is mostly unconsidered when observing single interactions. This thesis tackles the growing need of this systems perspective by exploring new relationships and mechanisms in molecular crosstalks via Boolean network models.

The physiological maintenance and ageing process of hematopoietic stem cells (HSCs) were investigated via both manually curated and automatically reconstructed approaches. The manually curated HSC model integrates cellular crosstalks and niche regulations to unravel mechanisms in the awakening of HSCs from dormancy. Model simulations shed light on a regulatory mechanism involving a niche-dependent rewinding of cell cycle and metabolic regulators, impacting tumour protein P53 (TP53) activity during the HSCs awakening. In particular, via a series of *in silico* knockout experiments, it was proposed that the TP53 downregulation is crucial in ensuring the entering in the cell cycle without firing apoptosis or senescence. The current understanding of HSC ageing is mostly depicted in descriptive terms. Thus, model simulations perturbing hallmarks of niche and HSC ageing were employed to dissect different hypotheses on the process. Results showed that only a co-adaptation of HSCs and niche signals ensures the survival of HSCs during ageing to the expense of a loss of quiescence.
The heterogenous activity states observed in HSCs populations are captured by single cell sequencing data. This type of expression data was exploited to construct pseudo-time series within human HSCs single cell expression profiles, which were then fed to a newly established automatic network reconstruction pipeline to investigate age-related alterations in the nuclear factor kappa-light chain-enhancer of activated B-cells (NF-κB) pathway. This strategy allowed for the first time to uncouple automatic network reconstructions from developmental trajectories. Network ensembles representing different human HSC populations were automatically reconstructed in a personalised fashion and their properties were compared among ensembles reconstructed from individuals of different ages. Topologically, aged ensembles showed a loss of regulations and structural networks motifs. Dynamic

analyses, instead, highlighted a decrease in NF-κB-related activities during ageing. While most of these alterated activities were not previously reported in ageing, they could be still associated with hallmarks of ageing such as loss of quiescence and increased inflammation. An inter-individual heterogeneity was also observed, pointing at a "young-behaving" aged ensemble. Based on its attractor pattern, P53-induced death domain protein 1 (PIDD1) was identified as a potential new player in delaying human HSCs ageing.

Pancreatic neuroendocrine tumours (pNETs) are heterogenous tumours, whose progression and prognosis are largely unpredictable. While some frequent mutations have been identified, molecular mechanisms of pNETs progression are largely unknown. A new Boolean model studying the main crosstalks involved in pNETs development was manually established. Simulations of most frequently reported alterations in pNETs suggested different mutation-dependent phenotypes. These results were integrated with the establishment of a foreign features classification strategy inferring similarities between human pNET expression profiles bearing different driving mutations. An *in silico* tumour driver screening was further designed. This analysis highlighted new potential first and second-hit drivers after Menin 1 (MEN1) loss, which were evaluated based on their influence in the dynamics after perturbation. First-hit perturbations from wildtype (WT) pNETs showed more heterogenous and less severe attractor landscapes, supporting a multi step tumour development hypothesis. Simulations for the frequently in use intervention on mammalian target of rapamycin complex 1 (mTORC1) confirmed the presence of a resistant phenotype, and could indicate a potential regulatory mechanism for its insurgence. Finally, an automatic drug screening indicated five new targeted interventions, namely cellular inhibitor of PP2A (CIP2A), E2F transcription factor (E2F), cyclin-dependent kinase inhibitor 1A (p21), phosphoprotein phosphatase 2A (PP2A), and TP53, all reverting the attractor landscape to a quiescent phenotype.

The last part of this thesis dealt with the identification of interaction graph-based measures able capture dynamic relevance. By studying a set of 35 published biologically motivated Boolean models, the intersection of vertex betweenness and determinative power performed best for the task. Within this intersection, a new class of nodes, called gatekeepers, was identified. Gatekeepers are characterised having a large dynamic impact while not being comparably highly connected. These properties are particularly interesting when investigating targeted interventions, since targeting directly hub nodes might cause unwanted side effects. The gatekepeers of the pNET model were enriched for nodes also selected as drivers or targeted interventions from the above mentioned dynamic screenings. Besides, all five dynamically-identified therapeutic interventions were also selected as gatekeepers. Thus, the newly established approach is an effective and fast method to screen for dynamic influencing nodes.

6

REFERENCES

[1] Abbas, H. A., Maccio, D. R., Coskun, S., Jackson, J. G., Hazen, A. L., Sills, T. M., You, M. J., Hirschi, K. K., and Lozano, G. Mdm2 is required for survival of hematopoietic stem cells/progenitors via dampening of ROS-induced p53 activity. *Cell stem cell 7*, 5 (2010), 606–617.

[2] Abbas, H. A., Pant, V., and Lozano, G. The ups and downs of p53 regulation in hematopoietic stem cells. *Cell Cycle 10*, 19 (2011), 3257–3262.

[3] Adelman, R. C., Britton, G. W., Rotenberg, S., Ceci, L., and Karoly, K. Endocrine regulation of enzyme activity in aging animals of different genotypes. *Birth defects original article series 14*, 1 (1978), 355–364.

[4] Adolfsson, J., Borge, O. J., Bryder, D., Theilgaard-Mönch, K., Åstrand-Grundström, I., Sitnicka, E., Sasaki, Y., and Jacobsen, S. E. W. Upregulation of Flt3 Expression within the Bone Marrow Lin-Sca1+c-kit+ Stem Cell Compartment Is Accompanied by Loss of Self-Renewal Capacity. *Immunity 15*, 4 (2001), 659–669.

[5] Agarwal, N. K., Qu, C., Kunkulla, K., Liu, Y., and Vega, F. Transcriptional regulation of serine/threonine protein kinase (akt) genes by glioma-associated oncogene homolog 1. *Journal of Biological Chemistry 288*, 21 (2013), 15390–15401.

[6] Akala, O. O., Park, I.-K., Qian, D., Pihalja, M., Becker, M. W., and Clarke, M. F. Long-term haematopoietic reconstitution by $Trp53^{-/-}p16^{Ink4a-/-}p19^{Arf-/-}$ multipotent progenitors. *Nautre 453* (2008), 228–232.

[7] Akirov, A., Larouche, V., Alshehri, S., Asa, S. L., and Ezzat, S. Treatment options for pancreatic neuroendocrine tumors. *Cancers 11*, 6 (2019), 828.

[8] Akutsu, T. *Algorithms for analysis, inference, and control of Boolean networks*. World Scientific Publishing, Singapore, 2018.

[9] Akutsu, T., Miyano, S., and Kuhara, S. Inferring qualitative relations in genetic networks and metabolic pathways. *Bioinformatics 16*, 8 (2000), 727–734.

[10] Albergante, L., Blow, J. J., and Newman, T. J. Buffered qualitative stability

explains the robustness and evolvability of transcriptional networks. *eLife 3* (2014), e02863.

[11] Albert, I., Thakar, J., Li, S., Zhang, R., and Albert, R. Boolean network simulations for life scientists. *Source Code for Biology and Medicine 3*, 16 (2008).

[12] Albert, R., Jeong, H., and Barabási, A.-L. Error and attack tolerance of complex networks. *Nature 406* (2000), 378–382.

[13] Albert, R., and Thakar, J. Boolean modeling: a logic-based dynamic approach for understanding signaling and regulatory networks and for making useful predictions. *WIREs Systems Biology and Medicine 6*, 5 (2014), 353–369.

[14] Alberts, A. S., Thorburn, A. M., Shenolikar, S., Mumby, M. C., and Feramisco, J. R. Regulation of cell cycle progression and nuclear affinity of the retinoblastoma protein by protein phosphatases. *Proceedings of the National Academy of Sciences 90*, 2 (1993), 388–392.

[15] Aldana, M., and Cluzel, P. A natural class of robust networks. *Proceedings of the National Academy of Sciences 100*, 15 (2003), 8710–8714.

[16] Alizad-Rahvar, A. R., and Sadeghi, M. Ambiguity in logic-based models of gene regulatory networks: An integrative multi-perturbation analysis. *PLOS ONE 13*, 11 (2018), e0206976.

[17] Alon, U. Network motifs: theory and experimental approaches. *Nature Reviews Genetics 8*, 6 (2007), 450–461.

[18] Amoah, A., Keller, A., Emini, R., Hoenicka, M., Liebold, A., Vollmer, A., Eiwen, K., Soller, K., Sakk, V., Zheng, Y., Florian, M. C., and Geiger, H. Aging of human hematopoietic stem cells is linked to changes in cdc42 activity. *Haematologica 107*, 2 (2022), 393–402.

[19] Amrein, M. A., Bührer, E. D., Ruckstuhl, C., Höpner, S., Riether, C., and Ochsenbein, A. F. The Traf2 and Nck-Interacting Kinase is a conserved regulator of self-renewal in hematopoietic and leukemia stem cells. *Blood 130*, Supplement 1 (2017), 1137.

[20] Andersson, S., D'Arcy, P., Larsson, O., and Sehat, B. Focal adhesion kinase (FAK) activates and stabilizes IGF-1 receptor. *Biochemical and Biophysical Research Communications 387*, 1 (2009), 36–41.

[21] Armata, H. L., Golebiowski, D., Jung, D. Y., Ko, H. J., Kim, J. K., and Sluss, H. K. Requirement of the atm/p53 tumor suppressor pathway for glucose homeostasis. *Molecular and Cellular Biology 30*, 24 (2010), 5787–5794.

[22] Asai, T., Liu, Y., Bae, N., and Nimer, S. D. The p53 tumor suppressor protein regulates hematopoietic stem cell fate. *Journal of Cellular Physiology 226*, 9 (2011), 2215–2221.

[23] Astro, V., Tonoli, D., Chiaretti, S., Badanai, S., Sala, K., Zerial, M., and De Curtis, I. Liprin-α1 and erc1 control cell edge dynamics by promoting focal adhesion turnover. *Scientific Reports 6*, 1 (2016), 1–16.

[24] Attema, J. L., Pronk, C. J., Norddahl, G. L., Nygren, J. M., and Bryder, D. Hematopoietic stem cell ageing is uncoupled from p16 ink4a-mediated senescence. *Oncogene 28*, 22 (2009), 2238–2243.

[25] Azpeitia, E., Weinstein, N., Benítez, M., Mendoza, L., and Alvarez-Buylla, E. R. Finding missing interactions of the *Arabidopsis thaliana* root stem cell niche gene regulatory network. *Frontiers in Plant Science 4*, 110 (2013).

[26] Baena, E., Ortiz, M., Martínez-A, C., and de Alborán, I. M. c-Myc is essential for hematopoietic stem cell differentiation and regulates Lin(-)Sca-1(+)c-Kit(-) cell generation through p21. *Experimental Hematology 35*, 9 (2007), 1333–1343.

[27] Bakker, S. T., and Passegué, E. Resilient and resourceful: genome maintenance strategies in hematopoietic stem cells. *Experimental Hematology 41*, 11 (2013), 915–923.

[28] Bakker, W. J., Harris, I. S., and Mak, T. W. FOXO3a is activated in response to hypoxic stress and inhibits HIF1-induced apoptosis via regulation of CITED2. *Molecular Cell 28*, 6 (2007), 941–953.

[29] Baldridge, M. T., King, K. Y., Boles, N. C., Weksberg, D. C., and Goodell, M. A. Quiescent haematopoietic stem cells are activated by IFN-γ in response to chronic infection. *Nature 465*, 7299 (2010), 793–797.

[30] Barabási, A.-L. *Network Science*. Cambridge university press, Cambridge, 2016.

[31] Batcher, E., Madaj, P., and Gianoukakis, A. G. Pancreatic neuroendocrine tumors. *Endocrine research 36*, 1 (2011), 35–43.

[32] Batista, I. d. A. A., and Helguero, L. A. Biological processes and signal transduction pathways regulated by the protein methyltransferase SETD7 and their significance in cancer. *Signal Transduction and Targeted Therapy 3*, 1 (2018), 1–14.

[33] Baumgartner, C., Toifl, S., Farlik, M., Halbritter, F., Scheicher, R., Fischer, I., Sexl, V., Bock, C., and Baccarini, M. An erk-dependent feedback mechanism prevents hematopoietic stem cell exhaustion. *Cell Stem Cell 22*, 6 (2018), 879–892.

[34] Bazzi, W., Renon, M., Vercherat, C., Hamze, Z., Lacheretz-Bernigaud, A., Wang, H., Blanc, M., Roche, C., Calender, A., Chayvialle, J.-A., Scoazec, J.-Y., and Cordier-Bussat, M. MEN1 missense mutations impair sensitization to apoptosis induced by wild-type menin in endocrine pancreatic tumor cells. *Gastroenterology 135*, 5 (2008), 1698–1709.

[35] Béal, J., Montagud, A., Traynard, P., Barillot, E., and Calzone, L. Personalization of logical models with multi-omics data allows clinical stratification of patients. *Frontiers in Physiology* (2019), 1965.

[36] Béal, J., Pantolini, L., Noël, V., Barillot, E., and Calzone, L. Personalized logical models to investigate cancer response to braf treatments in melanomas and colorectal cancers. *PLOS Computational Biology 17*, 1 (2021), e1007900.

[37] Beauloye, C., Marsin, A.-S., Bertrand, L., Krause, U., Hardie, D. G., Vanoverschelde, J.-L., and Hue, L. Insulin antagonizes AMP-activated protein kinase activation by ischemia or anoxia in rat hearts, without affecting total adenine nucleotides. *FEBS letters 505*, 3 (2001), 348–352.

[38] Ben-Dor, A., Bruhn, L., Friedman, N., Nachman, I., Schummer, M., and Yakhini, Z. Tissue classification with gene expression profiles. In *Proceedings of the fourth annual international conference on Computational molecular biology* (2000), pp. 54–64.

[39] Bewick, V., Cheek, L., and Ball, J. Statistics review 13: Receiver operating characteristic curves. *Critical Care 8*, 6 (2004), 508–512.

[40] Blagosklonny, M. V. Paradoxes of aging. *Cell Cycle 6*, 24 (2007), 2997–3003.

[41] Blank, U., and Karlsson, S. TGF-β signaling in the control of hematopoietic stem cells. *Blood 125*, 23 (2015), 3542–3550.

[42] Boons, G., Vandamme, T., Ibrahim, J., Roeyen, G., Driessen, A., Peeters, D., Lawrence, B., Print, C., Peeters, M., Van Camp, G., and Op de Beeck, K. PDX1 DNA methylation distinguishes two subtypes of pancreatic neuroendocrine neoplasms with a different prognosis. *Cancers 12*, 6 (2020), 1461.

[43] Borneman, A. R., Leigh-Bell, J. A., Yu, H., Bertone, P., Gerstein, M., and Snyder, M. Target hub proteins serve as master regulators of development in yeast. *Genes & Development 20*, 4 (2006), 435–448.

[44] Bornholdt, S. Less is more in modeling large genetic networks. *Science 310*, 5747 (2005), 449–451.

[45] Bösch, F., Altendorf-Hofmann, A., Jacob, S., Auernhammer, C. J., Spitzweg, C., Boeck, S., Schubert-Fritschle, G., Werner, J., Kirchner, T., Angele, M. K., and Knössel, T. Distinct expression patterns of VEGFR 1-3 in gastroenteropancreatic neuroendocrine neoplasms: Supporting clinical relevance, but not a prognostic factor. *Journal of Clinical Medicine 9*, 10 (2020), 3368.

[46] Boucher, M.-J., Selander, L., Carlsson, L., and Edlund, H. Phosphorylation marks IPF1/PDX1 protein for degradation by glycogen synthase kinase 3-dependent mechanisms. *Journal of Biological Chemistry 281*, 10 (2006), 6395–6403.

[47] Bowie, M. B., Kent, D. G., Dykstra, B., McKnight, K. D., McCaffrey, L., Hoodless, P. A., and Eaves, C. J. Identification of a new intrinsically timed developmental checkpoint that reprograms key hematopoietic stem cell properties. *Proceedings of the National Academy of Sciences 104*, 14 (2007), 5878–5882.

[48] Bradford, G. B., Williams, B., Rossi, R., and Bertoncello, I. Quiescence, cycling, and turnover in the primitive hematopoietic stem cell compartment. *Experimental Hematology 25*, 5 (1997), 445–453.

[49] Brandon, M., Howard, B., Lawrence, C., and Laubenbacher, R. Iron acquisition and oxidative stress response in aspergillus fumigatus. *BMC Systems Biology 9*, 19 (2015).

[50] Bray, F., Ferlay, J., Soerjomataram, I., Siegel, R. L., Torre, L. A., and Jemal, A. Global cancer statistics 2018: Globocan estimates of incidence and mortality worldwide for 36 cancers in 185 countries. *CA: A Cancer Journal for Clinicians 68*, 6 (2018), 394–424.

[51] Brehm, A., Miska, E. A., McCance, D. J., Reid, J. L., Bannister, A. J., and Kouzarides, T. Retinoblastoma protein recruits histone deacetylase to repress transcription. *Nature 391*, 6667 (1998), 597–601.

[52] Brennan-Crispi, D. M., Overmiller, A. M., Tamayo-Orrego, L., Marous, M. R., Sahu, J., McGuinn, K. P., Cooper, F., Georgiou, I. C., Frankfurter, M., Salas-Alanis, J. C., Charron, F., MIllar, S. R., Mahoney, M. y. G., and Riobo-Del Galdo, N. Overexpression of Desmoglein 2 in a mouse model of gorlin syndrome enhances spontaneous basal cell carcinoma formation through STAT3-Mediated Gli1 expression. *Journal of Investigative Dermatology 139*, 2 (2019), 300–307.

[53] Broxmeyer, H. E., Starnes, T., Ramsey, H., Cooper, S., Dahl, R., Williamson, E., and Hromas, R. The IL-17 cytokine family members are inhibitors of human hematopoietic progenitor proliferation. *Blood 108*, 2 (2006), 770–770.

[54] Brunet, A., Bonni, A., Zigmond, M. J., Lin, M. Z., Juo, P., Hu, L. S., Anderson, M. J., Arden, K. C., Blenis, J., and Greenberg, M. E. Akt promotes cell survival by phosphorylating and inhibiting a Forkhead transcription factor. *Cell 96*, 6 (1999), 857–868.

[55] Brunet, A., Kanai, F., Stehn, J., Xu, J., Sarbassova, D., Frangioni, J. V., Dalal, S. N., DeCaprio, J. A., Greenberg, M. E., and Yaffe, M. B. 14-3-3 transits to the nucleus and participates in dynamic nucleocytoplasmic transport. *The Journal of Cell Biology 156*, 5 (2002), 817–828.

[56] Buchadas, A., Vaz, A. S., Honrado, J. P., Alagador, D., Bastos, R., Cabral, J. A., Santos, M., and Vicente, J. R. Dynamic models in research and management of biological invasions. *Journal of Environmental Management 196* (2017), 594–606.

[57] Buffenstein, R. The naked mole-rat: A new long-living model for human aging research. *Journal of Gerontology: Biological Sciences 60A*, 11 (2005), 1369–1377.

[58] Buicko, J. L., Finnerty, B. M., Zhang, T., Kim, B. J., Fahey III, T. J., and

Du, Y.-C. N. Insights into the biology and treatment strategies of pancreatic neuroendocrine tumors. *Annals of Pancreatic Cancer 2* (2019).

[59] Bunz, F., Dutriaux, A., Lengauer, C., Waldman, T., Zhou, S., Brown, J., Sedivy, J., Kinzler, K. W., and Vogelstein, B. Requirement for p53 and p21 to sustain g2 arrest after dna damage. *Science 282*, 5393 (1998), 1497–1501.

[60] Burzynski, S. R. Aging: gene silencing or gene activation? *Medical Hypotheses 64*, 1 (2005), 201–208.

[61] Busch, K., Klapproth, K., Barile, M., Flossdorf, M., Holland-Letz, T., Schlenner, S. M., Reth, M., Höfer, T., and Rodewald, H.-R. Fundamental properties of unperturbed haematopoiesis from stem cells in vivo. *Nature 518*, 7540 (2015), 542–546.

[62] Butler, J. M., Nolan, D. J., Vertes, E. L., Varnum-Finney, B., Kobayashi, H., Hooper, A. T., Seandel, M., Shido, K., White, I. A., Kobayashi, M., Witte, L., May, C., Shawber, C., Kimura, Y., Kitajewski, J., Rosenwaks, Z., Bernstein, I. D., and Rafii, S. Endothelial cells are essential for the self-renewal and repopulation of Notch-dependent hematopoietic stem cells. *Cell Stem Cell 6*, 3 (2010), 251–264.

[63] Cabezas-Wallscheid, N., Buettner, F., Sommerkamp, P., Klimmeck, D., Ladel, L., Thalheimer, F. B., Pastor-Flores, D., Roma, L. P., Renders, S., Zeisberger, P., Przybylla, A., Schönberger, K., Scngnamiglio, R., Altamura, S., Florian, C. M., Fawaz, M., Vonficht, D., Tesio, M., Collier, P., Pavlinic, D., Geiger, H., Schroeder, T., Benes, V., Dick, T. P., Rieger, M. A., Stegle, O., and Trumpp, A. Vitamin A-retinoic acid signaling regulates hematopoietic stem cell dormancy. *Cell 169*, 5 (2017), 807–823.

[64] Calvert, J., and Fujimura, J. H. Calculating life? duelling discourses in interdisciplinary systems biology. *Studies in History and Philosophy of Science Part C: Studies in History and Philosophy of Biological and Biomedical Sciences 42*, 2 (2011), 155–163.

[65] Calzone, L., Tournier, L., Fourquet, S., Thieffry, D., Zhivotovsky, B., Barillot, E., and Zinovyev, A. Mathematical modelling of cell-fate decision in response to death receptor engagement. *PLOS Computational Biology 6*, 3 (2010), e1000702.

[66] Cantone, M., Santos, G., Wentker, P., Lai, X., and Vera, J. Multiplicity of mathematical modeling strategies to search for molecular and cellular insights into bacteria lung infection. *Frontiers in Physiology* (2017), 645.

[67] Cao, Y., Liu, R., Jiang, X., Lu, J., Jiang, J., Zhang, C., Li, X., and Ning, G. Nuclear-cytoplasmic shuttling of menin regulates nuclear translocation of β-catenin. *Molecular and Cellular Biology 29*, 20 (2009), 5477–5487.

[68] Capurso, G., Archibugi, L., and Delle Fave, G. Molecular pathogenesis and targeted therapy of sporadic pancreatic neuroendocrine tumors. *Journal*

of Hepato-Biliary-Pancreatic Sciences 22, 8 (2015), 594–601.

[69] Carr, R. M., Duran, P. A. R., Tolosa, E. J., Ma, C., Oseini, A. M., Moser, C. D., Banini, B. A., Huang, J., Asumda, F., Dhanasekaran, R., Graham, R. P., Toruner, M. D., Safgren, S. L., Almada, L. L., Wang, S., Patnaik, M. M., Roberts, L. R., and Fernandez-Zapico, M. E. The extracellular sulfatase SULF2 promotes liver tumorigenesis by stimulating assembly of a promoter-looping GLI1-STAT3 transcriptional complex. *Journal of Biological Chemistry 295*, 9 (2020), 2698–2712.

[70] Carracedo, A., and Pandolfi, P. The PTEN–PI3K pathway: of feedbacks and cross-talks. *Oncogene 27*, 41 (2008), 5527–5541.

[71] Casalou, C., Ferreira, A., and Barral, D. C. The role of ARF family proteins and their regulators and effectors in cancer progression: a therapeutic perspective. *Frontiers in Cell and Developmental Biology 8* (2020).

[72] Cavalcanti, E., Galleggiante, V., Coletta, S., Stasi, E., Chieppa, M., Armentano, R., and Serino, G. Altered mirnas expression correlates with gastroenteropancreatic neuroendocrine tumors grades. *Frontiers in Oncology 10* (2020), 1187.

[73] Cavigelli, M., Li, W. W., Lin, A., Su, B., Yoshioka, K., and Karin, M. The tumor promoter arsenite stimulates ap-1 activity by inhibiting a jnk phosphatase. *The EMBO Journal 15*, 22 (1996), 6269–6279.

[74] Chabanon, A., Desterke, C., Rodenburger, E., Clay, D., Guerton, B., Boutin, L., Bennaceur-Griscelli, A., Pierre-Louis, O., Uzan, G., Abecassis, L., Bourgeade, M.-F., Lataillade, J.-J., and Le Bousse-Kerdilès, M.-C. A cross-talk between stromal cell-derived factor-1 and transforming growth factor-β controls the quiescence/cycling switch of CD34+ progenitors through FoxO3 and mammalian target of rapamycin. *Stem Cells 26*, 12 (2008), 3150–3161.

[75] Chakrabarti, R., Hwang, J., Blanco, M. A., Wei, Y., Lukačišin, M., Romano, R.-A., Smalley, K., Liu, S., Yang, Q., Ibrahim, T., Mercatali, L., Amadori, D., Haffty, B. G., Sinha, S., and Kang, Y. Elf5 inhibits the epithelial–mesenchymal transition in mammary gland development and breast cancer metastasis by transcriptionally repressing Snail2. *Nature Cell Biology 14*, 11 (2012), 1212–1222.

[76] Chakravarti, B., and Abraham, G. N. Effect of age and oxidative stress on tyrosine phosphorylation of ZAP-70. *Mechanisms of Ageing and Development 123*, 4 (2002), 297–311.

[77] Challen, G. A., Boles, N., Lin, K.-Y. K., and Goodell, M. A. Mouse hematopoietic stem cell identification and analysis. *Cytometry Part A 75A*, 1 (2009), 14–24.

[78] Chambers, S. M., Shaw, C. A., Gatza, C., Fisk, C. J., Donehower, L. A.,

AND GOODELL, M. A. Aging hematopoietic stem cells decline in function and exhibit epigenetic dysregulation. *PLOS Biology 5*, 8 (2007), e201.

[79] CHAN, C. S., LADDHA, S. V., LEWIS, P. W., KOLETSKY, M. S., ROBZYK, K., DA SILVA, E., TORRES, P. J., UNTCH, B. R., LI, J., BOSE, P., ET AL. Atrx, daxx or men1 mutant pancreatic neuroendocrine tumors are a distinct alpha-cell signature subgroup. *Nature communications 9*, 1 (2018), 1–10.

[80] CHAN, J., AND KULKE, M. Targeting the mtor signaling pathway in neuroendocrine tumors. *Current Treatment Options in Oncology 15*, 3 (2014), 365–379.

[81] CHANDEL, N. S., JASPER, H., HO, T. T., AND PASSEGUE, E. Metabolic regulation of stem cell function in tissue homeostasis and organismal ageing. *Nature Cell Biology 18*, 8 (2016), 823–832.

[82] CHANG, F., LEMMON, C. A., PARK, D., AND ROMER, L. H. FAK potentiates Rac1 activation and localization to matrix adhesion sites: A role for βPIX. *Molecular Biology of the Cell 18*, 1 (2007), 253–264.

[83] CHANG, T.-M., SHAN, Y.-S., CHU, P.-Y., JIANG, S. S., HUNG, W.-C., CHEN, Y.-L., TU, H.-C., LIN, H.-Y., TSAI, H.-J., AND CHEN, L.-T. The regulatory role of aberrant phosphatase and tensin homologue and liver kinase b1 on akt/mtor/c-myc axis in pancreatic neuroendocrine tumors. *Oncotarget 8*, 58 (2017), 98068.

[84] CHEN, C., LIU, Y., LIU, R., IKENOUE, T., GUAN, K.-L., LIU, Y., AND ZHENG, P. TSC–mTOR maintains quiescence and function of hematopoietic stem cells by repressing mitochondrial biogenesis and reactive oxygen species . *Journal of Experimental Medicine 205*, 10 (09 2008), 2397–2408.

[85] CHEN, C., LIU, Y., LIU, Y., AND ZHENG, P. The axis of mTOR-mitochondria-ROS and stemness of the hematopoietic stem cells. *Cell Cycle 8*, 8 (2009), 1158–1160.

[86] CHEN, W., LV, X., LIU, C., CHEN, R., LIU, J., DAI, H., AND ZOU, G.-M. Hematopoietic stem/progenitor cell differentiation towards myeloid lineage is modulated by LIGHT/LIGHT receptor signaling. *Journal of Cellular Physiology 233*, 2 (2018), 1095–1103.

[87] CHEN, Y., HAVIERNIK, P., BUNTING, K. D., AND YANG, Y.-C. Cited2 is required for normal hematopoiesis in the murine fetal liver. *Blood 110*, 8 (2007), 2889–2898.

[88] CHESHIER, S. H., MORRISON, S. J., LIAO, X., AND WEISSMAN, I. L. In vivo proliferation and cell cycle kinetics of long-term self-renewing hematopoietic stem cells. *Proceedings of the National Academy of Sciences 96*, 6 (1999), 3120–3125.

[89] CHEUNG, T. H., AND RANDO, T. A. Molecular regulation of stem cell quiescence. *Nature reviews Molecular cell biology 14*, 6 (2013), 329–340.

[90] CHO, I. J., LUI, P. P., OBAJDIN, J., RICCIO, F., STROUKOV, W., WILLIS, T. L., SPAGNOLI, F., AND WATT, F. M. Mechanisms, hallmarks, and implications of stem

cell quiescence. *Stem Cell Reports 12*, 6 (2019), 1190–1200.

[91] Cho, K. H., Jeong, K. J., Shin, S. C., Kang, J., Park, C. G., and Lee, H. Y. STAT3 mediates TGF-β1-induced TWIST1 expression and prostate cancer invasion. *Cancer Letters 336*, 1 (2013), 167–173.

[92] Cho, S.-H., Park, S.-M., Lee, H.-S., Lee, H.-Y., and Cho, K.-H. Attractor landscape analysis of colorectal tumorigenesis and its reversion. *BMC Systems Biology 10*, 1 (2016), 1–13.

[93] Choi, J., Park, S. Y., and Joo, C.-K. Transforming growth factor-β1 represses E-cadherin production via slug expression in lens epithelial cells. *Investigative Ophthalmology & Visual Science 48*, 6 (2007), 2708–2718.

[94] Chung, D. C., Brown, S. B., Graeme-Cook, F., Seto, M., Warshaw, A. L., Jensen, R. T., and Arnold, A. Overexpression of cyclin d1 occurs frequently in human pancreatic endocrine tumors. *The Journal of Clinical Endocrinology & Metabolism 85*, 11 (2000), 4373–4378.

[95] Chung, E., Hsu, C.-L., and Kondo, M. Constitutive MAP kinase activation in hematopoietic stem cells induces a myeloproliferative disorder. *PLOS ONE 6*, 12 (2011), e28350.

[96] Ciccarelli, C., Di Rocco, A., Gravina, G. L., Mauro, A., Festuccia, C., Del Fattore, A., Berardinelli, P., De Felice, F., Musio, D., Bouché, M., Tombolini, V., Zani, B. M., and Marampon, F. Disruption of MEK/ERK/c-Myc signaling radiosensitizes prostate cancer cells in vitro and in vivo. *Journal of Cancer Research and Clinical Oncology 144*, 9 (2018), 1685–1699.

[97] Cicchillitti, L., Fasanaro, P., Biglioli, P., Capogrossi, M. C., and Martelli, F. Oxidative stress induces protein phosphatase 2A-dependent dephosphorylation of the pocket proteins pRb, p107, and p130. *Journal of Biological Chemistry 278*, 21 (2003), 19509–19517.

[98] Cingarlini, S., Bonomi, M., Trentin, C., Corbo, V., Scarpa, A., and Tortora, G. Profiling mtor pathway in neuroendocrine tumors. *Management of Neuroendocrine Tumors of the Pancreas and Digestive Tract* (2014), 9–27.

[99] Climent, J.-J., García, F. J., and Requena, V. Computing the Degree of a Boolean Function from its Support. In *2010 International Symposium On Information Theory & Its Applications* (2010), IEEE, pp. 123–128.

[100] Cohen, D. P., Martignetti, L., Robine, S., Barillot, E., Zinovyev, A., and Calzone, L. Mathematical modelling of molecular pathways enabling tumour cell invasion and migration. *PLOS Computational Biology 11*, 11 (2015), e1004571.

[101] Connell-Crowley, L., Harper, J. W., and Goodrich, D. W. Cyclin D1/Cdk4 regulates retinoblastoma protein-mediated cell cycle arrest by site-specific phosphorylation. *Molecular biology of the cell 8*, 2 (1997), 287–301.

[102] Corbo, V., Dalai, I., Scardoni, M., Barbi, S., Beghelli, S., Bersani, S., Al-

BARELLO, L., DOGLIONI, C., SCHOTT, C., CAPELLI, P., CHILOSI, M., BONINSEGNA, L., BECKER, K.-F., FALCONI, M., AND SCARPA, A. MEN1 in pancreatic endocrine tumors: analysis of gene and protein status in 169 sporadic neoplasms reveals alterations in the vast majority of cases. *Endocrine-Related Cancer 17*, 3 (2010), 771–783.

[103] CORMEN, T. H., LEISERSON, C. E., RIVEST, R. L., AND STEIN, C. *Introduction to Algorithms second edition*. The MIT Press, 2001.

[104] COSKUN, S., AND HIRSCHI, K. K. Establishment and regulation of the HSC niche: Roles of osteoblastic and vascular compartments. *Birth defects research. Part C, Embryo today : reviews 90*, 4 (2010), 229–242.

[105] CRESON, T. K., YUAN, P., MANJI, H. K., AND CHEN, G. Evidence for involvement of ERK, PI3K, and RSK in induction of Bcl-2 by valproate. *Journal of Molecular Neuroscience 37*, 2 (2009), 123–134.

[106] CRICK, F. Central dogma of molecular biology. *Nature 227*, 5258 (1970), 561–563.

[107] CROFT, M., DUAN, W., CHOI, H., EUN, S.-Y., MADIREDDI, S., AND MEHTA, A. Tnf superfamily in inflammatory disease: translating basic insights. *Trends in Immunology 33*, 3 (2012), 144–152.

[108] CSARDI, G., AND NEPUSZ, T. The igraph software package for complex network research. *InterJournal, Complex Systems 1695*, 5 (2006), 1–9.

[109] CUNANAN, K. M., IASONOS, A., SHEN, R., BEGG, C. B., AND GÖNEN, M. An efficient basket trial design. *Statistics in Medicine 36*, 10 (2017), 1568–1579.

[110] CURATOLO, P., AND MOAVERO, R. mtor inhibitors in tuberous sclerosis complex. *Current Neuropharmacology 10*, 4 (2012), 404–415.

[111] CVIJOVIC, M., HÖFER, T., AĆIMOVIĆ, J., ALBERGHINA, L., ALMAAS, E., BESOZZI, D., BLOMBERG, A., BRETSCHNEIDER, T., CASCANTE, M., COLLIN, O., DE ATAURI, P., DEPNER, C., DICKINSON, R., DOBRZYKNSKI, M., FLECK, C., GARCIA-OJALVO, J., GONZE, D., HAHN, J., HESS, H. M., HOLLMANN, S., KRANTZ, M., KUMMER, U., LUNDH, T., MARTIAL, G., DOS SANTOS, V. M., MAUER-OBERTHÜR, A., REGIERER, B., SKENE, B., STALIDZANS, E., STELLING, J., TEUSINK, B., WORKMAN, C. T., AND HOHMANN, S. Strategies for structuring interdisciplinary education in systems biology: an european perspective. *NPJ Systems Biology and Applications 2*, 16011 (2016).

[112] CZAJA, M. J. The future of gi and liver research: editorial perspectives. iii. jnk/ap-1 regulation of hepatocyte death. *American Journal of Physiology 284*, 1 (2003), G875–G879.

[113] DAHLHAUS, M., BURKOVSKI, A., HERTWIG, F., MÜSSEL, C., VOLLAND, R., FISCHER, M., DEBATIN, K.-M., KESTLER, H. A., AND BELTINGER, C. Boolean modeling identifies Greatwall/MASTL as an important regulator in the AURKA network of neuroblastoma. *Cancer Letters 371*, 1 (2016), 79–89.

[114] Daksis, J. I., Lu, R. Y., Facchini, L. M., Marhin, W. W., and Penn, L. Myc induces cyclin d1 expression in the absence of de novo protein synthesis and links mitogen-stimulated signal transduction to the cell cycle. *Oncogene 9*, 12 (1994), 3635–3645.

[115] Dasari, A., Shen, C., Halperin, D., Zhao, B., Zhou, S., Xu, Y., Shih, T., and Yao, J. C. Trends in the incidence, prevalence, and survival outcomes in patients with neuroendocrine tumors in the united states. *JAMA Oncology 3*, 10 (2017), 1335–1342.

[116] Davila-Velderrain, J., Villarreal, C., and Alvarez-Buylla, E. R. Reshaping the epigenetic landscape during early flower development: induction of attractor transitions by relative differences in gene decay rates. *BMC Systems Biology 9*, 1 (2015), 20.

[117] Davis, J. E., Xie, X., Guo, J., Huang, W., Chu, W.-M., Huang, S., Teng, Y., and Wu, G. Arf1 promotes prostate tumorigenesis via targeting oncogenic MAPK signaling. *Oncotarget 7*, 26 (2016), 39834.

[118] Dawar, S., Shahrin, N. H., Sladojevic, N., D'andrea, R. J., Dorstyn, L., Hiwase, D. K., and Kumar, S. Impaired haematopoietic stem cell differentiation and enhanced skewing towards myeloid progenitors in aged caspase-2-deficient mice. *Cell Death & Disease 7*, 12 (2016), e2509–e2509.

[119] De, P., Carlson, J., Leyland-Jones, B., and Dey, N. Oncongenic nexus of cancerous inhibitor of protein phosphatase 2A (CIP2A): an oncoprotein with many hands. *Oncotarget 5*, 13 (2014), 4581–4602.

[120] De, P., Rozeboom, B. J., Aske, J. C., and Dey, N. Active rac1 promotes tumorigenic phenotypes and therapy resistance in solid tumors. *Cancers 12*, 6 (2020).

[121] De, S., Karim, F., Kiessu, E., Cushing, L., Lin, L.-L., Ghandil, P., Hoarau, C., Casanova, J.-L., Puel, A., and Rao, V. R. Mechanism of dysfunction of human variants of the irak4 kinase and a role for its kinase activity in interleukin-1 receptor signaling. *Journal of Biological Chemistry 293*, 39 (2018), 15208–15220.

[122] De Haan, G., and Lazare, S. S. Aging of hematopoietic stem cells. *Blood 131*, 5 (2018), 479–487.

[123] De Siervi, A., Marinissen, M., Diggs, J., Wang, X.-F., Pages, G., and Senderowicz, A. Transcriptional activation of p21waf1/cip1 by alkylphospholipids: role of the mitogen-activated protein kinase pathway in the transactivation of the human p21waf1/cip1 promoter by Sp1. *Cancer Research 64*, 2 (2004), 743–750.

[124] Dean, W., and Morgan, R. F. In defense of the concept of biological aging measurement—current status. *Archives of Gerontology and Geriatrics 7*, 3 (1988), 191–210.

[125] Demaria, M., Giorgi, C., Lebiedzinska, M., Esposito, G., D'Angeli, L., Bartoli, A., Gough, D. J., Turkson, J., Levy, D. E., Watson, C. J., Wieckowski, M. R., Provero, P., Pinton, P., and Poli, V. A sTAT3-mediated metabolic switch is involved in tumour transformation and STAT3 addiction. *Aging 2*, 11 (2010), 823–842.

[126] Demaria, M., and Poli, V. PKM2, STAT3 and HIF-1α. *JAK-STAT 1*, 3 (2012), 194–196.

[127] Deng, Y., Luo, S., Deng, C., Luo, T., Yin, W., Zhang, H., Zhang, Y., Zhang, X., Lan, Y., Ping, Y., Xiao, Y., and Li, X. Identifying mutual exclusivity across cancer genomes: computational approaches to discover genetic interaction and reveal tumor vulnerability. *Briefings in Bioinformatics 20*, 1 (2019), 254–266.

[128] Di Agostino, S., Rossi, P., Geremia, R., and Sette, C. The mapk pathway triggers activation of nek2 during chromosome condensation in mouse spermatocytes. *Development 129*, 7 (2002), 1715–1727.

[129] Diehl, J. A., Cheng, M., Roussel, M. F., and Sherr, C. J. Glycogen synthase kinase-3β regulates cyclin D1 proteolysis and subcellular localization. *Genes & Development 12*, 22 (1998), 3499–3511.

[130] Dimri, G. P., Nakanishi, M., Desprez, P.-Y., Smith, J. R., and Campisi, J. Inhibition of E2F activity by the cyclin-dependent protein kinase inhibitor p21 in cells expressing or lacking a functional retinoblastoma protein. *Molecular and Cellular Biology 16*, 6 (1996), 2987–2997.

[131] Dinić, J., Efferth, T., García-Sosa, A. T., Grahovac, J., Padrón, J. M., Pajeva, I., Rizzolio, F., Saponara, S., Spengler, G., and Tsakovska, I. Repurposing old drugs to fight multidrug resistant cancers. *Drug Resistance Updates 52* (2020), 100713.

[132] Diop, O., Tourniel, L., and Fromion, V. Summarizing complex asynchronous boolean attractors, application to the analysis of a mammalian cell cycle model. In *2019 18th European Control Conference (ECC)* (2019), IEEE, pp. 1677–1682.

[133] Djukom, C., Proo, L. J., Mrazek, A., Townsend, C. M., Hellmich, M. R., and Chao, C. Dual inhibition of PI3K and mTOR signaling pathways decreases human pancreatic neuroendocrine tumor PNET metastatic progression. *Pancreas 43*, 1 (2010), 88–92.

[134] Dodd, K. M., Yang, J., Shen, M. H., Sampson, J. R., and Tee, A. R. mTORC1 drives HIF-1α and VEGF-A signalling via multiple mechanisms involving 4E-BP1, S6K1 and STAT3. *Oncogene 34*, 17 (2015), 2239–2250.

[135] Dolnikov, A., Xu, N., Shen, S., Song, E., Holmes, T., Klamer, G., and O'Brien, T. A. GSK-3β inhibition promotes early engraftment of ex vivo-expanded haematopoietic stem cells. *Cell Proliferation 47*, 2 (2014), 113–123.

[136] Domen, J. The role of apoptosis in regulating hematopoiesis and hematopoietic stem cells. *Immunologic Research 22*, 2-3 (2000), 83–94.

[137] Dong, X., Milholland, B., and Vijg, J. Evidence for a limit to human lifespan. *Nature 538*, 7624 (2016), 257–259.

[138] Dubrova, E., and Teslenko, M. A SAT-based algorithm for finding attractors in synchronous Boolean networks. *IEEE/ACM Transactions on Computational Biology and Bioinformatics 8*, 5 (2011), 1393–1399.

[139] Dufour, M., Dormond-Meuwly, A., Pythoud, C., Demartines, N., and Dormond, O. Reactivation of AKT signaling following treatment of cancer cells with PI3K inhibitors attenuates their antitumor effects. *Biochemical and Biophysical Research Communications 438*, 1 (2013), 32–37.

[140] Ehlers, R. A., Zhang, Y., Hellmich, M. R., and Evers, B. M. Neurotensin-mediated activation of MAPK pathways and AP-1 binding in the human pancreatic cancer cell line, MIA PaCa-2. *Biochemical and Biophysical Research Communications 269*, 3 (2000), 704–708.

[141] El-Deiry, W. S. p21/p53, cellular growth control and genomic integrity. In *Cyclin Dependent Kinase (CDK) Inhibitors*. Springer, 1998, pp. 121–137.

[142] Eliasson, P., and Jönsson, J.-I. The hematopoietic stem cell niche: low in oxygen but a nice place to be. *Journal of Cellular Physiology 222*, 1 (2010), 17–22.

[143] Eliasson, P., Rehn, M., Hammar, P., Larsson, P., Sirenko, O., Flippin, L. A., Cammenga, J., and Jönsson, J.-I. Hypoxia mediates low cell-cycle activity and increases the proportion of long-term-reconstituting hematopoietic stem cells during in vitro culture. *Experimental Hematology 38*, 4 (2010), 301–310.e2.

[144] Ema, H., Takano, H., Sudo, K., and Nakauchi, H. In vitro self-renewal division of hematopoietic stem cells. *The Journal of Experimental Medicine 192*, 9 (2000), 1281–1288.

[145] Ema, H., Takano, H., Sudo, K., and Nakauchi, H. In vitro self-renewal division of hematopoietic stem cells. *The Journal of Experimental Medicine 192*, 9 (2000), 1281–1288.

[146] Enciso, J., Mayani, H., Mendoza, L., and Pelayo, R. Modeling the pro-inflammatory tumor microenvironment in acute lymphoblastic leukemia predicts a breakdown of hematopoietic-mesenchymal communication networks. *Frontiers in Physiology 7*, 349 (2016).

[147] Enver, T., Heyworth, C. M., and Dexter, T. M. Do stem cells play dice? *Blood 92*, 2 (1998), 348–351.

[148] Fauré, A., Naldi, A., Chaouiya, C., and Thieffry, D. Dynamical analysis of a generic Boolean model for the control of the mammalian cell cycle. *Bioinformatics 22*, 14 (2006), e124–e131.

[149] Fawcett, T. An introduction to ROC analysis. *Pattern Recognition Letters 27*,

8 (2006), 861–874.

[150] Feldman, R. J., Sementchenko, V. I., and Watson, D. K. The epithelial-specific Ets factors occupy a unique position in defining epithelial proliferation, differentiation and carcinogenesis. *Anticancer Research 23*, 3 (2003), 2125–2132.

[151] Fendrich, V., Waldmann, J., Esni, F., Ramaswamy, A., Mullendore, M., Buchholz, M., Maitra, A., and Feldmann, G. Snail and Sonic Hedgehog activation in neuroendocrine tumors of the ileum. *Endocrine-Related Cancer 14*, 3 (2007), 865–874.

[152] Feng, J., Sheng, H., Zhu, C., Qian, X., Wan, D., Su, D., Chen, X., and Zhu, L. Correlation of neuroendocrine features with prognosis of non-small cell lung cancer. *Oncotarget 7*, 44 (2016), 71727.

[153] Feng, Z., and Levine, A. J. The regulation of energy metabolism and the IGF-1/mTOR pathways by the p53 protein. *Trends in Cell Biology 20*, 7 (2010), 427 – 434.

[154] Feng, Z., Ma, J., and Hua, X. Epigenetic regulation by the menin pathway. *Endocrine-Related Cancer 24*, 10 (2017), T147–T159.

[155] Feng, Z., Wang, L., Sun, Y., Jiang, Z., Domsic, J., An, C., Xing, B., Tian, J., Liu, X., Metz, D. C., Yang, X., Marmorstein, R., Ma, X., and Hua, X. Menin and Daxx interact to suppress neuroendocrine tumors through epigenetic control of the membrane metallo-endopeptidase. *Cancer Research 77*, 2 (2017), 401–411.

[156] Fiedler, K., Kokai, E., Bresch, S., and Brunner, C. Myd88 is involved in myeloid as well as lymphoid hematopoiesis independent of the presence of a pathogen. *American Journal of Blood Research 3*, 2 (2013), 124.

[157] Filmus, J., Robles, A. I., Shi, W., Wong, M. J., Colombo, L. L., and Conti, C. J. Induction of cyclin d1 overexpression by activated ras. *Oncogene 9*, 12 (1994), 3627–3633.

[158] Finnerty, B. M., Moore, M. D., Verma, A., Aronova, A., Huang, S., Edwards, D. P., Chen, Z., Seandel, M., Scognamiglio, T., Du, Y.-C. N., Element, O., Zarnegar, R., Min, I. M., and Fahey, T. J. UCHL1 loss alters the cell cycle in metastatic pancreatic neuroendocrine tumors. *Endocrine-Related Cancer 26*, 4 (2019), 411–423.

[159] Fleming, W., Alpern, E., Uchida, N., Ikuta, K., Spangrude, G., and Weissman, I. Functional heterogeneity is associated with the cell cycle status of murine hematopoietic stem cells. *Journal of Cell Biology 122*, 4 (08 1993), 897–902.

[160] Flügel, D., Görlach, A., Michiels, C., and Kietzmann, T. Glycogen synthase kinase 3 phosphorylates hypoxia-inducible factor 1α and mediates its destabilization in a VHL-independent manner. *Molecular and Cellular Biology*

27, 9 (2007), 3253–3265.

[161] Forsberg, E. C., Prohaska, S. S., Katzman, S., Heffner, G. C., Stuart, J. M., and Weissman, I. L. Differential expression of novel potential regulators in hematopoietic stem cells. *PLOS Genetics 1*, 3 (2005), e28.

[162] Foudi, A., Hochedlinger, K., Van Buren, D., Schindler, J. W., Jaenisch, R., Carey, V., and Hock, H. Analysis of histone 2B-GFP retention reveals slowly cycling hematopoietic stem cells. *Nature Biotechnology 27*, 1 (2009), 84–90.

[163] François, R. A., Maeng, K., Nawab, A., Kaye, F. J., Hochwald, S. N., and Zajac-Kaye, M. Targeting focal adhesion kinase and resistance to mtor inhibition in pancreatic neuroendocrine tumors. *Journal of the National Cancer Institute 107*, 8 (2015), djv123.

[164] Freeman, L. C. A Set of Measures of Centrality based on Betweenness. *Sociometry* (1977), 35–41.

[165] Friboulet, A., and Thomas, D. Systems biology—an interdisciplinary approach. *Biosensors and Bioelectronics 20*, 12 (2005), 2404–2407.

[166] Friedman, D. R., Davis, P. H., Lanasa, M. C., Moore, J. O., Gockerman, J. P., Nelson, T., Bond, K. M., Jiang, N., Davis, E. D., Allgood, S. D., Chen, Y., Sportelli, P., and Weinberg, B. Pre-clinical and interim results of a Phase II trial of perifosine in patients with relapsed or refractory chronic lymphocytic leukemia (CLL). *Blood 116*, 21 (2010), 1842.

[167] Friedman, E. J., Young, K., Tremper, G., Liang, J., Landsberg, A. S., Schuff, N., and Initiative, A. D. N. Directed network motifs in alzheimer's disease and mild cognitive impairment. *PLOS ONE 10*, 4 (2015), e0124453.

[168] Frisch, B. J., and Calvi, L. M. Hematopoietic stem cell cultures and assays. In *Skeletal Development and Repair. Methods in Molecular Biology* (2014), M. J. Hilton, Ed., vol. 1130, Humana Press, Totowa, NJ, pp. 315–324.

[169] Frost, M., Lines, K. E., and Thakker, R. V. Current and emerging therapies for PNETs in patients with or without MEN1. *Nature Reviews Endocrinology 14*, 4 (2018), 216–227.

[170] Fröbel, J., Landspersky, T., Percin, G., Schreck, C., Rahmig, S., Ori, A., Nowak, D., Essers, M., Waskow, C., and Oostendorp, R. A. J. The hematopoietic bone marrow niche ecosystem. *Frontiers in Cell and Developmental Biology 9* (2021), 1958.

[171] Futreal, P. A., Coin, L., Marshall, M., Down, T., Hubbard, T., Wooster, R., Rahman, N., and Stratton, M. R. A census of human cancer genes. *Nature Reviews Cancer 4*, 3 (2004), 177–183.

[172] Gammaitoni, L., Bruno, S., Sanavio, F., Gunetti, M., Kollet, O., Cavalloni, G., Falda, M., Fagioli, F., Lapidot, T., Aglietta, M., and Piacibello, W. Ex vivo expansion of human adult stem cells capable of primary and secondary hemopoietic reconstitution. *Experimental Hematology 31*, 3 (2003),

261–270.

[173] Gan, B., Sahin, E., Jiang, S., Sanchez-Aguilera, A., Scott, K. L., Chin, L., Williams, D. A., Kwiatkowski, D. J., and DePinho, R. A. mTORC1-dependent and -independent regulation of stem cell renewal, differentiation, and mobilization. *Proceedings of the National Academy of Sciences 105*, 49 (2008), 19384–19389.

[174] Gansauge, S., Gansauge, F., Ramadani, M., Stobbe, H., Rau, B., Harada, N., and Beger, H. G. Overexpression of cyclin D1 in human pancreatic carcinoma is associated with poor prognosis. *Cancer Research 57*, 9 (1997), 1634–1637.

[175] Gao, D., Inuzuka, H., Tseng, A., Chin, R. Y., Toker, A., and Wei, W. Phosphorylation by Akt1 promotes cytoplasmic localization of Skp2 and impairs APCCdh1-mediated Skp2 destruction. *Nature Cell Biology 11*, 4 (2009), 397–408.

[176] Gao, J., Aksoy, B. A., Dogrusoz, U., Dresdner, G., Gross, B., Sumer, S. O., Sun, Y., Jacobsen, A., Sinha, R., Larsson, E., Cerami, E., Sandler, C., and Schultz, N. Integrative analysis of complex cancer genomics and clinical profiles using the cBioPortal. *Science Signaling 6*, 269 (2013), pl1–pl1.

[177] Gao, J., Graves, S., Koch, U., Liu, S., Jankovic, V., Buonamici, S., El Andaloussi, A., Nimer, S. D., Kee, B. L., Taichman, R., Radtke, F., and Aifantis, I. Hedgehog signaling is dispensable for adult hematopoietic stem cell function. *Cell Stem Cell 4*, 6 (2009), 548–558.

[178] Gao, X., Zhao, L., Liu, S., Li, Y., Xia, S., Chen, D., Wang, M., Wu, S., Dai, Q., Vu, H., Zacharias, L., DeBerardinis, R., Lim, E., Metallo, C., Boggon, T. J., Lonial, S., Lin, R., Maon, H., Pan, Y., Shan, C., and Chen, J. γ-6-phosphogluconolactone, a byproduct of the oxidative pentose phosphate pathway, contributes to AMPK activation through inhibition of PP2A. *Molecular Cell 76*, 6 (2019), 857–871.

[179] García-Gómez, M. L., Azpeitia, E., and Álvarez-Buylla, E. R. A dynamic genetic-hormonal regulatory network model explains multiple cellular behaviors of the root apical meristem of *Arabidopsis thaliana*. *PLOS Computational Biology 13*, 4 (2017), e1005488.

[180] Gates, A. J., and Rocha, L. M. Control of complex networks requires both structure and dynamics. *Scientific Reports 6*, 1 (2016), 1–11.

[181] Geest, C. R., and Coffer, P. J. MAPK signaling pathways in the regulation of hematopoiesis. *Journal of Leukocyte Biology 86*, 2 (2009), 237–250.

[182] Geiger, H., Koehler, A., and Gunzer, M. Stem cells, aging, niche, adhesion and Cdc42: a model for changes in cell-cell interactions and hematopoietic stem cell aging. *Cell Cycle 6*, 8 (2007), 884–887.

[183] Gerber, H.-P., Malik, A. K., Solar, G. P., Sherman, D., Liang, X. H., Meng,

G., Hong, K., Marsters, J. C., and Ferrara, N. VEGF regulates haematopoietic stem cell survival by an internal autocrine loop mechanism. *Nature 417*, 6892 (2002), 954–958.

[184] Gershenson, C., Kauffman, S. A., and Shmulevich, I. The role of redundancy in the robustness of random Boolean networks. *In Artifical Life X, Proceedings of the Tenth International Conference on the Simulation and Synthesis of Living Systems* (2006).

[185] Ghayouri, M., Boulware, D., Nasir, A., Strosberg, J., Kvols, L., and Coppola, D. Activation of the serine/theronine protein kinase Akt in enteropancreatic neuroendocrine tumors. *Anticancer Research 30*, 12 (2010), 5063–5067.

[186] Giacinti, C., and Giordano, A. RB and cell cycle progression. *Oncogene 25*, 38 (2006), 5220–5227.

[187] Giacomantonio, C. E., and Goodhill, G. J. A Boolean model of the gene regulatory network underlying mammalian cortical area development. *PLOS Computational Biology 6*, 9 (2010), e1000936.

[188] Giatsidis, C., Thilikos, D. M., and Vazirgiannis, M. D-cores: measuring collaboration of directed graphs based on degeneracy. *Knowledge and Information Systems 35*, 2 (2013), 311–343.

[189] Gilbert, J. A., Adhikari, L. J., Lloyd, R. V., Halfdanarson, T. R., Muders, M. H., and Ames, M. M. Molecular markers for novel therapeutic strategies in pancreatic endocrine tumors. *Pancreas 42*, 3 (2013), 411.

[190] Gillingham, A. K., Bertram, J., Begum, F., and Munro, S. In vivo identification of gtpase interactors by mitochondrial relocalization and proximity biotinylation. *eLife 8* (2019).

[191] Glauche, I., Thielecke, L., and Roeder, I. Cellular aging leads to functional heterogeneity of hematopoietic stem cells: a modeling perspective. *Aging ell 10*, 3 (2011), 457–465.

[192] Glauser, D. A., and Schlegel, W. The emerging role of foxo transcription factors in pancreatic β cells. *Journal of Endocrinology 193*, 2 (2007), 195–207.

[193] Gonzalez, A. G., Naldi, A., Sanchez, L., Thieffry, D., and Chaouiya, C. GINsim: a software suite for the qualitative modelling, simulation and analysis of regulatory networks. *Biosystems 84*, 2 (2006), 91–100.

[194] Grande, E., Teulé, A., Alonso-Gordoa, T., Jiménez-Fonseca, P., Benavent, M., Capdevila, J., Custodio, A., Vera, R., Munarriz, J., La Casta, A., Díez, J. J., Gajate, P., Molina-Cerrillo, J., Matos, I., Cristóbal, E. M., Ruffinelli, J. C., Palacios, J., and García-Carbonero, R. The PALBONET Trial: A phase II study of palbociclib in metastatic grade 1 and 2 pancreatic neuroendocrine tumors (GETNE-1407). *The Oncologist 25*, 9 (2020), 745.

[195] Gregory, M. A., Qi, Y., and Hann, S. R. Phosphorylation by glycogen synthase kinase-3 controls c-Myc proteolysis and subnuclear localization. *The*

Journal of Biological Chemistry 278, 51 (2003), 51606–51612.

[196] Grieb, M., Burkovski, A., Sträng, J. E., Kraus, J. M., Gross, A., Palm, G., Kühl, M., and Kestler, H. A. Predicting variabilities in cardiac gene expression with a boolean network incorporating uncertainty. *PLOS ONE 10*, 7 (2015), e0131832.

[197] Gross, A., Kracher, B., Kraus, J. M., Kühlwein, S. D., Pfister, A. S., Wiese, S., Luckert, K., Pötz, O., Joos, T., Van Daele, D., De Readt, L., Kühl, M., and Kestler, H. A. Representing dynamic biological networks with multi-scale probabilistic models. *Communications Biology 2* (2019).

[198] Gu, Z., Xia, J., Xu, H., Frech, I., Tricot, G., and Zhan, F. NEK2 promotes aerobic glycolysis in multiple myeloma through regulating splicing of pyruvate kinase. *Journal of Hematology & Oncology 10*, 1 (2017), 1–11.

[199] Guerrouahen, B. S., Al-Hijji, I., and Tabrizi, A. R. Osteoblastic and vascular endothelial niches, their control on normal hematopoietic stem cells, and their consequences on the development of leukemia. *Stem Cells International 2011*, 1-2 (2011), 375857–8.

[200] Gui, T., Sun, Y., Shimokado, A., and Muragaki, Y. The roles of mitogen-activated protein kinase pathways in TGF-β-induced epithelial-mesenchymal transition. *Journal of Signal Transduction 2012* (2012).

[201] Guimera, R., and Amaral, L. A. N. Functional cartography of complex metabolic networks. *Nature 433*, 7028 (2005), 895–900.

[202] Guimerà, R., and Nunes Amaral, L. A. Functional cartography of complex metabolic networks. *Nature 433* (2005), 895–900.

[203] Gulhati, P., Bowen, K. A., Liu, J., Stevens, P. D., Rychahou, P. G., Chen, M., Lee, E. Y., Weiss, H. L., O'Connor, K. L., Gao, T., and Evers, B. M. mTORC1 and mTORC2 regulate EMT, motility, and metastasis of colorectal cancer via RhoA and Rac1 signaling pathways. *Cancer Research 71*, 9 (2011), 3246–3256.

[204] Guney, I., Wu, S., and Sedivy, J. M. Reduced c-myc signaling triggers telomere-independent senescence by regulating bmi-1 and p16ink4a. *Proceedings of the National Academy of Sciences 103*, 10 (2006), 3645–3650.

[205] Guo, S., Wu, X., Shimoide, A., Wong, J., Moatamed, F., and Sawicki, M. Frequent overexpression of cyclin d1 in sporadic pancreatic endocrine tumours. *Journal of Endocrinology 179*, 1 (2003), 73–80.

[206] Gupta, S., Bisht, S. S., Kukreti, R., Jain, S., and Brahmachari, S. K. Boolean network analysis of a neurotransmitter signaling pathway. *Journal of Theoretical Biology 244*, 3 (2007), 463–469.

[207] Gurung, B., Feng, Z., and Hua, X. Menin directly represses Gli1 expression independent of canonical Hedgehog signaling. *Molecular Cancer Research 11*, 10 (2013), 1215–1222.

[208] Gutierrez-Martinez, P., Hogdal, L., Nagai, M., Kruta, M., Singh, R.,

Sarosiek, K., Nussenzweig, A., Beerman, I., Letai, A., and Rossi, D. J. Diminished apoptotic priming and atm signalling confer a survival advantage onto aged haematopoietic stem cells in response to dna damage. *Nature Cell Biology 20*, 4 (2018), 413–421.

[209] Hage, P., and Harary, F. Eccentricity and centrality in networks. *Social Networks 17*, 1 (1995), 57–63.

[210] Hahn-Windgassen, A., Nogueira, V., Chen, C.-C., Skeen, J. E., Sonenberg, N., and Hay, N. Akt activates the mammalian target of rapamycin by regulating cellular atp level and ampk activity. *Journal of Biological Chemistry 280*, 37 (2005), 32081–32089.

[211] Haines, E., Saucier, C., and Claing, A. The adaptor proteins p66shc and grb2 regulate the activation of the gtpases ARF1 and ARF6 in invasive breast cancer cells. *Journal of Biological Chemistry 289*, 9 (2014), 5687–5703.

[212] Hajian-Tilaki, K. Receiver operating characteristic (ROC) curve analysis for medical diagnostic test evaluation. *Caspian Journal of Internal Medicine 4*, 2 (2013), 627–635.

[213] Hampsch, R. A., Shee, K., Bates, D., Lewis, L. D., Désiré, L., Leblond, B., Demidenko, E., Stefan, K., Huang, Y. H., and Miller, T. W. Therapeutic sensitivity to rac gtpase inhibition requires consequential suppression of mtorc1, akt, and mek signaling in breast cancer. *Oncotarget 8*, 13 (2017), 21806.

[214] Han, J. D. J., Bertin, N., Hao, T., Goldberg, D. S., Berriz, G. F., Zhang, L. V., Dupuy, D., Walhout, A. J., Cusick, M. E., Roth, F. P., and Vidal, M. Evidence for dynamically organized modularity in the yeast protein–protein interaction network. *Nature 430*, 6995 (2004), 88–93.

[215] Hanahan, D. Heritable formation of pancreatic β-cell tumours in transgenic mice expressing recombinant insulin/simian virus 40 oncogenes. *Nature 315*, 6015 (1985), 115–122.

[216] Hanahan, D. Dissecting multistep tumorigenesis in transgenic mice. *Annual Review of Genetics 22*, 1 (1988), 479–519.

[217] Hanahan, D. Rethinking the war on cancer. *The Lancet 383*, 9916 (2014), 558–563.

[218] Hanahan, D., and Weinberg, R. A. The hallmarks of cancer. *Cell 100*, 1 (2000), 57–70.

[219] Hanahan, D., and Weinberg, R. A. Hallmarks of cancer: the next generation. *cell 144*, 5 (2011), 646–674.

[220] Hannum, C., Culpepper, J., Campbell, D., McClanahan, T., Zurawski, S., Bazan, J. F., Kastelein, R., Hudak, S., Wagner, J., and Mattson, J. Ligand for FLT3/FLK2 receptor tyrosine kinase regulates growth of haematopoietic stem cells and is encoded by variant RNAs. *Nature 368*, 6472 (1994), 643–648.

[221] Hao, S., Chen, C., and Cheng, T. Cell cycle regulation of hematopoietic stem

or progenitor cells. *International Journal of Hematology 103*, 5 (2016), 487–497.

[222] Harman, D. The aging process. *Proceedings of the National Academy of Sciences 78*, 11 (1981), 7124–7128.

[223] Harman, D. Aging: overview. *Annals of the New York Academy of Sciences 928*, 1 (2001), 1–21.

[224] Harris, S. L., and Levine, A. J. The p53 pathway: positive and negative feedback loops. *Oncogene 24*, 17 (2005), 2899–2908.

[225] Harvey, I., and Bossomaier, T. Time Out of Joint: Attractors in Asynchronous Random Boolean Networks. In *Proceedings of the Fourth European Conference on Artificial Life* (1997), MIT Press, Cambridge, pp. 67–75.

[226] Haupt, Y., Maya, R., Kazaz, A., and Oren, M. Mdm2 promotes the rapid degradation of p53. *Nature 387*, 6630 (1997), 296–299.

[227] Hay, N. Interplay between FOXO, TOR, and Akt. *Biochimica et Biophysica Acta (BBA)-Molecular Cell Research 1813*, 11 (2011), 1965–1970.

[228] Hayflick, L. The future of ageing. *Nature 408*, 6809 (2000), 267–269.

[229] He, H., and Wang, J. Inflammation and hematopoietic stem cells aging. *Blood Science 3*, 1 (2021), 1–5.

[230] He, X., and Zhang, J. Why do hubs tend to be essential in protein networks? *PLOS Genetics 2*, 6 (2006), e88.

[231] Heckel, R., Schober, S., and Bossert, M. Harmonic analysis of Boolean networks: Determinative power and perturbations. *EURASIP Journal on Bioinformatics and Systems Biology 2013*, 1 (2013), 6.

[232] Helikar, T., Kowal, B., McClenathan, S., Bruckner, M., Rowley, T., Madrahimov, A., Wicks, B., Shrestha, M., Limbu, K., and Rogers, J. A. The Cell Collective: toward an open and collaborative approach to systems biology. *BMC Systems Biology 6*, 96 (2012).

[233] Hemmati, S., Sinclair, T., Tong, M., Bartholdy, B., Okabe, R. O., Ames, K., Ostrodka, L., Haque, T., Kaur, I., Mills, T. S., and others. PI3K alpha and delta promote hematopoietic stem cell activation. *JCI Insight 4*, 13 (2019).

[234] Heo, S.-K., Noh, E.-K., Gwon, G.-D., Kim, J. Y., Jo, J.-C., Choi, Y., Koh, S., Baek, J. H., Min, Y. J., and Kim, H. Light (tnfsf14) increases the survival and proliferation of human bone marrow-derived mesenchymal stem cells. *PLOS ONE 11*, 11 (2016), e0166589.

[235] Hermida, M. A., Kumar, J. D., and Leslie, N. R. GSK3 and its interactions with the PI3K/AKT/mTOR signalling network. *Advances in Biological Regulation 65* (2017), 5–15.

[236] Herrmann, F., Gross, A., Zhou, D., Kestler, H. A., and Kühl, M. A Boolean model of the cardiac gene regulatory network determining first and second heart field identity. *PLOS ONE 7*, 10 (2012), e46798.

[237] Hiebert, S., Chellappan, S., Horowitz, J., and Nevins, J. The interaction

of RB with E2F coincides with an inhibition of the transcriptional activity of E2F. *Genes & Development 6*, 2 (1992), 177–185.

[238] Hirai, H., Roussel, M. F., Kato, J., Ashmun, R. A., and Sherr, C. J. Novel INK4 proteins, p19 and p18, are specific inhibitors of the cyclin D-dependent kinases CDK4 and CDK6. *Molecular and Cellular Biology 15*, 5 (1995), 2672–2681.

[239] Hock, H., Hamblen, M. J., Rooke, H. M., Schindler, J. W., Saleque, S., Fujiwara, Y., and Orkin, S. H. Gfi-1 restricts proliferation and preserves functional integrity of haematopoietic stem cells. *Nature 431*, 7011 (Sept. 2004), 1002–1007.

[240] Hofmann, I., Stover, E. H., Cullen, D. E., Mao, J., Morgan, K. J., Lee, B. H., Kharas, M. G., Miller, P. G., Cornejo, M. G., Okabe, R., Armstrong, S. A., Ghilardi, N., Gould, S., de Sauvage, F. J., McMahon, A. P., and Gilliland, D. G. Hedgehog signaling is dispensable for adult murine hematopoietic stem cell function and hematopoiesis. *Cell Stem Cell 4*, 6 (2009), 559–567.

[241] Holmes, T., O'Brien, T. A., Knight, R., Lindeman, R., Shen, S., Song, E., Symonds, G., and Dolnikov, A. Glycogen synthase kinase-3beta inhibition preserves hematopoietic stem cell activity and inhibits leukemic cell growth. *Stem Cells 26*, 5 (2008), 1288–1297.

[242] Honda, R., Tanaka, H., and Yasuda, H. Oncoprotein MDM2 is a ubiquitin ligase E3 for tumor suppressor p53. *FEBS Letters 420*, 1 (1997), 25–27.

[243] Hong, K. H., Ryu, J., and Han, K. H. Monocyte chemoattractant protein-1–induced angiogenesis is mediated by vascular endothelial growth factor-a. *Blood 105*, 4 (2005), 1405–1407.

[244] Hopfensitz, M., Müssel, C., Maucher, M., and Kestler, H. A. Attractors in boolean networks: a tutorial. *Computational Statistics 28*, 1 (2013), 19–36.

[245] Hopfensitz, M., Müssel, C., Wawra, C., Maucher, M., Kühl, M., Neumann, H., and Kestler, H. A. Multiscale binarization of gene expression data for reconstructing boolean networks. *IEEE/ACM Transactions on Computational Biology and Bioinformatics (TCBB) 9*, 2 (2012), 487–498.

[246] Horman, S., Vertommen, D., Heath, R., Neumann, D., Mouton, V., Woods, A., Schlattner, U., Wallimann, T., Carling, D., Hue, L., and Rider, M. H. Insulin antagonizes ischemia-induced Thr172 phosphorylation of AMP-activated protein kinase α-subunits in heart via hierarchical phosphorylation of Ser485/491. *Journal of Biological Chemistry 281*, 9 (2006), 5335–5340.

[247] Huang, J., Zhang, Y., Bersenev, A., O'Brien, W. T., Tong, W., Emerson, S. G., Klein, P. S., and others. Pivotal role for glycogen synthase kinase–3 in hematopoietic stem cell homeostasis in mice. *The Journal of Clinical Investigation 119*, 12 (2009), 3519–3529.

[248] Huang, S., Eichler, G., Bar-Yam, Y., and Ingber, D. E. Cell fates as high-

dimensional attractor states of a complex gene regulatory network. *Physical Review Letters 94*, 12 (2005), 128701.

[249] Huang, S., and Ingber, D. E. Shape-dependent control of cell growth, differentiation, and apoptosis: switching between attractors in cell regulatory networks. *Experimental Cell Research 261*, 1 (2000), 91–103.

[250] Huang, Z., and Bao, S.-D. Roles of main pro-and anti-angiogenic factors in tumor angiogenesis. *World Journal of Gastroenterology 10*, 4 (2004), 463.

[251] Humphrey, R. K., Yu, S.-M., Flores, L. E., and Jhala, U. S. Glucose regulates steady-state levels of PDX1 via the reciprocal actions of GSK3 and AKT kinases. *Journal of Biological Chemistry 285*, 5 (2010), 3406–3416.

[252] I Ahmad, I. An insight into the therapeutic potential of quinazoline derivatives as anticancer agents. *MedChemComm 8*, 5 (2017), 871–885.

[253] Ideker, T., Galitski, T., and Hood, L. A new approach to decoding life: systems biology. *Annual Review of Genomics and Human Genetics 2* (2001), 343–372.

[254] Ikonomi, N., Kühlwein, S. D., Schwab, J. D., and Kestler, H. A. Awakening the hsc: dynamic modeling of hsc maintenance unravels regulation of the TP53 pathway and quiescence. *Frontiers in Physiology 11* (2020), 848.

[255] Ikonomi, N., Werle, S. D., Schwab, J. D., and Kestler, H. A. Discrete logic modeling of cell signaling pathways. In *TGF-Beta Signaling. Methods in Molecular Biology* (2022), Z. Zi and X. Liu, Eds., Humana, New York, NY, pp. 159–181.

[256] Ingram, P. J., Stumpf, M. P., and Stark, J. Network motifs: structure does not determine function. *BMC Genomics 7*, 1 (2006), 1–12.

[257] Inoki, K., Ouyang, H., Zhu, T., Lindvall, C., Wang, Y., Zhang, X., Yang, Q., Bennett, C., Harada, Y., Stankunas, K., yu Wang, C., He, X., MacDougald, O. A., You, M., Williams, B. O., and Guan, K.-L. TSC2 integrates wnt and energy signals via a coordinated phosphorylation by AMPK and GSK3 to regulate cell growth. *Cell 126*, 5 (2006), 955–968.

[258] Irons, D. Logical analysis of the budding yeast cell cycle. *Journal of Theoretical Biology 257*, 4 (2009), 543–559.

[259] Ishida, E., Yamada, M., Horiguchi, K., Taguchi, R., Ozawa, A., Shibusawa, N., Hashimoto, K., Satoh, T., Yoshida, S., Tanaka, Y., Yokota, M., Tosaka, M., Yamada, S., Yoshimoto, Y., and Mori, M. Attenuated expression of menin and p27 kip1 in an aggressive case of multiple endocrine neoplasia type 1 (MEN1) associated with an atypical prolactinoma and a malignant pancreatic endocrine tumor. *Endocrine journal 58*, 4 (2011), 287–296.

[260] Israel, L., and Mellett, M. Clinical and genetic heterogeneity of card14 mutations in psoriatic skin disease. *Frontiers in Immunology 9* (2018), 2239.

[261] Itkin, T., Gur-Cohen, S., Spencer, J. A., Schajnovitz, A., Ramasamy,

S. K., Kusumbe, A. P., Ledergor, G., Jung, Y., Milo, I., Poulos, M. G., Kalinkovich, A., Ludin, A., Kollet, O., Shakhar, G., Butler, J. M., Rafii, S., Adams, R. H., Scadden, D. T., Lin, C. P., and Lapidot, T. Distinct bone marrow blood vessels differentially regulate haematopoiesis. *Nature 532*, 7599 (2016), 323–328.

[262] Ito, K., Hirao, A., Arai, F., Matsuoka, S., Takubo, K., Hamaguchi, I., Nomiyama, K., Hosokawa, K., Sakurada, K., Nakagata, N., and others. Regulation of oxidative stress by ATM is required for self-renewal of haematopoietic stem cells. *Nature 431*, 7011 (2004), 997–1002.

[263] Ito, K., Hirao, A., Arai, F., Takubo, K., Matsuoka, S., Miyamoto, K., Ohmura, M., Naka, K., Hosokawa, K., Ikeda, Y., and others. Reactive oxygen species act through p38 MAPK to limit the lifespan of hematopoietic stem cells. *Nature Medicine 12*, 4 (2006), 446–451.

[264] Jackson, P. K., Chevalier, S., Philippe, M., and Kirschner, M. W. Early events in DNA replication require cyclin E and are blocked by p21CIP1. *The Journal of Cell Biology 130*, 4 (1995), 755–769.

[265] Jacobs, J. J., Kieboom, K., Marino, S., DePinho, R. A., and van Lohuizen, M. The oncogene and Polycomb-group gene bmi-1 regulates cell proliferation and senescence through the ink4a locus. *Nature 397*, 6715 (1999), 164–168.

[266] Jamali, M., and Chetty, R. Predicting prognosis in gastroentero-pancreatic neuroendocrine tumors: an overview and the value of Ki-67 immunostaining. *Endocrine Pathology 19*, 4 (2008), 282–288.

[267] Jang, Y.-Y., and Sharkis, S. J. A low level of reactive oxygen species selects for primitive hematopoietic stem cells that may reside in the low-oxygenic niche. *Blood 110*, 8 (2007), 3056–3063.

[268] Janssens, S., Tinel, A., Lippens, S., and Tschopp, J. PIDD mediates NF-κB activation in response to DNA damage. *Cell 123*, 6 (2005), 1079–1092.

[269] Janzen, V., Forkert, R., Fleming, H. E., Saito, Y., Waring, M. T., Dombkowski, D. M., Cheng, T., DePinho, R. A., Sharpless, N. E., and Scadden, D. T. Stem-cell ageing modified by the cyclin-dependent kinase inhibitor p16 ink4a. *Nature 443*, 7110 (2006), 421–426.

[270] Jeong, A. L., Lee, S., Park, J. S., Han, S., Jang, C.-Y., Lim, J.-S., Lee, M. S., and Yang, Y. Cancerous inhibitor of protein phosphatase 2A (CIP2A) protein is involved in centrosome separation through the regulation of NIMA (never in mitosis gene A)-related kinase 2 (NEK2) protein activity. *Journal of Biological Chemistry 289*, 1 (2014), 28–40.

[271] Jeong, H., Mason, S. P., Barabási, A.-L., and Oltvai, Z. N. Lethality and centrality in protein networks. *Nature 411* (2001), 41–42.

[272] Jeong, M., Piao, Z.-H., Kim, M. S., Lee, S. H., Yun, S., Sun, H.-n., Yoon, S. R., Chung, J. W., Kim, T.-D., Jeon, J. H., Lee, J., Kim, H.-N., Choi, J.-Y., and

Choi, I. Thioredoxin-interacting protein regulates hematopoietic stem cell quiescence and mobilization under stress conditions. *The Journal of Immunology 183*, 4 (2009), 2495–2505.

[273] Jiang, C., Wu, Y., Xia, Q., and Huang, Q. Novel molecular targets in malignant diseases of digestive system. *Gastroenterology research and practice 2013* (2013).

[274] Jiang, M., Chen, H., Lai, S., Wang, R., Qiu, Y., Ye, F., Fei, L., Sun, H., Xu, Y., Jiang, X., Zhou, Z., Zhang, T., Li, Y., Xie, J., Fang, Q., Gale, R. P., Han, X., Huang, H., and Guo, G. Maintenance of human haematopoietic stem and progenitor cells in vitro using a chemical cocktail. *Cell Discovery 4*, 1 (2018), 59.

[275] Jiang, Z., Shi, D., Tu, Y., Tian, J., Zhang, W., Xing, B., Wang, J., Liu, S., Lou, J., Gustafsson, J.-Å., Hua, X., and Ma, X. Human proislet peptide promotes pancreatic progenitor cells to ameliorate diabetes through FOXO1/menin-mediated epigenetic regulation. *Diabetes 67*, 7 (2018), 1345–1355.

[276] Jiang, Z., Xing, B., Feng, Z., Ma, J., Ma, X., and Hua, X. Menin upregulates FOXO1 protein stability by repressing Skp2-mediated degradation in β cells. *Pancreas 48*, 2 (2019), 267.

[277] Jiao, Y., Shi, C., Edil, B. H., De Wilde, R. F., Klimstra, D. S., Maitra, A., Schulick, R. D., Tang, L. H., Wolfgang, C. L., Choti, M. A., Velculescu, V. E., Diaz Jr, L. A., Vogelstein, B., Kinzler, K. W., Hruban, R. H., and Papadopoulos, N. DAXX/ATRX, MEN1, and mTOR pathway genes are frequently altered in pancreatic neuroendocrine tumors. *Science 331*, 6021 (2011), 1199–1203.

[278] Jones, D. L., and Wagers, A. J. No place like home: anatomy and function of the stem cell niche. *Nature Reviews Molecular Cell Biology 9*, 1 (2008), 11–21.

[279] Jones, S. N., Roe, A. E., Donehower, L. A., and Bradley, A. Rescue of embryonic lethality in mdm2-deficient mice by absence of p53. *Nature 378* (1995), 206–208.

[280] Jung, H., Kim, D. O., Byun, J.-E., Kim, W. S., Kim, M. J., Song, H. Y., Kim, Y. K., Kang, D.-K., Park, Y.-J., Kim, T.-D., Yoon, S. R., Lee, H. G., Choi, E.-J., Min, S.-H., and Choi, I. Thioredoxin-interacting protein regulates haematopoietic stem cell ageing and rejuvenation by inhibiting p38 kinase activity. *Nature Communications 7*, 1 (2016), 1–12.

[281] Jung, H., Kim, M. J., Kim, D. O., Kim, W. S., Yoon, S.-J., Park, Y.-J., Yoon, S. R., Kim, T.-D., Suh, H.-W., Yun, S., Min, J.-K., Lee, H. G., Lee, Y. H., Na, H.-J., Lee, D. C., Kim, H.-C., and Choi, I. TXNIP maintains the hematopoietic cell pool by switching the function of p53 under oxidative stress. *Cell Metabolism 18*, 1 (2013), 75–85.

[282] Jung, J.-W., Lee, S., Seo, M.-S., Park, S.-B., Kurtz, A., Kang, S.-K., and Kang,

K.-S. Histone deacetylase controls adult stem cell aging by balancing the expression of polycomb genes and jumonji domain containing 3. *Cellular and Molecular Life Sciences 67*, 7 (2010), 1165–1176.

[283] Juntilla, M. M., Patil, V. D., Calamito, M., Joshi, R. P., Birnbaum, M. J., and Koretzky, G. A. AKT1 and AKT2 maintain hematopoietic stem cell function by regulating reactive oxygen species. *Blood 115*, 20 (2010), 4030–4038.

[284] Junttila, M. R., Puustinen, P., Niemelä, M., Ahola, R., Arnold, H., Böttzauw, T., Ala-aho, R., Nielsen, C., Ivaska, J., Taya, Y., Lu, S.-L., Lin, S., Chan, E. K. L., Wang, X.-J., Grènman, Kast, J., Kallunki, T., Sears, R., Kähäri, V.-M., and Westermarck, J. CIP2A inhibits PP2A in human malignancies. *Cell 130*, 1 (2007), 51–62.

[285] Kabiri, Z., Numata, A., Kawasaki, A., Edison, Tenen, D. G., and Virshup, D. M. Wnts are dispensable for differentiation and self-renewal of adult murine hematopoietic stem cells. *Blood 126*, 9 (2015), 1086–1094.

[286] Kallergi, G., Agelaki, S., Markomanolaki, H., Georgoulias, V., and Stournaras, C. Activation of FAK/PI3K/Rac1 signaling controls actin reorganization and inhibits cell motility in human cancer cells. *Cellular Physiology and Biochemistry 20*, 6 (2007), 977–986.

[287] Kan, J., Guo, W., Huang, C., Bao, G., Zhu, Y., and Zhu, Y. Z. S-propargyl-cystein, a novel watter-soluble modulator of endogenous hydogen sulfide, promotes angiogenesis through activation of singal transducer and activator of transcription 3. *Antioxidants & Redox Signaling 20*, 15 (2014), 2303–2316.

[288] Kanehisa, M., and Goto, S. KEGG: kyoto encyclopedia of genes and genomes. *Nucleic Acids Research 28*, 1 (2000), 27–30.

[289] Kao, S.-H., Wang, W.-L., Chen, C.-Y., Chang, Y.-L., Wu, Y.-Y., Wang, Y.-T., Wang, S.-P., Nesvizhskii, A. I., Chen, Y.-J., Hong, T.-M., and Yang, P.-C. GSK3β controls epithelial–mesenchymal transition and tumor metastasis by CHIP-mediated degradation of Slug. *Oncogene 33*, 24 (2014), 3172–3182.

[290] Karger, S., Weidinger, C., Krause, K., Sheu, S.-Y., Aigner, T., Gimm, O., Schmid, K.-W., Dralle, H., and Fuhrer, D. FOXO3a: a novel player in thyroid carcinogenesis? *Endocrine-Related Cancer 16*, 1 (2009), 189.

[291] Karin, M., Liu, Z.-g., and Zandi, E. AP-1 function and regulation. *Current Opinion in Cell Biology 9*, 2 (1997), 240–246.

[292] Karnik, S. K., Hughes, C. M., Gu, X., Rozenblatt-Rosen, O., McLean, G. W., Xiong, Y., Meyerson, M., and Kim, S. K. Menin regulates pancreatic islet growth by promoting histone methylation and expression of genes encoding p27Kip1 and p18INK4c. *Proceedings of the National Academy of Sciences 102*, 41 (2005), 14659–14664.

[293] Kasajima, A., and Klöppel, G. Neuroendocrine neoplasms of lung, pancreas

and gut: a morphology-based comparison. *Endocrine-Related Cancer 27*, 11 (2020), R417–R432.

[294] Kastan, M. B., Lim, D.-S., Kim, S.-T., Xu, B., and Canman, C. Multiple signaling pathways involving ATM. In *Cold Spring Harbor Symposia on Quantitative Biology* (2000), Cold Spring Harbor Laboratory Press, pp. 521–526.

[295] Kato, S., Hokari, R., Crawley, S., Gum, J., Ahn, D.-H., Kim, J.-W., Kwon, S.-W., Miura, S., Basbaum, C. B., and Kim, Y. S. MUC5AC mucin gene regulation in pancreatic cancer cells. *International Journal of Oncology 29*, 1 (2006), 33–40.

[296] Kato, Y., Hou, L.-B., Miyagi, S., Nitta, E., Aoyama, K., Shinoda, D., Yamazaki, S., Kuribayashi, W., Isshiki, Y., Koide, S., Si, S., Saraya, A., Matsuzaki, Y., van Lohuizen, M., and Iwama, A. Bmi1 restricts the adipogenic differentiation of bone marrow stromal cells to maintain the integrity of the hematopoietic stem cell niche. *Experimental Hematology 76* (2019), 24–37.

[297] Kauffman, S. A. Metabolic stability and epigenesis in randomly constructed genetic nets. *Journal of Theoretical Biology 22*, 3 (1969), 437–467.

[298] Kauffman, S. A. *The Origins of order: Self-Organization and Selection in Evolution*. Oxford: Oxford University Press, 1993.

[299] Kauffman, S. A., Peterson, C., Samuelsson, B., and Troein, C. Genetic networks with canalyzing Boolean rules are always stable. *Proceedings of the National Academy of Sciences 101*, 49 (2004), 17102–17107.

[300] Kaushansky, K. Molecular mechanisms of thrombopoietin signaling. *Journal of Thrombosis and Haemostasis 7*, Suppl. 1 (2009), 235–238.

[301] Kennedy, S. G., Kandel, E. S., Cross, T. K., and Hay, N. Akt/Protein kinase B inhibits cell death by preventing the release of cytochrome c from mitochondria. *Molecular and Cellular Biology 19*, 8 (1999), 5800–5810.

[302] Keutgen, X. M., Kumar, S., Gara, S., Boufraqech, M., Agarwal, S., Hruban, R. H., Nilubol, N., Quezado, M., Finney, R., Cam, M., and Kebebew, E. Transcriptional alterations in hereditary and sporadic nonfunctioning pancreatic neuroendocrine tumors according to genotype. *Cancer 124*, 3 (2018), 636–647.

[303] Khanal, P., Kim, G., Yun, H. J., Cho, H.-G., and Choi, H. S. The prolyl isomerase Pin1 interacts with and downregulates the activity of AMPK leading to induction of tumorigenicity of hepatocarcinoma cells. *Molecular Carcinogenesis 52* (2013), 813–823.

[304] Khanin, R., and Wit, E. How scale-free are biological networks. *Journal of Computational Biology 13*, 3 (2006), 810–818.

[305] Khanna, A., Okkeri, J., Bilgen, T., Tiirikka, T., Vihinen, M., Visakorpi, T., and Westermarck, J. ETS1 mediates MEK1/2-dpendent overexpression of cancerous inhibitor of protein phosphatase 2A (CIP2A) in human cancer cells.

PLOS ONE 6, 3 (2011), e17979.

[306] KHATRI, S., YEPISKOPOSYAN, H., GALLO, C. A., TANDON, P., AND PLAS, D. R. FOXO3a regulates glycolysis via transcriptional control of tumor suppressor TSC1. *Journal of Biological Chemistry 285*, 21 (2010), 15960–15965.

[307] KHOO, S., GRIFFEN, S. C., XIA, Y., BAER, R. J., GERMAN, M. S., AND COBB, M. H. Regulation of insulin gene transcription by erk1 and erk2 in pancreatic β cells. *Journal of Biological Chemistry 278*, 35 (2003), 32969–32977.

[308] KIDOYA, H., MURAMATSU, F., SHIMAMURA, T., JIA, W., SATOH, T., HAYASHI, Y., NAITO, H., KUNISAKI, Y., ARAI, F., SEKI, M., SUZUKI, Y., OSAWA, T., AKIRA, S., AND TAKAKURA, N. Regnase-1-mediated post-transcriptional regulation is essential for hematopoietic stem and progenitor cell homeostasis. *Nature Communications 10*, 1 (2019), 1–16.

[309] KIEL, M. J., YILMAZ, O. H., IWASHITA, T., YILMAZ, O. H., TERHORST, C., AND MORRISON, S. J. SLAM family receptors distinguish hematopoietic stem and progenitor cells and reveal endothelial niches for stem cells. *Cell 121*, 7 (2005), 1109–1121.

[310] KIM, J., HWANGBO, J., AND WONG, P. K. Y. p38 MAPK-Mediated Bmi-1 down-regulation and defective proliferation in ATM-deficient neural stem cells can be restored by Akt activation. *PLOS ONE 6*, 1 (2011), e16615.

[311] KIM, S. W., KIM, H. J., CHUN, Y. J., AND KIM, M. Y. Ceramide produces apoptosis through induction of p27kip1 by protein phosphatase 2a-dependent akt dephosphorylation in pc-3 prostate cancer cells. *Journal of Toxicology and Environmental Health, Part A 73*, 21-22 (2010), 1465–1476.

[312] KIM, T. H., XIONG, H., ZHANG, Z., AND REN, B. β-catenin activates the growth factor endothelin-1 in colon cancer cells. *Oncogene 24*, 4 (2005), 597–604.

[313] KIM, Y.-C., KIM, S. Y., MELLADO-GIL, J. M., YADAV, H., NEIDERMYER, W., KAMARAJU, A. K., AND RANE, S. G. Rb regulates pancreas development by stabilizing pdx1. *The EMBO Journal 30*, 8 (2011), 1563–1576.

[314] KITANO, H. Computational systems biology. *Nature 420*, 6912 (2002), 206–210.

[315] KITANO, H. Systems biology: A brief overview. *Science 295*, 5560 (2002), 1662–1664.

[316] KLAMT, S., SAEZ-RODRIGUEZ, J., AND GILLES, E. D. Structural and functional analysis of cellular networks with CellNetAnalyzer. *BMC Systems Biology 1*, 1 (2007), 2.

[317] KLAMT, S., SAEZ-RODRIGUEZ, J., LINDQUIST, J. A., SIMEONI, L., AND GILLES, E. D. A methodology for the structural and functional analysis of signaling and regulatory networks. *BMC Bioinformatics 7*, 1 (2006), 56.

[318] KLAMT, S., SAEZ-RODRIGUEZ, J., LINDQUIST, J. A., SIMEONI, L., AND GILLES, E. D. A methodology for the structural and functional analysis of signaling and regulatory networks. *BMC Bioinformatics 7*, 56 (2006).

[319] Klaus, A., and Birchmeier, W. Wnt signalling and its impact on development and cancer. *Nature Reviews Cancer 8*, 5 (2008), 387–398.

[320] Klein, D. J., and Randić, M. Resistance distance. *Journal of Mathematical Chemistry 12*, 1 (1993), 81–95.

[321] Klemm, K., and Bornholdt, S. Stable and unstable attractors in boolean networks. *Physical Review E 72*, 5 (2005), 055101.

[322] Knight, J. R., Alexandrou, C., Skalka, G. L., Vlahov, N., Pennel, K., Officer, L., Teodosio, A., Kanellos, G., Gay, D. M., May-Wilson, S., Smith, E. M., Najumudeen, A. K., Gilroy, K., Ridgway, R. A., Flanagan, D. J., Smith, R. C. L., McDonald, L., MacKay, C., Cheastly, A., McArthur, K., Stanway, E., Leach, J. D., Jackstadt, R., Waldron, J. A., Campbell, A. D., Vlachogiannis, G., Valeri, N., Haigis, K. M., Sonenberg, N., Proud, C. G., Jones, N. P., Sweabrick, M. E., McKinnon, H. J., Faller, W. J., Le Quesne, J., Edwards, J., Willis, A. E., Bushell, M., and Sansom, O. J. MNK inhibition sensitizes KRAS-mutant colorectal cancer to mTORC1 inhibition by reducing eIF4E phosphorylation and c-MYC expression. *Cancer Discovery 11*, 5 (2021), 1228–1247.

[323] Kobayashi, H., Morikawa, T., Okinaga, A., Hamano, F., Hashidate-Yoshida, T., Watanuki, S., Hishikawa, D., Shindou, H., Arai, F., Kabe, Y., Suematsu, M., Shimizu, T., and Takubo, K. Environmental optimization enables maintenance of quiescent hematopoietic stem cells ex vivo. *Cell Reports 28*, 1 (2019), 145–158.e9.

[324] Kobayashi, H., and Takubo, K. Protocol for the maintenance of quiescent murine hematopoietic stem cells. *STAR Protocols 1*, 2 (2020), 100078.

[325] Kollek, M., Müller, A., Egle, A., and Erlacher, M. Bcl-2 proteins in development, health, and disease of the hematopoietic system. *The FEBS Journal 283*, 15 (2016), 2779–2810.

[326] Kolupaeva, V., and Janssens, V. PP1 and PP2A phosphatases – cooperating partners in modulating retinoblastoma protein activation. *The FEBS Journal 280*, 2 (2013), 627–643.

[327] Kong, M., Fox, C. J., Mu, J., Solt, L., Xu, A., Cinalli, R. M., Birnbaum, M. J., Lindsten, T., and Thompson, C. B. The PP2A-associated protein $\alpha 4$ is an essential inhibitor of apoptosis. *Science 306*, 5696 (2004), 695–698.

[328] Koo, M. Y., Park, J., Lim, J. M., Joo, S. Y., Shin, S.-P., Shim, H. B., Chung, J., Kang, D., Woo, H. A., and Rhee, S. G. Selective inhibition of the function of tyrosine-phosphorylated stat3 with a phosphorylation site-specific intrabody. *Proceedings of the National Academy of Sciences 111*, 17 (2014), 6269–6274.

[329] Kopp, H.-G., Avecilla, S. T., Hooper, A. T., and Rafii, S. The bone marrow vascular niche: home of HSC differentiation and mobilization. *Physiology (Bethesda, Md.) 20*, 5 (2005), 349–356.

[330] Kosan, C., and Godman, M. Genetic and epigenetic mechanisms that maintain hematopoietic stem cell function. *Stem Cells International 2016*, 5178965 (2016).

[331] Kotliarova, S., Pastorino, S., Kovell, L. C., Kotliarov, Y., Song, H., Zhang, W., Bailey, R., Maric, D., Zenklusen, J. C., Lee, J., and Fine, H. A. Glycogen synthase kinase-3 inhibition induces glioma cell death through c-MYC, nuclear factor-κb, and glucose regulation. *Cancer Research 68*, 16 (2008), 6643–6651.

[332] Kovacic, S., Soltys, C.-L. M., Barr, A. J., Shiojima, I., Walsh, K., and Dyck, J. R. Akt activity negatively regulates phosphorylation of AMP-activated protein kinase in the heart. *Journal of Biological Chemistry 278*, 41 (2003), 39422–39427.

[333] Krinner, A., and Roeder, I. Quantification and modeling of stem cell–niche interaction. *A Systems Biology Approach to Blood* (2014), 11–36.

[334] Krumsiek, J., Marr, C., Schroeder, T., and Theis, F. J. Hierarchical differentiation of myeloid progenitors is encoded in the transcription factor network. *PLOS ONE 6*, 8 (2011), e22649.

[335] Kubbutat, M. H., Jones, S. N., and Vousden, K. H. Regulation of p53 stability by Mdm2. *Nature 387*, 6630 (1997), 299–303.

[336] Kumar, S., and Geiger, H. HSC niche biology and HSC expansion ex vivo. *Trends in Molecular Medicine 23*, 9 (2017), 799–819.

[337] Kuroda, S., Fukata, M., Nakagawa, M., Fujii, K., Nakamura, T., Ookubo, T., Izawa, I., Nagase, T., Nomura, N., Tani, H., Shoji, I., Matsuura, Y., Yonehara, S., and Kaibuchi, K. Role of IQGAP1, a target of the small GTPases Cdc42 and Rac1, in regulation of E-cadherin-mediated cell-cell adhesion. *Science 281*, 5378 (1998), 832–835.

[338] Kurosawa, S., and Iwama, A. Aging and leukemic evolution of hematopoietic stem cells under various stress conditions. *Inflammation and Regeneration 40*, 1 (2020), 1–10.

[339] Lacava, G., Laus, F., Amaroli, A., Marchegiani, A., Censi, R., Di Martino, P., Yanagawa, T., Sabbieti, M. G., and Agas, D. P62 deficiency shifts mesenchymal/stromal stem cell commitment toward adipogenesis and disrupts bone marrow homeostasis in aged mice. *Journal of Cellular Physiology 234*, 9 (2019), 16338–16347.

[340] Lacorazza, H. D., Yamada, T., Liu, Y., Miyata, Y., Sivina, M., Nunes, J., and Nimer, S. D. The transcription factor MEF/ELF4 regulates the quiescence of primitive hematopoietic cells. *Cancer Cell 9*, 3 (2006), 175–187.

[341] Lähdesmäki, H., Shmulevich, I., and Yli-Harja, O. On learning gene regulatory networks under the boolean network model. *Machine Learning 52*, 1 (2003), 147–167.

[342] Lamberti, G., Brighi, N., Maggio, I., Manuzzi, L., Peterle, C., Ambrosini, V., Ricci, C., Casadei, R., and Campana, D. The role of mtor in neuroendocrine tumors: future cornerstone of a winning strategy? *International Journal of Molecular Sciences 19*, 3 (2018), 747.

[343] Lane, H. A., Wood, J. M., McSheehy, P. M., Allegrini, P. R., Boulay, A., Brueggen, J., Littlewood-Evans, A., Maira, S.-M., Martiny-Baron, G., Schnell, C. R., Sini, P., and O´Reily, T. mTOR inhibitor RAD001 (everolimus) has antiangiogenic/vascular properties distinct from a VEGFR tyrosine kinase inhibitor. *Clinical Cancer Research 15*, 5 (2009), 1612–1622.

[344] Lannutti, B. J., and Drachman, J. G. Lyn tyrosine kinase regulates thrombopoietin-induced proliferation of hematopoietic cell lines and primary megakaryocytic progenitors. *Blood 103*, 10 (2004), 3736–3743.

[345] Lansbergen, G., Grigoriev, I., Mimori-Kiyosue, Y., Ohtsuka, T., Higa, S., Kitajima, I., Demmers, J., Galjart, N., Houtsmuller, A. B., Grosveld, F., and Akhmanova, A. CLASPs attach microtubule plus ends to the cell cortex through a complex with LL5β. *Developmental Cell 11*, 1 (2006), 21–32.

[346] Laplante, M., and Sabatini, D. M. Regulation of mTORC1 and its impact on gene expression at a glance. *Journal of Cell Science 126* (2013), 1713–1719.

[347] Larson, A., Hedgire, S., Deshpande, V., Stemmer-Rachamimov, A., Harisinghani, M., Ferrone, C., Shah, U., and Thiele, E. Pancreatic neuroendocrine tumors in patients with tuberous sclerosis complex. *Clinical Genetics 82*, 6 (2012), 558–563.

[348] Lavrova, A. I., Postnikov, E. B., Zyubin, A. Y., and Babak, S. V. Ordinary differential equations and boolean networks in application to modelling of 6-mercaptopurine metabolism. *Royal Society Open Science 4*, 4 (2017), 160872.

[349] Lee, D., Kim, D. W., and Cho, J.-Y. Role of growth factors in hematopoietic stem cell niche. *Cell Biology and Toxicology 87*, 6 (2020), 2162.

[350] Lee, L., Ito, T., and Jensen, R. T. Everolimus in the treatment of neuroendocrine tumors: Efficacy, side-effects, resistance, and factors affecting its place in the treatment sequence. *Expert Opinion on Pharmacotherapy 19*, 8 (2018), 909–928.

[351] Lee, L., Ito, T., and Jensen, R. T. Imaging of pancreatic neuroendocrine tumors: recent advances, current status, and controversies. *Expert Review of Anticancer Therapy 18*, 9 (2018), 837–860.

[352] Lee, M.-Y., Moreno, C. S., and Saavedra, H. I. E2F activators signal and maintain centrosome amplification in breast cancer cells. *Molecular and Cellular Biology 34*, 14 (2014), 2581–2599.

[353] Leonard, D., Huang, W., Izadmehr, S., O'Connor, C. M., Wiredja, D. D., Wang, Z., Zaware, N., Chen, Y., Schlatzer, D. M., Kiselar, J., Vasireddi, N., Schüchner, S., Perl, A. L., Galsky, M. D., Xu, W., Brautigan, D. L.,

Ogris, E., Taylor, D. J., and Narla, G. Selective PP2A enhancement through biased heterotrimer stabilization. *Cell 181*, 3 (2020), 688–701.

[354] Lessard, J., and Sauvageau, G. Bmi-1 determines the proliferative capacity of normal and leukaemic stem cells. *Nature 423*, 6937 (2003), 255–260.

[355] Li, J. Quiescence regulators for hematopoietic stem cell. *Experimental Hematology 39*, 5 (2011), 511–520.

[356] Li, J., Gu, L., Zhang, H., Liu, T., Tian, D., Zhou, M., and Zhou, S. Berberine represses daxx gene transcription and induces cancer cell apoptosis. *Laboratory Investigation 93*, 3 (2013), 354–364.

[357] Li, K., Guo, Y., Yang, X., Zhang, Z., Zhang, C., and Xu, Y. ELF5-mediated ar activation regulates prostate cancer progression. *Scientific Reports 7* (2017), 42759.

[358] Li, L., and Bhatia, R. Stem cell quiescence. *Clinical Cancer Research 17*, 15 (2011), 4936–4941.

[359] Li, L.-Z., Zhang, C. Z., Liu, L.-L., Yi, C., Lu, S.-X., Zhou, X., Zhang, Z.-J., Peng, Y.-H., Yang, Y.-Z., and Yun, J.-P. miR-720 inhibits tumor invasion and migration in breast cancer by targeting TWIST1. *Carcinogenesis 35*, 2 (2014), 469–478.

[360] Li, X., Deng, W., Lobo-Ruppert, S., and Ruppert, J. Gli1 acts through Snail and E-cadherin to promote nuclear signaling by β-catenin. *Oncogene 26*, 31 (2007), 4489–4498.

[361] Li, X., Deng, W., Nail, C. D., Bailey, S. K., Kraus, M. H., Ruppert, J. M., and Lobo-Ruppert, S. M. Snail induction is an early response to Gli1 that determines the efficiency of epithelial transformation. *Oncogene 25*, 4 (2006), 609–621.

[362] Li, X., Zeng, X., Xu, Y., Wang, B., Zhao, Y., Lai, X., Qian, P., and Huang, H. Mechanisms and rejuvenation strategies for aged hematopoietic stem cells. *Journal of Hematology & Oncology 13*, 1 (2020), 1–16.

[363] Li, Z., Fu, X., Wu, W., Liu, Z., Chen, Z., Zhou, C., Liu, Y., Kuang, M., Sun, F., Xiao, F., Huang, Y., Zhang, X., Fan, S., Huang, X., Zheng, G., Chen, J., and Hou, Y. Zfp521 is essential for the quiescence and maintenance of adult hematopoietic stem cells under stress. *iScience 24*, 2 (2021), 102039.

[364] Liang, Y., Van Zant, G., and Szilvassy, S. J. Effects of aging on the homing and engraftment of murine hematopoietic stem and progenitor cells. *Blood 106*, 4 (2005), 1479–1487.

[365] Likić, V. A., McConville, M. J., Lithgow, T., and Bacic, A. Systems biology: The next frontier for bioinformatics. *Advances in Bioinformatics 2010*, 268925 (2010).

[366] Lilly, A. J., Johnson, W. E., and Bunce, C. M. The haematopoietic stem cell niche: new insights into the mechanisms regulating haematopoietic stem cell

behaviour. *Stem Cells International 2011*, 6 (2011), 274564–10.

[367] Lim, J.-H., Lee, Y.-M., Lee, G., Choi, Y.-J., Lim, B.-O., Kim, Y. J., Choi, D.-K., and Park, J.-W. PRMT5 is essential for the eIF4E-mediated 5-cap dependent translation. *Biochemical and Biophysical Research Communications 452*, 4 (2014), 1016–1021.

[368] Lim, Y., Park, H., Jeon, J., Han, I., Kim, J., Jho, E.-H., and Oh, E.-S. Focal adhesion kinase is negatively regulated by phosphorylation at tyrosine 407. *Journal of Biological Chemistry 282*, 14 (2007), 10398–10404.

[369] Lin, C.-W., Wang, L.-K., Wang, S.-P., Chang, Y.-L., Wu, Y.-Y., Chen, H.-Y., Hsiao, T.-H., Lai, W.-Y., Lu, H.-H., Chang, Y.-H., Yang, S.-C., Lin, M.-W., Hong, T.-M., and Yang, P.-C. Daxx inhibits hypoxia-induced lung cancer cell metastasis by suppressing the HIF-1α/HDAC/Slug axis. *Nature Communications 7*, 1 (2016), 1–16.

[370] Liu, B., Chen, Y., and Clair, D. K. S. ROS and p53: a versatile partnership. *Free Radical Biology and Medicine 44*, 8 (2008), 1529–1535.

[371] Liu, C.-Y., Huang, T.-T., Huang, C.-T., Hu, M.-H., Wang, D.-S., Wang, W.-L., Tsai, W.-C., Lee, C.-H., Lau, K.-Y., Yang, H.-P., Chen, M.-H., Shiau, C.-W., Tseng, L.-M., and Chen, K.-F. EGFR-independent Elk1/CIP2A signalling mediates apoptotic effect of an erlotinib derivative TD52 in triple-negative breast cancer cells. *European journal of cancer (Oxford, England : 1990) 72* (2017), 112–123.

[372] Liu, J., Cao, L., Chen, J., Song, S., Lee, I. H., Quijano, C., Liu, H., Keyvanfar, K., Chen, H., Cao, L.-Y., Ahn, B.-H., Kumar, N. G., Rovira, I. I., Xu, X.-L., van Lohuizen, M., Motoyama, N., Deng, C.-X., and Finkel, T. Bmi1 regulates mitochondrial function and the DNA damage response pathway. *Nature 459*, 7245 (2009), 387–392.

[373] Liu, L., Luo, Y., Chen, L., Shen, T., Xu, B., Chen, W., Zhou, H., Han, X., and Huang, S. Rapamycin inhibits cytoskeleton reorganization and cell motility by suppressing rhoa expression and activity. *Journal of Biological Chemistry 285*, 49 (2010), 38362–38373.

[374] Liu, S., Chang, Y., Ma, J., Li, X., Li, X., Fan, J., Huang, R., Duan, G., and Sun, X. Prognostic impact of p16 and p21 on gastroenteropancreatic neuroendocrine tumors. *Oncology Letters 6*, 6 (2013), 1641–1645.

[375] Liu, X., Huang, J., Chen, T., Wang, Y., Xin, S., Li, J., Pei, G., and Kang, J. Yamanaka factors critically regulate the developmental signaling network in mouse embryonic stem cells. *Cell research 18*, 12 (2008), 1177–1189.

[376] Liu, Y., Elf, S. E., Miyata, Y., Sashida, G., Liu, Y., Huang, G., Di Giandomenico, S., Lee, J. M., Deblasio, A., Menendez, S., Antipin, J., Reva, B., Koff, A., and Nimer, S. D. p53 regulates hematopoietic stem cell quiescence. *Cell Stem Cell 4*, 1 (2009), 37–48.

[377] López, L., Cruz, C., Godoy, G., M Robledo, S., and D Vélez, I. Thermoterapy effective and safer than miltefosine in the treatment of cutaneous leishmaniasis in colombia. *Revista do Instituto de Medicina Tropical de São Paulo 55* (2013), 197–204.

[378] López-Otín, C., Blasco, M. A., Partridge, L., Serrano, M., and Kroemer, G. The hallmarks of aging. *Cell 153*, 6 (2013), 1194–1217.

[379] Lorz, C., Oteo, M., and Santos, M. Neuroendocrine lung cancer mouse models: An overview. *Cancers 13*, 1 (2020), 14.

[380] Lowe, S. W., and Sherr, C. J. Tumor suppression by Ink4a-Arf: progress and puzzles. *Current Opinion in Genetics & Development 13*, 1 (2003), 77–83.

[381] Lu, X., Jain, V. V., Finn, P. W., and Perkins, D. L. Hubs in biological interaction networks exhibit low changes in expression in experimental asthma. *Molecular Systems Biology 3*, 1 (2007).

[382] Ludin, A., Gur-Cohen, S., Golan, K., Kaufmann, K. B., Itkin, T., Medaglia, C., Lu, X.-J., Ledergor, G., Kollet, O., and Lapidot, T. Reactive oxygen species regulate hematopoietic stem cell self-renewal, migration and development, as well as their bone marrow microenvironment. *Antioxidants & Redox Signaling 21*, 11 (2014), 1605–1619.

[383] Ludlow, J. W., Glendening, C. L., Livingston, D. M., and DeCarprio, J. A. Specific enzymatic dephosphorylation of the retinoblastoma protein. *Molecular and Cellular Biology 13*, 1 (1993), 367–372.

[384] Luley, K. B., Biedermann, S. B., Künstner, A., Busch, H., Franzenburg, S., Schrader, J., Grabowski, P., Wellner, U. F., Keck, T., Brabant, G., Schmid, S. M., Lehnert, H., and Ungefroren, H. A comprehensive molecular characterization of the pancreatic neuroendocrine tumor cell lines BON-1 and QGP-1. *Cancers 12*, 3 (2020), 691.

[385] Maccario, H., Perera, N. M., Davidson, L., Downes, C. P., and Leslie, N. R. PTEN is destabilized by phosphorylation on thr^{366}. *Biochemical Journal 405* (2007), 439–444.

[386] MacDonald, B. T., Tamai, K., and He, X. Wnt/β-catenin signaling: components, mechanisms, and diseases. *Developmental Cell 17*, 1 (2009), 9–26.

[387] MacLean, D., and Studholme, D. J. A Boolean model of the *Pseudomonas syringae* hrp regulon predicts a tightly regulated system. *PLOS ONE 5*, 2 (2010), e9101.

[388] Macleod, K. F. The role of the RB tumour suppressor pathway in oxidative stress responses in the haematopoietic system. *Nature Reviews Cancer 8*, 10 (2008), 769–781.

[389] Maharjan, C. K., Ear, P. H., Tran, C. G., Howe, J. R., Chandrasekharan, C., and Quelle, D. E. Pancreatic neuroendocrine tumors: Molecular mechanisms and therapeutic targets. *Cancers 13*, 20 (2021), 5117.

[390] Mai, Z., and Liu, H. Boolean network-based analysis of the apoptosis network: Irreversible apoptosis and stable surviving. *Journal of Theoretical Biology 259*, 4 (2009), 760–769.

[391] Maillard, I., Koch, U., Dumortier, A., Shestova, O., Xu, L., Sai, H., Pross, S. E., Aster, J. C., Bhandoola, A., Radtke, F., and Pear, W. S. Canonical notch signaling is dispensable for the maintenance of adult hematopoietic stem cells. *Cell Stem Cell 2*, 4 (2008), 356–366.

[392] Mancini, S. J. C., Mantei, N., Dumortier, A., Suter, U., MacDonald, H. R., and Radtke, F. Jagged1-dependent Notch signaling is dispensable for hematopoietic stem cell self-renewal and differentiation. *Blood 105*, 6 (2005), 2340–2342.

[393] Mann, B., Gelos, M., Siedow, A., Hanski, M., Gratchev, A., Ilyas, M., Bodmer, W., Moyer, M., Riecken, E., Buhr, H., and Hanski, C. Target genes of β-catenin–T cell-factor/lymphoid-enhancer-factor signaling in human colorectal carcinomas. *Proceedings of the National Academy of Sciences 96*, 4 (1999), 1603–1608.

[394] Mann, M., Mehta, A., de Boer, C. G., Kowalczyk, M. S., Lee, K., Haldeman, P., Rogel, N., Knecht, A. R., Farouq, D., Regev, A., and Baltimore, D. Heterogeneous responses of hematopoietic stem cells to inflammatory stimuli are altered with age. *Cell Reports 25*, 11 (2018), 2992–3005.

[395] Marini, F., Giusti, F., Tonelli, F., and Brandi, M. L. Pancreatic neuroendocrine neoplasms in multiple endocrine neoplasia type 1. *International Journal of Molecular Sciences 22*, 8 (2021), 4041.

[396] Marinoni, I. Prognostic value of daxx/atrx loss of expression and alt activation in pannets: is it time for clinical implementation? *Gut 71*, 5 (2022), 847–848.

[397] Marinoni, I., Kurrer, A. S., Vassella, E., Dettmer, M., Rudolph, T., Banz, V., Hunger, F., Pasquinelli, S., Speel, E.-J., and Perren, A. Loss of daxx and atrx are associated with chromosome instability and reduced survival of patients with pancreatic neuroendocrine tumors. *Gastroenterology 146*, 2 (2014), 453–460.

[398] Marques-Pita, M., and Rocha, L. M. Canalization and control in automata networks: body segmentation in *Drosophila melanogaster*. *PLOS ONE 8*, 3 (2013), e55946.

[399] Martelli, A. M., Evangelisti, C., Chiarini, F., Grimaldi, C., Cappellini, A., Ognibene, A., and McCubrey, J. A. The emerging role of the phosphatidylinositol 3-kinase/Akt/mammalian target of rapamycin signaling network in normal myelopoiesis and leukemogenesis. *Biochimica et Biophysica Acta 1803*, 9 (2010), 991–1002.

[400] Martin, L. R., Williams, S. L., Haskard, K. B., and DiMatteo, M. R. The

challenge of patient adherence. *Therapeutics and Clinical Risk Management 1*, 3 (2005), 189.

[401] Martinez, S. C., Cras-Méneur, C., Bernal-Mizrachi, E., and Permutt, M. A. Glucose regulates foxo1 through insulin receptor signaling in the pancreatic islet β-cell. *Diabetes 55*, 6 (2006), 1581–1591.

[402] Martinez-Sanchez, M. E., Mendoza, L., Villarreal, C., and Alvarez-Buylla, E. R. A minimal regulatory network of extrinsic andintrinsic factors recovers observed patterns of CD4+ T cell differentiation and plasticity. *PLOS Computational Biology 11*, 6 (2015), e1004324.

[403] Marty-Santos, L., and Cleaver, O. Pdx1 regulates pancreas tubulogenesis and e-cadherin expression. *Development 143*, 1 (2016), 101–112.

[404] Maryanovich, M., Oberkovitz, G., Niv, H., Vorobiyov, L., Zaltsman, Y., Brenner, O., Lapidot, T., Jung, S., and Gross, A. The ATM-BID pathway regulates quiescence and survival of haematopoietic stem cells. *Nature Bell Biology 14*, 5 (2012), 535–541.

[405] Massagué, J. G1 cell-cycle control and cancer. *Nature 432*, 7015 (2004), 298–306.

[406] Masui, K., Tanaka, K., Akhavan, D., Babic, I., Gini, B., Matsutani, T., Iwanami, A., Liu, F., Villa, G. R., Gu, Y., Campos, C., Zhu, S., Yang, H., Yong, W. H., Cloughesy, T. F., Mellinghof, I. K., Cavenee, W. K., Shaw, R. J., and Mischel, P. S. mtor complex 2 controls glycolytic metabolism in glioblastoma through FoxO acetylation and upregulation of c-myc. *Cell Metabolism 18*, 5 (2013), 726–739.

[407] Matache, M. T., and Matache, V. Logical reduction of biological networks to their most determinative components. *Bulletin of Mathematical Biology 78*, 7 (2016), 1520–1545.

[408] Matkar, S., Thiel, A., and Hua, X. Menin: a scaffold protein that controls gene expression and cell signaling. *Trends in Biochemical Sciences 38*, 8 (2013), 394–402.

[409] Matsuda, T., Muromoto, R., Sekine, Y., Togi, S., Kitai, Y., Kon, S., and Oritani, K. Signal transducer and activator of transcription 3 regulation by novel binding partners. *World Journal of Biological Chemistry 6*, 4 (2015), 324.

[410] Matsumoto, A., Takeishi, S., Kanie, T., Susaki, E., Onoyama, I., Tateishi, Y., Nakayama, K., and Nakayama, K. I. p57 is required for quiescence and maintenance of adult hematopoietic stem cells. *Cell Stem Cell 9*, 3 (2011), 262–271.

[411] Matsumoto, R., Dainichi, T., Tsuchiya, S., Nomura, T., Kitoh, A., Hayden, M. S., Ishii, K. J., Tanaka, M., Honda, T., Egawa, G., Otsuka, A., Nakajima, S., Sakurai, K., Nakano, Y., Kobayashi, T., Sugimoto, Y., and Kabashima, K. Epithelial TRAF6 drives IL-17–mediated psoriatic inflammation. *JCI In-*

sight 3, 15 (2018).

[412] Maucher, M., Kracher, B., Kühl, M., and Kestler, H. A. Inferring Boolean network structure via correlation. *Bioinformatics 27*, 11 (2011), 1529–1536.

[413] Maurer, U., Preiss, F., Brauns-Schubert, P., Schlicher, L., and Charvet, C. GSK-3 - at the crossroads of cell death and survival. *Journal of Cell Science 127*, Pt 7 (2014), 1369–1378.

[414] Mavroudi, I., and Papadaki, H. A. The role of cd40/cd40 ligand interactions in bone marrow granulopoiesis. *The Scientific World Journal 11* (2011), 2011–2019.

[415] Maxwell, J. E., Sherman, S. K., and Howe, J. R. Translational diagnostics and therapeutics in pancreatic neuroendocrine tumors. *Clinical Cancer Research 22*, 20 (2016), 5022–5029.

[416] Maya, R., Balass, M., Kim, S.-T., Shkedy, D., Leal, J.-F. M., Shifman, O., Moas, M., Buschmann, T., Ronai, Z., Shiloh, Y., and others. ATM-dependent phosphorylation of Mdm2 on serine 395: role in p53 activation by DNA damage. *Genes & Development 15*, 9 (2001), 1067–1077.

[417] McCubrey, J. A., Steelman, L. S., Bertrand, F. E., Davis, N. M., Abrams, S. L., Montalto, G., D'Assoro, A. B., Libra, M., Nicoletti, F., Maestro, R., Basecke, J., Cocco, L., Cervello, M., and Martelli, A. M. Multifaceted roles of GSK-3 and Wnt/β-catenin in hematopoiesis and leukemogenesis: opportunities for therapeutic intervention. *Leukemia 28*, 1 (2014), 15–33.

[418] McCubrey, J. A., Steeman, L., Chappell, W., Abrams, S., Montalto, G., Cervello, M., Nicoletti, F., Fagone, P., Malaponte, G., Mazzarino, M., Candido, S., Libra, M., Basecke, J., Mijatovic, S., Maksimovic-Ivanic, D., Milella, M., Tafuri, A., Cocco, L., Evangelisti, C., Chiarini, F., and Martelli, A. Mutations and deregulation of RAS/RAF/MEK/ERK and PI3K/PTEN/AKT/mTOR cascades which alter therapy resonse. *Oncotraget 3*, 9 (2012), 954–987.

[419] Meek, D. W. Tumour suppression by p53: a role for the DNA damage response? *Nature Reviews Cancer 9*, 10 (2009), 714–723.

[420] Mejia-Ramirez, E., and Florian, M. C. Understanding intrinsic hematopoietic stem cell aging. *Haematologica 105*, 1 (2020), 22.

[421] Mellett, M., Meier, B., Mohanan, D., Schairer, R., Cheng, P., Satoh, T. K., Kiefer, B., Ospelt, C., Nobbe, S., Thome, M., Contassot, E., and French, L. E. CARD14 gain-of-function mutation alone is sufficient to drive IL-23/IL-17–mediated psoriasiform skin inflammation in vivo. *Journal of Investigative Dermatology 138*, 9 (2018), 2010–2023.

[422] Méndez, A., and Mendoza, L. A network model to describe the terminal differentiation of B cells. *PLOS Computational Biology 12*, 1 (2016), e1004696.

[423] Méndez-López, L. F., Davila-Velderrain, J., Domínguez-Hüttinger, E.,

Enríquez-Olguín, C., Martínez-García, J. C., and Alvarez-Buylla, E. R. Gene regulatory network underlying the immortalization of epithelial cells. *BMC Systems Biology 11*, 1 (2017), 24.

[424] Mendoza, L., and Xenarios, I. A method for the generation of standardized qualitative dynamical systems of regulatory networks. *Theoretical Biology and Medical Modelling 3*, 13 (2006).

[425] Mendoza, M. C., Er, E. E., and Blenis, J. The Ras-ERK and PI3K-mTOR pathways: cross-talk and compensation. *Trends in Biochemical Sciences 36*, 6 (2011), 320–328.

[426] Meric-Bernstam, F., and Gonzalez-Angulo, A. M. Targeting the mTOR signaling network for cancer therapy. *Journal of Clinical Oncology 27*, 13 (2009), 2278–2287.

[427] Meulmeester, E., Pereg, Y., Shiloh, Y., and Jochemsen, A. G. Atm-mediated phosphorylations inhibit mdmx/mdm2 stabilization by hausp in favor of p53 activation. *Cell Cycle 4*, 9 (2005), 1166–1170.

[428] Meyer, P., Maity, P., Burkovski, A., Schwab, J., Müssel, C., Singh, K., Ferreira, F. F., Krug, L., Maier, H. J., Wlaschek, M., Wirth, T., Kestler, H. A., and Scharffetter-Kochanek, K. A model of the onset of the senescence associated secretory phenotype after DNA damage induced senescence. *PLOS Computational Biology 13*, 12 (2017), e1005741.

[429] Mikheeva, S. A., Mikheev, A. M., Petit, A., Beyer, R., Oxford, R. G., Khorasani, L., Maxwell, J.-P., Glackin, C. A., Wakimoto, H., González-Herrero, I., Sánchez-García, I., Silber, J. R., Horner, P. J., and Rostomily, R. C. TWIST1 promotes invasion through mesenchymal change in human glioblastoma. *Molecular Cancer 9*, 1 (2010), 194.

[430] Milne, T. A., Hughes, C. M., Lloyd, R., Yang, Z., Rozenblatt-Rosen, O., Dou, Y., Schnepp, R. W., Krankel, C., LiVolsi, V. A., Gibbs, D., Hua, X., Roeder, R. G., Meyerson, M., and Hess, J. L. Menin and mll cooperatively regulate expression of cyclin-dependent kinase inhibitors. *Proceedings of the National Academy of Sciences 102*, 3 (2005), 749–754.

[431] Milo, R., Shen-Orr, S., Itzkovitz, S., Kashtan, N., Chklovskii, D., and Alon, U. Network motifs: simple building blocks of complex networks. *Science 298*, 5594 (2002), 824–827.

[432] Missiaglia, E., Dalai, I., Barbi, S., Beghelli, S., Falconi, M., Della Peruta, M., Piemonti, L., Capurso, G., Di Florio, A., Delle Fave, G., Pederzoli, P., Croce, C. M., and Scarpa, A. Pancreatic endocrine tumors: expression profiling evidences a role for AKT-mTOR pathway. *Journal of Clinical Oncology 28*, 2 (2010), 245.

[433] Miyamoto, K., Araki, K. Y., Naka, K., Arai, F., Takubo, K., Yamazaki, S., Matsuoka, S., Miyamoto, T., Ito, K., Ohmura, M., Chen, C., Hosokawa, K.,

Nakauchi, H., Nakayama, K., Nakayama, K. I., Harada, M., Motoyama, N., Suda, T., and Hirao, A. Foxo3a is essential for maintenance of the hematopoietic stem cell pool. *Cell Stem Cell 1*, 1 (2007), 101–112.

[434] Model, M. C. A small-molecule e2f inhibitor blocks growth in. *Cancer Research 68* (2008), 6292–6299.

[435] Mohrin, M., Bourke, E., Alexander, D., Warr, M. R., Barry-Holson, K., Le Beau, M. M., Morrison, C. G., and Passegué, E. Hematopoietic stem cell quiescence promotes error-prone DNA repair and mutagenesis. *Cell Stem Cell 7*, 2 (2010), 174 – 185.

[436] Mojsa, B., Lassot, I., and Desagher, S. Mcl-1 ubiquitination: unique regulation of an essential survival protein. *Cells 3*, 2 (2014), 418–437.

[437] Mojsilović, S., Jauković, A., Santibañez, J. F., and Bugarski, D. Interleukin-17 and its implication in the regulation of differentiation and function of hematopoietic and mesenchymal stem cells. *Mediators ofi Inflammation 2015* (2015).

[438] Momand, J., Zambetti, G. P., Olson, D. C., George, D., and Levine, A. J. The mdm-2 oncogene product forms a complex with the p53 protein and inhibits p53-mediated transactivation. *Cell 69*, 7 (1992), 1237–1245.

[439] Montagud, A., Béal, J., Tobalina, L., Traynard, P., Subramanian, V., Szalai, B., Alföldi, R., Puskás, L., Valencia, A., Barillot, E., Saez-Rodriguez, J., and Calzone, L. Patient-specific Boolean models of signalling networks guide personalised treatments. *(eLife) 11* (2022), e72626.

[440] Montes de Oca Luna, R., Wagner, D. S., and Lozano, G. Rescue of early embryonic lethality in mdm2-deficient mice by deletion of p53. *Nature 378* (1995), 203–206.

[441] Moore, J. C., Mulligan, T. S., Yordán, N. T., Castranova, D., Pham, V. N., Tang, Q., Lobbardi, R., Anselmo, A., Liwski, R. S., Berman, J. N., Sadreyev, R. I., Weinstein, B. M., and Langenau, D. M. T cell immune deficiency in zap70 mutant zebrafish. *Molecular and Cellular Biology 36*, 23 (2016), 2868–2876.

[442] Morris, M. K., Saez-Rodriguez, J., Sorger, P. K., and Lauffenburger, D. A. Logic-based models for the analysis of cell signaling networks. *Biochemistry 49*, 15 (2010), 3216–3224.

[443] Mortensen, M., Watson, A. S., and Simon, A. K. Lack of autophagy in the hematopoietic system leads to loss of hematopoietic stem cell function and dysregulated myeloid proliferation. *Autophagy 7*, 9 (2011), 1069–1070.

[444] Mpilla, G., Aboukameel, A., Muqbil, I., Kim, S., Beydoun, R., Philip, P. A., Mohammad, R. M., Kamgar, M., Shidham, V., Senapedis, W., Baloglu, E., Li, J., Dyson, G., Xue, Y., El-Rayes, B., and Azmi, A. S. PAK4-NAMPT dual inhibition as a novel strategy for therapy resistant pancreatic neuroendocrine

tumors. *Cancers 11*, 12 (2019), 1902.

[445] Mpilla, G. B., Philip, P. A., El-Rayes, B., and Azmi, A. S. Pancreatic neuroendocrine tumors: Therapeutic challenges and research limitations. *World Journal of Gastroenterology 26*, 28 (2020), 4036.

[446] Mujtaba, T., and Dou, Q. P. Advances in the understanding of mechanisms and therapeutic use of bortezomib. *Discovery Medicine 12*, 67 (2011), 471.

[447] Muller, M. Cellular senescence: molecular mechanisms, in vivo significance, and redox considerations. *Antioxidants & Redox Signaling 11*, 1 (2009), 59–98.

[448] Muller-Sieburg, C. E., Sieburg, H. B., Bernitz, J. M., and Cattarossi, G. Stem cell heterogeneity: implications for aging and regenerative medicine. *Blood 119*, 17 (2012), 3900–3907.

[449] Münzberg, C., Höhn, K., Krndija, D., Maass, U., Bartsch, D. K., Slater, E. P., Oswald, F., Walther, P., Seufferlein, T., and von Wichert, G. IGF-1 drives chromogranin A secretion via activation of Arf1 in human neuroendocrine tumour cells. *Journal of Cellular and Molecular Medicine 19*, 5 (2015), 948–959.

[450] Muromoto, R., Nakao, K., Watanabe, T., Sato, N., Sekine, Y., Sugiyama, K., Oritani, K., Shimoda, K., and Matsuda, T. Physical and functional interactions between Daxx and STAT3. *Oncogene 25*, 14 (2006), 2131–2136.

[451] Murphy, L. O., MacKeigan, J. P., and Blenis, J. A network of immediate early gene products propagates subtle differences in mitogen-activated protein kinase signal amplitude and duration. *Molecular and Cellular Biology 24*, 1 (2004), 144–153.

[452] Murphy, M. J., Wilson, A., and Trumpp, A. More than just proliferation: Myc function in stem cells. *Trends in Cell Biology 15*, 3 (2005), 128–137.

[453] Murrugarra, D., and Dimitrova, E. S. Molecular network control through boolean canalization. *EURASIP Journal on Bioinformatics and Systems Biology 2015*, 1 (2015), 9.

[454] Müssel, C., Hopfensitz, M., and Kestler, H. A. BoolNet – an R package for generation, reconstruction and analysis of Boolean networks. *Bioinformatics 26*, 10 (2010), 1378–1380.

[455] Müssel, C., Schmid, F., Blätte, T. J., Hopfensitz, M., Lausser, L., and Kestler, H. A. BiTrinA—multiscale binarization and trinarization with quality analysis. *Bioinformatics 32*, 3 (2016), 465–468.

[456] Nakagawa, M. M., Chen, H., and Rathinam, C. V. Constitutive activation of nf-κb pathway in hematopoietic stem cells causes loss of quiescence and deregulated transcription factor networks. *Frontiers in Cell and Developmental Biology 6* (2018), 143.

[457] Nakano, H., Oshima, H., Chung, W., Williams-Abbott, L., Ware, C. F., Yagita, H., and Okumura, K. TRAF5, an activator of NF-κB and putative

signal transducer for the lymphotoxin-β receptor. *Journal of Biological Chemistry 271*, 25 (1996), 14661–14664.

[458] Nakano, H., Sakon, S., Koseki, H., Takemori, T., Tada, K., Matsumoto, M., Munechika, E., Sakai, T., Shirasawa, T., Akiba, H., Kobata, T., Santee, S. M., Ware, C. F., Rennert, P. D., Taniguchi, M., Yagita, H., and Okumura, K. Targeted disruption of Traf5 gene causes defects in CD40-and CD27-mediated lymphocyte activation. *Proceedings of the National Academy of Sciences 96*, 17 (1999), 9803–9808.

[459] National Center for Health Statistics, U. S., National Office of Vital Statistics, U. S., National Vital Statistics Division United States, U. S., and Public Health Service, U. S. *Monthly vital statistics report*, vol. 7. Federal Security Agency, Public Health Service, National Office of Vital Statistics, 1958.

[460] Newman, M. E. The mathematics of networks. *The New Palgrave Encyclopedia of Economics 2*, 2008 (2008), 1–12.

[461] Nguyen, D., Liao, W., Zeng, S. X., and Lu, H. Reviving the guardian of the genome: Small molecule activators of p53. *Pharmacology & Therapeutics 178* (2017), 92–108.

[462] Nii, T., Marumoto, T., and Tani, K. Roles of p53 in various biological aspects of hematopoietic stem cells. *Journal of Biomedicine and Biotechnology 2012*, 11 (2012), 903435–10.

[463] Ning, L., Chen, H., and Kunnimalaiyaan, M. Focal adhesion kinase, a downstream mediator of Raf-1 signaling, suppresses cellular adhesion, migration, and neuroendocrine markers in bon carcinoid cells. *Molecular Cancer Research 8*, 5 (2010), 775–782.

[464] Nishikawa, K., Nakashima, T., Takeda, S., Isogai, M., Hamada, M., Kimura, A., Kodama, T., Yamaguchi, A., Owen, M. J., Takahashi, S., and Takayanagi, H. Maf promotes osteoblast differentiation in mice by mediating the age-related switch in mesenchymal cell differentiation. *The Journal of Clinical Investigation 120*, 10 (2010), 3455–3465.

[465] Nitta, E., Yamashita, M., Hosokawa, K., Xian, M., Takubo, K., Arai, F., Nakada, S., and Suda, T. Telomerase reverse transcriptase protects atm-deficient hematopoietic stem cells from ros-induced apoptosis through a telomere-independent mechanism. *Blood 117*, 16 (2011), 4169–4180.

[466] Noritake, J., Watanabe, T., Sato, K., Wang, S., and Kaibuchi, K. IQGAP1: a key regulator of adhesion and migration. *Journal of Cell Science 118*, 10 (2005), 2085–2092.

[467] Nuñez, J. E., Donadio, M., Rocha Filho, D., Rego, J. F., Barros, M., Formiga, M. N., Lopez, R., and Riechelmann, R. The efficacy of everolimus and sunitinib in patients with sporadic or germline mutated metastatic pan-

creatic neuroendocrine tumors. *Journal of Gastrointestinal Oncology 10*, 4 (2019), 645.

[468] Ogawa, T., Kitagawa, M., and Hirokawa, K. Age-related changes of human bone marrow: a histometric estimation of proliferative cells, apoptotic cells, T cells, B cells and macrophages. *Mechanisms of Ageing and Development 117*, 1-3 (2000), 57–68.

[469] Ogihara, T., Vanderford, N. L., Maier, B., Stein, R. W., and Mirmira, R. G. Expression and function of Set7/9 in pancreatic islets. *Islets 1*, 3 (2009), 269–272.

[470] Oguro, H., and Iwama, A. Life and death in hematopoietic stem cells. *Current Opinion in Immunology 19*, 5 (2007), 503–509.

[471] Ohta, M., Tateishi, K., Kanai, F., Watabe, H., Kondo, S., Guleng, B., Tanaka, Y., Asaoka, Y., Jazag, A., Imamura, J., Ijichi, H., Ikenoue, T., Sata, M., Miyagishi, M., Taira, K., Tada, M., Kawabe, T., and Omata, M. p53-independent negative regulation of p21/cyclin-dependent kinase–interacting protein 1 by the sonic hedgehog-glioma-associated oncogene 1 pathway in gastric carcinoma cells. *Cancer Research 65*, 23 (2005), 10822–10829.

[472] Ohtani, K., Degregori, J., and Nevins, J. R. Regulation of the cyclin e gene by transcription factor e2f1. *Proceedings of the National Academy of Sciences 92*, 26 (1995), 12146–12150.

[473] Oostendorp, R. A. J. Secretion of Wnts is dispensable for hematopoiesis. *Blood 126*, 9 (2015), 1051–1052.

[474] Opferman, J. T., Iwasaki, H., Ong, C. C., Suh, H., Mizuno, S.-i., Akashi, K., and Korsmeyer, S. J. Obligate role of anti-apoptotic MCL-1 in the survival of hematopoietic stem cells. *Science 307*, 5712 (2005), 1101–1104.

[475] O'Reilly, K. E., Rojo, F., She, Q.-B., Solit, D., Mills, G. B., Smith, D., Lane, H., Hofmann, F., Hicklin, D. J., Ludwig, D. L., Baselga, J., and Rosen, N. mTOR inhibition induces upstream receptor tyrosine kinase signaling and activates Akt. *Cancer Research 66*, 3 (2006), 1500–1508.

[476] Orelio, C., and Dzierzak, E. Bcl-2 expression and apoptosis in the regulation of hematopoietic stem cells. *Leukemia & Lymphoma 48*, 1 (2007), 16–24.

[477] Orford, K. W., and Scadden, D. T. Deconstructing stem cell self-renewal: genetic insights into cell-cycle regulation. *Nature Reviews Genetics 9*, 2 (2008), 115–128.

[478] Orlando, D. A., Lin, C. Y., Bernard, A., Wang, J. Y., Socolar, J. E., Iversen, E. S., Hartemink, A. J., and Haase, S. B. Global control of cell-cycle transcription by coupled CDK and network oscillators. *Nature 453* (2008), 944–947.

[479] Orr-Asman, M. A., Chu, Z., Jiang, M., Worley, M., LaSance, K., Koch, S. E., Carreira, V. S., Dahche, H. M., Plas, D. R., Komurov, K., Qi, X., Mercer,

C. A., Anthony, L. B., Rubinstein, J., and Thomas, H. E. mTOR kinase inhibition effectively decreases progression of a subset of neuroendocrine tumors that progress on rapalog therapy and delays cardiac impairment. *Molecular Cancer Therapeutics 16*, 11 (2017), 2432–2441.

[480] Orschell, C. M., Borneo, J., Munugalavadla, V., Ma, P., Sims, E., Ramdas, B., Yoder, M. C., and Kapur, R. Deficiency of src family kinases compromises the repopulating ability of hematopoietic stem cells. *Experimental Hematology 36*, 5 (2008), 655–666.

[481] Ortiz-Gutiérrez, E., García-Cruz, K., Azpeitia, E., Castillo, A., de la Paz Sánchez, M., and Álvarez-Buylla, E. R. A dynamic gene regulatory network model that recovers the cyclic behavior of *Arabidopsis thaliana* cell cycle. *PLOS Computational Biology 11*, 9 (2015), e1004486.

[482] Palma, A., Iannuccelli, M., Rozzo, I., Licata, L., Perfetto, L., Massacci, G., Castagnoli, L., Cesareni, G., and Sacco, F. Integrating patient-specific information into logic models of complex diseases: application to acute myeloid leukemia. *Journal of Personalized Medicine 11*, 2 (2021), 117.

[483] Palmer, A. C., and Sorger, P. K. Combination cancer therapy can confer benefit via patient-to-patient variability without drug additivity or synergy. *Cell 171*, 7 (2017), 1678–1691.

[484] Pang, W. W., Price, E. A., Sahoo, D., Beerman, I., Maloney, W. J., Rossi, D. J., Schrier, S. L., and Weissman, I. L. Human bone marrow hematopoietic stem cells are increased in frequency and myeloid-biased with age. *Proceedings of the National Academy of Sciences 108*, 50 (2011), 20012–20017.

[485] Pant, V., Quintás-Cardama, A., and Lozano, G. The p53 pathway in hematopoiesis: lessons from mouse models, implications for humans. *Blood 120*, 26 (2012), 5118–5127.

[486] Paramore, A., and Frantz, S. Fresh from the pipeline. *Nature Reviews | Drug Discovery 2* (2003), 611.

[487] Park, I.-K., Qian, D., Kiel, M., Becker, M. W., Pihalja, M., Weissman, I. L., Morrison, S. J., and Clarke, M. F. Bmi-1 is required for maintenance of adult self-renewing haematopoietic stem cells. *Nature 423*, 6937 (2003), 302–305.

[488] Partridge, L. The new biology of ageing. *Philosophical Transactions of the Royal Society B: Biological Sciences 365*, 1537 (2010), 147–154.

[489] Passegué, E., Wagers, A. J., Giuriato, S., Anderson, W. C., and Weissman, I. L. Global analysis of proliferation and cell cycle gene expression in the regulation of hematopoietic stem and progenitor cell fates. *The Journal of Experimental Medicine 202*, 11 (2005), 1599–1611.

[490] Paulevé, L. Pint: a static analyzer for transient dynamics of qualitative networks with IPython interface. In *International Conference on Computational*

Methods in Systems Biology (2017), Springer, pp. 309–316.

[491] Paulevé, L., Kolčák, J., Chatain, T., and Haar, S. Reconciling qualitative, abstract, and scalable modeling of biological networks. *Nature Communications 11*, 1 (2020), 1–7.

[492] Pentzien, T., Puniya, B. L., Helikar, T., and Matache, M. T. Identification of biologically essential nodes via Determinative Power in logical models of cellular processes. *Frontiers in Physiology 9* (2018).

[493] Perry, M. E. The regulation of the p53-mediated stress response by MDM2 and MDM4. *Cold Spring Harbor Perspectives in Biology 2*, 1 (2010), a000968.

[494] Piccoli, C., Agriesti, F., Scrima, R., Falzetti, F., Di Ianni, M., and Capitanio, N. To breathe or not to breathe: the haematopoietic stem/progenitor cells dilemma. *British Journal of Pharmacology 169*, 8 (2013), 1652–1671.

[495] Pietras, E. M. Inflammation: a key regulator of hematopoietic stem cell fate in health and disease. *Blood 130*, 15 (2017), 1693–1698.

[496] Pietras, E. M., Warr, M. R., and Passegué, E. Cell cycle regulation in hematopoietic stem cells. *The Journal of Cell Biology 195*, 5 (2011), 709–720.

[497] Pietrobono, S., Gagliardi, S., and Stecca, B. Non-canonical hedgehog signaling pathway in cancer: Activation of GLI transcription factors beyond smoothened. *Frontiers in Genetics 10* (2019), 556.

[498] Ping, Z., Chen, S., Hermans, S. J., Kenswil, K. J., Feyen, J., van Dijk, C., Bindels, E. M., Mylona, A. M., Adisty, N. M., Hoogenboezem, R. M., Sanders, M. A., Cremers, E. M. P., Lindenbergh-Kortleve, D. J., Samsom, J. N., van de Loosdrecht, A. A., and Raaijmakers, M. H. G. P. Activation of NF-κB driven inflammatory programs in mesenchymal elements attenuates hematopoiesis in low-risk myelodysplastic syndromes. *Leukemia 33*, 2 (2019), 536–541.

[499] Pinho, S., and Frenette, P. S. Haematopoietic stem cell activity and interactions with the niche. *Nature Reviews Molecular Cell Biology 20*, 5 (2019), 303–320.

[500] Porta, C., Paglino, C., and Mosca, A. Targeting PI3K/Akt/mTOR signaling in cancer. *Frontiers in Oncology 4*, 64 (2014).

[501] Qian, H., Buza-Vidas, N., Hyland, C. D., Jensen, C. T., Antonchuk, J., Månsson, R., Thoren, L. A., Ekblom, M., Alexander, W. S., and Jacobsen, S. E. W. Critical role of thrombopoietin in maintaining adult quiescent hematopoietic stem cells. *Cell Stem Cell 1*, 6 (2007), 671–684.

[502] Qu, X., Aldana, M., and Kadanoff, L. P. Numerical and Theoretical Studies of Noise Effects in the Kauffman Model. *Journal of Statistical Physics 109*, 5 (2002), 967–986.

[503] R Development Core Team. *R: A Language and Environment for Statistical Computing*. R Foundation for Statistical Computing, Vienna, Austria, 2008.

ISBN 3-900051-07-0.

[504] Ramos, J. W. The regulation of extracellular signal-regulated kinase (ERK) in mammalian cells. *The international Journal of Biochemistry & Cell Biology 40*, 12 (2008), 2707–2719.

[505] Rando, T. A. Stem cells, ageing and the quest for immortality. *Nature 441*, 7097 (2006), 1080–1086.

[506] Rao, M. S., and Mattson, M. P. Stem cells and aging: expanding the possibilities. *Mechanisms of Ageing and Development 122*, 7 (2001), 713–734.

[507] Ratliff, M. L., Garton, J., James, J. A., and Webb, C. F. ARID3a expression in human hematopoietic stem cells is associated with distinct gene patterns in aged individuals. *Immunity & Ageing 17*, 1 (2020), 1–15.

[508] Ray, A., James, M. K., Larochelle, S., Fisher, R. P., and Blain, S. W. p27Kip1 inhibits cyclin D-cyclin-dependent kinase 4 by two independent modes. *Molecular and Cellular Biology 29*, 4 (2009), 986–999.

[509] Rayess, H., Wang, M. B., and Srivatsan, E. S. Cellular senescence and tumor suppressor gene p16. *International Journal of Cancer 130*, 8 (2012), 1715–1725.

[510] Redza-Dutordoir, M., and Averill-Bates, D. A. Activation of apoptosis signalling pathways by reactive oxygen species. *Biochimica et Biophysica Acta 1863*, 12 (2016), 2977–2992.

[511] Reiske, H. R., Zhao, J., Han, D. C., Cooper, L. A., and Guan, J.-L. Analysis of FAK-associated signaling pathways in the regulation of cell cycle progression. *FEBS Letters 486*, 3 (2000), 275–280.

[512] Reya, T., Morrison, S. J., Clarke, M. F., and Weissman, I. L. Stem cells, cancer, and cancer stem cells. *Nature 414*, 6859 (2001), 105–111.

[513] Rhyasen, G. W., Bolanos, L., and Starczynowski, D. T. Differential irak signaling in hematologic malignancies. *Experimental Hematology 41*, 12 (2013), 1005.

[514] Ringshausen, I., O'Shea, C. C., Finch, A. J., Swigart, L. B., and Evan, G. I. Mdm2 is critically and continuously required to suppress lethal p53 activity in vivo. *Cancer Cell 10*, 6 (2006), 501–514.

[515] Ríos, O., Frias, S., Rodríguez, A., Kofman, S., Merchant, H., Torres, L., and Mendoza, L. A Boolean network model of human gonadal sex determination. *Theoretical Biology and Medical Modelling 12*, 26 (2015).

[516] Rizo, A., Olthof, S., Han, L., Vellenga, E., de Haan, G., and Schuringa, J. J. Repression of BMI1 in normal and leukemic human CD34+ cells impairs self-renewal and induces apoptosis. *Blood, The Journal of the American Society of Hematology 114*, 8 (2009), 1498–1505.

[517] Rizo, A., Vellenga, E., de Haan, G., and Schuringa, J. J. Signaling pathways in self-renewing hematopoietic and leukemic stem cells: do all stem cells need a niche? *Human Molecular Genetics 15*, Issue Suppl 2 (2006), R210–

R219.

[518] Rizzolio, S., Cagnoni, G., Battistini, C., Bonelli, S., Isella, C., Van Ginderachter, J. A., Bernards, R., Di Nicolantonio, F., Giordano, S., and Tamagnone, L. Neuropilin-1 upregulation elicits adaptive resistance to oncogene-targeted therapies. *The Journal of Clinical Investigation 128*, 9 (2018), 3976–3990.

[519] Ro, C., Chai, W., Victoria, E. Y., and Yu, R. Pancreatic neuroendocrine tumors: biology, diagnosis, and treatment. *Chinese Journal of Cancer 32*, 6 (2013), 312.

[520] Robertson, H., Hayes, J. D., and Sutherland, C. A partnership with the proteasome; the destructive nature of GSK3. *Biochemical Pharmacology 147* (2018), 77–92.

[521] Robin, X., Turck, N., Hainard, A., Tiberti, N., Lisacek, F., Sanchez, J.-C., and Müller, M. pROC: an open-source package for R and S+ to analyze and compare ROC curves. *BMC Bioinformatics 12*, 77 (2011).

[522] Robine, J.-M., and Allard, M. The oldest human. *Science 279*, 5358 (1998), 1831.

[523] Rodgers, J. T., King, K. Y., Brett, J. O., Cromie, M. J., Charville, G. W., Maguire, K. K., Brunson, C., Mastey, N., Liu, L., Tsai, C.-R., Goodell, M. A., and Rando, T. A. mTORC1 controls the adaptive transition of quiescent stem cells from G 0 to G Alert. *Nature 510*, 7505 (2014), 393–396.

[524] Rodrigue, J.-P. *The Geography of Transport Systems*. Taylor & Francis, 2016.

[525] Roeder, I., Horn, K., Sieburg, H.-B., Cho, R., Muller-Sieburg, C., and Loeffler, M. Characterization and quantification of clonal heterogeneity among hematopoietic stem cells: a model-based approach. *Blood 112*, 13 (2008), 4874–4883.

[526] Roeder, I., and Lorenz, R. Asymmetry of stem cell fate and the potential impact of the niche. *Stem Cell Reviews 2*, 3 (2006), 171–180.

[527] Roland, C. L., Bian, A., Mansour, J. C., Yopp, A. C., Balch, G. C., Sharma, R., Xie, X.-J., and Schwarz, R. E. Survival impact of malignant pancreatic neuroendocrine and islet cell neoplasm phenotypes. *Journal of Surgical Oncology 105*, 6 (2012), 595–600.

[528] Romeo, Y., Zhang, X., and Roux, P. P. Regulation and function of the RSK family of protein kinases. *Biochemical Journal 441*, 2 (2012), 553–569.

[529] Rosanò, L., Spinella, F., and Bagnato, A. Endothelin 1 in cancer: biological implications and therapeutic opportunities. *Nature Reviews Cancer 13*, 9 (2013), 637–651.

[530] Rossi, D. J., Bryder, D., Seita, J., Nussenzweig, A., Hoeijmakers, J., and Weissman, I. L. Deficiencies in dna damage repair limit the function of haematopoietic stem cells with age. *Nature 447*, 7145 (2007), 725–729.

[531] Rossi, D. J., Bryder, D., and Weissman, I. L. Hematopoietic stem cell aging: mechanism and consequence. *Experimental Gerontology 42*, 5 (2007), 385–390.

[532] Rossi, D. J., Bryder, D., Zahn, J. M., Ahlenius, H., Sonu, R., Wagers, A. J., and Weissman, I. L. Cell intrinsic alterations underlie hematopoietic stem cell aging. *Proceedings of the National Academy of Sciences 102*, 26 (2005), 9194–9199.

[533] Rossi, D. J., Jamieson, C. H., and Weissman, I. L. Stems cells and the pathways to aging and cancer. *Cell 132*, 4 (2008), 681–696.

[534] Rossi, L., Challen, G. A., Sirin, O., Lin, K. K.-Y., and Goodell, M. A. Hematopoietic stem cell characterization and isolation. In *Stem Cell Migration. Methods in Molecular Biology (methods and protocols)* (2011), M.-D. Filippi and H. Geiger, Eds., vol. 750, Humana Press, Totowa, NJ, pp. 47–59.

[535] Roux, P. P., and Topisirovic, I. Regulation of mRNA translation by signaling pathways. *Cold Spring Harbor Perspectives in Biology 4*, 11 (2012), a012252.

[536] Roy, N., Takeuchi, K. K., Ruggeri, J. M., Bailey, P., Chang, D., Li, J., Leonhardt, L., Puri, S., Hoffman, M. T., Gao, S., Halbrook, C. J., Song, Y., Ljungman, M., Malik, S., Wright, C. V. E., Dawson, D. W., Biankin, A. V., Hebrok, M., and Crawford, H. C. PDX1 dynamically regulates pancreatic ductal adenocarcinoma initiation and maintenance. *Genes & Development 30*, 24 (2016), 2669–2683.

[537] Rozmus, J., McDonald, R., Fung, S.-Y., Del Bel, K. L., Roden, J., Senger, C., Schultz, K. R., McKinnon, M. L., Davis, J., and Turvey, S. E. Successful clinical treatment and functional immunological normalization of human malt1 deficiency following hematopoietic stem cell transplantation. *Clinical Immunology 168* (2016), 1–5.

[538] Rubio-Escudero, C., Harari, O., Cordón, O., and Zwir, I. Modeling genetic networks: comparison of static and dynamic models. In *Evolutionary Computation, Machine Learning and Data Mining in Bioinformatics* (2007), E. Marchiori, J. H. Moore, and J. C. Rajapakse, Eds., vol. LNCS 4447 of *5th European Conference, EvoBIO 2007*, Springer, pp. 79–89.

[539] Rumman, M., Dhawan, J., and Kassem, M. Concise review: quiescence in adult stem cells: biological significance and relevance to tissue regeneration. *Stem Cells 33*, 10 (2015), 2903–2912.

[540] Ryu, S.-W., Woo, J. H., Kim, Y.-H., Lee, Y.-S., Park, J. W., and Bae, Y.-S. Downregulation of protein kinase ckii is associated with cellular senescence. *FEBS Letters 580*, 3 (2006), 988–994.

[541] Saadatpour, A., and Albert, R. Boolean modeling of biological regulatory networks: A methodology tutorial. *Methods 62*, 1 (2013), 3–12.

[542] Saadatpour, A., and Albert, R. A comparative study of qualitative and quantitative dynamic models of biological regulatory networks. *EPJ Nonlinear*

Biomedical Physics 4, 5 (2016).

[543] Saadatpour, A., Albert, R., and Reluga, T. C. A reduction method for Boolean network models proven to conserve attractors. *SIAM Journal on Applied Dynamical Systems 12*, 4 (2013), 1997–2011.

[544] Saadatpour, A., Wang, R.-S., Liao, A., Liu, X., Loughran, T. P., Albert, I., and Albert, R. Dynamical and structural analysis of a T cell survival network identifies novel candidate therapeutic targets for large granular lymphocyte leukemia. *PLOS Computational Biology 7*, 11 (2011), e1002267.

[545] Saçma, M., Pospiech, J., Bogeska, R., de Back, W., Mallm, J.-P., Sakk, V., Soller, K., Marka, G., Vollmer, A., Karns, R., Cabezas-Wallscheid, N., Trumpp, A., Méndez-Ferrer, S., Milsom, M. D., Mulaw, M. A., Geiger, H., and Florian, M. C. Haematopoietic stem cells in perisinusoidal niches are protected from ageing. *Nature Cell Biology 21*, 11 (2019), 1309–1320.

[546] Sadanandam, A., Wullschleger, S., Lyssiotis, C. A., Grötzinger, C., Barbi, S., Bersani, S., Körner, J., Wafy, I., Mafficini, A., Lawlor, R. T., Simbolo, M., Asara, J. M., Bläker, H., Cantley, L. C., Wiedenmann, B., Scarpa, A., and Hanahan, D. A cross-species analysis in pancreatic neuroendocrine tumors reveals molecular subtypes with distinctive clinical, metastatic, developmental, and metabolic characteristics. *Cancer Discovery 5*, 12 (2015), 1296–1313.

[547] Saha, M., Kumar, S., Bukhari, S., Balaji, S. A., Kumar, P., Hindupur, S. K., and Rangarajan, A. AMPK–Akt double-negative feedback loop in breast cancer cells regulates their adaptation to matrix deprivation. *Cancer Research 78*, 6 (2018), 1497–1510.

[548] Sahin, Ö., Fröhlich, H., Löbke, C., Korf, U., Burmester, S., Majety, M., Mattern, J., Schupp, I., Chaouiya, C., Thieffry, D., Poustka, A., Wiemann, S., Beissbarth, T., and Arlt, D. Modeling ERBB receptor-regulated G1/S transition to find novel targets for *de novo* trastuzumab resistance. *BMC Systems Biology 3*, 1 (2009).

[549] Saito, Y., Kitamura, H., Hijikata, A., Tomizawa-Murasawa, M., Tanaka, S., Takagi, S., Uchida, N., Suzuki, N., Sone, A., Najima, Y., Ozawa, H., Wake, A., Taniguchi, S., Schultz, L. D., Ohara, O., and Ishikawa, F. Identification of therapeutic targets for quiescent, chemotherapy-resistant human leukemia stem cells. *Science Translational Medicine 2*, 17 (2010), 17ra9–17ra9.

[550] Samaga, R., and Klamt, S. Modeling approaches for qualitative and semi-quantitative analysis of cellular signaling networks. *Cell Communication and Signaling 11*, 43 (2013).

[551] Sánchez-Aguilera, A., Arranz, L., Martín-Pérez, D., García-García, A., Stavropoulou, V., Kubovcakova, L., Isern, J., Martín-Salamanca, S., Langa, X., Skoda, R. C., Schwaller, J., and Méndez-Ferrer, S. Estro-

gen signaling selectively induces apoptosis of hematopoietic progenitors and myeloid neoplasms without harming steady-state hematopoiesis. *Cell Stem Cell 15*, 6 (2014), 791–804.

[552] Sankar, M., Osmont, K. S., Rolcik, J., Gujas, B., Tarkowska, D., Strnad, M., Xenarios, I., and Hardtke, C. S. A qualitative continuous model of cellular auxin and brassinosteroid signaling and their crosstalk. *Bioinformatics 27*, 10 (2011), 1404–1412.

[553] Sapkota, G. P., Kieloch, A., Lizcano, J. M., Lain, S., Arthur, J. S. C., Williams, M. R., Morrice, N., Deak, M., and Alessi, D. R. Phosphorylation of the protein kinase mutated in Peutz-Jegehrs cancer syndrome, LKB1/STK11, at Ser^{431} by $p90^{RSK}$ and cAMP-dependent protein kinase, but not its farnesylation at $Cys^{4}33$, is essential for LKB1 to suppress cell growth. *The Journal of Biological Chemistry 276*, 22 (2001), 19469–19482.

[554] Sarfstein, R., Belfiore, A., and Werner, H. Identification of insulin-like growth factor-I receptor (IGF-IR) gene promoter-binding proteins in estrogen receptor (ER)-positive and ER-depleted breast cancer cells. *Cancers 2*, 2 (2010), 233–261.

[555] Sashida, G., Liu, Y., Elf, S., Miyata, Y., Ohyashiki, K., Izumi, M., Menendez, S., and Nimer, S. D. ELF4/MEF activates MDM2 expression and blocks oncogene-induced p16 activation to promote transformation. *Molecular and Cellular Biology 29*, 13 (2009), 3687–3699.

[556] Satoh, Y., Matsumura, I., Tanaka, H., Ezoe, S., Sugahara, H., Mizuki, M., Shibayama, H., Ishiko, E., Ishiko, J., Nakajima, K., and Kanakura, Y. Roles for c-myc in self-renewal of hematopoietic stem cells. *Journal of Biological Chemistry 279*, 24 (2004), 24986–24993.

[557] Sawai, C. M., Babovic, S., Upadhaya, S., Knapp, D. J. H. F., Lavin, Y., Lau, C. M., Goloborodko, A., Feng, J., Fujisaki, J., Ding, L., Mirny, L. A., Merad, M., Eaves, C. J., and Reizis, B. Hematopoietic stem cells are the major source of multilineage hematopoiesis in adult animals. *Immunity 45*, 3 (2016), 597–609.

[558] Scandura, J. M., Boccuni, P., Massagué, J., and Nimer, S. D. Transforming growth factor β-induced cell cycle arrest of human hematopoietic cells requires p57KIP2 up-regulation. *Proceedings of the National Academy of Sciences 101*, 42 (2004), 15231–15236.

[559] Scarpa, A., Chang, D. K., Nones, K., Corbo, V., Patch, A.-M., Bailey, P., Lawlor, R. T., Johns, A. L., Miller, D. K., Mafficini, A., Rusev, B., Scardoni, M., Davide, A., Barbi, S., O dikora, K., Cingarlini, S., Vicentini, C., McKay, S., Quinn, M. C. J., Bruxner, T. J. C., Christ, A. N., Harliwong, I., Idrisoglu, S., McLean, S., Nourse, C., Nourbakhsh, E., Wilson, P. J., Anderson, M. J., Fink, L. J., Newell, F., Waddell, N., Holmes, O., Kazakoff,

S. H., Leonard, C., Wood, S., Xu, Q., Nagaraj, S. H., Amato, E., Dalai, I., Bersani, S., Cataldo, I., Dei Tos, A. P., Capelli, P., Davi, M. V., Landoni, L., Malpaga, A., Miotto, M., Whitehall, V. L. J., Leggett, B. A., Harris, J. L., Harris, J., Jones, M. D., Humphris, J., Chantrill, L. A., Chin, V., Nagrial, A. M., Pajic, M., Scarlett, C. J., Pihno, A., Rooman, I., Toon, C., Wu, J., Pinese, M., Cowley, M., Barbour, A., Mawson, A., Humphrey, E. S., Colvin, E. K., Chou, A., Lovell, J. A., Kamieson, N. B., Duthie, F., Cingras, M.-C., Fisher, W. E., Dagg, R. A., Lau, L. M. S., Lee, M., Pickett, H. A., Reddel, R. R., Samra, J. S., Kench, J. G., Merrett, N. D., Epari, J., Nguyen, N. Q., Zeps, N., Falconi, M., Simbolo, M., Burrutini, G., Van Buren, G., Partelli, S., Fassan, M., Khanna, K. K., Gill, A. J., Wheeler, D. A., Gibbs, R. A., Musgrove, E. A., Bassi, C., Tortora, G., Pederzoli, P., Pearson, J. V., Waddell, N., Biankin, A. V., and Grimmond, S. M. Whole-genome landscape of pancreatic neuroendocrine tumours. *Nature 543*, 7643 (2017), 65–71.

[560] Schaible, R., Scheuerlein, A., Dańko, M. J., Gampe, G., and Martínez, D. E. Constant mortality and fertility over age in hydra. *Proceedings of the National Academy of Sciences of the United States of America 112*, 51 (2015), 15701–15706.

[561] Scheidegger, K. J., Du, J., and Delafontaine, P. Distinct and common pathways in the regulation of insulin-like growth factor-1 receptor gene expression by angiotensin ii and basic fibroblast growth factor. *Journal of Biological Chemistry 274*, 6 (1999), 3522–3530.

[562] Schlienger, S., Ramirez, R. A. M., and Claing, A. ARF1 regulates adhesion of MDA-MB-231 invasive breast cancer cells through formation of focal adhesions. *Cellular Signalling 27*, 3 (2015), 403–415.

[563] Schmitt, A., Schmid, S., Rudolph, T., Anlauf, M., Prinz, C., Klöppel, G., Moch, H., Heitz, P., Komminoth, P., and Perren, A. VHL inactivation is an important pathway for the development of malignant sporadic pancreatic endocrine tumors. *Endocrine-Related Cancer 16*, 4 (2009), 1219–1227.

[564] Schnepp, R. W., Chen, Y.-X., Wang, H., Cash, T., Silva, A., Diehl, J. A., Brown, E., and Hua, X. Mutation of tumor suppressor gene men1 acutely enhances proliferation of pancreatic islet cells. *Cancer Research 66*, 11 (2006), 5707–5715.

[565] Schofield, R. The relationship between the spleen colony-forming cell and the haemopoietic stem cell. *Blood Cells 4*, 1-2 (1978), 7–25.

[566] Schrader, J., Henes, F., Perez, D., Burdak-Rothkamm, S., Stein, A., Izbicki, J., and Lohse, A. Successful mtor inhibitor therapy for a metastastic neuroendocrine tumour in a patient with a germline tsc2 mutation. *Annals of Oncology 28*, 4 (2017), 904–905.

[567] Schuringa, J. J., and Vellenga, E. Role of the polycomb group gene BMI1

in normal and leukemic hematopoietic stem and progenitor cells. *Current Opinion in Hematology 17*, 4 (2010), 294–299.

[568] Schwab, J. Modeling regulatory processes with qualitative networks. Doctoral dissertation, Medical Faculty, Ulm University, 2019.

[569] Schwab, J., Burkovski, A., Siegle, L., Müssel, C., and Kestler, H. A. ViSiBooL—visualization and simulation of Boolean networks with temporal constraints. *Bioinformatics 33*, 4 (2016), 601–604.

[570] Schwab, J. D., Ikonomi, N., Kühlwein, S. D., Weidner, F. M., Geiger, H., and Kestler, H. A. Reconstructing Boolean network ensembles from single-cell data for unraveling dynamics in the aging of human hematopoietic stem cells. *Computational and Structural Biotechnology 19* (2021), 5321–5332.

[571] Schwab, J. D., and Kestler, H. A. Automatic screening for perturbations in Boolean networks. *Frontiers in Physiology 9*, 431 (2018).

[572] Schwab, J. D., Kühlwein, S. D., Ikonomi, N., Kühl, M., and Kestler, H. A. Concepts in Boolean network modeling: What do they all mean? *Computational and Structural Biotechnology 18* (2020), 571–582.

[573] Schwab, J. D., Siegle, L., Kühlwein, S. D., Kühl, M., and Kestler, H. A. Stability of signaling pathways during aging—A Boolean network approach. *Biology 6*, 4 (2017), 46.

[574] Sengupta, T., Abraham, G., Xu, Y., Clurman, B. E., and Minella, A. C. Hypoxia-inducible factor 1 is activated by dysregulated cyclin E during mammary epithelial morphogenesis. *Molecular and Cellular Biology 31*, 18 (2011), 3885–3895.

[575] Sennino, B., Ishiguro-Oonuma, T., Wei, Y., Naylor, R. M., Williamson, C. W., Bhagwandin, V., Tabruyn, S. P., You, W.-K., Chapman, H. A., Christensen, J. G., Aftab, D. T., and McDonald, D. M. Suppression of tumor invasion and metastasis by concurrent inhibition of c-Met and VEGF signaling in pancreatic neuroendocrine tumors. *Cancer Discovery 2*, 3 (2012), 270–287.

[576] Serrano, M., and Blasco, M. A. Cancer and ageing: convergent and divergent mechanisms. *Nature Reviews Molecular Cell Biology 8*, 9 (2007), 715–722.

[577] Serrano, M., Lin, A. W., McCurrach, M. E., Beach, D., and Lowe, S. W. Oncogenic ras provokes premature cell senescence associated with accumulation of p53 and p16INK4a. *Cell 88*, 5 (1997), 593–602.

[578] Sgariglia, D., Conforte, A. J., Pedreira, C. E., de Carvalho, L. A. V., Carneiro, F. R. G., Carels, N., and da Silva, F. A. B. Data-driven modeling of breast cancer tumors using Boolean networks. *Frontiers in Big Data 4* (2021).

[579] Shah, M. H., Young, D., Kindler, H. L., Webb, I., Kleiber, B., Wright, J., and Grever, M. Phase ii study of the proteasome inhibitor bortezomib $(\mathrm{ps}-341)$ in patients with metastatic neuroendocrine tumors. *Clinical Cancer*

Research 10, 18 (2004), 6111–6118.

[580] Shahbazian, D., Roux, P. P., Mieulet, V., Cohen, M. S., Raught, B., Taunton, J., Hersehy, J. W., Blenis, J., Pende, M., and Sonenberg, N. The mTOR/PI3K and MAPK pahtways converge on eIF4B to control its phosphorylation and activity. *The EMBO Journal 25*, 12 (2006), 2781–2791.

[581] Shalini, S., Dorstyn, L., Wilson, C., Puccini, J., Ho, L., and Kumar, S. Impaired antioxidant defence and accumulation of oxidative stress in caspase-2-deficient mice. *Cell Death & Differentiation 19*, 8 (2012), 1370–1380.

[582] Shanks, N., Greek, R., and Greek, J. Are animal models predictive for humans? *Philosophy, Ethics, and Humanities in Medicine 4*, 1 (2009), 1–20.

[583] Shao, L., Li, H., Pazhanisamy, S. K., Meng, A., Wang, Y., and Zhou, D. Reactive oxygen species and hematopoietic stem cell senescence. *International Journal of Hematology 94*, 1 (2011), 24–32.

[584] Shaw, R. J. LKB1 and AMP-activated protein kinase control of mTOR signalling and growth. *Acta Physiologica 196* (2009), 65–80.

[585] Sherr, C. J. The INK4a/ARF network in tumour suppression. *Nature Reviews Molecular Cell Biology 2*, 10 (2001), 731–737.

[586] Sherr, C. J., and Roberts, J. M. CDK inhibitors: positive and negative regulators of G1-phase progression. *Genes & Development 13*, 12 (1999), 1501–1512.

[587] Sherr, C. J., and Weber, J. D. The ARF/p53 pathway. *Current Opinion in Genetics & Development 10*, 1 (2000), 94–99.

[588] Shida, T., Kishimoto, T., Furuya, M., Nikaido, T., Koda, K., Takano, S., Kimura, F., Shimizu, H., Yoshidome, H., Ohtsuka, M., Tanizawa, T., Nakatani, Y., and Miyazaki, M. Expression of an activated mammalian target of rapamycin (mTOR) in gastroenteropancreatic neuroendocrine tumors. *Cancer Chemotherapy and Pharmacology 65*, 5 (2010), 889–893.

[589] Shimbel, A. Applications of matrix algebra to communication nets. *The Bulletin of Mathematical Biophysics 13*, 3 (1951), 165–178.

[590] Shimbel, A. Structural parameters of communication networks. *The Bulletin of Mathematical Biophysics 15*, 4 (1953), 501–507.

[591] Shivakumar, L., Minna, J., Sakamaki, T., Pestell, R., and White, M. A. The RASSF1A tumor suppressor blocks cell cycle progression and inhibits Cyclin D1 accumulation. *Molecular and Cellular Biology 22*, 12 (2002), 4309–4318.

[592] Shmulevich, I., Dougherty, E. R., Kim, S., and Zhang, W. Probabilistic Boolean networks: a rule-based uncertainty model for gene regulatory networks. *Bioinformatics 18*, 2 (2002), 261–274.

[593] Shock, N. W., Greulich, R. C., Costa, Paul T, J., Andres, R., Lakatta, E. G., Arenberg, D., and Tobin, J. D. *Normal human aging: the Baltimore longitudinal study on aging*. NIH Publication, Washington, DC, 1985.

[594] Shome, K., Vasudevan, C., and Romero, G. Arf proteins mediate insulin-

dependent activation of phospholipase D. *Current Biology 7*, 6 (1997), 387–396.

[595] Shumway, S. D., Li, Y., and Xiong, Y. 14-3-3β binds to and negatively regulates the tuberous sclerosis complex 2 (tsc2) tumor suppressor gene product, tuberin. *Journal of Biological Chemistry 278*, 4 (2003), 2089–2092.

[596] Shvarts, A., Steegenga, W. T., Riteco, N., Van Laar, T., Dekker, P., Bazuine, M., Van Ham, R. C., van der Houven van Oordt, W., Hateboer, G., Van Der Eb, A. J., and Jochemsen, A. G. MDMX: a novel p53-binding protein with some functional properties of MDM2. *The EMBO Journal 15*, 19 (1996), 5349–5357.

[597] Siegel, R. L., Miller, K. D., Fuchs, H. E., and Jemal, A. Cancer statistics, 2021. *CA: a Cancer Journal for Clinicians 71*, 1 (2021), 7–33.

[598] Siegle, L., Schwab, J. D., Kühlwein, S. D., Lausser, L., Tümpel, S., Pfister, A. S., Kühl, M., and Kestler, H. A. A Boolean network of the crosstalk between IGF and Wnt signaling in aging satellite cells. *PLOS ONE 13*, 3 (2018), e0195126.

[599] Sigala, J. L. D., Bottero, V., Young, D. B., Shevchenko, A., Mercurio, F., and Verma, I. M. Activation of transcription factor NF-κB requires ELKS, an IκB kinase regulatory subunit. *Science 304*, 5679 (2004), 1963–1967.

[600] Sinenko, S. A., Starkova, T. Y., Kuzmin, A. A., and Tomilin, A. N. Physiological signaling functions of reactive oxygen species in stem cells: from flies to man. *Frontiers in Cell and Developmental Biology 9* (2021).

[601] Sirkisoon, S. R., Carpenter, R. L., Rimkus, T., Anderson, A., Harrison, A., Lange, A. M., Jin, G., Watabe, K., and Lo, H.-W. Interaction between STAT3 and GLI1/tGLI1 oncogenic transcription factors promotes the aggressiveness of triple-negative breast cancers and HER2-enriched breast cancer. *Oncogene 37*, 19 (2018), 2502–2514.

[602] Sladky, V. C., and Villunger, A. Uncovering the piddosome and caspase-2 as regulators of organogenesis and cellular differentiation. *Cell Death & Differentiation 27*, 7 (2020), 2037–2047.

[603] Snel, B., Lehmann, G., Bork, P., and Huynen, M. A. STRING: a web-server to retrieve and display the repeatedly occurring neighbourhood of a gene. *Nucleic Acids Research 28*, 18 (2000), 3442–3444.

[604] Soltys, C.-L. M., Kovacic, S., and Dyck, J. R. Activation of cardiac amp-activated protein kinase by lkb1 expression or chemical hypoxia is blunted by increased akt activity. *American Journal of Physiology-Heart and Circulatory Physiology 290*, 6 (2006), H2472–H2479.

[605] Sonawane, A. R., Platig, J., Fagny, M., Chen, C.-Y., Paulson, J. N., Lopes-Ramos, C. M., DeMeo, D. L., Quackenbush, J., Glass, K., and Kuijjer, M. L. Understanding tissue-specific gene regulation. *Cell Reports 21*, 4 (2017), 1077–1088.

[606] Song, G., Ouyang, G., and Bao, S. The activation of Akt/PKB signaling pathway and cell survival. *Journal of Cellular and Molecular Medicine 9*, 1 (2005), 59–71.

[607] Song, M., Song, S., Kim, S., Nakayama, K., Nakayama, K., and Lim, D.-S. Skp2 regulates the antiproliferative function of the tumor suppressor RASSF1A via ubiquitin-mediated degradation at the G 1–S transition. *Oncogene 27*, 22 (2008), 3176–3185.

[608] Song, M. S., Song, S. J., Kim, S. Y., Oh, H. J., and Lim, D.-S. The tumour suppressor RASSF1A promotes MDM2 self-ubiquitination by disrupting the MDM2–DAXX–HAUSP complex. *The EMBO Journal 27*, 13 (2008), 1863–1874.

[609] Song, Q., Sun, X., Guo, H., and Yu, Q. Concomitant inhibition of receptor tyrosine kinases and downstream AKT synergistically inhibited growth of KRAS/BRAF mutant colorectal cancer cells. *Oncotarget 8*, 3 (2017), 5003.

[610] Song, X., Call, G. B., Kirilly, D., and Xie, T. Notch signaling controls germline stem cell niche formation in the drosophila ovary. *Development 134* (2007), 1071–1080.

[611] Sontag, E. D. Monotone and near-monotone biochemical networks. *Systems and Synthetic Biology 1*, 2 (2007), 59–87.

[612] Soofiyani, S. R., Hejazi, M. S., and Baradaran, B. The role of CIP2A in cancer: A review and update. *Biomedicine & Pharmacotherapy 96* (2017), 626–633.

[613] Spangrude, G., Heimfeld, S., and Weissman, I. Purification and characterization of mouse hematopoietic stem cells. *Science 241*, 4861 (1988), 58–62.

[614] Spradling, A., Drummond-Barbosa, D., and Kai, T. Stem cells find their niche. *Nature 414*, 6859 (2001), 98–104.

[615] Sridharan, S., Layek, R., Datta, A., and Venkatraj, J. Boolean modeling and fault diagnosis in oxidative stress response. *BMC Genomics 13*, S4 (2012).

[616] Stalberg, P., Grimfjard, P., Santesson, M., Zhou, Y., Lindberg, D., Gobl, A., Oberg, K., Westin, G., Rastad, J., Wang, S., and Skogseid, B. Transfection of the multiple endocrine neoplasia type 1 gene to a human endocrine pancreatic tumor cell line inhibits cell growth and affects expression of JunD, δ-like protein 1/preadipocyte factor-1, proliferating cell nuclear antigen, and QM/Jif-1. *The Journal of Clinical Endocrinology & Metabolism 89*, 5 (2004), 2326–2337.

[617] Stark, C., Breitkreutz, B.-J., Reguly, T., Boucher, L., Breitkreutz, A., and Tyers, M. BioGRID: a general repository for interaction datasets. *Nucleic Acids Research 34*, suppl_1 (2006), D535–D539.

[618] Stark, G. R., Wang, Y., and Lu, T. Lysine methylation of promoter-bound transcription factors and relevance to cancer. *Cell research 21*, 3 (2011), 375–380.

[619] Storz, P. Forkhead homeobox type O transcription factors in the responses to oxidative stress. *Antioxidants & Redox Signaling 14*, 4 (2011), 593–605.

[620] Suda, T., Takubo, K., and Semenza, G. L. Metabolic regulation of hematopoietic stem cells in the hypoxic niche. *Cell Stem Cell 9*, 4 (2011), 298–310.

[621] Sugiyama, T., Kohara, H., Noda, M., and Nagasawa, T. Maintenance of the hematopoietic stem cell pool by CXCL12-CXCR4 chemokine signaling in bone marrow stromal cell niches. *Immunity 25*, 6 (2006), 977 – 988.

[622] Sun, J., Lu, Z., Deng, Y., Wang, W., He, Q., Yan, W., and Wang, A. Up-regulation of INSR/IGF1R by C-myc promotes TSCC tumorigenesis and metastasis through the nf-κb pathway. *Biochimica et Biophysica Acta (BBA)-Molecular Basis of Disease 1864*, 5 (2018), 1873–1882.

[623] Sun, M., Cheng, X., and Socolar, J. E. Regulatory logic and pattern formation in the early sea urchin embryo. *Journal of Theoretical Biology 363* (2014), 80–92.

[624] Sun, P., Xiong, H., Kim, T. H., Ren, B., and Zhang, Z. Positive interregulation between β-Catenin/T cell factor-4 signaling and endothelin-1 signaling potentiates proliferation and survival of prostate cancer cells. *Molecular Pharmacology 69*, 2 (2006), 520–531.

[625] Sun, T., Rodriguez, M., and Kim, L. Glycogen synthase kinase 3 in the world of cell migration. *Development, Growth & Differentiation 51*, 9 (2009), 735–742.

[626] Sung, H., Ferlay, J., Siegel, R. L., Laversanne, M., Soerjomataram, I., Jemal, A., and Bray, F. Global cancer statistics 2020: Globocan estimates of incidence and mortality worldwide for 36 cancers in 185 countries. *CA: a Cancer Journal for Clinicians 71*, 3 (2021), 209–249.

[627] Szklarczyk, D., Gable, A. L., Lyon, D., Junge, A., Wyder, S., Huerta-Cepas, J., Simonovic, M., Doncheva, N. T., Morris, J. H., Bork, P., Jensen, L. J., and von Mering, C. STRING v11: protein–protein association networks with increased coverage, supporting functional discovery in genome-wide experimental datasets. *Nucleic Acids Research 47*, D1 (2019), D607–D613.

[628] Szklarczyk, D., Morris, J. H., Cook, H., Kuhn, M., Wyder, S., Simonovic, M., Santos, A., Doncheva, N. T., Roth, A., Bork, P., Jensen, L. J., and Von Mering, C. The STRING database in 2017: quality-controlled protein–protein association networks, made broadly accessible. *Nucleic Acids Research* (2016), gkw937.

[629] Taguchi, R., Yamada, M., Horiguchi, K., Tomaru, T., Ozawa, A., Shibusawa, N., Hashimoto, K., Okada, S., Satoh, T., and Mori, M. Haploinsufficient and predominant expression of multiple endocrine neoplasia type 1 (MEN1)-related genes, MLL, p27Kip1 and p18Ink4C in endocrine organs. *Biochemical and Biophysical Research Communications 415*, 2 (2011), 378–383.

[630] Takizawa, H., Fritsch, K., Kovtonyuk, L. V., Saito, Y., Yakkala, C., Jacobs,

K., Ahuja, A. K., Lopes, M., Hausmann, A., Hardt, W.-D., Gomariz, A., Nombela-Arrieta, C., and Manz, M. G. Pathogen-induced TLR4-TRIF innate immune signaling in hematopoietic stem cells promotes proliferation but reduces competitive fitness. *Cell Stem Cell 21*, 2 (2017), 225–240.

[631] Takizawa, H., Regoes, R. R., Boddupalli, C. S., Bonhoeffer, S., and Manz, M. G. Dynamic variation in cycling of hematopoietic stem cells in steady state and inflammation. *Journal of Experimental Medicine 208*, 2 (2011), 273–284.

[632] Tanaka, H., Fauré, A., and Matsuno, H. Boolean modeling of mammalian cell cycle and cancer pathways. In *International Conference on Artificial Life and Robotics* (2017), pp. 507–510.

[633] Tang, L. H., Contractor, T., Clausen, R., Klimstra, D. S., Du, Y.-C. N., Allen, P. J., Brennan, M. F., Levine, A. J., and Harris, C. R. Attenuation of the retinoblastoma pathway in pancreatic neuroendocrine tumors due to increased cdk4/cdk6. *Clinical Cancer Research 18*, 17 (2012), 4612–4620.

[634] TeKippe, M., Harrison, D. E., and Chen, J. Expansion of hematopoietic stem cell phenotype and activity in Trp53-null mice. *Experimental Hematology 31*, 6 (2003), 521–527.

[635] Tesio, M., Tang, Y., Müdder, K., Saini, M., Von Paleske, L., Macintyre, E., Pasparakis, M., Waisman, A., and Trumpp, A. Hematopoietic stem cell quiescence and function are controlled by the CYLD–TRAF2–p38MAPK pathway. *Journal of Experimental Medicine 212*, 4 (2015), 525–538.

[636] Tesio, M., and Trumpp, A. Breaking the cell cycle of HSCs by p57 and friends. *Cell Stem Cell 9*, 3 (2011), 187–192.

[637] Thakar, J., Pathak, A. K., Murphy, L., Albert, R., and Cattadori, I. M. Network model of immune responses reveals key effectors to single and co-infection dynamics by a respiratory bacterium and a gastrointestinal helminth. *PLOS Computational Biology 8*, 1 (2012), e1002345.

[638] Thomas-Marques, L., Murat, A., Delemer, B., Penfornis, A., Cardot-Bauters, C., Baudin, E., Niccoli-Sire, P., Levoir, D., du Boullay Choplin, H., Chabre, O., Jovenin, N., and Cadiot, G. Prospective endoscopic ultrasonographic evaluation of the frequency of nonfunctioning pancreaticoduodenal endocrine tumors in patients with multiple endocrine neoplasia type 1. *Official journal of the American College of Gastroenterology | ACG 101*, 2 (2006), 266–273.

[639] Thorén, L. A., Liuba, K., Bryder, D., Nygren, J. M., Jensen, C. T., Qian, H., Antonchuk, J., and Jacobsen, S. E. W. Kit Regulates Maintenance of Quiescent Hematopoietic Stem Cells. *The Journal of Immunology 180*, 4 (2008), 2045–2053.

[640] Tiainen, M., Vaahtomeri, K., Ylikorkala, A., and Mäkelä, T. P. Growth arrest by the lkb1 tumor suppressor: induction of p21waf1/cip1. *Human*

molecular genetics 11, 13 (2002), 1497–1504.

[641] Tian, X., Liu, Z., Niu, B., Zhang, J., Tan, T. K., Lee, S. R., Zhao, Y., Harris, D. C., and Zheng, G. E-cadherin/β-catenin complex and the epithelial barrier. *Journal of Biomedicine and Biotechnology 2011* (2011).

[642] Todd, R. G., and Helikar, T. Ergodic sets as cell phenotype of budding yeast cell cycle. *PLOS ONE 7*, 10 (2012), e45780.

[643] Toledo, F., and Wahl, G. M. Regulating the p53 pathway: in vitro hypotheses, in vivo veritas. *Nature Reviews Cancer 6*, 12 (2006), 909–923.

[644] Tomczyk, S., Fischer, K., Austad, S., and Galliot, B. Hydra, a powerful model for aging studies. *Invertebrate Reproduction & Development 59*, S1 (2015), 11–16.

[645] Tong, Y., Ying, H., Liu, R., Li, L., Bergholz, J., and Xiao, Z. Pin1 inhibits PP2A-mediated rb dephosphorylation in regulation of cell cycle and S-phase DNA damage. *Cell death & disease 6*, 2 (2015), e1640–e1640.

[646] Tothova, Z., and Gilliland, D. G. FoxO transcription factors and stem cell homeostasis: insights from the hematopoietic system. *Cell Stem Cell 1*, 2 (2007), 140–152.

[647] Tothova, Z., Kollipara, R., Huntly, B. J., Lee, B. H., Castrillon, D. H., Cullen, D. E., McDowell, E. P., Lazo-Kallanian, S., Williams, I. R., Sears, C., Armstrong, S. A., Passegué, E., DePinho, R. A., and Gilliland, D. G. FoxOs are critical mediators of hematopoietic stem cell resistance to physiologic oxidative stress. *Cell 128*, 2 (2007), 325–339.

[648] Toyoshima, H., and Hunter, T. p27, a novel inhibitor of g1 cyclin-cdk protein kinase activity, is related to p21. *Cell 78*, 1 (1994), 67–74.

[649] Tran, H., Brunet, A., Griffith, E. C., and Greenberg, M. E. The many forks in FOXO's road. *Science's STKE 2003*, 172 (2003), re5.

[650] Troen, B. R. The biology of aging. *Mount Sinai Journal of Medicine 70*, 1 (2003), 3–22.

[651] Trowbridge, J. J., and Starczynowski, D. T. Innate immune pathways and inflammation in hematopoietic aging, clonal hematopoiesis, and mds. *Journal of Experimental Medicine 218*, 7 (2021), e20201544.

[652] Trumpp, A., Essers, M., and Wilson, A. Awakening dormant haematopoietic stem cells. *Nature Reviews Immunology 10*, 3 (2010), 201–209.

[653] Umemoto, T., Yamato, M., Nishida, K., Yang, J., Tano, Y., and Okano, T. p57Kip2 is expressed in quiescent mouse bone marrow side population cells. *Biochemical and Biophysical Research Communications 337*, 1 (2005), 14–21.

[654] Umesalma, S., Kaemmer, C. A., Kohlmeyer, J. L., Letney, B., Schab, A. M., Reilly, J. A., Sheehy, R. M., Hagen, J., Tiwari, N., Zhan, F., Leidinger, M. R., O'Dorisio, T. M., Dillon, J., Merrill, R. A., Meyerholz, D. K., Perl, A. L., Brown, B. J., Braun, T. A., Scott, A. T., Ginader, T., Taghiyev, A. F.,

Zamba, G. K., Howe, J. R., Strack, S., Bellizzi, A. M., Narla, G., Darbro, B. W., Quelle, F. W., and Quelle, D. E. RABL6A inhibits tumor-suppressive PP2A/AKT signaling to drive pancreatic neuroendocrine tumor growth. *The Journal of Clinical Investigation 129*, 4 (2019), 1641–1653.

[655] Vacca, F., Bagnato, A., Catt, K. J., and Tecce, R. Transactivation of the epidermal growth factor receptor in endothelin-1-induced mitogenic signaling in human ovarian carcinoma cells. *Cancer Research 60*, 18 (2000), 5310–5317.

[656] Valenta, T., Hausmann, G., and Basler, K. The many faces and functions of β-catenin. *The EMBO Journal 31*, 12 (2012), 2714–2736.

[657] Van Zant, G., and Liang, Y. The role of stem cells in aging. *Experimental Hematology 31*, 8 (2003), 659–672.

[658] Vandamme, T., Beyens, M., Op de Beek, K., Dogan, F., van Koestsveld, P. M., Pauwels, P., Mortier, G., Vangestel, C., de Herder, W., Van Camp, G., Peeters, M., and Hofland, L. J. Long-term acquired everolimus resistance in pancreatic neuroendocrine tumours can be overcome with novel PI3K-AKT-mTOR inhibitors. *Britisch Journal of Cancer 114* (2016), 650–658.

[659] Vandoorne, K., Rohde, D., Kim, H.-Y., Courties, G., Wojtkiewicz, G., Honold, L., Hoyer, F. F., Frodermann, V., Nayar, R., Herisson, F., Jung, Y., Désorgerè, P. A., Vinegoni, C., Caravan, P., Weissleder, R., Sosnovik, D. E., Lin, C. P., and Swirski, F. K. Imaging the vascular bone marrow niche during inflammatory stress. *Circulation Research 123*, 4 (2018), 415–427.

[660] Varghese, L. N., Defour, J.-P., Pecquet, C., and Constantinescu, S. N. The Thrombopoietin Receptor: Structural Basis of Traffic and Activation by Ligand, Mutations, Agonists, and Mutated Calreticulin. *Frontiers in Endocrinology 8* (2017), 59.

[661] Varnat, F., Siegl-Cachedenier, I., Malerba, M., Gervaz, P., and Ruiz i Altaba, A. Loss of wnt-tcf addiction and enhancement of hh-gli1 signalling define the metastatic transition of human colon carcinomas. *EMBO Molecular Medicine 2*, 11 (2010), 440–457.

[662] Varnum-Finney, B., Xu, L., Brashem-Stein, C., Nourigat, C., Flowers, D., Bakkour, S., Pear, W. S., and Bernstein, I. D. Pluripotent, cytokine-dependent, hematopoietic stem cells are immortalized by constitutive Notch1 signaling. *Nature Medicine 6*, 11 (2000), 1278–1281.

[663] Veliz-Cuba, A., and Stigler, B. Boolean models can explain bistability in the lac operon. *Journal of Computational Biology 18*, 6 (2011), 783–794.

[664] Verovskaya, E., Broekhuis, M. J., Zwart, E., Ritsema, M., van Os, R., de Haan, G., and Bystrykh, L. V. Heterogeneity of young and aged murine hematopoietic stem cells revealed by quantitative clonal analysis using cellular barcoding. *Blood 122*, 4 (2013), 523–532.

[665] Verovskaya, E. V., Dellorusso, P. V., and Passegué, E. Losing sense of self

and surroundings: hematopoietic stem cell aging and leukemic transformation. *Trends in Molecular Medicine 25*, 6 (2019), 494–515.

[666] Vijayvergia, N., Boland, P. M., Handorf, E., Gustafson, K. S., Gong, Y., Cooper, H. S., Sheriff, F., Astsaturov, I., Cohen, S. J., and Engstrom, P. F. Molecular profiling of neuroendocrine malignancies to identify prognostic and therapeutic markers: a fox chase cancer center pilot study. *British Journal of Cancer 115*, 5 (2016), 564–570.

[667] Vivanco, I., and Sawyers, C. L. The phosphatidylinositol 3-kinase–AKT pathway in human cancer. *Nature Reviews Cancer 2*, 7 (2002), 489–501.

[668] Vogt, P. K., Jiang, H., and Aoki, M. Triple layer control: phosphorylation, acetylation and ubiquitination of foxo proteins. *Cell Cycle 4*, 7 (2005), 908–913.

[669] Völkel, G., Laban, S., Fürstberger, A., Kühlwein, S. D., Ikonomi, N., Hoffman, T. K., Brunner, C., Neuberg, D. S., Gaidzik, V., Döhner, H., Kraus, J. M., and Kestler, H. A. Analysis, identification and visualization of subgroups in genomics. *Briefings in Bioinformatics* (2020), bbaa217.

[670] von Wichert, G., Jehle, P. M., Hoeflich, A., Koschnick, S., Dralle, H., Wolf, E., Wiedenmann, B., Boehm, B. O., Adler, G., and Seufferlein, T. Insulin-like growth factor-i is an autocrine regulaotr of Chromogranin A secretion and growth in human neuroendocrine tumor cells. *Cancer Research 60*, 16 (2000), 4573–4581.

[671] Vousden, K. H., and Lane, D. P. p53 in health and disease. *Nature Reviews Molecular Cell Biology 8*, 4 (2007), 275–283.

[672] Wagner, W., Horn, P., Bork, S., and Ho, A. D. Aging of hematopoietic stem cells is regulated by the stem cell niche. *Experimental Gerontology 43*, 11 (2008), 974–980.

[673] Walter, D., Lier, A., Geiselhart, A., Thalheimer, F. B., Huntscha, S., Sobotta, M. C., Moehrle, B., Brocks, D., Bayindir, I., Kaschutnig, P., Mudder, K., Klein, C., Jauch, A., Schroeder, T., Geiger, H., Dick, T. P., Holland-Letz, T., Scmezer, P., Lane, S. W., Rieger, M. A., Essers, M. A. G., Williams, D. A., Trumpp, A., and Milsom, M. D. Exit from dormancy provokes DNA-damage-induced attrition in haematopoietic stem cells. *Nature 520*, 7548 (2015), 549–552.

[674] Wang, D.-G., Johnston, C. F., and Buchanan, K. D. Oncogene expression in gastroenteropancreatic neuroendocrine tumors: implications for pathogenesis. *Cancer: Interdisciplinary International Journal of the American Cancer Society 80*, 4 (1997), 668–675.

[675] Wang, M. W., Consoli, U., Lane, C. M., Durett, A., Lauppe, M. J., Champlin, R., Andreeff, M., and Deisseroth, A. B. Rescue from apoptosis in early (CD34-selected) versus late (non-CD34-selected) human hematopoietic cells by very late antigen 4- and vascular cell adhesion molecule (VCAM)

1-dependent adhesion to bone marrow stromal cells. *Cell Growth & Differentiation 9*, 2 (1998), 105–112.

[676] Wang, Q., Sun, Z., and Yang, H. Downregulation of tumor suppressor Pdcd4 promotes invasion and activates both β-catenin/Tcf and AP-1-dependent transcription in colon carcinoma cells. *Oncogene 27*, 11 (2008), 1527–1535.

[677] Wang, R., Xia, L., Gabrilove, J., Waxman, S., and Jing, Y. Downregulation of Mcl-1 through GSK-3β activation contributes to arsenic trioxide-induced apoptosis in acute myeloid leukemia cells. *Leukemia 27*, 2 (2013), 315–324.

[678] Wang, Y., Ozawa, A., Zaman, S., Prasad, N. B., Chandrasekharappa, S. C., Agarwal, S. K., and Marx, S. J. The tumor suppressor protein menin inhibits AKT activation by regulating its cellular localization. *Cancer Research 71*, 2 (2011), 371–382.

[679] Wang, Y.-t., Tang, F., Hu, X., Zheng, C.-x., Gong, T.-j., Zhou, Y., Luo, Y., and Min, L. Role of crosstalk between stat3 and mtor signaling in driving sensitivity to chemotherapy in osteosarcoma cell lines. *IUBMB life 72*, 10 (2020), 2146–2153.

[680] Warr, M. R., Binnewies, M., Flach, J., Reynaud, D., Garg, T., Malhotra, R., Debnath, J., and Passegué, E. FOXO3A directs a protective autophagy program in haematopoietic stem cells. *Nature 494*, 7437 (2013), 323–327.

[681] Warr, M. R., Kohli, L., and Passegué, E. Born to survive: autophagy in hematopoietic stem cell maintenance. *Cell Cycle 12*, 13 (2013), 1979–1980.

[682] Warr, M. R., Pietras, E. M., and Passegué, E. Mechanisms controlling hematopoietic stem cell functions during normal hematopoiesis and hematological malignancies. *Wiley Interdisciplinary Reviews: Systems Biology and Medicine 3*, 6 (2011), 681–701.

[683] Wasylishen, A. R., Sun, C., Moyer, S. M., Qi, Y., Chau, G. P., Aryal, N. K., McAllister, F., Kim, M. P., Barton, M. C., Estrella, J. S., Su, X., and Lozano, G. Daxx maintains endogenous retroviral silencing and restricts cellular plasticity in vivo. *Science Advances 6*, 32 (2020), eaba8415.

[684] Watson, D. K., Turner, D. P., Scheiber, M. N., Findlay, V. J., and Watson, P. M. ETS transcription factor expression and conversion during prostate and breast cancer progression. *The Open Cancer Journal 3*, 1 (2010), 24–39.

[685] Watson, I. R., Irwin, M. S., and Ohh, M. NEDD8 pathways in cancer, sine quibus non. *Cancer cell 19*, 2 (2011), 168–176.

[686] Wei, Z., Jiang, X., Qiao, H., Zhai, B., Zhang, L., Zhang, Q., Wu, Y., Jiang, H., and Sun, X. Stat3 interacts with skp2/p27/p21 pathway to regulate the motility and invasion of gastric cancer cells. *Cellular signalling 25*, 4 (2013), 931–938.

[687] Weidner, F. M. Inferring dynamic properties of Boolean Netoworks from

static graph-based measures. Master thesis, Medical Faculty, Ulm University, 2019.

[688] Weidner, F. M., Schwab, J. D., Werle, S. D., Ikonomi, N., Lausser, L., and Kestler, H. A. Capturing dynamic relevance in boolean networks using graph theoretical measures. *Bioinformatics 37*, 20 (2021), 3530–3537.

[689] Weiss, M. B., Abel, E. V., Mayberry, M. M., Basile, K. J., Berger, A. C., and Aplin, A. E. TWIST1 is an ERK1/2 effector that promotes invasion and regulates MMP-1 expression in human melanoma cells. *Cancer Research 72*, 24 (2012), 6382–6392.

[690] Weissman, I. L., and Shizuru, J. A. The origins of the identification and isolation of hematopoietic stem cells, and their capability to induce donor-specific transplantation tolerance and treat autoimmune diseases. *Blood 112*, 9 (2008), 3543–3553.

[691] Werle, S. D., Ikonomi, N., Schwab, J. D., Kraus, J. M., Weidner, F. M., Rudolph, K. L., Pfister, A. S., Schuler, R., Kühl, M., and Kestler, H. A. Identification of dynamic driver sets controlling phenotypical landscapes. *Computational and Structural Biotechnology Journal 20* (2022), 1603–1617.

[692] Werle, S. D., Schwab, J. D., Tatura, M., Kirchhoff, S., Szekely, R., Diels, R., Ikonomi, N., Sipos, B., Sperveslage, J., Gress, T. M., Buchholz, M., and Kestler, H. A. Unraveling the molecular tumor-promoting regulation of Cofilin-1 in pancreatic cancer. *Cancers 13*, 4 (2021).

[693] Werner, H., Karnieli, E., Rauscher, F. J., and LeRoith, D. Wild-type and mutant p53 differentially regulate transcription of the insulin-like growth factor I receptor gene. *Proceedings of the National Academy of Sciences of the United States of America 93*, 16 (1996), 8318–8323.

[694] Werner, H. M., Mills, G. B., and Ram, P. T. Cancer systems biology: a peek into the future of patient care? *Nature Reviews Clinical Oncology 11*, 3 (2014), 167–176.

[695] Wiegering, A., Pfann, C., Uthe, F. W., Otto, C., Rycak, L., Mäder, U., Gasser, M., Waaga-Gasser, A.-M., Eilers, M., and Germer, C.-T. Cip2a influences survival in colon cancer and is critical for maintaining myc expression. *PLOS ONE 8*, 10 (2013), e75292.

[696] Wilson, A., Laurenti, E., Oser, G., van der Wath, R. C., Blanco-Bose, W., Jaworski, M., Offner, S., Dunant, C. F., Eshkind, L., Bockamp, E., Lió, P., MacDonald, H. R., and Trumpp, A. Hematopoietic stem cells reversibly switch from dormancy to self-renewal during homeostasis and repair. *Cell 135*, 6 (2008), 1118–1129.

[697] Wilson, A., Laurenti, E., and Trumpp, A. Balancing dormant and self-renewing hematopoietic stem cells. *Current Opinion in Genetics & Development 19*, 5 (2009), 461–468.

[698] Wilson, A., Murphy, M. J., Oskarsson, T., Kaloulis, K., Bettess, M. D., Oser, G. M., Pasche, A.-C., Knabenhans, C., MacDonald, H. R., and Trumpp, A. c-Myc controls the balance between hematopoietic stem cell self-renewal and differentiation. *Genes & Development 18*, 22 (2004), 2747–2763.

[699] Wilson, A., Oser, G. M., Jaworski, M., Blanco-Bose, W. E., Laurenti, E., Adolphe, C., Essers, M. A., MacDonald, H. R., and Trumpp, A. Dormant and self-renewing hematopoietic stem cells and their niches. *Annals of the New York Academy of Sciences 1106*, 1 (2007), 64–75.

[700] Wilson, A., and Trumpp, A. Bone-marrow haematopoietic-stem-cell niches. *Nature Reviews Immunology 6*, 2 (2006), 93–106.

[701] Wolkenhauer, O., Auffray, C., Jaster, R., Steinhoff, G., and Dammann, O. The road from systems biology to systems medicine. *Pediatric Research 73*, 4 (2013), 502–507.

[702] Wong, C., Tang, L. H., Davidson, C., Vosburgh, E., Chen, W., Foran, D. J., Notterman, D. A., Levine, A. J., and Xu, E. Y. Two well-differentiated pancreatic neuroendocrine tumor mouse models. *Cell Death & Differentiation 27*, 1 (2020), 269–283.

[703] Wu, T., and Hua, X. Menin represses tumorigenesis via repressing cell proliferation. *American journal of cancer research 1*, 6 (2011), 726.

[704] Wu, X., Tu, X., Joeng, K. S., Hilton, M. J., Williams, D. A., and Long, F. Rac1 activation controls nuclear localization of β-catenin during canonical wnt signaling. *Cell 133*, 2 (2008), 340–353.

[705] Wu, Y., Meitzler, J. L., Antony, S., Juhasz, A., Lu, J., Jiang, G., Liu, H., Hollingshead, M., Haines, D. C., Butcher, D., Pnter, M. S., Roy, K., and Doroshow, J. H. Dual oxidase 2 and pancreatic adenocarcinoma: IFN-γ-mediated dual oxidase 2 overexpression results in H2O2-induced, ERK-associated up-regulation of HIF-1α and VEGF-A. *Oncotarget 7*, 42 (2016), 68412.

[706] Wu, Z.-H., Mabb, A., and Miyamoto, S. Pidd: a switch hitter. *Cell 123*, 6 (2005), 980–982.

[707] Wullschleger, S., Loewith, R., and Hall, M. N. TOR signaling in growth and metabolism. *Cell 124*, 3 (2006), 471–484.

[708] Xao, J. C., Phan, A. T., Jehl, V., Shah, G., and Meric-Bernstam, F. Everolimus in advanced pancreatic neuroendocrine tumors: The clinical experience. *Cancer Research 73*, 5 (2013), 1449–1453.

[709] Xiao, Y. A tutorial on analysis and simulation of boolean gene regulatory network models. *Current Genomics 10*, 7 (2009), 511–525.

[710] Xu, C., Kim, N.-G., and Gumbiner, B. M. Regulation of protein stability by GSK3 mediated phosphorylation. *Cell Cycle 8*, 24 (2009), 4032–4039.

[711] Xu, Q., Liu, X., Zheng, X., Yao, Y., Wang, M., and Liu, Q. The transcriptional

activity of gli1 is negatively regulated by ampk through hedgehog partial agonism in hepatocellular carcinoma. *International Journal of Molecular Medicine 34*, 3 (2014), 733–741.

[712] Xu, Y., Lee, D.-K., Feng, Z., Xu, Y., Bu, W., Li, Y., Liao, L., and Xu, J. Breast tumor cell-specific knockout of Twist1 inhibits cancer cell plasticity, dissemination, and lung metastasis in mice. *Proceedings of the National Academy of Sciences 114*, 43 (2017), 11494–11499.

[713] Yachida, S., Vakiani, E., White, C. M., Zhong, Y., Saunders, T., Morgan, R., De Wilde, R. F., Maitra, A., Hicks, J., DeMarzo, A. M., Shi, C., Sharma, R., Laheru, D., Edil, B. H., Wolfgang, C. L., Schulick, R. D., Heuban, R. H., Tang, L. H., Klimstra, D. S., and Iacubuzio-Donahue, C. A. Small cell and large cell neuroendocrine carcinomas of the pancreas are genetically similar and distinct from well-differentiated pancreatic neuroendocrine tumors. *The American Journal of Surgical Pathology 36*, 2 (2012), 173 –184.

[714] Yahata, T., Takanashi, T., Muguruma, Y., Ibrahim, A. A., Matsuzawa, H., Uno, T., Sheng, Y., Onizuka, M., Ito, M., Kato, S., and Ando, K. Accumulation of oxidative DNA damage restricts the self-renewal capacity of human hematopoietic stem cells. *Blood 118*, 11 (2011), 2941–2950.

[715] Yalcin, S., Zhang, X., Luciano, J. P., Mungamuri, S. K., Marinkovic, D., Vercherat, C., Sarkar, A., Grisotto, M., Taneja, R., and Ghaffari, S. Foxo3 is essential for the regulation of ataxia telangiectasia mutated and oxidative stress-mediated homeostasis of hematopoietic stem cells. *Journal of Biological Chemistry 283*, 37 (2008), 25692–25705.

[716] Yamaguchi, S., Kaneko, M., and Narukawa, M. Approval success rates of drug candidates based on target, action, modality, application, and their combinations. *Clinical and Translational Science 14*, 3 (2021), 1113–1122.

[717] Yamashita, K., Discher, D. J., Hu, J., Bishopric, N. H., and Webster, K. A. Molecular regulation of the endothelin-1 gene by hypoxia. *Journal of Biological Chemistry 276*, 16 (2001), 12645–12653.

[718] Yamashita, M., and Passegué, E. Tnf-α coordinates hematopoietic stem cell survival and myeloid regeneration. *Cell Stem Cell 25*, 3 (2019), 357–372.

[719] Yamauchi, Y., Kodama, Y., Shiokawa, M., Kakiuchi, N., Marui, S., Kuwada, T., Sogabe, Y., Tomono, T., Mima, A., Morita, T., Matsumore, T., Ueda, T., Tsuda, M., Nishikawa, Y., Kuriyama, K., Sakuma, Y., Ota, Y., Maruno, T., Uza, N., Masuda, A., Tatsuoka, H., Yabe, D., Minamiguchi, S., Masui, T., Inagaki, N., Uemoto, S., Chiba, T., and Seno, H. Rb and p53 execute distinct roles in the development of pancreatic neuroendocrine tumors. *Cancer Research 80*, 17 (2020), 3620–3630.

[720] Yamazaki, S., Iwama, A., Morita, Y., Eto, K., Ema, H., and Nakauchi, H. Cytokine signaling, lipid raft clustering, and HSC hibernation. *Annals of the*

New York Academy of Sciences 1106, 1 (2007), 54–63.

[721] Yamazaki, S., Iwama, A., Takayanagi, S.-i., Eto, K., Ema, H., and Nakauchi, H. TGF-beta as a candidate bone marrow niche signal to induce hematopoietic stem cell hibernation. *Blood 113*, 6 (2009), 1250–1256.

[722] Yamazaki, S., Iwama, A., Takayanagi, S.-i., Morita, Y., Eto, K., Ema, H., and Nakauchi, H. Cytokine signals modulated via lipid rafts mimic niche signals and induce hibernation in hematopoietic stem cells. *The EMBO Journal 25*, 15 (2006), 3515–3523.

[723] Yan, J., Yang, Y., Zhang, H., King, C., Kan, H.-M., Cai, Y., Yuan, C.-X., Bloom, G. S., and Hua, X. Menin interacts with IQGAP1 to enhance intercellular adhesion of β-cells. *Oncogene 28*, 7 (2009), 973–982.

[724] Yang, H. W., Shin, M.-G., Lee, S., Kim, J.-R., Park, W. S., Cho, K.-H., Meyer, T., and Heo, W. D. Cooperative activation of PI3K by Ras and Rho family small GTPases. *Molecular Cell 47*, 2 (2012), 281–290.

[725] Yao, B., Zhao, J., Li, Y., Li, H., Hu, Z., Pan, P., Zhang, Y., Du, E., Liu, R., and Xu, Y. Elf5 inhibits TGF-β-driven epithelial-mesenchymal transition in prostate cancer by repressing SMAD3 activation. *The Prostate 75*, 8 (2015), 872–882.

[726] Yao, J. C., Hassan, M., Phan, A., Dagohoy, C., Leary, C., Mares, J. E., Abdalla, E. K., Fleming, J. B., Vauthey, J.-N., Rashid, A., and Evans, D. B. One hundred years after "carcinoid": epidemiology of and prognostic factors for neuroendocrine tumors in 35,825 cases in the united states. *Journal of Clinical Oncology 26*, 18 (2008), 3063–3072.

[727] Yilmaz, O. H., Valdez, R., Theisen, B. K., Guo, W., Ferguson, D. O., Wu, H., and Morrison, S. J. Pten dependence distinguishes haematopoietic stem cells from leukaemia-initiating cells. *Nature 441*, 7092 (2006), 475–482.

[728] Yim, K.-L. Everolimus and mTOR inhibition in pancreatic neuroendocrine tumors. *Cancer Management and Research 4* (2012), 2017–214.

[729] Yin, Y., Hua, H., Li, M., Liu, S., Kong, Q., Shao, T., Wang, J., Luo, Y., Wang, Q., Luo, T., and Jiang, Y. mTORC2 promotes type i insulin-like growth factor receptor and insulin receptor activation through the tyrosine kinase activity of mTOR. *Cell Research 26*, 1 (2016), 46–65.

[730] Yonemori, K., Kurahara, H., Maemura, K., Mataki, Y., Sakoda, M., Iino, S., Ueno, S., Shinchi, H., and Natsugoe, S. Impact of snail and E-cadherin expression in pancreatic neuroendocrine tumors. *Oncology Letters 14*, 2 (2017), 1697–1702.

[731] Yoon, J. W., Gallant, M., Lamm, M. L., Iannaccone, S., Vieux, K.-F., Proytcheva, M., Hyjek, E., Iannaccone, P., and Walterhouse, D. Noncanonical regulation of the hedgehog mediator GLI1 by c-MYC in Burkitt lymphoma. *Molecular Cancer Research 11*, 6 (2013), 604–615.

[732] Yoshihara, H., Arai, F., Hosokawa, K., Hagiwara, T., Takubo, K., Nakamura, Y., Gomei, Y., Iwasaki, H., Matsuoka, S., Miyamoto, K., Miyazaki, H., Takahashi, T., and Suda, T. Thrombopoietin/MPL signaling regulates hematopoietic stem cell quiescence and interaction with the osteoblastic niche. *Cell Stem Cell 1*, 6 (2007), 685–697.

[733] Yoshimoto, G., Miyamoto, T., Jabbarzadeh-Tabrizi, S., Iino, T., Rocnik, J. L., Kikushige, Y., Mori, Y., Shima, T., Iwasaki, H., Takenaka, K., Nagafuji, K., Mizuno, S.-i., Niiro, H., Gilliland, G. D., and Akashi, K. FLT3-ITD up-regulates MCL-1 to promote survival of stem cells in acute myeloid leukemia via FLT3-ITD-specific STAT5 activation. *Blood 114*, 24 (2009), 5034–5043.

[734] Yousefi, M. R., and Dougherty, E. R. Intervention in gene regulatory networks with maximal phenotype alteration. *Bioinformatics 29*, 14 (2013), 1758–1767.

[735] Yu, B., Huo, L., Liu, Y., Deng, P., Szymanski, J., Li, J., Luo, X., Hong, C., Lin, J., and Wang, C.-Y. PGC-1α controls skeletal stem cell fate and bone-fat balance in osteoporosis and skeletal aging by inducing TAZ. *Cell Stem Cell 23*, 2 (2018), 193–209.

[736] Yu, B., Miao, Z.-H., Jiang, Y., Li, M.-H., Yang, N., Li, T., and Ding, J. c-Jun protects hypoxia-inducible factor-1α from degradation via its oxygen-dependent degradation domain in a nontranscriptional manner. *Cancer Research 69*, 19 (2009), 7704–7712.

[737] Yu, H., Hung, M., Chen, Y., Chu, P., Wang, C., Chao, T., Liu, C., Shiau, C., and Chen, K. Erlotinib derivative inhibits hepatocellular carcinoma by targeting cip2a to reactivate protein phosphatase 2a. *Cell death & Disease 5*, 7 (2014), e1359–e1359.

[738] Yu, H., Kim, P. M., Sprecher, E., Trifonov, V., and Gerstein, M. The Importance of Bottlenecks in Protein Networks: Correlation with Gene Essentiality and Expression Dynamics. *PLOS Computational Biology 3*, 4 (2007), e59.

[739] Yu, J. T., Foster, R. G., and Dean, D. C. Transcriptional repression by Rb-E2F and regulation of anchorage-independent survival. *Molecular and Cellular Biology 21*, 10 (2001), 3325–3335.

[740] Zamboni, V., Jones, R., Umbach, A., Ammoni, A., Passafaro, M., Hirsch, E., and Merlo, G. R. Rho gtpases in intellectual disability: from genetics to therapeutic opportunities. *International Journal of Molecular Sciences 19*, 6 (2018), 1821.

[741] Zanini, S., Renzi, S., Giovinazzo, F., and Bermano, G. mTOR pathway in gastroenteropancreatic neuroendocrine tumor (GEP-NETs). *Frontiers in Endocrinology 11* (2020), 746.

[742] Zañudo, J. G. T., Yang, G., and Albert, R. Structure-based control of complex networks with nonlinear dynamics. *Proceedings of the National Academy*

of Sciences 114, 28 (2017), 7234–7239.

[743] Zaytseva, Y. Y., Valentino, J. D., Gulhati, P., and Evers, B. M. mTOR inhibitors in cancer therapy. *Cancer Letters 319*, 1 (2012), 1–7.

[744] Zeller, E., Hammer, K., Kirschnick, M., and Braeuning, A. Mechanisms of RAS/β-catenin interactions. *Archives of Toxikology 87* (2013), 611–632.

[745] Zeng, H., Yücel, R., Kosan, C., Klein-Hitpass, L., and Möröy, T. Transcription factor Gfi1 regulates self-renewal and engraftment of hematopoietic stem cells. *The EMBO Journal 23*, 20 (2004), 4116–4125.

[746] Zeng, P.-Y., and Berger, S. L. LKB1 is recruited to the p21/WAF1 promoter by p53 to mediate transcriptional activation. *Cancer Research 66*, 22 (2006), 10701–10708.

[747] Zeng, X., Li, X., Shao, M., Xu, Y., Shan, W., Wei, C., Li, X., Wang, L., Hu, Y., Zhao, Y., Qian, P., and Huang, H. Integrated single-cell bioinformatics analysis reveals intrinsic and extrinsic biological characteristics of hematopoietic stem cell aging. *Frontiers in genetics* (2021), 2071.

[748] Zhang, J., Francois, R., Iyer, R., Seshadri, M., Zajac-Kaye, M., and Hochwald, S. N. Current understanding of the molecular biology of pancreatic neuroendocrine tumors. *Journal of the National Cancer Institute 105*, 14 (2013), 1005–1017.

[749] Zhang, J., Li, L., Baldwin Jr, A. S., Friedman, A. D., and Paz-Priel, I. Loss of IKKβ but not NF-κB p65 skews differentiation towards myeloid over erythroid commitment and increases myeloid progenitor self-renewal and functional long-term hematopoietic stem cells. *PLOS ONE 10*, 6 (2015), e0130441.

[750] Zhang, J., Niu, C., Ye, L., Huang, H., He, X., Tong, W.-G., Ross, J., Haug, J., Johnson, T., Feng, J. Q., Harris, S., Wiedemann, L. M., Mishina, Y., and Li, L. Identification of the haematopoietic stem cell niche and control of the niche size. *Nature 425*, 6960 (2003), 836–841.

[751] Zhang, L., Mack, R., Breslin, P., and Zhang, J. Molecular and cellular mechanisms of aging in hematopoietic stem cells and their niches. *Journal of Hematology & Oncology 13*, 1 (2020), 1–22.

[752] Zhang, R., Huang, S. Y., Ka-Wai Li, K., Li, Y.-H., Hsu, W.-H., Zhang, G., Chang, C.-J., and Yang, J.-Y. Dual degradation signals destruct GLI1: AMPK inhibits GLI1 through β-TrCP-mediated proteasome degradation. *Oncotarget 8*, 30 (2017), 49869–49881.

[753] Zhang, S., Zhou, X., Lang, R. A., and Guo, F. Rhoa of the rho family small gtpases is essential for b lymphocyte development. *PLOS ONE 7*, 3 (2012), e33773.

[754] Zhang, W., Girard, L., Zhang, Y.-A., Haruki, T., Papari-Zareei, M., Stastny, V., Ghayee, H. K., Pacak, K., Oliver, T. G., Minna, J. D., et al. Small cell lung cancer tumors and preclinical models display heterogeneity

of neuroendocrine phenotypes. *Translational Lung Cancer Research 7*, 1 (2018), 32.

[755] Zhang, W., Hart, J., McLeod, H. L., and Wang, H. L. Differential expression of the AP-1 transcription factor family members in human colorectal epithelial and neuroendocrine neoplasms. *American Journal of Clinical Pathology 124*, 1 (2005), 11–19.

[756] Zhang, Z., Zhou, L., Xie, N., Nice, E. C., Zhang, T., Cui, Y., and Huang, C. Overcoming cancer therapeutic bottleneck by drug repurposing. *Signal Transduction and Targeted Therapy 5*, 1 (2020), 1–25.

[757] Zheng, J., Zhang, D., Przytycki, P. F., Zielinski, R., Capala, J., and Przytycka, T. M. SimBoolNet—a Cytoscape plugin for dynamic simulation of signaling networks. *Bioinformatics 26*, 1 (2010), 141–142.

[758] Zhong, L., Georgia, S., Tschen, S.-i., Nakayama, K., Nakayama, K., and Bhushan, A. Essential role of Skp2-mediated p27 degradation in growth and adaptive expansion of pancreatic β cells. *The Journal of Clinical Investigation 117*, 10 (2007), 2869–2876.

[759] Zhong, L., Yao, L., Tower, R. J., Wei, Y., Miao, Z., Park, J., Shrestha, R., Wang, L., Yu, W., Holdreith, N., Huang, X., Zhang, Y., Tong, W., Gong, Y., Ahn, J., Susztak, K., Dyment, N., Li, M., Long, F., Chen, C., Seale, P., and Qin, L. Single cell transcriptomics identifies a unique adipose lineage cell population that regulates bone marrow environment. *eLife 9* (2020), e54695.

[760] Zhou, D., Müssel, C., Lausser, L., Hopfensitz, M., Kühl, M., and Kestler, H. A. Boolean networks for modeling and analysis of gene regulation. Ulmer Informatik-Berichte, Fakultät für Ingenieurwissenschaften und Informatik Universität Ulm, 2009.

[761] Zhou, F., Huang, D., Li, Y., Hu, G., Rao, H., Lu, Q., Luo, S., and Wang, Y. Nek2A/SuFu feedback loop regulates Gli-mediated Hedgehog signaling pathway. *International Journal of Oncology 50* (2017), 373–380.

[762] Zhu, J. W., DeRyckere, D., Li, F. X., Wan, Y. Y., and DeGregori, J. A role for E2F1 in the induction of ARF, p53, and apoptosis during thymic negative selection. *Cell Growth & Differentiation 10*, 12 (1999), 829–838.

[763] Zhu, X., Gerstein, M., and Snyder, M. Getting connected: analysis and principles of biological networks. *Genes & Development 21*, 9 (2007), 1010–1024.

[764] Zou, P., Yoshihara, H., Hosokawa, K., Tai, I., Shinmyozu, K., Tsukahara, F., Maru, Y., Nakayama, K., Nakayama, K. I., and Suda, T. p57(Kip2) and p27(Kip1) cooperate to maintain hematopoietic stem cell quiescence through interactions with Hsc70. *Cell Stem Cell 9*, 3 (2011), 247–261.

7

APPENDIX

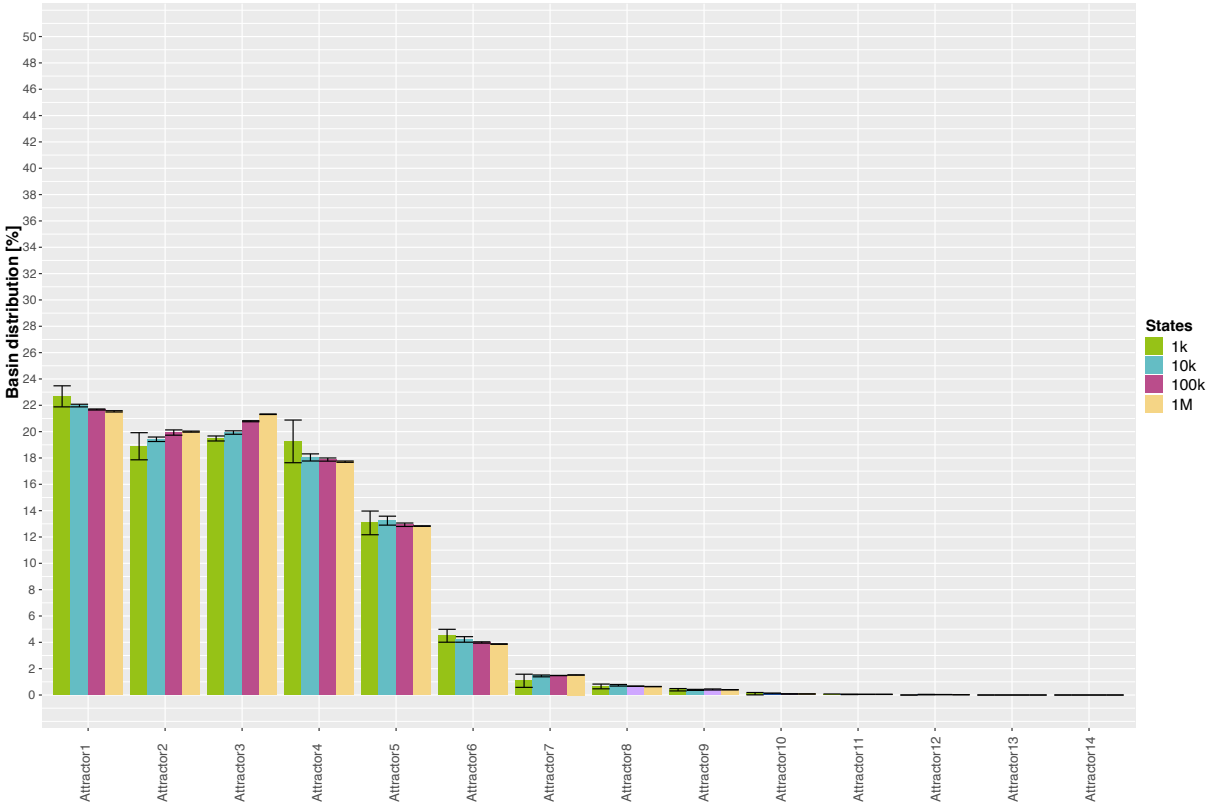


Figure A1: **Basin distribution analysis based on attractors.** The basin distribution of the 14 attractors of the MEN1 loss condition in the pNET model is reported above. The abundance of an attractor in the basin was evaluated for 1000 (1k, in green), 10,000 (10k, in blue), 100,000 (100k, in purplr), and 1,000,000 (1M, in yellow) randomly drawn starting states. The evaluation has been performed three times for each initial condition. Standard deviations are reported as bars in the graphs and the height of the histogram represents the means. The initial sampling of starting states does not significantly affect the basin distributions of the attractor landscape.

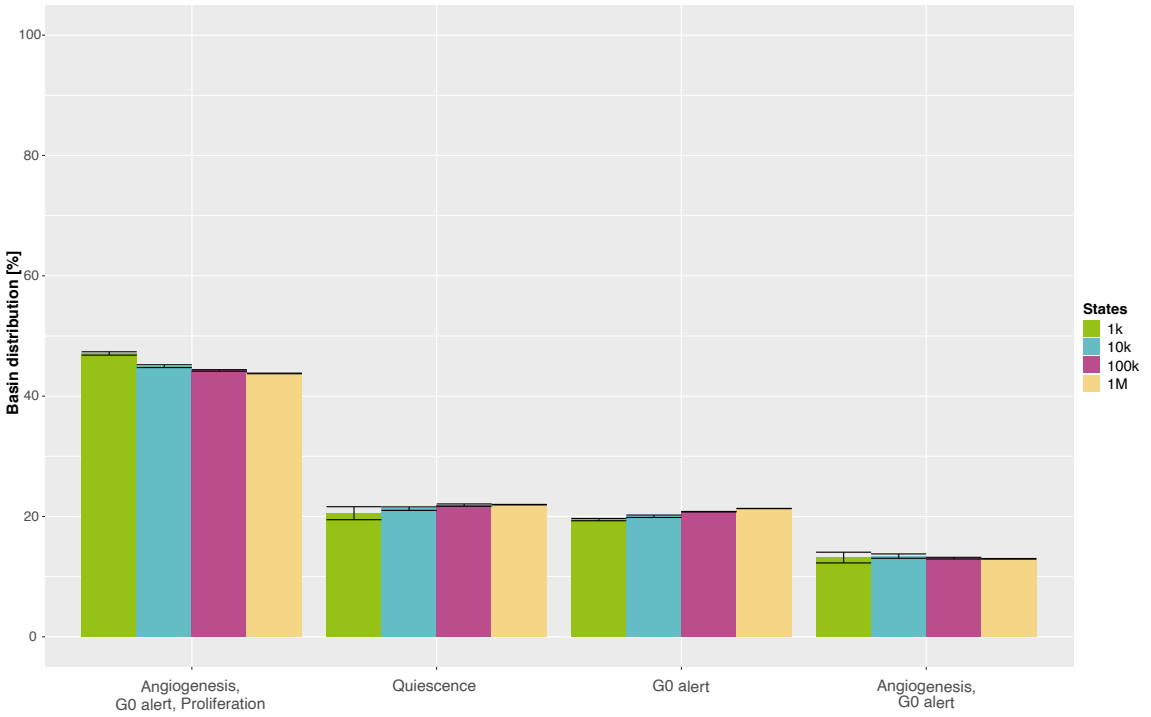


Figure A2: **Basin distribution analysis based on grouped phenotypes**. The basin distribution of the four retrieved phenotypes of MEN1 loss condition in the pNET model is depicted above. The abundance each in the basin was evaluated for 1000 (1k, in green), 10,000 (10k, in blue), 100,000 (100k, in purple), and 1,000,000 (1M, in yellow) randomly drawn starting states. Attractors matching the reported phenotypes were summed up in their basin abundance. The evaluation has been performed three times for each initial condition. Standard deviations are reported as bars in the graphs and the height of the histogram represents the means. The initial sampling of starting states does not significantly affect the basin distributions of the final evaluated phenotypes.

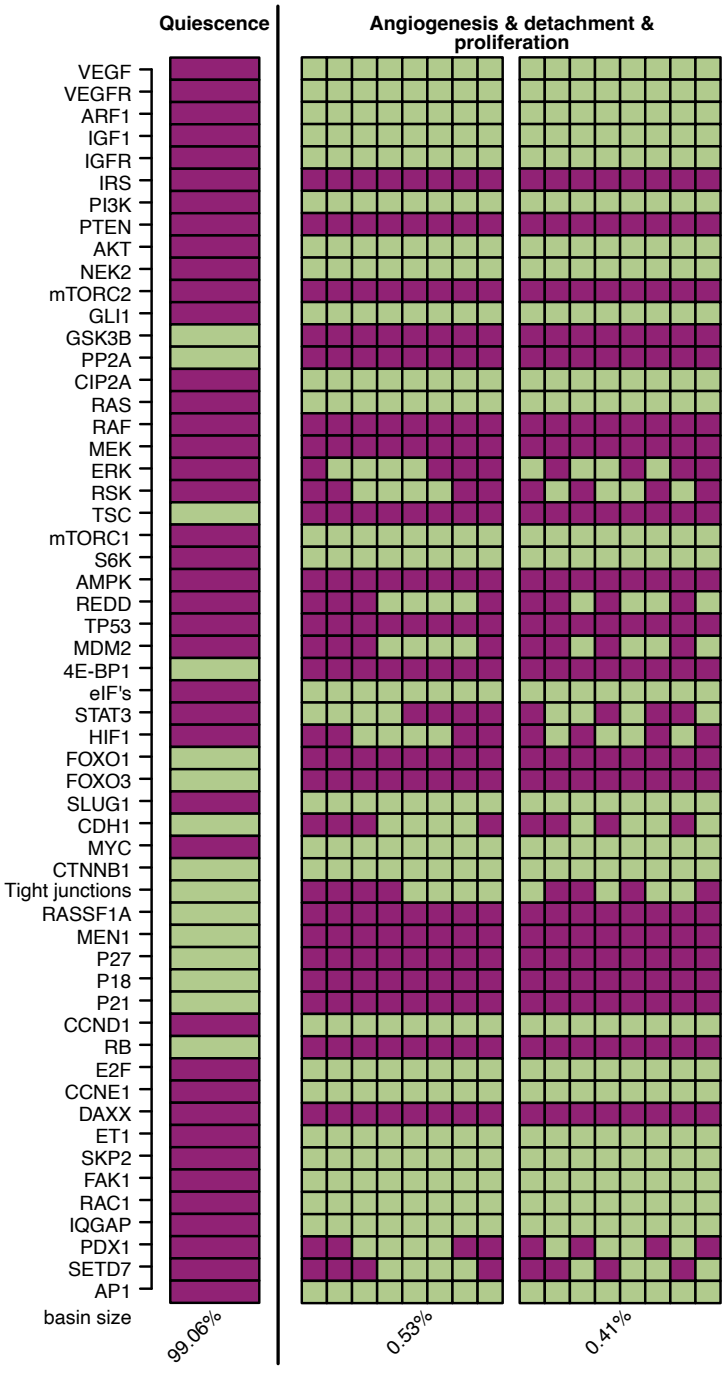


Figure A3: **Unperturbed attractor patterns of the pNETs model.** The attractor landscape of the unperturbed (WT) pNETs network is reported. Attractors are grouped based on their matched phenotypes. Below each attractor the basin size is reported. Activities are reported in the coloured boxes. Here, green indicates active (1) and dark purple indicates inactive (0) genes/proteins.

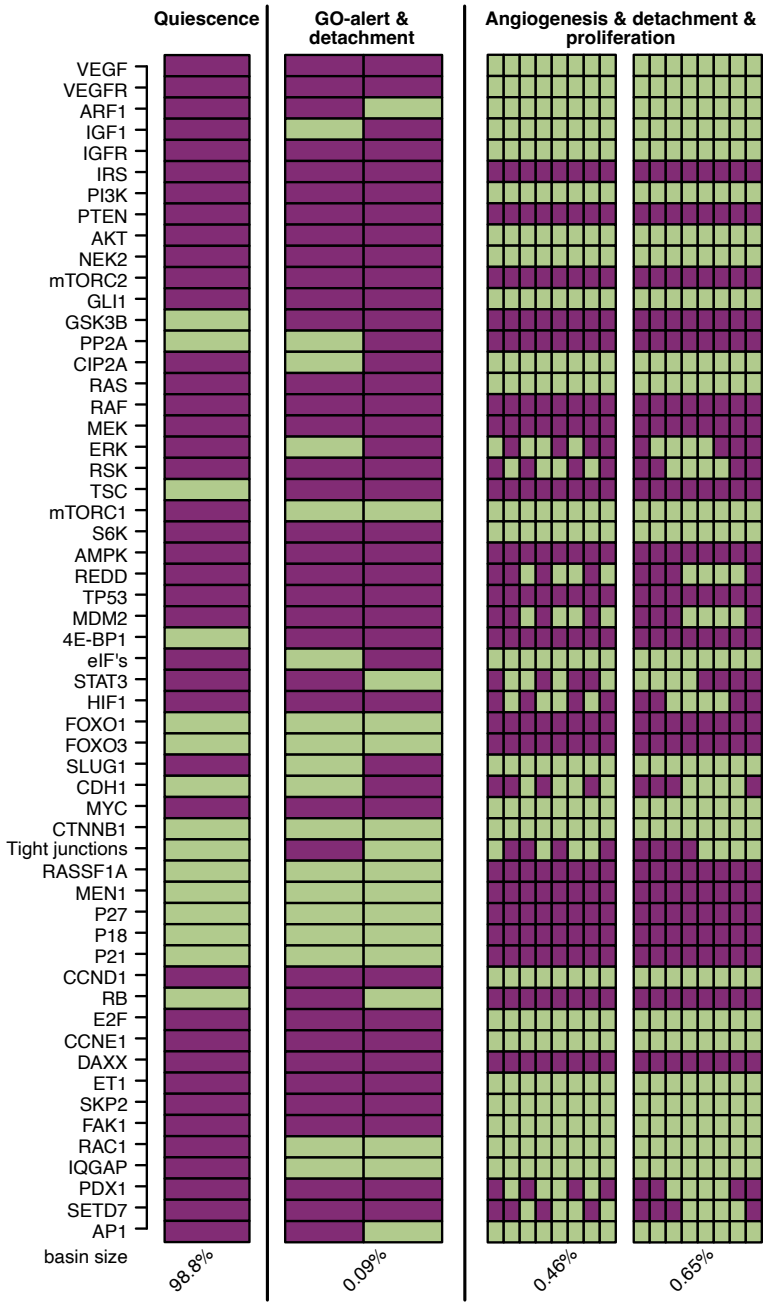


Figure A4: **DAXX loss attractor patterns of the pNETs model.** The attractor landscape of the DAXX loss (DAXX KO) pNETs network is reported. Attractors are grouped based on their matched phenotypes. Below each attractor the basin size is reported. Activities are reported in the coloured boxes. Here, green indicates active (1) and dark purple indicates inactive (0) genes/proteins.

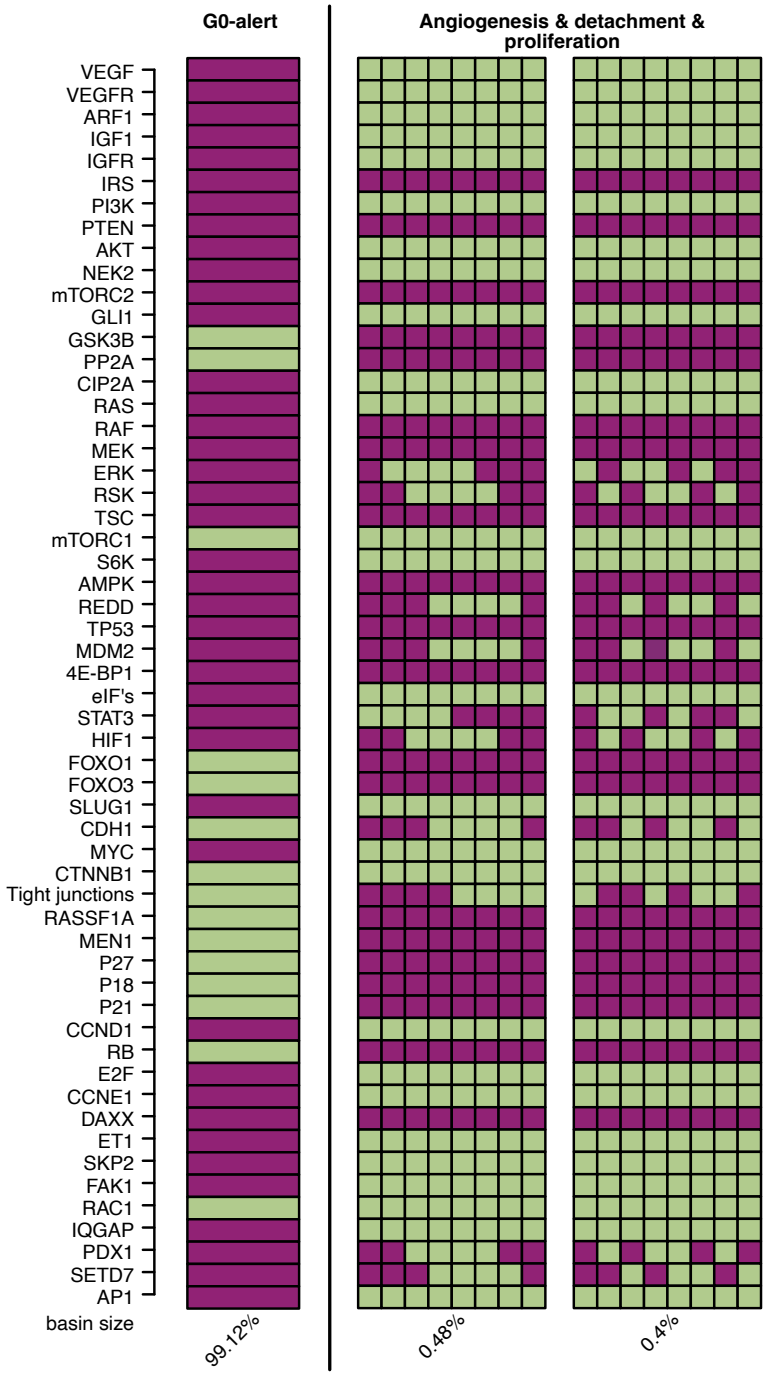


Figure A5: **TSC loss attractor patterns of the pNETs model.** The attractor landscape of the TSC loss (TSC KO) pNETs network is reported. Attractors are grouped based on their matched phenotypes. Below each attractor the basin size is reported. Activities are reported in the coloured boxes. Here, green indicates active (1) and dark purple indicates inactive (0) genes/proteins.

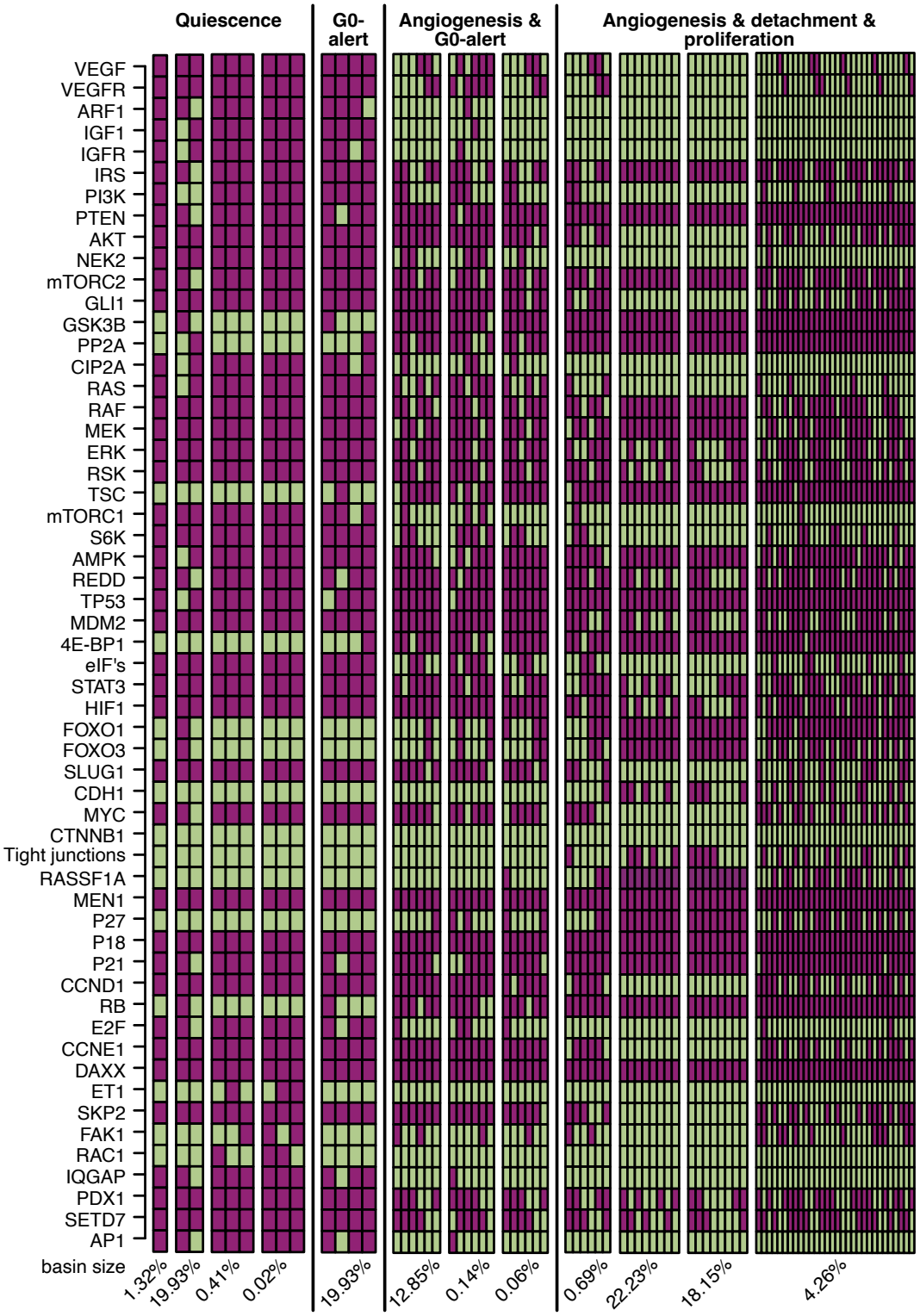


Figure A6: **MEN1 loss attractor patterns of the pNETs model.** The attractor landscape of the MEN1 loss (MEN1 KO) pNETs network is reported. Attractors are grouped based on their matched phenotypes. Below each attractor the basin size is reported. Activities are reported in the coloured boxes. Here, green indicates active (1) and dark purple indicates inactive (0) genes/proteins.

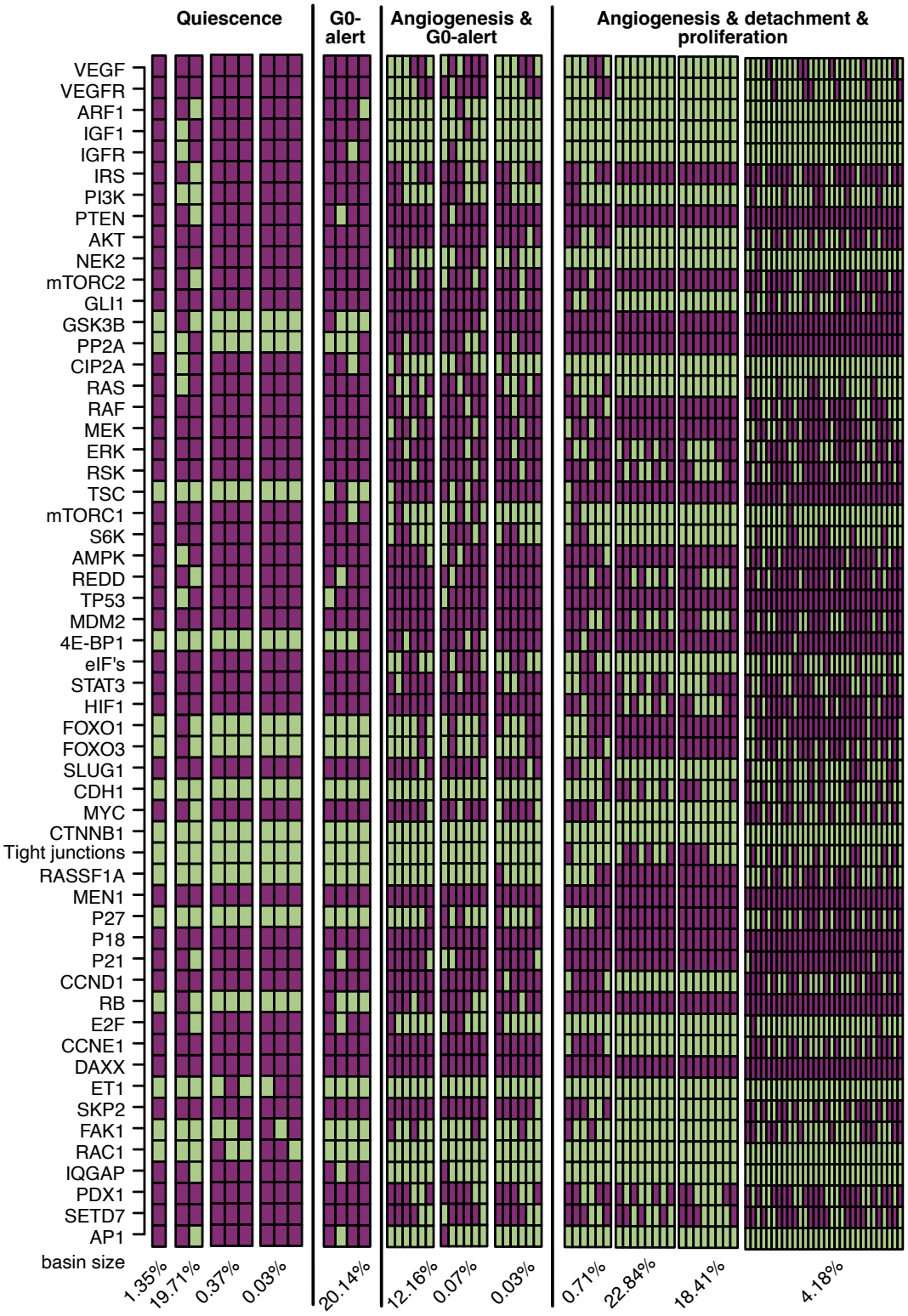


Figure A7: **MEN1 and DAXX loss attractor patterns of the pNETs model.** The attractor landscape of the MEN1 and DAXX loss (MEN1/DAXX KO) pNETs network is reported. Attractors are grouped based on their matched phenotypes. Below each attractor the basin size is reported. Activities are reported in the coloured boxes. Here, green indicates active (1) and dark purple indicates inactive (0) genes/proteins.

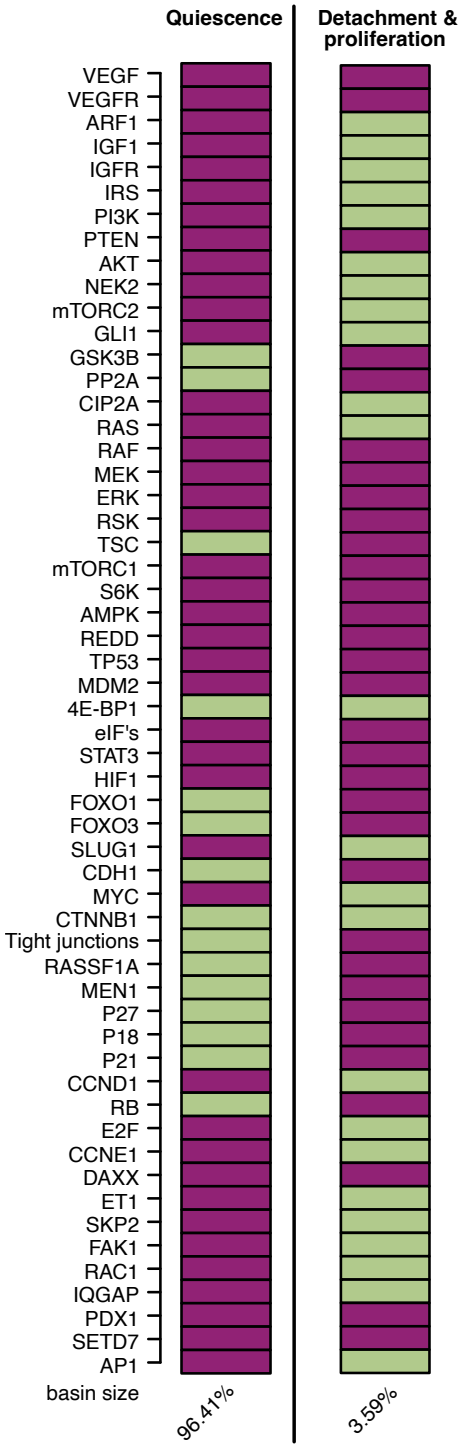


Figure A8: **mTORC1 knockout on unperturbed pNETs.** The attractor landscape of the mTORC1 *in silico* knockout on the unperturbed (WT) pNET network is reported. Attractors are grouped based on their matched phenotypes. Below each attractor the basin size is reported. Activities are reported in the coloured boxes. Here, green indicates active (1) and dark purple indicates inactive (0) genes/proteins.

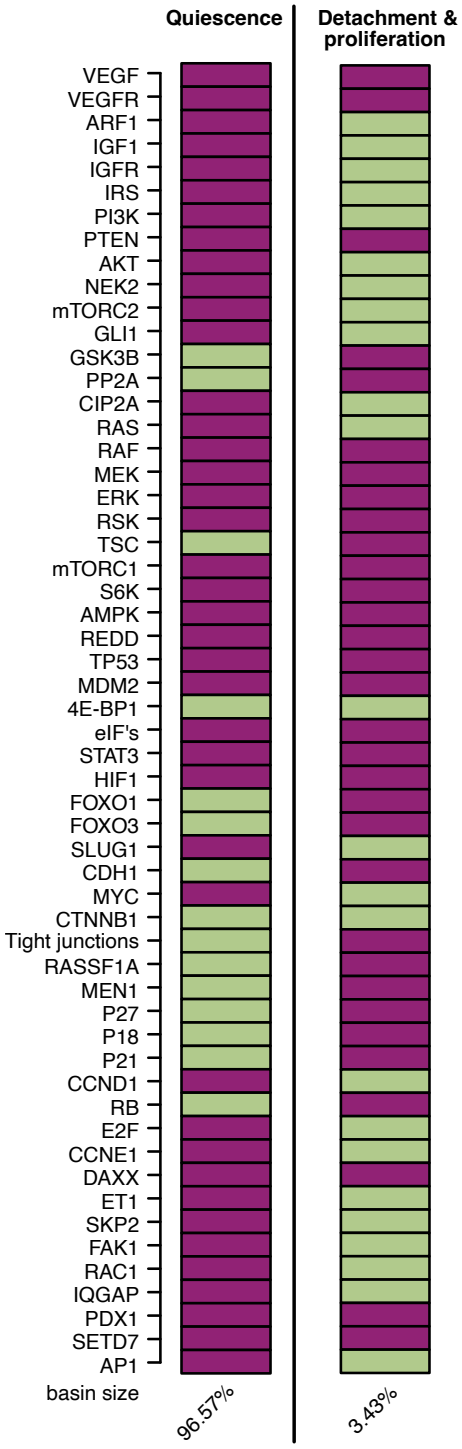


Figure A9: **mTORC1 knockout on DAXX loss pNETs.** The attractor landscape of the mTORC1 *in silico* knockout on the DAXX loss pNET network is reported. Attractors are grouped based on their matched phenotypes. Below each attractor the basin size is reported. Activities are reported in the coloured boxes. Here, green indicates active (1) and dark purple indicates inactive (0) genes/proteins.

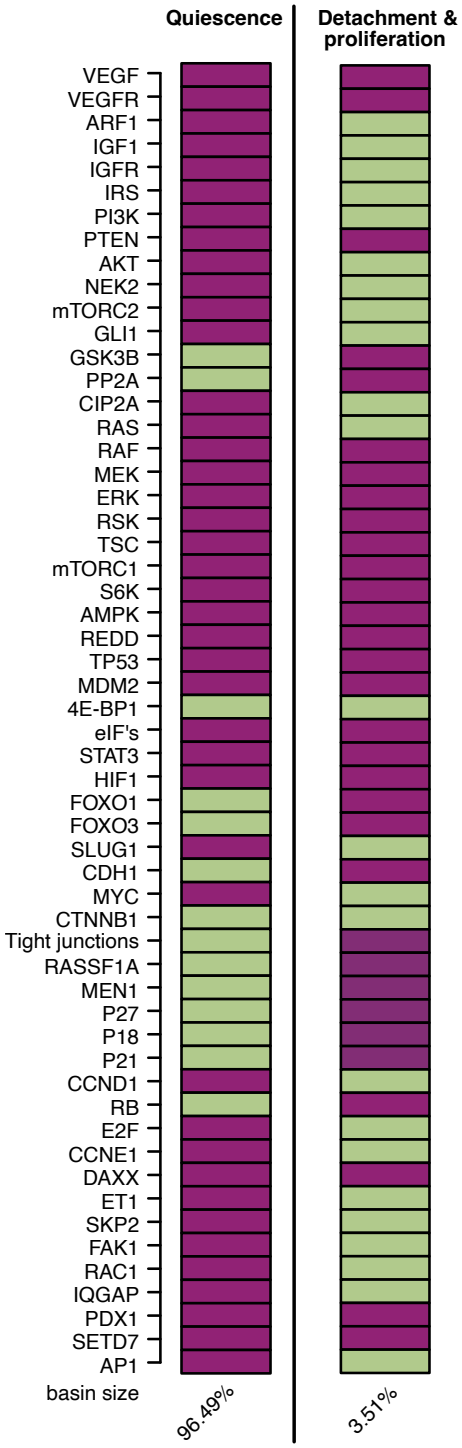


Figure A10: **mTORC1 knockout on TSC loss pNETs.** The attractor landscape of the mTORC1 *in silico* knockout on the TSC loss pNET network is reported. Attractors are grouped based on their matched phenotypes. Below each attractor the basin size is reported. Activities are reported in the coloured boxes. Here, green indicates active (1) and dark purple indicates inactive (0) genes/proteins.

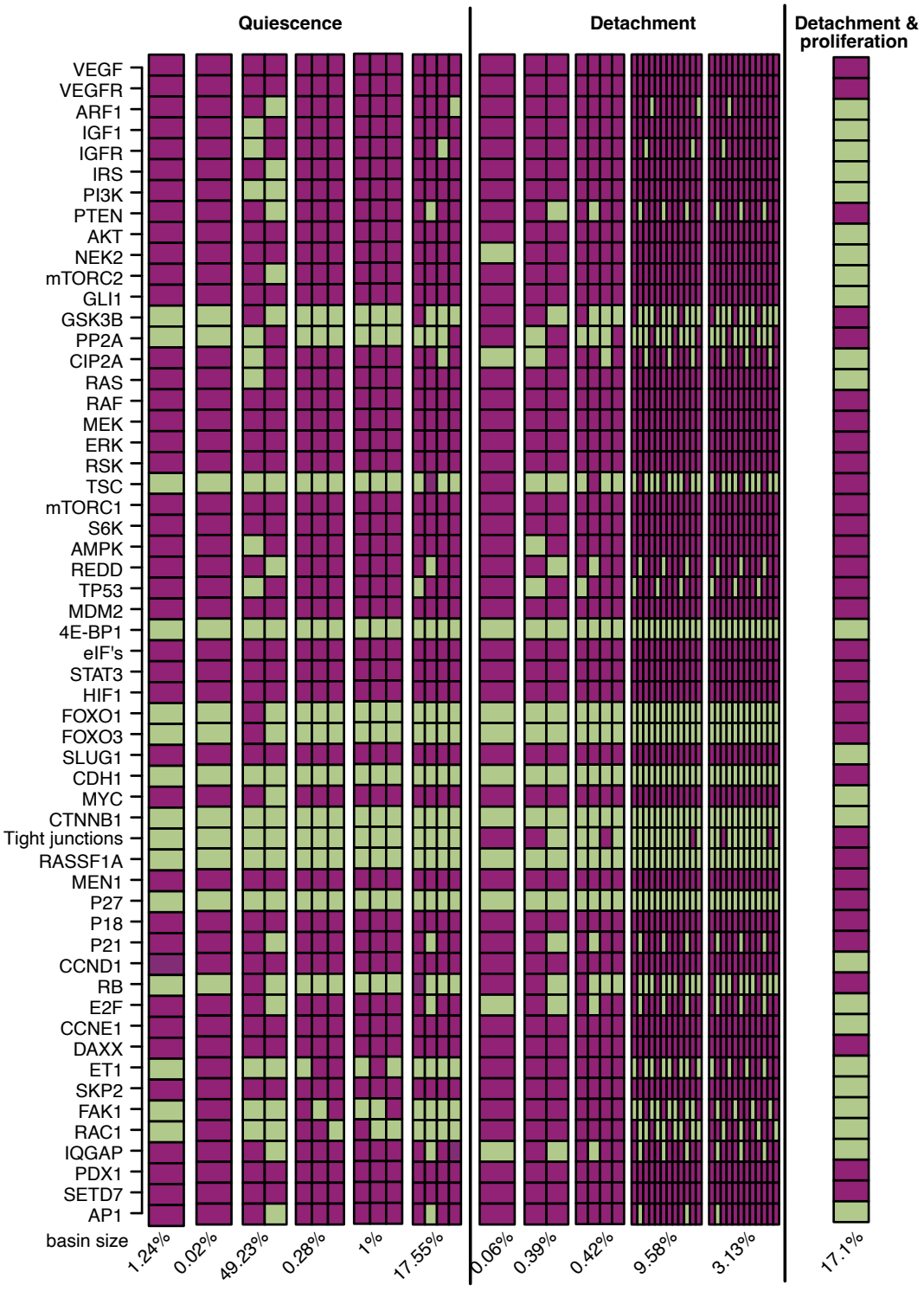


Figure A11: **mTORC1 knockout on MEN1 loss pNETs.** The attractor landscape of the mTORC1 *in silico* knockout on the MEN1 loss pNET network is reported. Attractors are grouped based on their matched phenotypes. Below each attractor the basin size is reported. Activities are reported in the coloured boxes. Here, green indicates active (1) and dark purple indicates inactive (0) genes/proteins.

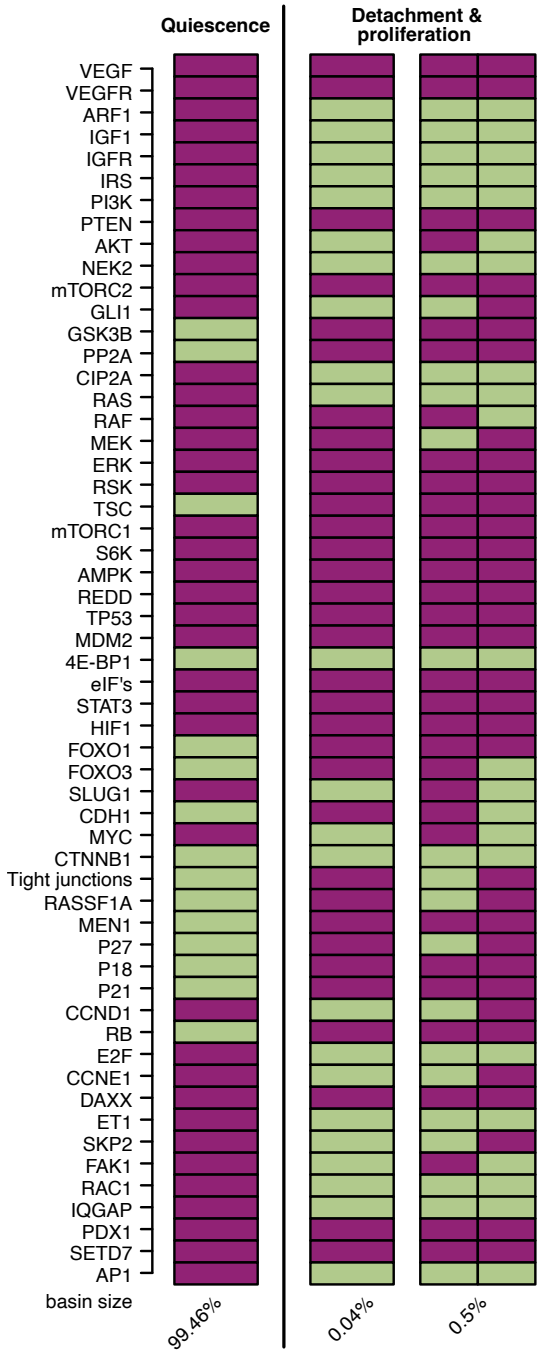


Figure A12: **mTORC1 and mTORC2 knockouts on unperturbed pNETs.** The attractor landscape of the mTORC1 and mTORC2 *in silico* knockouts on the unperturbed (WT) pNET network is reported. Attractors are grouped based on their matched phenotypes. Below each attractor the basin size is reported. Activities are reported in the coloured boxes. Here, green indicates active (1) and dark purple indicates inactive (0) genes/proteins.

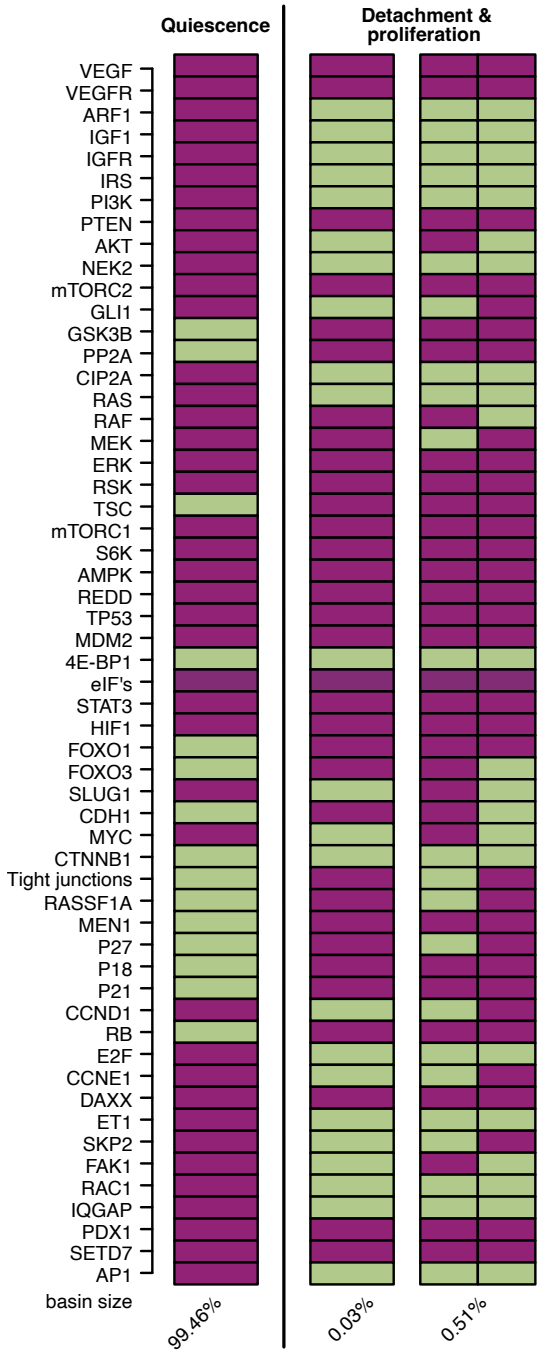


Figure A13: **mTORC1 and mTORC2 knockouts on DAXX loss pNETs.** The attractor landscape of the mTORC1 and mTORC2 *in silico* knockouts on the DAXX loss pNET network is reported. Attractors are grouped based on their matched phenotypes. Below each attractor the basin size is reported. Activities are reported in the coloured boxes. Here, green indicates active (1) and dark purple indicates inactive (0) genes/proteins.

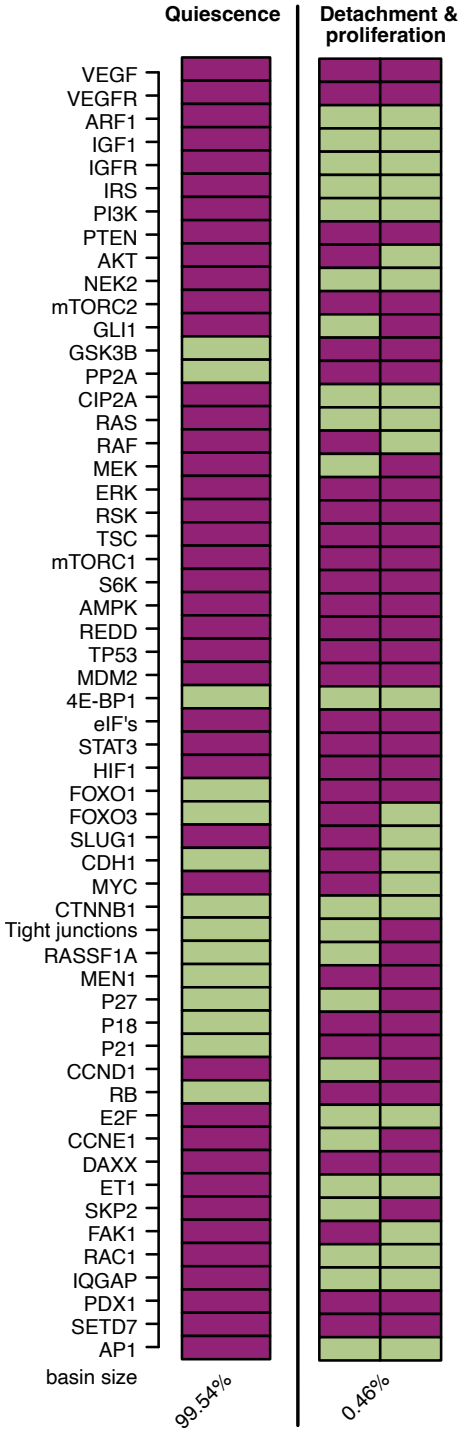


Figure A14: **mTORC1 and mTORC2 knockouts on TSC loss pNETs.** The attractor landscape of the mTORC1 and mTORC2 *in silico* knockouts on the MEN1 loss pNET network is reported. Attractors are grouped based on their matched phenotypes. Below each attractor the basin size is reported. Activities are reported in the coloured boxes. Here, green indicates active (1) and dark purple indicates inactive (0) genes/proteins.

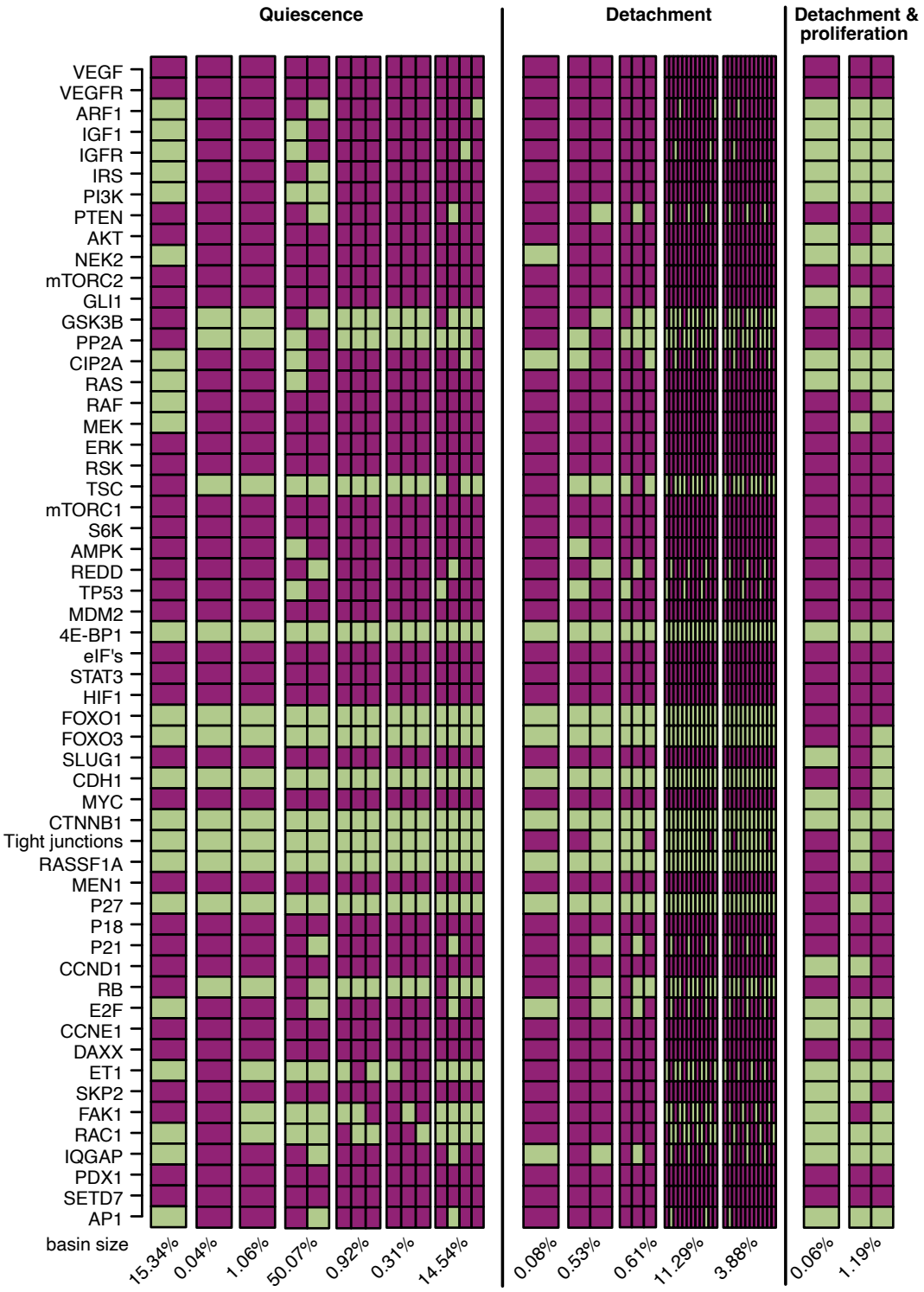


Figure A15: **mTORC1 and mTORC2 knockouts on MEN1 loss pNETs.** The attractor landscape of the mTORC1 and mTORC2 *in silico* knockouts on the TSC loss pNET network is reported. Attractors are grouped based on their matched phenotypes. Below each attractor the basin size is reported. Activities are reported in the coloured boxes. Here, green indicates active (1) and dark purple indicates inactive (0) genes/proteins.

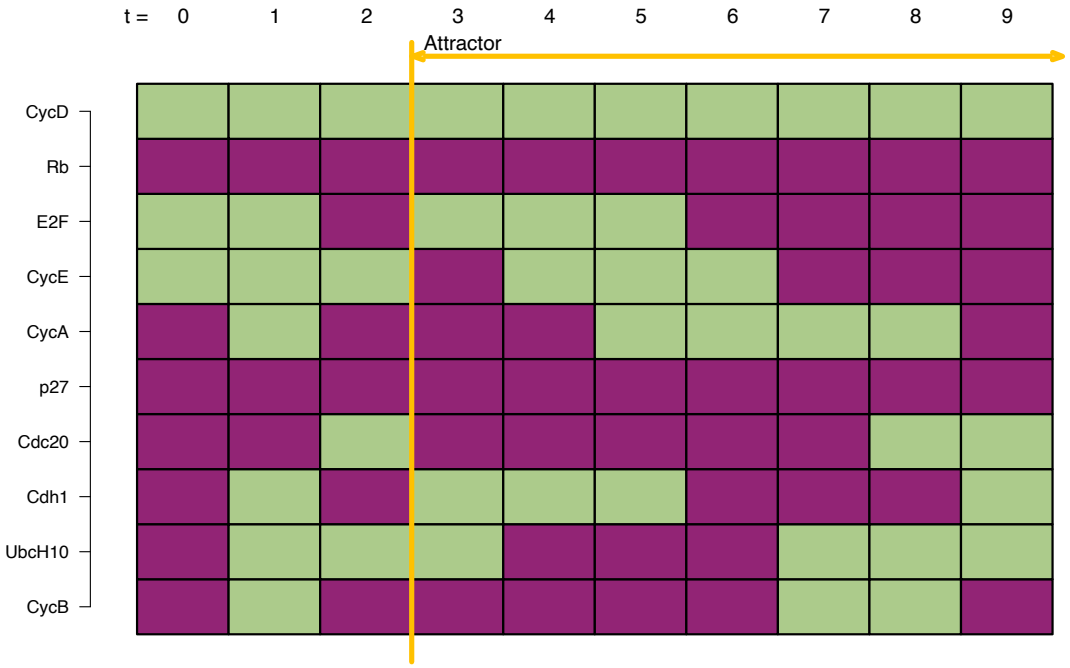


Figure A16: **The the cycling HSC phenotype can lead to a cyclic behaviour.** The activity of CCND1 (CycD), Rb, E2F, CCNE1 (CycE), and P27 were used as start states for attractor search in the cell cycle model from [148]. It is shown that the starting states for the established HSC model lead to a cyclic attractor. The state of each component is depicted by coloured rectangles. Green indicates active components; dark purple indicates inactive ones. The figure has been modified from Ikonomi et al. [254], licensed under CC BY 4.0, https://creativecommons.org/licenses/by/4.0/.

Table A1: Co-expression analysis. Analysis of co-expressed genes via STRING-DB[628], with the high confidence given by the tool (confidence level of high, 0.7). Table modified from Weidner, Schwab, Kühlwein, Ikonomi et al. [688] licensed under CC BY 4.0, https://creativecommons.org/licenses/by/4.0/.

Node class	co-occurance	co-expression
PM (Gatekeepers)	1	1
NM	0	3
NS	0	1

Table A2: Mutual exclusion analysis. Analysis of mutually exclusive genes via cBioPortal [176]. Table modified from Weidner, Schwab, Kühlwein, Ikonomi et al. [688] licensed under CC BY 4.0, https://creativecommons.org/licenses/by/4.0/.

Network reference	Mutually exclusive pair	Type	p-value
Klamt et al. [317]	BRAS - KRAS	PM-PM	< 0.001
	KRAS - NRAS	PM-PM	< 0.001
Sridharan et al. [615]	KRAS-NRAS	PM-PM	< 0.001
	NRAS-PI3KCA	PM-PM	0.017

Table A3: Selection of nodes in the three case studies for the 35 biologically motivated networks. Gatekeepers, negative mismatches and non selected nodes of the three case studies presented among the 35 biologically motivated models are listed. Table modified from Weidner, Schwab, Kühlwein, Ikonomi et al. [688], licensed under CC BY 4.0, https://creativecommons.org/licenses/by/4.0/.

Class	Network	Nodes
Gatekeeper	Cohen et al. [100]	TWIST1
		Migration
		CDH1
		ERK
		TGFβ
		CDH2
		CTNNB1
		miR203
		ZEB2
		miR200
		AKT1
	Méndez-López et al. [423]	ESE2
		p16
	Krumsiek et al. [334]	CEBPα
		FLI1
		PU1
		GATA2
		GFI1

Table A3: Selection of nodes in the three case studies for the 35 biologically motivated networks. Gatekeepers, negative mismatches and non selected nodes of the three case studies presented among the 35 biologically motivated models are listed. Table modified from Weidner, Schwab, Kühlwein, Ikonomi et al. [688], licensed under CC BY 4.0, https://creativecommons.org/licenses/by/4.0/.

Negative mismatch	Cohen et al. [100]	p53
		p63
		p73
		SNAI2
		miR24
		NICD
		AKT2
		SNAI1
		ZEB1
		SMAD
	Méndez-López et al. [423]	p53
		SNAI2
		NF-κB
	Krumsiek et al. [334]	GATA1
		EgrNab
Non selected	Cohen et al. [100]	DNAdamage
		ECM
		p21
		Apoptosis
		EMT
		GF
		Invasion
		CellCycleArrest
		DKK1
		Metastasis
		VIM
	Méndez-López et al. [423]	Cyclin
		TELase
		RB
		E2F

Table A3: Selection of nodes in the three case studies for the 35 biologically motivated networks. Gatekeepers, negative mismatches and non selected nodes of the three case studies presented among the 35 biologically motivated models are listed. Table modified from Weidner, Schwab, Kühlwein, Ikonomi et al. [688], licensed under CC BY 4.0, https://creativecommons.org/licenses/by/4.0/.

	Krumsiek et al. [334]	FOG1
		EKLF
		SCL
		cJUN

Table A4: Comparison of gatekeepers and dynamic-based screening results. Gatekeepers, negative mismatches and non selected nodes of the PNET model are listed. Gatekeepers are ranked based on the mismatch between their connectivity and dynamic impact (reported in brackets). For each node, its selection as tumour driver and as intervention targets is also reported. The intervention targets that yielded a complete quiescent phenotype are highlighted in green, while intervention only suggested in combination with others are indicated as "(double)".

Class	Node	Tumour driver	Therapeutic target
Gatekeeper	CIP2A (0.70)	✓	✓
	mTORC1 (0.70)		✓
	PI3K (0.49)		✓(double)
	RAC1 (0.47)		✓
	FOXO1 (0.46)	✓	✓
	RAF (0.46)		
	ARF1 (0.42)		✓(double)
	RAS (0.41)		
	E2F (0.38)	✓	✓
	TSC (0.38)		✓
	SKP2 (0.24)		
	PP2A (0.33)	✓	✓
	eIFs (0.32)		✓
	TP53 (0.30)	✓	✓
	PDX1 (0.29)		✓
	CDH1 (0.28)		

Table A4: Comparison of gatekeepers and dynamic-based screening results. Gatekeepers, negative mismatches and non selected nodes of the PNET model are listed. Gatekeepers are ranked based on the mismatch between their connectivity and dynamic impact (reported in brackets). For each node, its selection as tumour driver and as intervention targets is also reported. The intervention targets that yielded a complete quiescent phenotype are highlighted in green, while intervention only suggested in combination with others are indicated as "(double)".

Gatekeeper	STAT3 (0.26)		✓
	ETS1 (0.23)	✓	
	IRS (0.18)		
	NEK2 (0.17)		✓(double)
	P21 (0.17)		✓
	IGFR (0.15)		✓
	RSK (0.13)	✓	
	CTNNB1(0.09)		✓
	GSK3β (0.08)	✓	✓
	FAK1 (0.08)		
	SETD7 (0.08)		✓
	AKT (0.04)	✓	✓
	HIF1 (0.02)		
Negative mismatch	VEGF		✓(double)
	PTEN		✓(double)
	mTORC2	✓	✓(double)
	GLI1	✓	✓
	ERK	✓	✓
	S6K		
	AMPK	✓	✓
	MDM2		
	SLUG1		
	MYC		✓
	MEN1	✓	
	ET1		
	AP1		
	VEGFR		
	IGF		
	PP1		✓(double)

Table A4: Comparison of gatekeepers and dynamic-based screening results. Gatekeepers, negative mismatches and non selected nodes of the PNET model are listed. Gatekeepers are ranked based on the mismatch between their connectivity and dynamic impact (reported in brackets). For each node, its selection as tumour driver and as intervention targets is also reported. The intervention targets that yielded a complete quiescent phenotype are highlighted in green, while intervention only suggested in combination with others are indicated as "(double)".

Non selected	MEK		
	PAK4		✓
	LKB1		
	Sestrin1		
	REDD		
	MEF		
	4EB-P1		✓
	MNK		
	FOXO3	✓	✓
	SP1		
	IEG		
	Tight Junctions		
	RASSF1A		
	P27		✓
	P18		
	CCND1		
	RB		✓
	CCNE1		
	DAXX		✓
	IQGAP1		
	JNK		

STATUTORY DECLARATION

I hereby declare that I wrote the present dissertation with the topic:
Logical modelling of molecular crosstalks for the prediction of complex phenotypes
independently and used no other aids that those cited. In each individual case, I have clearly identified the source of the passages that are taken word for word or paraphrased from other works.
I also hereby declare that I have carried out my scientific work according to the principles of good scientific practice in accordance with the current „Satzung der Universität Ulm zur Sicherung guter wissenschaftlicher Praxis“ [Rules of the University of Ulm for Assuring Good Scientific Practice].
Ulm,

Nensi Ikonomi